Two newly defined inherited disorders due to cholinergic transporter dysfunction with distinct clinical outcomes, disease mechanisms and modes of inheritance

Katy Elizabeth Sara Barwick

PhD Thesis

April 2016

Two newly defined inherited disorders due to cholinergic transporter dysfunction with distinct clinical outcomes, disease mechanisms and modes of inheritance

Submitted by

Katy Elizabeth Sara Barwick

To the University of Exeter as a thesis for the degree of Doctor of Philosophy of Medical Studies, April 2016.

I certify that all material in this thesis which is not my own work has been identified and that no material has previously been submitted and approved for the award of a degree by this or any other University.

(Signature)…….

ACKNOWLEDGMENTS

First and foremost I would like to thank the families who participated in this study and to the McDowall family for their support of my research.

My sincerest gratitude goes to my primary supervisor Professor Andrew Crosby for allowing the opportunity to undertake my PhD studies, for the endless and invaluable academic and personal support provided by him, and for the many fantastic experiences this degree has brought me.

I would also like to extend my thanks to Professor Lorna Harries for her support, enthusiasm and encouragement since joining my supervisory team on my arrival in Exeter. Dr Ali Al-Memar, Dr. Meriel McEntagart, Professor Steve Jefferies and Dr Pia Ostergaard at St. George's University of London have provided invaluable support and advice throughout my academic education.

Since arriving in Exeter, Dr. Mark Russell, Dr Jacquelin Whatmore, Dr. David Allard, Professor Robert Pawlak and Dr Craig Beall have provided guidance and support for planning and carrying out new areas of research, for which I am hugely appreciative. Thanks also to Dr Pia Leete for her advice and friendship.

I would like to thank all members of the Crosby group for their help and support, but in particular Dr Barry Chioza, Dr Emma Baple, Dr Ajith Nair and Dr Gaurav Harlalka whose continual patience, guidance and support with regards to my work made completion of this thesis possible, but also whose friendship and encouragement made the undertaking of my studies most enjoyable.

During my PhD I have fortunate to collaborate with many other scientists and clinicians, all of whom I would like to thank for their contributions. I am particularly grateful to Professor Randy Blakely and Jane Wright at Vanderbilt University, USA for having me to their lab, as well as for their teaching and contribution to my cellular studies, and for their continued support and advice. Thanks to Dr Sebastian Gerety and Eve Coomber for producing and phenotyping our mouse model, and for having me to the Sanger Institute to observe their work.

On a personal level I would like to thank my cheerleaders: my mother, Elizabeth Mair, and my nieces, Grace and Lily Annesley- without whom none of this wouldn’t have been possible.

The work in this this thesis was funded by Neurosciences Research Foundation and the John McDowall Bursary (for MND research).

ABSTRACT

Neurodegenerative diseases are becoming increasingly prevalent due to the ageing population, and are among the major contributors to disability and disease worldwide. The identification of the gene defects responsible for many of these conditions has played a major role in our understanding of the pathogenic processes involved, and provided opportunity to develop targeted treatment strategies.

Cholinergic neurotransmission supports a wide range of physiological and behavioural processes and its dysfunction of cholinergic signalling has been associated with a number of disorders, including myasthenias, cardiovascular disease(1), attention-deficit hyperactivity disorder (ADHD) (2), Alzheimer's disease (ADi), schizophrenia, addiction(3), and depression(4). *SLC5A7* encodes the Na^+/Cl^- dependent, high-affinity choline transporter (CHT) which represents the rate limiting step in acetylcholine (Ach) synthesis and is critical for normal cholinergic signalling. The work in this thesis details two new inherited disorders, caused by distinct pathogenic disease mechanisms, associated with novel *SLC5A7* mutations.

Chapter three documents the discovery of two autosomal-dominantly acting *SLC5A7*/CHT mutations associated with adult onset motor neurone disorders. Initially we identified a frameshift mutation that results in premature truncation of the transporter protein in a large Welsh kindred affected with distal hereditary motor neuropathy type VII (dHMN-VII), in which neurodegeneration and muscle paresis is largely restricted to the distal limb muscles and vocal cords. The mutation responsible results in the dominant-negative interference of the mutant molecule with function of the wild type choline transporter, resulting in significantly reduced (although not completely abolished) transporter activity. This finding is further evidenced by the discovery of a second dHMN family associated with a distinct frameshift *SLC5A7* mutation indicative of a similar dominant-negative disease mechanism. Together these findings corroborate a dominant-negative disease mechanism arising from C-terminal truncating *SLC5A7* mutations associated with dHMN, and provide further insight into the role of aberrant choline transporter function in neurological disease.

Chapter four describes N-terminal missense mutations located in the transmembrane spanning region of *SLC5A7*/CHT, associated with a severe infantile neuromuscular disorder characterised by predominantly central hypotonia and developmental delay. The phenotypic effects of these mutations are likely to result from the near abolition of CHT-mediated choline transport in homozygous individuals, and are in keeping with those observed in CHT *knock-out* mouse models(5).

The development of a mouse model of the human motor neurone disease arising from *SLC5A7* frameshift mutations should allow for further investigation of the mechanism by which truncated CHT leads to the dHMN phenotype. Chapter 5 details treatment hypotheses for dHMN, as well as the generation of a patient-specific *knock-in* mouse model carrying an *Slc5a7* mutation orthologous to that identified in dHMN-VII families in chapter 3, and results from preliminary neurological phenotyping of the mouse model. This model will be crucially important for the exploration of treatment options in dHMN-VII motor neurone disease as a prelude to clinical trials in humans.

TABLE OF CONTENTS

1 INTRODUCTION 24

1.1 Neurogenetics 24

1.2 Neurodegenerative disease 25

1.3 Embryogenesis and development of the nervous system 26
1.3.1 Gastrulation and embryonic germ layer formation 26
1.3.2 Neural induction 28
1.3.3 Brain and spinal cord development 30
1.3.4 Genetic and molecular regulation of spinal cord development 31
1.3.5 Histological differentiation 33
1.3.5.1 Neurone development 33
1.3.5.2 Glial cells, neural crest cells, and spinal nerves 34
1.3.5.3 Myelination 35
1.3.6 Brain development 35
1.3.6.1 Genetic and molecular regulation of brain development 36

1.4 The adult motor system 38
1.4.1 The upper motor system 38
1.4.1.1 The corticospinal/pyramidal tract 39
1.4.1.2 The corticobulbar tract 39
1.4.2 The lower motor system 40
1.4.2.1 Alpha and gamma motor neurones 40
1.4.2.2 The neuromuscular junction 42

1.5 Mechanisms of neurodegeneration 43
1.5.1 Selective neuronal vulnerability 44
1.5.2 Intracellular mechanisms 45
1.5.3 Local tissue environment 47
1.5.4 Systemic environment 48

1.6 Motor neurone degenerative disorders 48

1.7 Overview of hereditary peripheral nerve disorders 50
1.7.1 Charcot-Marie-Tooth disease and distal hereditary motor neuropathy 51
1.7.1.1 Demyelinating Charcot-Marie-Tooth disease (Type I) 53
1.7.1.2 Axonal Charcot-Marie-Tooth disease (Type II) 55
1.7.1.3 Intermediate Charcot-Marie-Tooth disease 55
1.7.1.4 X-linked Charcot-Marie-Tooth disease 56
1.7.1.5 The distal hereditary motor neuropathies 57

2 MATERIALS AND METHODS 60

2.1 Buffers, reagents and stock materials 60

2.2 Family recruitment and sample acquisition 61
2.2.1 Ethical Approval 61
2.2.2 Data management 62

2.3 Molecular methods 62
2.3.1 DNA extraction 62

2.3.2 RNA extraction 63
2.3.3 Reverse transcription PCR (RT-PCR) 65
2.3.4 Whole-exome sequencing in dHMN-VII family 67
2.3.5 Targeted next-generation sequencing in dHMN-V family 68
2.3.6 Whole-exome sequencing in Turkish hypotonia family 68
2.3.7 Whole-exome sequencing in Hispanic hypotonia family 69
2.3.8 Primer design 69
2.3.9 Polymerase chain reaction (PCR) 70
2.3.10 Optimisation of PCR primer conditions 71
2.3.11 Agarose gel electrophoresis 72
2.3.12 PCR product purification 73
2.3.13 Sequencing reaction 73
2.3.14 Sequencing reaction product purification 74
2.3.15 Restriction digest 75
2.3.16 Denaturing polyacrylamide gel electrophoresis (PAGE) 76
2.3.17 Bacterial culture: growth and maintenance 77
2.3.18 Heat shock transformation of chemically competent bacteria 77
2.3.19 Sub-cloning of PCR products 78
2.3.20 Site-directed mutagenesis (SDM) 80
2.3.21 Plasmid preparation and sequence verification 82

2.4 *In silico* methods 83
2.4.1 *In silico* sequencing data analysis 83
2.4.2 Mutation Analysis 83
2.4.3 Conservation Analysis 83

2.5 Cell culture techniques 83
2.5.1 Cell culture 83
2.5.2 Freezing cell line stocks 84
2.5.3 Cell plating 84
2.5.4 Transient transfection of cultured cells 84

2.6 Protein methods 85
2.6.1 Cell extract preparations 85
2.6.2 Bicinchoninic acid (BCA) protein assay 85
2.6.3 SDS-PAGE 86
2.6.4 Membrane transfer 87
2.6.5 Western blotting 88

2.7 Functional studies 89
2.7.1 Cell surface biotinylation experiments in transiently transfected HEK-293 cells 89
2.7.2 Saturation analysis of choline uptake in HA-SLC5A7^{WT} and HA-SLC5A7^{K499N} transfected HEK-293 cells 90
2.7.3 [^{3}H]-choline uptake assay in transiently transfected HEK-293 cells 90
2.7.4 [^{3}H]-Choline uptake assay in whole blood monocytes 91
2.7.5 Co-immunoprecipitation of tagged *SLC5A7* wild type protein products and *SLC5A7* (NM_021815.2: c.1497delG; NP_068587.1: p.K499Nfs*13) mutant protein from transiently transfected HEK-293T cells 92
2.7.6 Pulse chase analysis of CHT-WT and CHT-K499Nfs*13 in transiently transfected HEK-293 cells 92

3 READING FRAME ALTERATION OF THE SLC5A7/CHT C-TERMINUS IS ASSOCIATED WITH DHMN PHENOTYPES VIA A DOMINANT-NEGATIVE DISEASE MECHANISM 94

3.1 Introduction 94

3.2 Results 98

PART A 98
3.2.1 Identification of the disease causing mutation in *SLC5A7* in a dHMN-VII family by whole-exome sequence analysis 98
3.2.1.1 History of clinical and pathological features of dHMN-VII family (family 1) members and previous genetic analysis 98
3.2.1.2 Exome sequencing identifies a mutation in *SLC5A7* as the likely cause of dHMN-VII 104
3.2.1.3 *In silico* analysis of *SLC5A7* c.1497delG 107
3.2.1.4 Functional investigation of CHT p.K499Nfs*13 111
3.2.1.4.1 *SLC5A7*^{K499Nfs*13} alters CHT expression levels and surface delivery 111
3.2.1.4.2 The p.K499Nfs*13 mutation significantly reduces choline transport activity in both transfected and patient cells 114
3.2.1.5 Electrophysiology recording in dHMN-VII subjects 116
3.2.1.6 Identification of a second family (family 4), also from Wales, in which the same *SLC5A7* c.1497delG truncating mutation underlies dHMN-VII 117
3.2.1.7 Genetic studies 118

PART B 120
3.2.2 Identification of a likely pathogenic, distinct *SLC5A7* truncating mutation in a family with dHMN-V (family 5) by targeted next generation sequencing 120
3.2.2.1 History and clinical findings in dHMN-V family 5 members 120
3.2.2.2 Targeted next-generation sequence analysis identifies a novel likely pathogenic variant in *SLC5A7* 128
3.2.2.3 *In silico* analysis of *SLC5A7* c.1563_1564delCA 129
3.2.2.4 *SLC5A7*^{H521Qfs*2} truncates CHT, alters expression levels and reduces choline transport 132

3.3 Discussion 134

4 N- TERMINAL AUTOSOMAL RECESSIVELY-ACTING SLC5A7/CHT MISSENSE MUTATIONS ASSOCIATED WITH SEVERE CONGENITAL HYPOTONIA 144

4.1 Introduction 144

4.2 Results 146
4.2.1 Identification of a autosomal recessive mutations in *SLC5A7* in two consanguineous families with severe congenital hypotonia 146
4.2.1.1 History and clinical pathological features in Turkish hypotonia family (family 6) 146
4.2.1.2 History and clinical pathological features in Hispanic hypotonia family (family 7) 147
4.2.2 Exome sequencing and mutation identification 151
4.2.3 *In silico* analysis of *SLC5A7* missense mutations 152
4.2.4 Functional investigation of CHT p.V112E and CHT p.S94R 156
4.2.4.1 *SLC5A7*^{S94R} and *SLC5A7*^{V112E} reduce surface, but not overall, CHT expression 156
4.2.4.2 *SLC5A7*^{S94R} and *SLC5A7*^{V112E} abolish choline transport activity in transfected cells 161

4.3 Discussion 163

5 DHMN-VII MOUSE MODEL 170

5.1 Introduction 170
5.1.1 Animal models of human disease 170
5.1.2 The importance of animal models of motor neurone disorders 171
5.1.3 CHT-related disease treatment hypotheses 172
5.1.3.1 Treatment with a nAChR agonist 173
5.1.3.2 Treatment with an AChE inhibitor 175

5.2 Generation of dHMN-VII mouse line, and results of preliminary phenotyping .. 175
5.2.1 Open field and grip strength testing 176
5.2.2 Grip strength results for *Slc5a7*$^{indelAC/+}$ mice 176
5.2.3 Grip strength results for *Slc5a7*$^{+/TM1A}$ mice 177

5.3 Discussion 179
5.3.1 Future work- creation of a hypomorphoc compound heterozygous *Slc5a7*$^{indelAC/TM1A}$ 180

6 FINAL DISCUSSION AND FUTURE WORK 184

7 APPENDIX 190

7.1 APPENDIX CHAPTER 1 190
7.1.1 Table 31. Demyelinating CMT subtypes, their distinguishing features, and their associated genes and their functions 191
7.1.2 Table 32. Axonal CMT subtypes, their distinguishing features, and their associated genes and their functions 194
7.1.3 Table 33. Intermediate CMT subtypes, their distinguishing features, and their associated genes and their functions 198
7.1.4 Table 34. X-linked CMT subtypes, their distinguishing features, and their associated genes and their functions. 200
7.1.5 Table 35. Distal hereditary motor neuropathy subtypes, their distinguishing features, and their associated genes and their functions 201

7.2 APPENDIX CHAPTER 2 205
7.2.1 Table 36. Amounts of human *SLC5A7* cDNA construct transfected/500,000 cells ... 205
7.2.2 Table 37. Amounts of human *SLC5A7* cDNA construct transfected/100,000 cells ... 206

7.3 APPENDIX CHAPTER 3 207
7.3.1 Table 38. dHMN-VII family 1 identification numbers across studies 207
7.3.2 Table 39. Primer sequences for cosegregation analysis of four candidate variants within dHMN-VII locus 208
7.3.3 Table 40. *SLC5A7* primer sequences 209
7.3.4 *SLC5A7* c.1497delG screening in regional control subjects 209
7.3.5 Species conservation of CHT C-terminus compared to p.K499Nfs*13 mutant protein 210
7.3.6 TMHMM analysis of CHT p.K499Nfs*13 211
7.3.7 *SLC5A7* c.1563_1564delCA/p.H521Qfs*2 site-directed mutagenesis (SDM) primers 212
7.3.8 Co-immunoprecipitation of tagged *SLC5A7* wild type protein products and *SLC5A7* c.1497delG/p.K499Nfs*13 mutant protein from transiently transfected HEK-293T cells 212
7.3.8.1 Methodology 212
7.3.8.2 Results 214
7.3.9 Pulse chase analysis of CHT-WT and CHT-K499Nfs*13 in transiently transfected HEK-293T cells 215
7.3.9.1 Methodology 215

7.3.9.2 Results 216
7.3.10 Species conservation of CHT C-terminus compared to p.H521Q*fs2 mutant protein 218
7.3.11 TMHMM analysis of CHT p.H521Q*fs2 219

7.4 APPENDIX CHAPTER 4 220
7.4.1 Table 41. Disorders featuring congenital central, peripheral, and combined hypotonia 220
7.4.2 Species conservation of CHT C-terminus compared to p.S94R and p.V112E mutant proteins 222
7.4.3 TMHMM analysis of CHT p.S94R and p.V112E 223
7.4.4 *SLC5A7* c.282T>A/ p.S94R and c.335T>A/V112E site-directed mutagenesis (SDM) primers 224

7.5 APPENDIX CHAPTER 5 225
7.5.1 CHT-related disease treatment hypotheses figures 225
7.5.2 Approach to mouse model generation 229
7.5.3 Assay for *knock-in* allele expression 230
7.5.4 Open field testing - methodology and results 231
7.5.5 Grip strength testing - methodology and results raw data 232
7.5.5.1 Grip strength testing in *Slc5a7*$^{indelAC/+}$ mice 233
7.5.5.2 Grip strength testing in *Slc5a7*$^{+/TM1A}$ mice 236

LIST OF FIGURES

Figure 1:	Invagination	27
Figure 2:	Stages of neurulation. Modified (Mitchell & Sharma, 2009)	29
Figure 3:	Cross section of the spinal cord during development. Modified (Tarant County College, 2014)	31
Figure 4:	Cross section of the spinal cord showing a typical motor neurone originating in the ventral horn. Modified (http://classes.midlandstech.edu/carterp/Courses/bio110/chap08/chap08.htm)	35
Figure 5:	Diagram of the organisation of the motor system.	41
Figure 6:	Schematic diagram showing upper and lower motor neurones. Modified (http://highscope.ch.ntu.edu.tw/wordpress/?p=11860)	42
Figure 7:	Conceptual model of candidate pathways leading to neurodegeneration grouped according to their major site or mode of action. Modified (Ramanan, 2013)	44
Figure 8:	The architecture of the myelinated axon in the peripheral nervous system and the myelin proteins defected in CMT-I. Modified (Scherer, 2015)	54
Figure 9:	Diagram of a myelinated nerve fibre showing the locations of the proteins mutated in autosomal dominant and autosomal recessive forms of intermediate CMT. Modified (Liu, 2014)	56
Figure 10:	dHMN-VII family (family 1) pedigree	99
Figure 11:	Distal muscle wasting of family 1_V:9. Modified (Young & Harper, 1980)	100
Figure 12:	Family pedigree of large Welsh kindred in which dHMN-VII locus was refined. Modified (Dick, 2008)	103
Figure 13:	Schematic diagram of the refined dHMN-VII locus represented by microsatellite markers. Modified (Dick, 2008)	103
Figure 14:	dHMN-VII family pedigree showing cosegregation analysis results for each of the variants in the dHMN-VII loci.	106
Figure 15:	Chromatogram showing DNA sequence around the c.1497delG variant.	107
Figure 16:	dHMN-VII-like family pedigrees.	109
Figure 17:	Alignment of wild type and CHT K499Nfs*13 amino acid sequences.	110
Figure 18:	Diagram of the predicted secondary structure of the *SLC5A7* and *SLC5A7* c.1497delG gene products. Modified (Apparsundaram, 2000; Apparsundaram, 2001)	111
Figure 19:	Total protein levels of HA-tagged CHT WT and CHT p.K499Nfs*13 in transiently transfected HEK-293 cells.	113
Figure 20:	Total and surface levels of CHT WT and CHT p.K499Nfs*13 protein in transiently transfected HEK-293 cells.	113
Figure 21:	Saturation analysis of [3H]-choline transport activity in CHT WT and CHT p.K499Nfs*13 transfected HEK-293 cells.	114
Figure 22:	[3H]-choline transport activity in CHT WT and CHT p.K499Nfs*13 co-transfected HEK-293 cells.	115
Figure 23:	HC-3 sensitive choline transport activity in whole blood monocytes natively expressing CHT WT and CHT p.K499Nfs*13.	116
Figure 24:	dHMN-VII family (family 4) pedigree.	119
Figure 25:	Distal muscle wasting of family 4_II:2.	119
Figure 26:	dHMN-V family (family 5) pedigree	122
Figure 27:	Next generation sequencing data for individual family 5_III-2.	128

Figure 28: Chromatogram showing DNA sequence around the c.1563_1564delCA variant in family 5_III:2 and family 5_IV:1 129
Figure 29: Alignment of wild type and CHT H521Qfs*2 amino acid sequences. 130
Figure 30: Diagram of the predicted secondary structure of the *SLC5A7* and *SLC5A7* c.1563_1564delCA gene products. Modified (Apparsundaram, 2000; Apparsundaram, 2001) 131
Figure 31: Preliminary western blot analysis of HA-CHT WT, HA-CHT p.K499Nfs*13 and HA-CHT p.H521Qfs*2. 133
Figure 32: Preliminary choline uptake assay in HEK-293 cells transiently transfected with wild type and CHT p.H521Qfs*2 cDNAs. 133
Figure 33: Schematic diagram of the anatomical-clinical correlation of infantile hypotonia, illustrating differential diagnosis. Modified (Leyenaar, 2005) 145
Figure 34: Turkish hypotonia family (family 6) pedigree 147
Figure 35: Hispanic hypotonia family (family 7) pedigree 148
Figure 36: Brain MRI of family 7_V:3. 149
Figure 37: Chromatogram showing DNA sequence around *SLC5A7* c.282T>A and c.335T>A. 152
Figure 38: Alignment of wild type and CHT p.S94R and p.V112E amino acid sequences. 154
Figure 39: Diagram of the predicted secondary structure of the *SLC5A7* showing the p.S94R and p.V112E variants. Modified (Apparsundaram, 2000; Apparsundaram, 2001) 155
Figure 40: Total protein levels of myc-CHT WT, myc-CHT p.S94R and myc-CHT p.V112E expressed in HEK-293 cells assessed by western blot and ELISA. 158
Figure 41: Preliminary western blot analysis of total protein levels of HA-CHT WT, HA-CHT p.S94R and HA-CHT p.V112E in transiently transfected cells. 159
Figure 42: Surface protein levels of myc-CHT WT, myc-CHT p.S94R and myc-CHT p.V112E expressed in HEK-293 cells assessed by western blot and ELISA. 160
Figure 43: Immunostaining of myc-CHT WT, myc-CHT p.S94R and myc-CHT p.V112E transfected HEK-293T cells. 161
Figure 44: Preliminary choline uptake assay in HEK-293 cells transiently transfected with wild type and CHT p.S94R and p.V112E cDNAs. 162
Figure 45: Restriction digest showing the presence of the c.1497delG variant in one dHMN-VII affected individual, and its absence in 151 subjects control individuals. 209
Figure 46: Protein homology of the C-terminus of the *SLC5A7* genes protein product in various species compared with the c.1497delG mutant molecule. 210
Figure 47: TMHMM transmembrane predictions of the SLC5A7 protein product of wild type and p.K499Nfs*13 mutant molecules. 211
Figure 48: Preliminary pulse chase analysis HEK-293 cells transiently transfected with 2X HA-*SLC5A7*^{WT}, 2X HA-*SLC5A7*^{K499Nfs*13}, or 1X HA-*SLC5A7*^{WT} with 1X HA-*SLC5A7*^{K499Nfs*13}. 217
Figure 49: Protein homology of the C-terminus of the SLC5A7 genes protein product in various species compared with the c.1563_1564delCA mutant molecule. 218
Figure 50: TMHMM transmembrane predictions of the SLC5A7 protein product of wild type and p.H521Qfs*2 mutant molecules. 219
Figure 51: Protein homology of CHT at the amino acid positions of CHT p.S94R and p.V112E in various species and human wild type. 222
Figure 52: TMHMM transmembrane predictions of the SLC5A7 protein 223

product of wild type and p.S94R and p.V112E mutant molecules.
Figure 53: Normal cholinergic transmission at the NMJ. 225
Figure 54: Defective cholinergic transmission at the NMJ due to the SLC5A7 c.1497delG. 226
Figure 55: dHMN-VII treatment hypothesis (i) nAChR agonist. 227
Figure 56: dHMN-VII treatment hypothesis (ii) AChE inhibitor. 228
Figure 57: Confirmation of knock-in allele expression. 230
Figure 58: Distance covered in open field testiong of 18-22 week old mice. 231
Figure 59: Grip strength test results taken at time points 1 (18-22 weeks), 2 (23-26 weeks) and 3 (27-31 weeks) from wild type vs. *Slc5a7*$^{indelAC/+}$ mice 233
Figure 60: Grip strength test results taken at time points 1 (18-22 weeks), 2 (23-26 weeks) and 3 (27-31 weeks) from wild type vs. *Slc5a7*$^{+/TM1A}$ mice 236

LIST OF TABLES

Table 1: Simplified overview of broad clinical features arising from UMN or LMN lesions 49
Table 2: Common motor neurone degenerative disorders and their features, in which either UMNs, LMNs, or both are affected 50
Table 3: Buffers, reagents and stock solutions and their constituents 60
Table 4: RT-PCR constituents and their volumes 66
Table 5: RT-PCR thermal cycling program 66
Table 6: PCR constituents and their volumes 70
Table 7: Touchdown PCR thermal cycling program 71
Table 8: Sequencing reaction constituents and their volumes 74
Table 9: Sequencing reaction thermal cycling program 74
Table 10: Ligation reaction constituents and their volumes 79
Table 11: SDM sample reaction constituents and their volumes 81
Table 12: SDM control reaction constituents and their volumes 81
Table 13: SDM reaction thermal cycling program 81
Table 14: 10% SDS-PAGE running gel constituents and their volumes 87
Table 15: 10% SDS-PAGE stacking gel constituents and their volumes 87
Table 16: Electrophysiological findings from both branches of dHMN-VII family 1 101
Table 17: Clinical findings from both branches of dHMN-VII family 1 102
Table 18: Sequencing matrices 104
Table 19: dHMN-VII family 1 loci variants 104
Table 20: Fatigability and decrement EMG response 117
Table 21: Medical Research Councils manual muscle testing scale 123
Table 22: Manual muscle testing 124
Table 23: Motor nerve conduction in family 5_IV:1 125
Table 24: F-wave analysis in family 5_IV:1 125
Table 25: Sensory nerve conduction in family 5_IV:1 126
Table 26: Electromyography findings in family 5_IV:1 127
Table 27: Clinical phenotypes of family 7 150
Table 28: Online *in silico* mutation analysis software results for CHT p.S94R and p.V112E 155
Table 29: Comparison of *SLC5A7*/CHT mutations investigated in this study, their structural and function effects on the choline transporter, and their associated conditions 165
Table 30: Genotyping and initial phenotyping of litter born from intercrossing *Slc5a7*$^{indelAC/+}$ and *Slc5a7*$^{+/TM1A}$ mice 181
Table 31: Demyelinating CMT subtypes, their distinguishing features, and their associated genes and their functions 191
Table 32: Axonal CMT subtypes, their distinguishing features, and their associated genes and their functions 194
Table 33: Intermediate CMT subtypes, their distinguishing features, and their associated genes and their functions 198
Table 34: X-linked CMT subtypes, their distinguishing features, and their associated genes and their functions. 200

Table 35: Distal hereditary motor neuropathy subtypes, their distinguishing features, and their associated genes and their functions 201
Table 36: Amounts of human SLC5A7 cDNA construct transfected/500,000 cells 205
Table 37: Amounts of human SLC5A7 cDNA construct transfected/100,000 cells 206
Table 38: dHMN-VII family 1 identification numbers across studies 207
Table 39: Primer sequences for cosegregation analysis of four candidate variants within dHMN-VII locus 208
Table 40: *SLC5A7* primer sequences 209
Table 41: Disorders featuring congenital central, peripheral, and combined hypotonia 220
Table 42: Female *Slc5a7*$^{indelCA/+}$ mice grip strength summary statistics 234
Table 43: Male *Slc5a7*$^{indelCA/+}$ mice grip strength summary statistics 235
Table 44: Female *Slc5a7*$^{+/TM1A}$ mice grip strength summary statistics 237
Table 45: Male *Slc5a7*$^{+/TM1A}$ mice grip strength summary statistics 238

ABBREVIATIONS

3’	……..Three prime
3H	……..Methyl-^{3}H
5’	……..Five prime
Ab elb	……..Above the elbow
ACh	……..Acetylcholine
AChE	……..Acetylcholinesterase
adm	……..Abductor digiti minimi
ah	……..Abductor hallucis
Amp	……..Ampicillin
Amp.	……..Amplitude
AD	……..Autosomal dominant
ADi	……..Alzheimer’s disease
ADST	……..Antibody diluting solution with 0.2% Triton X-100
ALS	……..Amyotrophic lateral sclerosis
ANS	……..Autonomic nervous system
AP-3	……..Adaptor protein-3
apb	……..Abductor pollicis brevis
APS	……..Ammonium persulphate
ARS	……..Aminoacyl-tRNA synthetase protein
Asn	……..Asparagine
Be elb	……..Below the elbow
BMP	……..Bone morphogenetic protein
Bp	……..Base pair
BSA	……..Bovine serum albumin
$CaCl_2$	……..Calcium chloride
Carb	……..Carbenicillin
cDNA	……..Coding deoxyribonucleic acid
ChAT	……..Choline acetyltransferase
CHT	……..High affinity choline transporter
CHT p.H521Qfs*2	……..High affinity choline transporter expressing the c. 1563_1564delCA variant resulting in the H521Qfs*2 amino acid change
CMAP	……..Compound muscle action potential
CMS	……..Congenital myasthenic syndrome
CMT	……..Charcot-Marie-Tooth disease
CNS	……..Central nervous system
CNV	……..Copy number variant
CoA	……..Coenzyme A
CTL1	……..Choline transporter-like 1
Cys	……..Cysteine
°C	……..Degrees Celsius

edb	……..Extensor digitorum brevis
ddH_2O	……..Double distilled H_2O
dHMN	……..Distal hereditary motor neuropathy
dl	……..Decilitre
DMEM	……..Dulbecco’s modified Eagle’s medium
DMSO	……..Dimethylsulphoxide
DNA	……..Deoxyribonucleic acid
dNTP	……..Deoxyribonucleotide trisphosphate
ds	……..Double stranded
DTT	……..Dithiothreitol
E. Coli	……..Escherichia coli
edc	……..Extensor digitorum communis
EDTA	……..Ethylenediaminetetraacetic acid
EMG	……..Electromyography
Erb	……..Erb’s point
EVA	……..Exome based variant analysis suite
Exo	……..Exonuclease
Fasc.	……..Fasciculation
FBS	……..Foetal bovine serum
fdi	……..First dorsal interosseous
FGF	……..Fibroblast growth factor
fh	……..Fibular head
Fib	……..Fibrillation
GAM	……..Goat anti mouse
Gastroc. Caput med	……..Gastocnemius caput mediale
GC	……..Guanine-cytosine
Gln	……..Glycine
Glu	……..Glutamine
GWAS	……..Genome wide association study
HA	……..Hemagglutinin
HC-3	……..Hemicholinium-3
HD	……..Huntington’s disease
HEPES	……..4-(2-hydroxyethyl)piperazine-1-ethanesulphonic acid
H	……..Histidine
Het	……..Heterozygous
His	……..Histidine
HMSN	……..Hereditary motor sensory neuropathy
hr	……..Hour
IGV	……..Integrative Genome Viewer
Incr.	……..Increased
Ins. Act	……..Insertional action
K	……..Lysine

Kb	……..Kilobases
KCl	……..Potassium chloride
KH_2PO_4	……..Monopotassium phosphate
K_M	……..Michaelis constant
KRHB	……..Krebs-Ringer-HEPES buffer
L	……..Litre
LEMS	……..Lambert-Eaton myasthenic syndrome
Lft	……..Left
LB Broth	……..Luria Bernati Broth
LMN	……..Lower motor neurone
Lys	……..Lysine
NaCl	……..Sodium chloride
NaOH	……..Sodium hydroxide
µg	……..Microgram
µl	……..Microlitre
µm	……..Micrometre
µM	……..Micromolar
m	……..Metre
M	……..Molar
MAR	……..Mouse anti rabbit
Mb	……..Megabase
MeOH	……..Methanol
Met	……..Methionine
MG	……..Myasthenia Gravis
$MgCl_2$	……..Magnesium chloride
$MgSO_4$	……..Magnesium sulphate
min	……..Minute
ml	……..Millilitre
mm	……..Millimetre
mM	……..Millimolar
m.m.	……..Mouse monoclonal
MMT	……..Manual muscle testing
MND	……..Motor neurone disorder
mNVC	……..Motor nerve conduction velocity
m.p.	……..Mouse polyclonal
MRC	……..Medical Research Council
MRI	……..Magnetic resonance imaging
mRNA	……..Messenger Ribonucleic acid
mtDNA	……..Mitochondrial deoxyribonucleic acid
N	……..Asparagine
NaCl	……..Sodium chloride
Na deoxycholate	……..Sodium deoxycholate

NCV	……..Nerve conduction velocity
NHS	……..National Health Service
NMJ	……..Neuromuscular junction
Norm.	……..Normal
OATs	……..Organic anion transporters
OCTNs	……..Organic zwitterion/cation transporters
OCTs	……..Organic cation transporters
PAGE	……..Polyacrylamide gel electrophoresis
PBP	……..Progressive bulbar palsy
PBS	……..Phosphate buffered saline
PCR	……..Polymerase chain reaction
PD	……..Parkinson's disease
PDL	……..Poly-D-Lysine
Pen-Strep	……..Penicillin-Streptomycin solution
pf	……..Popliteal fossa
PFA	……..Paraformaldehyde
PLS	……..Primary lateral sclerosis
PMA	……..Progressive muscular atrophy
PNS	……..Peripheral nervous system
Poly.	……..Poly phasic potential
PSW	……..Positive sharp waves
Q	……..Glutamine
RA	……..Retinoic acid
Recruit.	……..Recruitment pattern
RIPA	……..Radioimmunoprecipitation assay
ROS	……..Reactive oxygen species
r.p.	……..Rabbit polyclonal
rpm	……..Revolutions per minute
Rt	……..Right
RT	……..Room temperature
SAP	……..Shrimp alkaline phosphatase
SDM	……..Site directed mutagenesis
SDS	……..Sodium dodecyl sulphate
SDS-PAGE	……..Sodium dodecyl sulphate - polyacrylamide gel electrophoresis
Sec	……..Second
SLC5A7	……..Solute carrier family 5; member 7
SLC5A7^{K499Nfs*13}	……..*SLC5A7* gene cDNA construct containing the c.1497delG deletion in a pRK5 plasmid vector
SLC5A7^{WT}	……..Wild type *SLC5A7* gene cDNA construct in a pRK5 vector
SLMV	……..Synaptic-like microvesicles
SMA	……..Spinal muscular atrophy
SNAP	……..Synaptosome-associated protein

SNAP	……..Sensory nerve action potential
SNP	……..Single nucleotide polymorphism
SNV	……..Single nucleotide variant
SP-SMA	……..Scapuloperoneal spinal muscular atrophy
STE	……..Sodium chloride-Tris-EDTA
TAE	……..Tris-acetate-EDTA
TBE	……..Tris-Borate-EDTA
TBS	……..Tris buffered saline
TBST	……..Tris buffered saline Tween-20
TE	……..Tris-EDTA
TEMED	……..N,N,N^{1},N^{1}-tetramethyl-ethylenediamine
TFG-β	……..Transforming growth factor-β
Tris	……..Tris(hydroxymethyl)aminomethane
Tris-Cl	……..Tris base adjusted with HCl
Triton X-100	……..Polyethylene glycol p-(1,1,3,3-tetramethylbutyl)-phenyl ether
Tween-20	……..Polysorbate 20
U	……..Units
UCSC	……..University of Calinfornia, Santa Cruz
UV	……..Ultraviolet
V	……..Volt
Val	……..Valine
VAMP	……..Vesicle-associated protein
VCPDM	……..Vocal cord and pharyngeal weakness with distal myopathy
V_{MAX}	……..Maximum rate of reaction
w/v	……..Weight per volume

1

CHAPTER ONE

INTRODUCTION

1 INTRODUCTION

1.1 Neurogenetics

One of the fundamental goals in human genetics is to link gene function to disease phenotype, yet the functions of the majority of the genes and their encoded molecules in the human body are still poorly understood. Neurogenetics is a field of research which, with interplay between the fields of molecular biology and clinical neurology, aims to provide better understanding of the genetic basis of the normal (and abnormal) development in regard to the function (and malfunction) of the nervous system. Identification of disease causing gene mutations in monogenic neurological disorders has provided invaluable insights into specific molecular pathways important to normal neuronal function, and which may lead to neurodegenerative disease when defective. In recent years, genome wide association studies (GWAS) have identified polymorphisms associated with increased risk for a number of neurological diseases, including autism, schizophrenia, Alzheimer's disease (ADi), Parkinson's disease (PD), and the frontotemporal lobar degeneration/amyotrophic lateral sclerosis (FTLD/ALS) spectrum(6, 7). These studies have also highlighted variations in genes with low penetrance, which contribute to polygenic, multifactorial neurological conditions. Investigation into copy number variants (CNVs), epigenetic, and epistatic effects have also more recently become recognised as important contributors to the heritability of neurological disease. Elucidation of the biochemical and physiological mechanisms which result in the genotype-phenotype correlation connecting disease gene mutations to the manifestation of their resultant neurological disorders leads to a more precise disease classification, an understanding of the underlying molecular pathways involved, recognition of neurodegenerative common pathways, and ultimately the identification of possible targeted treatments.

1.2 Neurodegenerative disease

The term ‘neurodegenerative disease’ is broad and encompasses a large group of highly clinically and genetically heterogeneous diseases which result in the loss of structure and function of neurones, and can be either sporadic or inherited. The most common neurodegenerative diseases are ADi and PD, however there are a huge diversity of other disorders involving nervous system dysfunction including other forms of dementia, epilepsy, multiple sclerosis, amyotrophic lateral sclerosis, Huntington’s disease (HD), and Prion disease. Both the central and peripheral nervous systems may be involved, and the diseases can be widespread or restricted to certain neurones or body regions, and may also be associated with other non-neurological features.

Neurodegenerative diseases are among the major contributors to disability and disease, and are becoming increasingly prevalent with the aging of the general population(8). Together these diseases are amongst the most costly and devastating of diseases to both the patients and their families. According to the Neurological Alliance, in 2014 there were estimated to be 12.5 million cases of various neurological diseases in England alone, resulting in an annual cost of £4.5 billion to the National Health Service (NHS), representing 4.2% of overall NHS expenditure(9). Of these 12.5 million cases, ~350,000 (~2.8%) individuals require help for most of their daily activities. Between the years of 2003/4 and 2013/13, NHS expenditure on neurological conditions increased by >200% and, in addition to this, it is estimated that £2.4 billion is spent on social care services for people suffering from neurological conditions each year. Parkinson’s disease (PD) alone, the second most common neurodegenerative disorder, has an estimated direct and indirect cost of care and treatment of approximately £2 billion in the UK.

The advent of modern genomic technologies has recently enabled pioneering research into the pathogenic disease mechanisms and putative treatment strategies of a range of neurodegenerative diseases(8). Mutations causative of neurodegenerative conditions have been identified in a number of disease genes, providing a better understanding of the underlying molecular pathways involved as well as identifying possible future treatments. Genetic analysis has also shed invaluable light on a number of the pathways underlying

neurodegenerative disease, and identified common biological processes that appear to be shared between different disease phenotypes. These studies have shown that neurodegenerative disease may relate to a wide range of pathogenic mechanisms, including oxidative modification, mitochondrial dysfunction, impaired protein degradation, and defective axonal transport mechanisms. Factors contributing to neurodegeneration include genetic factors, including the normal aging of the nervous system, and environmental factors (10-12).

1.3 Embryogenesis and development of the nervous system

In order to understand degenerative diseases of the nervous system, it is first important to understand normal neurological development. The information that follows gives an up-to-date outline of the current understanding of neurological development and is collated from well-established medical text books(13-17) and review articles(18-22).

1.3.1 Gastrulation and embryonic germ layer formation

There are a number of essential processes and cell differentiation steps during the very early stages of embryogenesis which lay down the initial foundations for the development of the nervous system. About 4 days following fertilisation, once the embryo reaches 8-16 cells (morula), the cells differentiate into two groups: the trophoblast (outer cell layer) and the embryoblast (inner cell mass), collectively known as a blastocyst. The trophoblast develops to form a large part of the placenta. The embryoblast will give rise to the embryo itself as well is its associated extraembryonic membranes. By the end of the first week of development the embryoblast splits into the hypoblast and epiblast layers to form the embryonic disk. At the start of the third week of development, by a process of cell migration called gastrulation the epiblast layer subdivides to form the three germ cell layers: ectoderm (outer), mesoderm (middle), and endoderm (inner).

Gastrulation commences with the appearance of the primitive streak, which by a process known as invagination, deepens as epiblast cells move through it to

form the ectoderm layer beneath (figure 1). At the caudal end, the addition of cells causes it to elongate, whilst its cranial end proliferates to form the primitive node. The primitive node contains a circular depression called the primitive pit, from which a trough like depression called the primitive groove runs caudally down the midline of the primitive streak. After the primitive streak is well established, most cells leave via the primitive pit and groove into the interior of the embryonic disc where some invade the hypoblast and replace its cells with a layer of definitive endoderm, whilst others move between endoderm and ectoderm where they form the intraembryonic mesoderm. At this stage, the three primary germ layers have formed, each of which will eventually give rise to all of the bodies tissues and organs. It is also during gastrulation that body axes of the developing embryo are established.

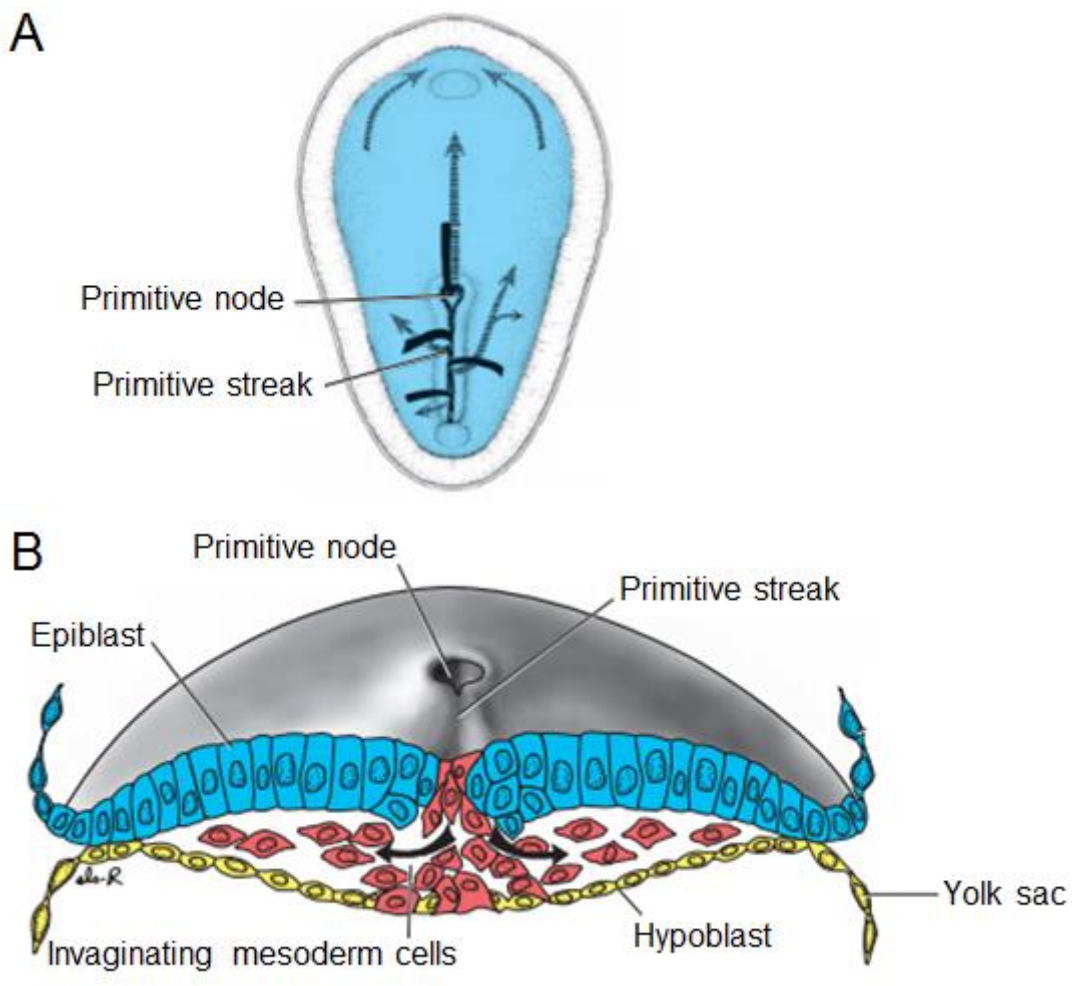

Figure 1. Invagination. A) Dorsal side of the embryonic disk showing the movement of epiblast cells (solid black lines) through the primitive streak and primitive node, and the subsequent movement of cells between hypoblast and epiblast (greyed lines). B) Cross section through the primitive streak showing invagination. Modified (Sadler, 2012(15))

1.3.2 Neural induction

During gastrulation, cells derived from the primitive node migrate cranially resulting in the appearance of the notochord plate which folds to form a solid cylinder called the notochord. This cellular rod which underlies the future neural tube, further defines the axis of the embryo, gives it some rigidity, and indicates the future site of the vertebral bodies. The notochord functions as the primary inductor in the early embryo and induces overlying ectoderm to thicken forming the neural plate. This is the first allocation of a group of ectodermal cells as the earliest rudiment of the nervous system.

Neurulation is the name given to the process whereby the neural plate forms the neural tube, the embryo's precursor to the brain and spinal cord. Towards the end of the third week of development the ectoderm thickens and forms the neural plate. The lateral margins of the neural plate then elevate to form neural folds (figure 2A), which meet and fuse to form the neural tube (figure 2B). Some cells from the lateral edges of the neural plate subsequently separate to form neural crest cells (figure 2A). These migrate to various locations in the embryo where they differentiate into a number of structures and cell types, including spinal ganglion cells, glial cells, and peripheral Schwann cells (figure 2C). Late in the fourth week of development, the neural tube closes and sinks beneath the ectoderm, and neurulation is complete. The central nervous system (CNS) is represented by a closed tubular structure of which the narrow caudal end will give rise to the spinal cord, and the thicker cranial end will form the brain (figure 2D).

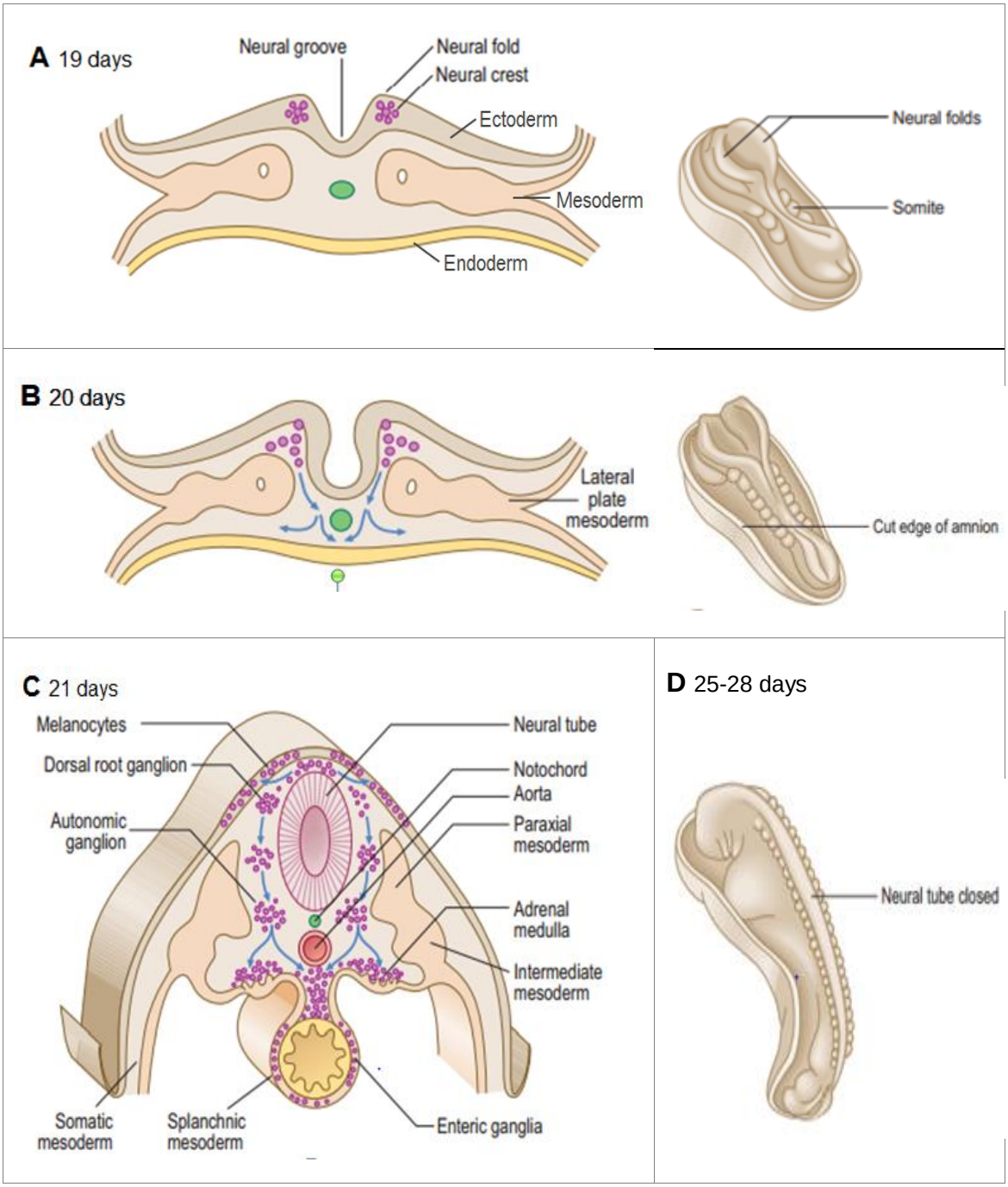

Figure 2. Stages of neurulation. Shown as diagrams of transverse sections of the embryo and the whole embryo A) At 19 days the lateral margins of the neural plate start to elevate and the neural crest cells form. B) At 20 days the neural groove deepens and neural folds further elevate, meet, and fuse to form the neural tube. Neural crest cells detatch and migration in the direction of the blue arrows initiates. C) At 21 days the neural tube has started to close and, after migration, neural crest cells contribute to a heterogeneous array of structures. D) At around 25 days, the cranial opening (neuropore) closes, the caudal neuropore closes 2-3 days later (27 or 28 days), and neurulation is complete. Modified (Mitchell & Sharma, 2009 (13))

1.3.3 Brain and spinal cord development

The cranial end of the neural tube forms three dilations that correspond to the primary brain vesicles: the prosencephalon (forebrain), the mesencephalon (midbrain), and the rhombencephalon (hindbrain). During the fifth week growth of the head exceeds that of other body regions and the three primary vesicles develop into five secondary vesicles. The prosencephalon forms the telencephalon and diencephalon, and the rhombencephalon becomes the metencephalon and the myelencephalon. The telencephalon is formed of a mid-portion between two bilateral portions, which represent the primitive cerebral hemispheres.

The extension of the neural tube caudal to the rhombomeric vesicles gives rise to the spinal cord. The lateral walls of the neural tube thicken and form a pseudostratified, columnar epithelium known as the ventricular layer, consisting of neuroepithelial cells. Neuroblasts migrate peripherally through the wall to form a layer directly around the ventricular layer called the mantle layer, the precursor of grey matter. The outer most layer of the spinal cord is the marginal layer, containing the axons of the neuroblasts entering and leaving the mantle layer, which appears white after myelination (white matter).

During the sixth embryonic week, the walls of the neural tube exhibit ventral and dorsal thickening, forming the alar plates (dorsal) and basal plates (ventral), separated by the sulcus limitans groove. Alar plates will form the dorsal horn and will generally become part of the sensory system, while the basal plates become the ventral horn and will contribute predominantly to motor functions (figure 3A). The dorsal and ventral aspects of the now diamond shaped lumen of the neural tube become the roof and floor plates respectively, and do not contain neuroblasts, but act as connecting pathways for nerve fibres crossing from one side to the other. The cell bodies of the efferent sensory neurones are in the posterior dorsal root ganglia, on the dorsal side of the spinal cord, and will give rise to axons that enter the dorsal root and synapse with neuronal cell bodies in the dorsal horn (figure 3B). Neurones in the ventral horn give rise to axons that enter directly into the ventral root. A group of neurones also accumulates between the dorsal and ventral horns to form a small intermediate

horn present only at thoracic and upper lumbar levels of the spinal cord, containing the sympathetic neurones of the autonomic nervous system (ANS).

From the third month the vertebral column and dura start to lengthen more quickly than the neural tube, the terminal end of which starts gradually shifting to a higher level. This disproportionate growth causes the spinal nerves, which till now have passed through the intervertebral foramina adjacent to their level of origin, to run obliquely from their place of origin within the spinal cord to their corresponding level of the vertebral column. Therefore in adults, the lower extremity of the spinal cord is located at the L2-L3 level of the vertebral column but its nerve fibres descend to lowers levels to leave from their respective intervertebral foramina at the sacral level of the spine.

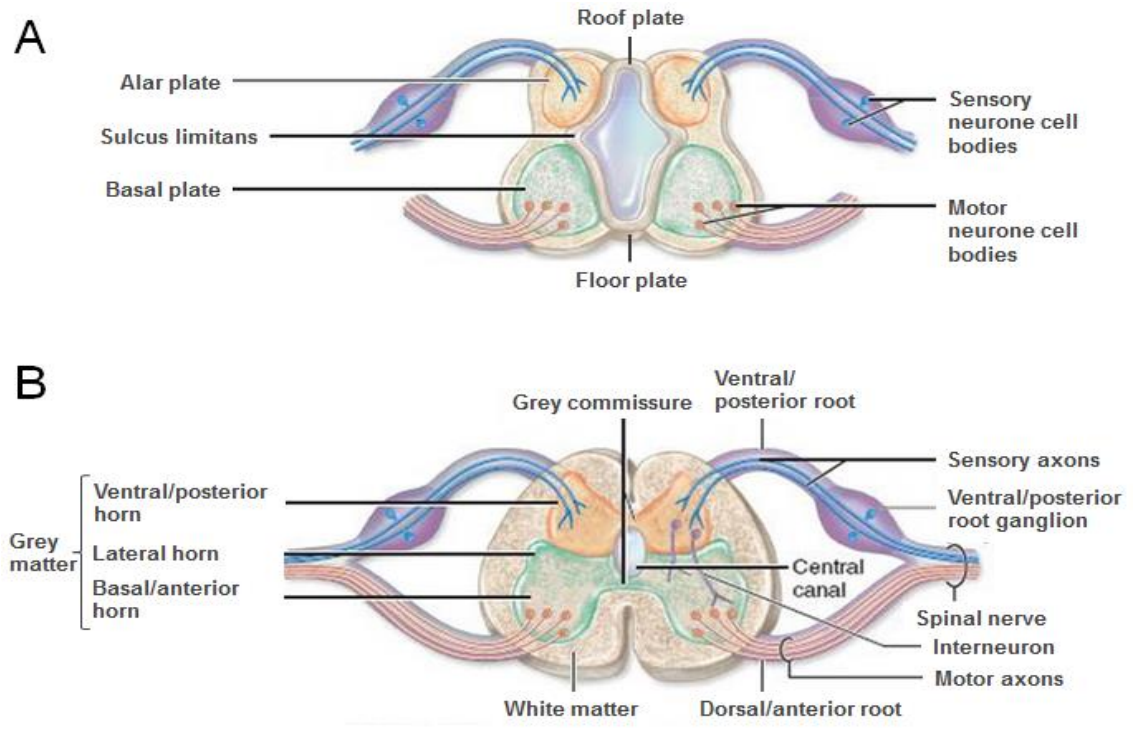

Figure 3. Cross section of the spinal cord during development. A) In the sixth week the alar and basal plates form. B) in the ninth week, grey horns form from the basal and alar plates. Modified (Tarant County College, 2014(23))

1.3.4 Genetic and molecular regulation of spinal cord development

Normal functioning of the nervous system allowing motor coordination and sensory perception is reliant on the formation of extraordinarily spatiotemporally precise and complex cell connections between distinct cell types. Generation of neuronal diversity, and proliferation and migration of the various neuronal cells,

is a multistep process requiring finely balanced control from both intrinsic and extrinsic influences.

At the neural plate stage, the entire plate in the spinal cord region of the embryo expresses homeodomain containing transcription factors: paired box genes 3 and 7 (PAX3 and PAX7) and muscle segment homeobox genes 1 and 2 (MSX1 and MSX2). Sonic hedgehog (SHH) and bone morphogenetic proteins 4 and 7 (BMP4 and BMP7) control the expression pattern of these transcription factors, and provide positional cues. SHH secreted from the notochord is essential for roof plate and floor plate induction, as well as motor neurone specification. Ventral (floor plate) patterning commences prior to dorsal (roof plate) patterning and results in the production of specific motor neurone subtypes in localised domains of the ventral cord. SHH represses transcription of class I homeodomain transcription factors (PAX6, PAX7, brain developing homeobox 2 [DBX2], Iroquois-class homeodomain protein [IRX3]), ventralising the neural tube. Once formed, the floor plate also secretes SHH forming a concentration gradient across the spinal cord which generates 5 subclasses of ventral neurones. Downstream class II homeodomain proteins such as NKX6.1, NKX6.2 and IRX3 have roles in motor neurone specification, positioning of motor neurone initiation, and maintenance of progenitors potential to become motor neurones. BMP4 and BMP7 are secreted by the non-neuronal ectoderm overlying the neural tube establishing a second signalling centre in the roof plate. BMP4 and 7 trigger their own production in a positive feedback loop, and stimulate the production of *wingless*-related mouse mammary tumour virus integration site (WNT) proteins. WNT signalling is vital for the control of proliferation, migration, and axon guidance of neighbouring dorsal interneurones. The presence of BMP4 in the roof plate initiates a cascade of the following transforming growth factor beta (TGF-β) proteins within the roof plate and its surroundings: BMP5, BMP7, activin and dorsalin-1. As in ventral patterning, temporal and spatial organisation of this cascade creates concentration gradient of the mentioned morphogens from the floor plate - ventrally. BMP7 also plays a role in axon guidance. BMP inhibitors noggin, follistatin, and chordin also play an important role in dorsal patterning. On the dorsal side of the neural tube, the expression of BMP4 and BMP7 also regulates and maintains PAX3 and PAX7, major regulators of the early

development of neural crest cells in the top of the neural fold. However, their role and those of MSX1 and MSX2 in differentiation of sensory neurones and interneurones is yet to be elucidated. It has been suggested that MSX1 and 2 may act as transcriptional activators of atonal homologue 1 (*ATOH1)*(24). Their expression throughout the neural plate during earlier stages is essential for the formation of ventral cell types, despite their being excluded from ventral regions in later stages by SHH. With exception to the midline, PAX6 is expressed throughout the elevating neural fold and is maintained following the neural tube closure.

An important aspect of spinal cord development is the grouping of neurones with common functions into longitudinal columns. Signals from the presomitic mesoderm, particularly fibroblast growth factor (FGF) and retinoic acid (RA) appear vital for inducing appropriate columns at appropriate spinal levels. A number of columns and sub-columns form, identifiable by their unique patterns of homeodomain transcription factor expression. This patterning and longitudinal column formation is regulated by a number of factors including the LIM/homeodomain family of transcription factors (ISL1, ISL2, LIM1,LIM 3) and HOX restriction factors, which act in cooperation with RA, FGF, WNT and TGF-β superfamily members.

1.3.5 Histological differentiation

1.3.5.1 Neurone development

All neurones, glia, and ependymal cells of the CNS arise exclusively from neuroepithelial cells of the ventricular layer. Once neuroblasts form from these cells, they lose their ability to divide. Neuroblasts initially have a central process extending to the lumen. As they migrate into the mantle layer they become temporarily round and apolar before further differentiation results in the appearance of two new processes on opposite sides of the cell, forming a bipolar neuroblast. One of these processes undergoes rapid elongation to form the primitive axon, and the other develops a number of cytoplasmic arborisations which represent primitive dendrites. This *multipolar neuroblast* is the direct precursor of the neurone. Neuronal axons in the basal plate migrate through the marginal layer to form the ventral motor root of the spinal nerve, where they conduct motor impulses from the spinal cord to the muscle fibres

(figure 4). Axons of sensory neurones in the alar plate (dorsal horn) also penetrate to the marginal layer of the spinal cord; however from here they ascend to either higher or lower levels to form interneurones.

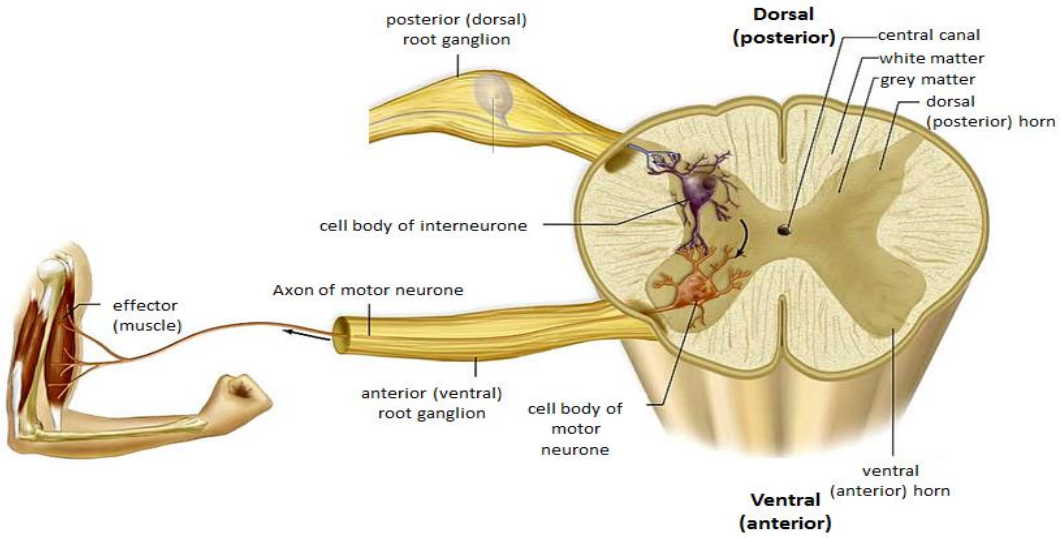

Figure 4. Cross section of the spinal cord showing a typical motor neurone originating in the ventral horn. A single axon extends from the cell body to the effector (muscle) cell. Modified (http://classes.midlandstech.edu/carterp/Courses/bio110/chap08/chap08.htm)

1.3.5.2 Glial cells, neural crest cells, and spinal nerves

After cessation of neuroblast production, the ventricular layer starts to form a new cell type from the neuroepithelial cells, glioblasts. These migrate to the mantle and marginal layers where they differentiate into protoplasmic and fibrillar astrocytes. In the marginal layer glioblasts form oligodendroglial cells. Later in development glioblasts form a third cell type, microglial cells, in the CNS. All glioblast derived cells act as supporting cells, and following cessation of their production by neuroepithelial cells, they differentiate into ependymal cells and line the central canal. Neural crest cells form along each edge of the neural folds during neural plate elevation and extend throughout the length of the neural tube and give rise to the sensory dorsal root ganglia of the spinal nerves. Neuroblasts that do not become neurones or glial cells develop into sensory nerve cells. Neuroblasts of the sensory ganglia form two processes. One is centrally growing and penetrates the dorsal portion of the neural tube to form the dorsal sensory root of the spinal nerve and either end in the dorsal

horn, or ascend through the marginal layer to one of the higher brain centres. The other peripherally growing processes join fibres of the ventral motor root and terminate in the sensory receptor organs. Sympathetic neuroblasts, Schwann cells, pigment cells, odontoblasts, meninges, and mesenchyme of the pharyngeal arches also derive from neural crest cells. Motor neurones arise from cells in the ventral horns collecting into bundles called ventral roots. Dorsal roots form from bundles of sensory nerve fibres originating in the dorsal root ganglia. Bundles of central processes from the dorsal root ganglia grow into the spinal cord opposite the dorsal horns and distal processes join the ventral roots to form a spinal nerve. Spinal nerves then almost instantly start to divide into ventral and dorsal primary rami. The ventral primary rami form the brachial and lumbosacral plexuses.

1.3.5.3 Myelination

The myelin sheath is a multilamellar spiral of modified plasma membrane wrapped around neuronal axons larger than 1µm in diameter that acts as an electrical insulator allowing for fast and efficient impulse conduction. Myelin sheaths surrounding nerve fibres within the spinal cord are formed by oligodendrocytes, and those surrounding the axons of peripheral nerve fibres are formed by Schwann cells. Schwann cells originate from the neural crest, where from they migrate peripherally and each wraps around a single axon of a peripheral nerve to form a neurilemma sheath. Oligodendrocytes are able to myelinate upto 50 axons. Myelination of nerve fibres within the spinal cord begins during the fourth month of foetal life into the first postnatal year. Fibre tracts generally become myelinated at around the same time they become functional.

1.3.6 Brain development

Towards the end of the fourth week of development the cranial end of the neural tube forms three dilations corresponding to the primary brain vesicles: the prosencephalon (forebrain), the mesencephalon (midbrain), and the rhombencephalon (hindbrain). Simultaneously with their appearance, the brain bends to produce two flexures; the midbrain (cephalic) flexure located in the

mesencephalon, and the cervical flexure at the junction between the rhombencephalon and the spinal cord. In the rhombencephalon and mesencephalon there are distinct basal and alar plates on either side of the midline representing motor and sensory areas, respectively. This is known as the brainstem, and as a direct continuation of the spinal cord, it has a similar organisation. Conversely, in the prosencephalon, or higher centres, accentuation of the alar plates and regression of the basal plates is seen. In the fifth week the forebrain further divides into the telencephalon and diencephalon, and the hindbrain divides into the metencephalon and myelencephalon. The midbrain does not divide and thus the brain now comprises five secondary vesicles. The telencephalon will give rise to the cerebral cortex, the corpus striatum, and the olfactory bulb (cerebral hemispheres), and the diencephalon will develop into the thalamus, hypothalamus and the neural portion of the retina. In the hindbrain, the myelencephalon is the predecessor of the medulla oblongata, and the metencephalon that of the pons and cerebellum. A third flexure, the pontine flexure, develops later in the brain's development between the metencephalon and myelencephalon. The central cavity that forms within the brain as it folds becomes the ventricular system.

1.3.6.1 Genetic and molecular regulation of brain development

The brain is patterned along the craniocaudal and dorsoventral axes. Craniocaudal patterning of the CNS commences during gastrulation and neural induction. Following establishment of the neural plate, homeobox genes expressed in the notochord, prechordal plate, and neural plate signal formation of the brain's three primary vesicles. The *Antennapedia* class of homeobox (*HOX)* genes, are a family of transcription factors located in clusters on the genome that are expressed in overlapping patterns. Genes at the 3' end of the cluster have more anterior boundaries and are expressed earlier than those at the 5' end, establishing a temporal expression pattern of these genes along the craniocaudal axis of the hindbrain, activating cascades of genes regulating processes such as axis and segmentation. *HOX* genes thus pattern the craniocaudal axis in the rhombencephalon and specify segment identity. Other homeodomain containing transcription factors such as LIM/homeobox protein 1 (LHX1) and orthodenticle homolog 2 (OTX2) pattern the craniocaudal axis of

the prosencephalon and mesencephalon. Following formation of the neural fold, further homeobox genes are expressed: orthodenticle homolog 1 (OTX1), and empty spiracles homolog 1 and 2 (EMX1 and EMX2). Like *HOX* gene expression in the hindbrain, these genes are expressed in specific and overlappig patterns specifiying the identity of the prosencephalon and mesencephalon. The anterior neural ridge and the encephalic isthmus are two other organising centers which form after establishment of the primary vesicles and secrete fibroblast growth factor 8 (FGF8). In both locations, FGF8 serves as an inducing factor of subsequent gene expression that regulates differentiation. Transcription factor forkhead box protein 1 (FOXG1) is expressed in the anterior neural ridge in response to FGF8 release and which regulates development of the telencephalon. In the isthmus, FGF8 induces the expression of engrailed homeobox 1 and 2 (EN1 and EN2) which regulate differentiation of the cerebelum and the roof of the mesencephalon. FGF8 also induces WNT family member 1 (WNT1) expression, which interacts with EN1 and EN2 to regulate development of a circumferential area anterior to the region of growth factor expression that includes the cerebellum. As in the spinal cord, SHH is secreted by the prechordal plate and nototcord ventralising the prosencephalon and mesencephalon, and inducing expression of homeobox protein NK-2 homologue A (NKX2.1), which regulates development of the hypothalamus. BMP4 and BMP7, expressed in the noneuronal ectoderm, induce and maintain expression of dorsalising genes such as *MSX1*.

As the brain is patterned both along the craniocaudal and dorsoventral axes, the expression patterns of the genes regulating these processes overlap and interact at the borders of these regions. Additionally, some areas of the brain are able to respond to specific signals that others are not, which assists in specifying regional differentiation. The molecular mechanisms controlling the neuronal diversity of the CNS are not well known or understood, and are only now starting to be unravelled. For example, the transcription factor SRY (sex determining region Y)-box 5 (SOX5) was recently shown to control differentiation of corticofugal neurone subtypes by preventing the premature formation of normally later-born corticifugal neurones(25), and the roles of a number of transcription factors and transmembrane receptors have been

described in the regulation of differentiation of the diverse dopaminergic system(26).

1.4 The adult motor system

The following information gives a description of the current understanding of neurological development and is collated from well-established medical and anatomy text books(17, 27-31).

The human motor system controls a complex neuromuscular network, and must do so in response to sensory information including visual and auditory, and can be divided into several interconnecting parts (figure 5). The motor system includes cortical and subcortical areas of grey matter; the corticobulbar, corticospinal, corticopontine, rubrospinal, reticulospinal, vestibulospinal, and tectospinal descending tracts; grey matter of the spinal cord; efferent nerves; and the cerebellum and basal ganglia. However, control of movement is generally regarded as being dependent on the interplay of two major descending neuronal motor systems: the extrapyramidal motor system which controls involuntary movement and is comprised entirely of fibres originating in the brainstem and higher centres; and the pyramidal motor system (corticospinal tract) , which controls voluntary movement of skeletal muscle and can be further subdivided into two pathways; the upper motor neurone (UMN) pathway, and the lower motor neurone (LMN) pathway (figure 6).

1.4.1 The upper motor system

UMNs are neurones of the brain that innervate, either directly or via interneurones, the lower motor neurones of the brainstem and spinal cord. The most significant UMNs are those that originate in the cerebral cortex and project to either the spinal cord via the pyramidal, or corticospinal tract, or to the brainstem via the corticobulbar tract (figure 5). They do not directly innervate muscles, yet are essential for the control of LMNs and the coordination of movement. Lesions or degeneration of UMNs can lead to severe movement defects often referred to as pyramidal tract signs: hyperreflexia, including

muscle spasticity, brisk reflexes, Babinsky sign, and loss of ability to perform fine movements.

1.4.1.1 The corticospinal/pyramidal tract

The corticospinal tract is the most important pathway for voluntary control over fine movements and is involved in regulation of posture. Corticospinal tract fibres primarily arise from pyramidal cells in the motor cortex. They begin their descent as corona radiata before descending to pass through the pyramidal decussation in the lower medulla oblongata. Here approximately 90% of the fibres cross to the opposite side and descend into the spinal cord where they form the lateral corticospinal tract. The other 10% of fibres continue to descend on the same side from which they originated as the anterior corticospinal tract. 80% of these fibres will also cross to the contralateral side and terminate in synaptic contact with LMNs and with interneurones of the anterior horn on both sides of the spinal cord. Ultimately, 98% of corticospinal tract fibres provide contralateral innervation and only 2% remain ipsilateral over their entire course. Disruption of the corticospinal tract at or below its cortical origin leads to impairment of movement on the opposite side of the body. Corticospinal tract fibres signal to alpha motor neurones (see 1.4.2.1) either directly or via interneurones. The presence of direct connections between the higher brain centres and LMNs allows for rapid transmission from the CNS to the periphery. The lateral corticospinal tract serves to regulate voluntary control over fine movements of the extremities such as the hands, and the anterior corticospinal tract is involved in regulation of postural mechanisms. Some corticospinal neurones that innervate the dorsal horn do not signal to muscles to produce movement, but act as modulators of primary sensory afferent information directed toward the cerebral cortex. The pyramidal tract signs mentioned earlier are thus often seen in combination with sensory symptoms.

1.4.1.2 The corticobulbar tract

The corticobulbar tract is also considered a pyramidal tract with its fibres arising from the lateral aspect of the primary motor cortex, and closely following the descending pathway of the corticospinal tract. However, unlike those of the

corticospinal tract, these fibres contribute to the control of the spinal cord indirectly by acting on neurones of the brainstem that project to the spinal cord. Other corticobulbar fibres serve as upper motor neurones to all cranial nerves, with which they make either direct or indirect synaptic contact. Most corticobulbar fibres that supply cranial nerves do so bilaterally. Lesions of the corticobulbar fibres that supply cranial nerves causes weakness of the affected muscles, known as facial palsy. Lesions to those that supply muscles involved in breathing, speech, mastication, swallowing and movement of the tongue cause weakness known as pseudobulbar palsy.

1.4.2 The lower motor system

LMNs are cranial nerves, located in the cranial nerve nuclei of the brainstem, or spinal nerves, located in the anterior horn of the spinal cord. The axons of these cells leave the spinal cord through the ventral root and extend to the muscles of the head and neck, and skeletal muscle respectively, and serve as the final motor neurones that innervate skeletal muscles at the neuromuscular junction. They receive sensory information via interneurones as part of the reflex arc, as well as motor signals from the pyramidal and extrapyramidal systems. LMNs are important for both spinal and cranial nerve reflex pathways, and for voluntary movement. Lesions or degeneration in, or distal of, the anterior horn cell result in weakness of the affected muscles with decreased tone and atrophy, absent or diminished reflexes, and muscle fasciculations.

1.4.2.1 Alpha and gamma motor neurones

There are two types of LMN important for muscle movement and reflexes: alpha (α) and gamma (γ) motor neurones. α-motor neurones are large LMNs with axon diameters of 12-20μm that transmit rapid action potentials (conduction velocity = 70-120m/s) and innervate extrafusal muscle fibres via the neuromuscular junction (NMJ) to initiate contraction. Extrafusal muscle fibres are the main skeletal muscle fibres responsible for muscle contraction. Inhibitory interneurones called Renshaw cells located in the ventral horn receive excitatory input via branches of α-motor neurones and project back to α-alpha motor neurones to form part of local feedback circuits that prevent over activity

of the α-motor neurones. γ-motor neurones have small axons compared with α-motor neurones (3-6μm in diameter) and make up 25-30% of the fibres in the ventral root. Firing of γ-motor neurones does not lead to directly detectable muscle contraction, but has a role in keeping muscle spindles taut by increasing tension on them, increasing sensitivity to overall stretch. γ-motor neurones innervate intrafusal muscle fibres of skeletal muscle. Each muscle spindle contains 2-10 small intrafusal muscle fibres which stretch and shorten in correspondence with contraction and relaxation of the whole muscle, and serve as proprioceptors to modulate the muscle contraction. This is important for allowing α-motor neurones to continue discharging without losing the contraction, and for maintaining posture.

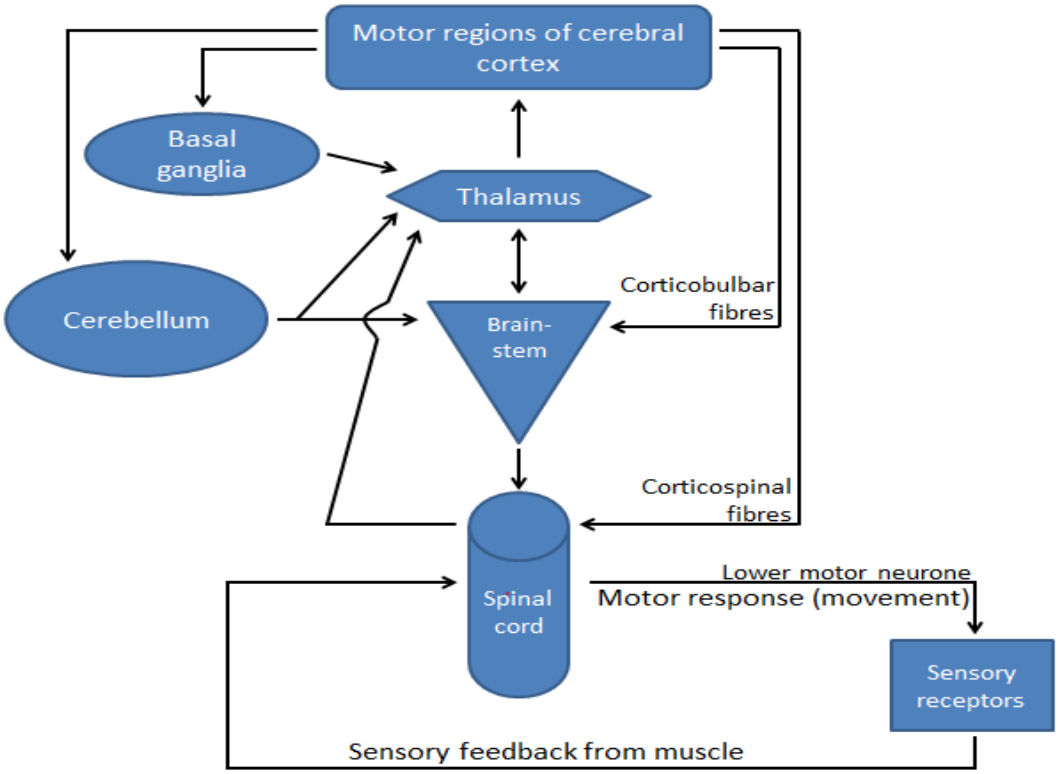

Figure 5. Diagram of the organisation of the motor system. Lower motor neurones make up the final common pathway to the muscles, and are under the control of upper motor neurones, as well as supraspinal control for spinal cord reflex mechanisms. The brainstem and the cerebral cortex are the only brain regions with direct control of the spinal cord. The basal ganglia receive innervation from the cerebral cortex, and control movement by feeding back signals to motor regions of the frontal cortex that are involved in movement initiation. The cerebellum receives signals from most parts of the CNS involved in motor functions, creating feedback loops with each and synchronising the output signals, serving as the main intergrater of motor function.

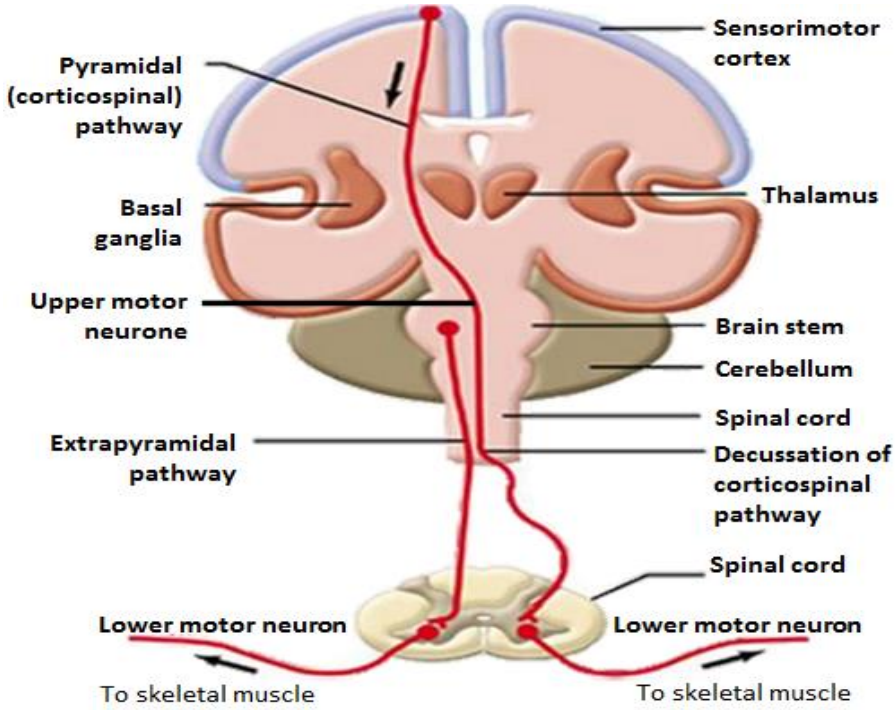

Figure 6. Schematic diagram showing upper and lower motor neurones of the pyramidal pathway originating in the cerebral cortex, and fibres of the extrapyramidal pathway orginating in the brainstem. Both pathways transmit to lower motor neurones, which in turn elicite muscle movement. Modified (http://highscope.ch.ntu.edu.tw/wordpress/?p=11860)

1.4.2.2 The neuromuscular junction

The neuromuscular junction (NMJ) is a specialised synapse that provides for reliable transmission between the presynaptic nerve terminal of the α-motor neurone and postsynaptic muscle cells (figure 53, appendix). Transmission of an electrical impulse across the NMJ is achieved by the release of the neurotransmitter acetylcholine (ACh). Its precursors, choline which is synthesised in the neuronal soma and then transported to the axon terminals via the high affinity choline transporter, and acetyl coenzyme A (CoA) which is synthesised in mitochondria, are acetylated by choline acetyltransferase (ChAT) to produce ACh. ACh transported into presynaptic vesicles by the vesicular acetylcholine transporter (VAChT), and stored until depolarisation of the cell's membrane stimulates its release into the synaptic cleft. This release is modulated by receptors at the presynaptic nerve ending, synaptosome-associated proteins (SNAPs), and vesicle-associated membrane proteins (VAMPs). ACh can bind to both inotropic receptors and metabotropic receptors

on the postsynaptic muscle cell membrane to stimulate a depolarisation response in the muscle cell. In order to prevent multiple synaptic depolarisations, ACh is cleaved back into its two component molecules by the enzyme acetylcholine esterase (AChE), which are then taken up into the presynaptic nerve terminal for reprocessing. Choline is transported into the presynaptic nerve terminal by the hemicholinium-3 (HC-3) sensitive, Na^+/Cl^- dependent, high affinity choline transporter (CHT).

There are two forms of NMJ; "*en plaque*", or twitch fibers, where the NMJ consists of a typical motor end plate and the terminal axon contains many synaptic vesicles, and "*en grappe*", where the NMJ consists of multiple contacts of nerves much thinner than the *en plaque*. *En grappe* synapses innervate tonic fibers that are present on only a small number of mammalian muscle fibers (extraocular, stapedius, tensor tympani, laryngeal and tongue muscle fibers), and have been shown to release ACh by almost an order of magnitude longer than twitch terminals. Evidence suggests a role for CHT primarily in sustained, high frequency ACh signalling(32), and that reserve stores of ACh are available to sustain low frequency ACh signalling(33). Choline can also be acquired through other mechanisms for low frequency signalling, such as the transporters that maintain choline phospholipid synthesis in all cells.

1.5 Mechanisms of neurodegeneration

Neurodegeneration is the progressive loss of structure and function of specific populations of neurones. In the last 20 years many of the genetic defects underlying familial neurodegenerative diseases have been identified, which have defined common molecular pathogenic mechanisms. Biological processes frequently associated with neurodegenerative disease are summarised in figure 7 and include aberrant protein structures, mitochondrial dysfunction, oxidative DNA damage and repair mechanisms, altered axonal transport and function, lipid homeostasis, and neuroinflammation(10, 11, 34-37). The definition of the genetic causes of neurodegenerative disease or disease susceptibility has furthered our understanding of the mechanisms underlying neurodegenerative disease. It is likely that better understanding of the dysfunctional cellular processes shared between common neurodegenerative disorders will lead to

the development of disease modifying pharmacotherapeutic interventions that may be beneficial to a variety of clinical phenotypes(10, 11, 34, 38-45).

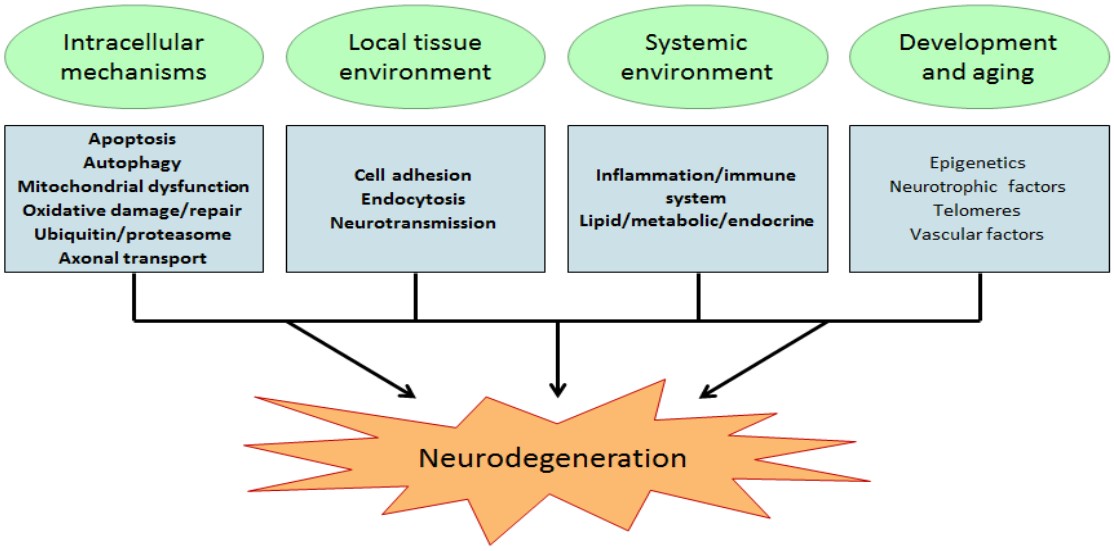

Figure 7. Conceptual model of candidate pathways leading to neurodegeneration grouped according to their major site or mode of action (intracellular mechanisms, local tissue environment influences, systemic influences, and mechanisms related to neurodevelopment and aging). Those in bold are discussed in their involvement in neurodegenerative disease in this section. Modified (Ramanan, 2013(11))

1.5.1 Selective neuronal vulnerability

Neurodegenerative diseases often selectively target subpopulations of neurones and involve characteristic ranges of pathological and molecular features(38). It is important in understanding genotype-phenotype correlation to elucidate why only certain cell types may become dysfunctional, degenerate, and die, as not only will the vulnerable cell type direct the clinical presentation, but may also highlight potential targets for treatment(46). In ADi, cholinergic neurones are the most vulnerable to degeneration, yet in PD it is the dopaminergic neurones that fall victim, while in ALS upper and lower motor neurones degenerate. Although various hypotheses have been proposed, precisely why certain groups of neurones are more susceptible than others in various neurodegenerative disorders is not well understood. Various hypotheses have been suggested to explain the susceptibility of neurones of the substantia nigra to oxidative stress by reactive oxygen species (ROS)-induced injury in PD, including their high levels of copper and iron compared to other cells types which can catalyse ROS formation(10), or their low stores of

antioxidant molecules, but these do not explain the selective neuronal vulnerability of other affected brain regions. In demyelinating forms of the peripheral nerve disorder Charcot-Marie-Tooth disease (CMT-I) where cellular vulnerability results from peripheral myelin protein-22 (PMP22) and myelin protein zero (MPZ) mutations, both associated with the neuronal insulator myelin, the factors determining cellular vulnerability are more obvious and better understood.

1.5.2 Intracellular mechanisms

A range of intracellular mechanisms involved in the normal functioning of neuronal cells as well as other cell types have been identified as having a role in neurodegeneration. The pathways implicated are highly interrelated, and in many cases have overlapping or interacting components, and are reviewed in this section.

Apoptosis: Apoptosis and autophagy are basic physiological processes encompassing pathways that contribute to the maintenance of cellular homeostasis. Apoptosis is generally defined as 'programmed cell death', and is the predominant form of cell death in chronic neurodegenerative disease. Normal cellular apoptotic processes remove old and damaged cells to maintain tissue homeostasis without harming adjacent cells(47). Dysregulation of apoptosis is associated with many diseases, and is not limited to those that are neurodegenerative. However, a characteristic of many hereditary or acquired neurodegenerative diseases including stroke, brain trauma, spinal cord injury, amyotrophic lateral sclerosis (ALS), HD, ADi, and PD, is aberrant neuronal cell death(48). Examples of neurodegenerative disease resulting from dysregulation of apoptosis include CMT types -4A, -IIK, and recessive intermediate type A (tables 31 and 32, appendix), caused by mutations in ganglioside-induced differentiation-associated protein 1 (*GDAP1*), a regulator of mitochondrial dynamics and inducer of apoptosis by promotion of mitochondrial fission(40, 49, 50); and CMT-4X (table 31, appendix), resulting from mutations *AIFM1*, an apoptosis inducing factor which acts via caspase activation(41).

Autophagy: Autophagy is the controlled digestion of long-lived, unnecessary, or dysfunctional cytosolic proteins and organelles. Failure to degrade and

remove misfolded or potentially toxic proteins can lead to organelle damage, and the formation of aberrant protein aggregates and inclusion bodies. There are two pathways known to be responsible for the elimination of damaged cellular components: the ubiquitin-proteasome system, and the autophagy-lysosome pathway (ALP), both integral to cell function and survival, especially in the case of neurones and other long-lived, non-regenerative cell types(51). Mitochondria and their physical dynamics play a vital role during numerous stages of autophagy (51). Failure to recruit autophagy-associated anchoring proteins to the mitochondrial membrane by mutant mitofusin (*MFN2*), a mediator of mitochondrial anchoring to the endoplasmic reticulum, results in CMT-IIA2 (table 32, appendix) (51, 52), and failure of protein sorting and redistribution of lysosomes essential for the ALP by mutant DYNC1H1, a crucial subunit of the cytoplasmic dynein complex, results in lower limb predominating spinal muscular atrophy 1 (SMALED1) and CMT-IIO (table 35 and 32, appendix) (43, 53).

Mitochondrial dysfunction: Neuronal cells have an exceptionally high energy demand, the primary supply of which comes from mitochondrial oxidative phosphorylation(54). Disruption of any one of a number of mitochondrial processes, including ATP production, generation or removal of ROS, and calcium buffering can lead to mitochondrial dysfunction. Such mutations contribute to a number of neurodegenerative diseases, including α-synuclein and parkin mutations in PD, superoxide dismutase [Cu-Zn] mutations in ALS, huntingtin in HD, and GDAP1 in CMT-4A (table 31, appendix).

Oxidative stress: The normal aerobic metabolism of oxygen by cells produces cytotoxic ROS, or free radicals, as a by-product. Therefore in all cells, but in particular in highly metabolically active cells such as neurones, there is constant ROS production and subsequent need for their elimination. Oxidative stress occurs when there is an imbalance between ROS generation, its metabolism, and damage repair(55). Repairing the DNA damage caused by ROS requires substantial metabolic energy, presenting a yet greater demand on the mitochondria of already highly metabolically demanding cells such as neurones. Mutations in genes encoding proteins involved in both ROS production (components of the NADPH oxidase enzyme complex) and elimination DJ-1

and (SOD1) can lead to increased oxidative stress and subsequent neuronal cell death(10).

Aberrant protein structures: The ubiquitin-proteasome system (UPS) is responsible for the targeted degradation of misfolded, aggregated, or otherwise abnormal proteins. Where the ALP degrades long-lived proteins, the UPS degrades aberrant short-lived proteins in the cytoplasm and nucleus(51). The UPS is activated by the ubiquitin labelling of a protein for degradation, causing it to be directed to proteasomes in cellular compartments containing protease enzymes and/or the ability to recognise ubiquitin-labelled proteins. While diverse neurodegenerative disorders involve unique proteins and selectively disparate brain regions, they often share two common features: formation of insoluble deposits of protein aggregates and neurone degeneration(56). Many of the defective proteins that result in mitochondrial dysfunction in neurodegenerative disease also cause the formation of protein aggregates.

Axonal transport: As protein synthesis is restricted to the cell body of neurones, and because the axons can extend for great distances from the cell body, neuronal cells are presented with unique challenges in transporting proteins between the cell body and their synaptic domains. While anterograde transport is important in supplying proteins, lipids and mitochondria to the distal synapse, retrograde transport is responsible for both the clearance of misfolded and aggregated proteins from the axon, and for the transport of distal trophic signals to the soma(57). A number proteins involved in axonal transport have been identified as being defective in neurodegenerative disease, with roles ranging from regulation of neurofilament and microtubule formation and stability (mutant NEFL in CMT-IIE: table 32, appendix), to retrograde and anterograde vesicle transport (mutant $p150^{Glued}$ subunit of the dynactin complex and DYNC1H1 in dHMN-VIIB, and SMALED1 and CMT-IIO respectively: tables 32 and 35, appendix)(43, 53, 58-60).

1.5.3 Local tissue environment

Cell adhesion is the binding of a cell to another cell or to an extracellular surface, and is important for the maintenance of synaptic contacts, blood-brain barrier integrity, and for efficient neurotransmission and intracellular

signalling(11). Altered expression of cell adhesion genes is a consistent finding in ADi (*APOE* ε4), PD (*L1CAM*) and CMT (*MPZ*).

Mutations in genes that interfere with endosomal signalling are among the many pathways implicated in neurodegenerative disease such as *DYNC1H1* in SMALED1 (table 35, appendix) which plays a role in the redistribution of organelles such as endosomes and lysosomes, and *FIG4* mutations in CMT-4J (table 31, appendix) involved in the biogenesis of endosome carrier vesicles.

Neurotransmitters are endogenous substances that transmit signals across a chemical synapse. Pathways involved in neurotransmission, such as calcium signalling, and neurotransmitter synthesis, recycling, transport and degradation, have been implicated in many neurodegenerative diseases, and can affect all types of neurotransmitter signalling (dopaminergic, serotoninergic, noradrenergic, GABAergic and cholinergic)(11, 45)

1.5.4 Systemic environment

Neuronal membranes contain a substantial amount of cholesterol and other lipids, and the myelin sheath of peripheral nerves is formed of proteins and phospholipids. Thus, disruption in lipid pathways has often been proposed to affect synaptic signalling, neuronal plasticity, and neurodegeneration(11). *PARK2* and *LRRK2* are PD associated genes known to regulate cellular uptake of lipid rich structures(11). Immune reactions inside the central nervous system are carefully regulated, and undergo several check-points in order to optimise protection of the fragile tissue(61). Disturbances in inflammation and immune pathways have been reported in ADi, PD, and multiple sclerosis(11, 61).

1.6 Motor neurone degenerative disorders

The term motor neurone disease (MND), although often used interchangeably with the most common form of MND, which is ALS, in fact encompasses a range of neurodegenerative disorders which selectively affect motor neurones of the spinal cord, brainstem, and motor cortex. The process of neurodegeneration in these conditions is often remarkably selective, leaving special senses and cerebellar, sensory and autonomic functions intact. There is

variation in patterns of involvement between different motor neurone disorders, however common early signs motor neurone dysfunction or degeneration allow for diagnosis and include: muscle weakness, and eventually wasting that may be restricted to a single muscle group; often the lower or upper limbs, a single limb, or muscles involved in swallowing, speech and breathing. Clinically, subtypes of motor neurone disease are distinguished according to the major site of motor neurone degeneration and of the affected muscles. The common major subtypes of motor neurone disease include ALS, spinal muscular atrophy, progressive bulbar palsy, progressive muscular atrophy, CMT, and primary lateral sclerosis (62). MNDs are also classified according to whether they are inherited or sporadic, and whether degeneration occurs in the upper or lower motor neurones, or both (tables 1 and 2)(63). Diagnosis is made from a detailed patient and family history, blood tests, physical examination and neurological examination, including electromyography (EMG) and magnetic resonance imaging (MRI).

Table 1. Simplified overview of broad clinical features arising from UMN or LMN lesions

Clinical test	UMN	LMN
Reflexes	Hyperreflexia	Hyporeflexia
Muscle tone	Increased (spastic)	Decreased (flaccid)
Fasciculation	None	Present
Wasting	None	Present
Babinski sign	Present	Absent

Abbreviations: **LMN**=Lower motor neurone; **UMN**=Upper motor neurone

Table 2. Common motor neurone degenerative disorders and their features, in which either UMNs, LMNs, or both are affected

Affected neurones	Associated condition	Features
LMNs	SMA	Usually infant to juvenile onset. Distal muscle weakness and wasting- often more sever in the trunk and upper leg and arm muscles than in muscles of hands and feet. Areflexia. Respiratory difficulties.
	CMT	Usually childhood or early adulthood onset. Distal muscle weakness and wasting- usually presenting and predominating in the muscles of the feet and hands.
UMNs	PLS	Progressive weakness of voluntary muscle movements of the arms, legs and face causing spasticity and stiffness, and speech slowing or slurring
LMNs & UMNs	PBP	Weakness of pharyngeal, jaw, facial, and tongue muscles causing loss of speech and difficulty swallowing. Limb weakness with upper and lower motor neurone signs. Emotional outbursts.
	ALS	Onset usually between 40 and 60 years. Bilateral weakness and wasting of the bulbar muscles and muscles of the arms and legs. Spasticity and rigidity of affected muscles, and loss of ability to sit upright.

Abbreviations: **LMN**=Lower motor neurone; **UMN**=Upper motor neurone; **SMA**=Spinal muscular atrophy; **CMT**=Charcot-Marie-Tooth disease; **PLS**=Primary lateral sclerosis; **PBP**=Progressive bulbar palsy; **ALS**=Amyotrophic lateral sclerosis

1.7 Overview of hereditary peripheral nerve disorders

Hereditary peripheral neuropathies have been the focus of investigation by both the research and medical communities since the 1800's when Charcot, Marie, and Tooth first descried families with what we now know as a dominantly inherited form of CMT. CMT, also known as hereditary motor and sensory neuropathy (HMSN) or peroneal muscular atrophy (PMA), is a clinically and genetically heterogeneous group of disorders characterised by distal muscle weakness and atrophy, and sensory loss(64). With an estimated prevalence of 17 to 40 per 10,000(65), CMT is one of the most common neurogenetic disorders, and the most commonly inherited disorder of the peripheral nervous system and thus clinically, an important problem.

Interplay between fields of genetics, molecular biology and clinical neurology in recent years has allowed for pioneering research into the genetic and molecular basis of neurodegenerative disease, allowing for more complex and accurate disease classification. Common pathways underlie a number of hereditary disorders of the peripheral nervous system; often single phenotypes have been found to have multiple genetic aetiologies, and conversely, there are many

reports of mutations of a single gene producing different and sometimes very distinct phenotypes(46). These disorders are highly heterogeneous, and for CMT alone, over 1,000 distinct mutations have been reported in over 70 disease-associated genes(66), encompassing a diverse range of pathogenic mechanisms.

In order to make an accurate diagnosis of a particular neuropathy, it is important to first establish that the disorder under investigation is in fact inherited, and not sporadic or acquired. In addition to observation of any of the mentioned clinical features, neuromuscular analysis such as nerve conduction studies, laboratory testing, and histopathologic evaluation may be used to assist in the identification of the inherited component beyond family history(67).

The inherited peripheral neuropathies can be broadly divided into two groups: those that are associated with a syndrome (syndromic) and those that are not (non-syndromic)(68). Syndromic neuropathies are those which occur as part of a group of symptoms that consistently occur together, and characterise a disease or medical condition. Neuropathy may or may not be the presenting and dominating feature of the syndrome. Giant axonal neuropathy-1 (GAN-1) is an example of an axonal syndromic inherited peripheral neuropathy. GAN-1 and is characterised by mental retardation, spasticity, early onset peripheral neuropathy with giant axons and slowed motor and sensory nerve conduction velocities (NCVs), and distinct ‘frizzly’ hair, and is caused my mutations in *GAN1* and *BAG3*(68, 69). Further classification can be made according to the mode of inheritance, penetrance, age of onset, the presence of absence of sensory involvement, whether the neuropathy is demyelinating, axonal, or mitochondria related, and the presence of clinical features.

1.7.1 Charcot-Marie-Tooth disease and distal hereditary motor neuropathy

As mentioned earlier, CMT accounts for the majority of cases of inherited peripheral neuropathy, and is both clinically and genetically heterogeneous. Age of onset is typically during the first or second decade and disease progression slow; however both vary between disease subtypes. The cardinal features of CMT arise from progressive length-dependent axonal loss resulting in impaired

motor and sensory nerve function and subsequent distal muscle weakness and atrophy. In addition to peripheral muscle weakness and wasting, key features of the disease include diminished or absent deep tendon reflexes and bony deformities of the feet such as *pes cavus*. However, these characteristics present with variable expression both between subtypes and between individual subjects affected with the same subtype. Individuals affected by CMT usually present with symptoms related to weakness, most commonly originating in the feet and progressing to the upper limbs. Weakness often presents as an abnormal gait as well as frequent tripping and falling, and difficulty running. Atrophy of the hand muscles may develop a claw-like positioning of the hand. There are several forms of CMT which are often difficult to diagnose due to the high clinical and genetic heterogeneity of the disease. This has led to a complex classification system(70) that is in a state of constant change as the original clinical classification benefits from newer genetic information.

CMT can be transmitted via all types of Mendelian inheritance and in 2005, was broadly subdivided into three distinct forms; a demyelinating form (CMT-I or HMSN-I), an axonal form (CMT-II or HMSN-II), and the distal hereditary motor neuropathies (dHMNs) or spinal CMT(71). For distinction between the demyelinating and axonal forms of CMT, motor nerve conduction velocities (mNCVs) of <38m/s are considered indicative of CMT-I, and those above 38m/s, of CMT-II. Autosomal dominant and recessive intermediate forms of CMT (DI-CMT and RI-CMT) also exist in which median mNCVs range from 25-45m/s. CMT and other related hereditary neuropathies have also been classified according to which features predominate. Hereditary neuropathies are classified as hereditary motor and sensory neuropathy (HMSN) where muscle weakness predominates with mild sensory deficits, distal hereditary motor neuropathy (dHMN) if the deficit is purely or predominantly motor, and hereditary sensory neuropathy (HSN) is sensory deficits dominate.

To date, genetic variants associated with CMT have been reported in more than 70 different genes, encompassing a broad range of protein functions, including: structural proteins (PMP22 and lamin A/C)(68, 72), adhesion molecules (MPZ/P_0)(73), mitochondrial transport proteins (KIF1B and DYNC1H1)(53, 74), vesicular transport proteins (DNM2)(75), intracellular membrane trafficking regulation proteins (RAB7)(76), neurofilament proteins (NEFL)(58), transcription

factors (EGR2)(77), and proteins involved in protein degradation (LITAF)(78) (tables 31-35, appendix). Members of groups of functionally related proteins have been implicated in various forms of CMT. For example, members of the heat-shock family of related housekeeping proteins that are up-regulated in response to various cellular stressors, have been reported as being defective in CMT. *HSPB8* mutations have been reported in axonal CMT-IIL(79) and purely motor dHMN-IIA(80), *HSPB1* variants have been observed in CMT-IIF and dHMN-IIB(81), *HSPB3* mutations have been found to cause dHMN-IIC(82), and mutations in *DNAJB2,* encoding heat-shock protein 40 (HSP40) have been implicated in both CMT-IIT and distal spinal muscular atrophy type 5 (dSMA5)(83, 84) (tables 32 and 35, appendix). Six aminoacyl-transfer RNA (tRNA) synthetase (ARS) proteins (GARS, YARS, AARS, KARS, HARS and MARS) have been associated with CMT-IID, DI-CMTC, CMT-IIN, and RI-CMTB, dHMN-II respectively (tables 32, 33 and 35, appendix)(85-89). ARSs are ubiquitously expressed, essential enzymes responsible for attaching amino acids to cognate tRNA molecules, the first step of protein translation(90).

1.7.1.1 Demyelinating Charcot-Marie-Tooth disease (Type I)

Charcot-Marie-Tooth disease Type I (CMT-I) is a demyelinating form of hereditary motor and sensory neuropathy and is the most frequent subtype of CMT. CMT-I is caused by mutations in genes encoding proteins involved in the myelination of neurones such as PMP22 (peripheral myelin protein 22) and myelin protein zero (MPZ or P_0) (figure 8). As described in section 1.3.5.3, myelin is a sheath formed of proteins and phospholipids by Schwann cells that is wrapped at regular intervals around certain neuronal axons and, when normal, aids neurons to transmit impulses more rapidly than non-myelinated nerve fibres. Due to the demyelination of axons in CMT-I, it is distinguishable from other forms of CMT by markedly reduced nerve conduction velocities (NCVs) of less than 38m/s. Neurological features also include enlargement of the peripheral nerves, and a segmental pattern of extensive de- and re-myelination with onion bulb formation, which may lead to diminished feeling in the feet and essential tremor of the hands(91, 92). The muscle weakness seen in this form of CMT typically results in gait abnormalities and clumsiness with increased instability in the ankle(92). CMT-I is divided into further subtypes

classified according to genetic characteristics, unusual clinical features, and age of onset and severity of the disease (table 31, appendix). However, all cases display a combination of the classic CMT features with a great degree of overlap of features with other CMT subtypes, with or without additional unusual clinical features. Penetrance and severity varies between subtypes, and even within the same subtype. Recessively inherited demyelinating forms of CMT have been reclassified as CMT-4(68)(table 31, appendix)

PMP22 and *MPZ* mutations are the most common causes of CMT-I and have each been implicated in a number of subtypes (table 31, appendix), as well as Déjérine-Sottas neuropathy, congenital hypomyelinating neuropathy, and in the case of *MPZ*, intermediate and axonal forms of CMT(68).Where duplication of *PMP22* results in a CMT-IA phenotype (the most common form of CMT), *PMP22* deletions lead to hereditary neuropathy with liability to pressure palsies (HNPP), and different point mutations in this gene may cause either phenotype(93).

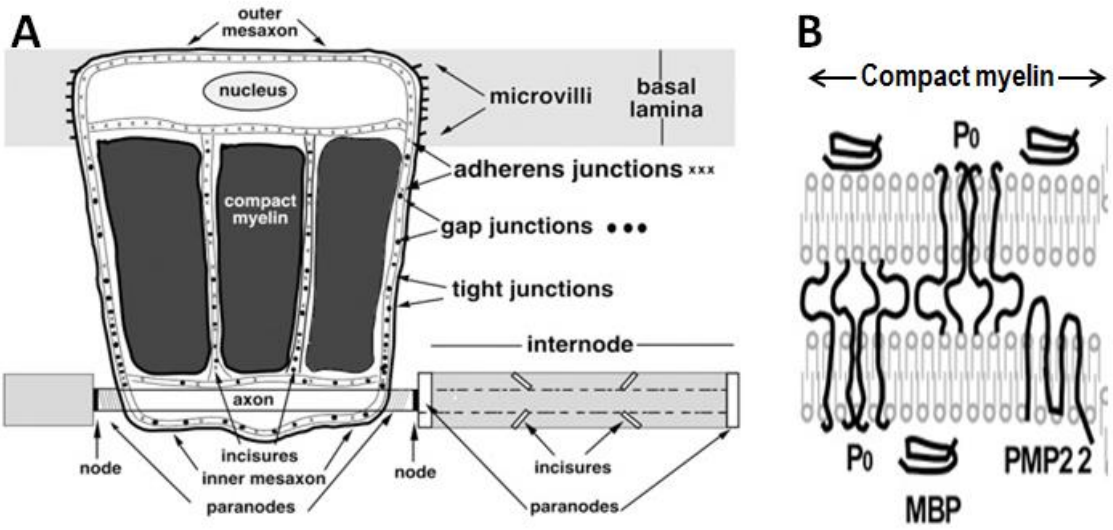

Figure 8. The architecture of the myelinated axon in the peripheral nervous system and the myelin proteins defected in CMT-I. A) Shows Schwann cells positioned along the axon, one of which has been "unrolled" to expose the regions forming compact myelin and non-compact myelin (paranodes and incisures). B) Shows that CMT-I associated proteins P_0 (MPZ), PMP22, are situtated within the compact myelin. Modified (Scherer, 2015 (68))

1.7.1.2 Axonal Charcot-Marie-Tooth disease (Type II)

Where CMT-I is due to myelination abnormalities, CMT-II is caused by defects in proteins with a role within the axon or cell body of the nerves. These include proteins involved in vesicular, mitochondrial and ion transport, in organelle structure, and in a cells response to oxidative stress. The classic CMT features described earlier are seen in CMT-II patients. In addition, restless leg syndrome is seen in almost 40% of CMT-II cases(94). However, the majority of CMT cases are distinguished as being either the demyelinating form or axonal form by use of a motor median NCV cut off value of 38m/s, whereby CMT-II is associated with NCVs above this value. Diagnosis of CMT-II may be hindered by axonal loss making it impossible to measure motor NCVs in some patients. Histological examination of CMT-II patients has shown axonal neuropathy with loss of large myelinated axons and indication of axonal regeneration with many small, thinly myelinated axons(95). In some cases, this secondary demyelination causes NCVs to be reduced leading to further diagnostic complication. Similarly to CMT-I, CMT-II can be subdivided into further subtypes according to genetic characteristics and the presence of unusual clinical features, such as involvement of both upper and lower limb muscles, presentation and predominance of muscle weakness and atrophy in the hands, pyramidal tract signs, pupillary abnormalities and varying degrees of hearing loss, and the presence of ulcers and infections which lead to the amputation of toes (table 32, appendix). As in CMT-I, age of onset and severity of the disease varies both between subtypes and within the same subtype.

1.7.1.3 Intermediate Charcot-Marie-Tooth disease

Increasing numbers of CMT patients manifest features of both CMT types I and II, further complicating classification and diagnosis. The term intermediate CMT was proposed to described CMT patients in which median motor NCVs are between 25 and 45m/s(96). Intermediate motor NCVs are often found in males with X-linked CMT, however, both autosomal dominant (DI-CMT) and autosomal recessive (RI-CMT) forms of intermediate CMT have been described (table 33, appendix and figure 9). Interestingly, different mutations in some of the genes implicated in either demyelinating or axonal CMT result in CMT with

intermediate NCVs. It has been suggested that MPZ is the second most frequent gene resulting in intermediate CMT(65).

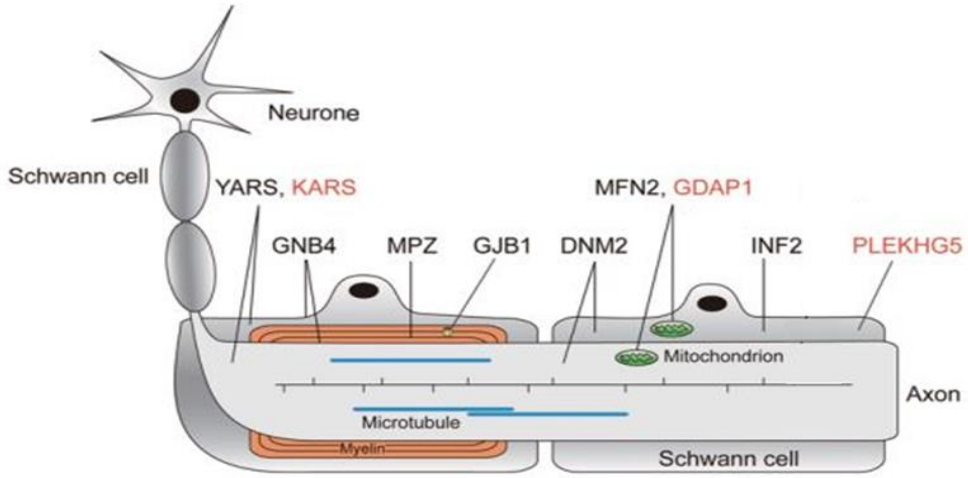

Figure 9. Diagram of a myelinated nerve fibre showing the locations of the proteins mutated in autosomal dominant (black) and autosomal recessive (red) forms of intermediate CMT. Modified (Liu, 2014 (65))

1.7.1.4 X-linked Charcot-Marie-Tooth disease

A number of CMT families have been described in which men are affected more severely than women(41, 97-102). Features of both demyelinating(103), axonal(104), and purely motor(102) have been observed in forms of X-linked CMT (CMTX), as have both X-linked dominant(97, 101) and X-linked recessive(102, 104-106) modes of inheritance (table 34, appendix). It has been estimated that X-linked CMT account for 7-10% of all CMT cases(41). X-linked forms of CMT which fit into one of the CMT-I, -II, or dHMN subtypes may be mentioned more than once in this chapter.

GJB1, or connexin32 (Cx32), is one of the connexin family of membrane-spanning proteins that assemble to form gap junction channels which facilitate the transport of ions and small molecules between cells(103). It has been shown to be expressed in myelinated peripheral nerves in the paranodal myelin loops, and Schmidt-Lanterman incisures of myelinating Schwann cells(103, 107). *GJB1* mutations, responsible for CMT-1X result in variable CMT phenotypes, including a stroke-like presentation(108) and CNS involvement(109).

CMT-X4 and CMT-X5 represent X-linked forms of CMT which present as part of a syndrome: Cowchock syndrome and Rosenberg-Chutorian syndrome,

respectively. Cowchock syndrome is characterised by a triad of slowly progressive axonal neuropathy, bilateral sensorineural hearing loss, and varying degrees of cognitive impairment, with childhood onset. Cowchock syndrome results from mutations in *AIMF1*, encoding a mitochondrial flavoprotein involved in caspase-independent cell death(41). Rosenberg-Chutorian syndrome is also characterised by a triad of symptoms: pre-lingual sensorineural hearing loss, followed by peripheral neuropathy and visual loss due to optic neuropathy at ~10 years. Rosenberg-Chutorian syndrome is caused by mutations in a metabolic enzyme, Ribose-phosphate pyrophosphokinase 1 (PRPS1), which catalyses the synthesis of phosphoribosylpyrophosphate, essential for purine metabolism and nucleotide biosynthesis. Mutant PRPS1 has also been implicated in phosphoribosylpyrophosphate Synthetase Superactivity, characterised by hyperuricemia, neurodevelopmental abnormalities, sensorineural deafness, and gout(110), Arts syndrome, characterised by early onset hypotonia, ataxia, delayed motor development, intellectual disability, hearing impairment and optic atrophy(111), and X-linked deafness 1, a form of nonsyndromic hearing loss(112).

1.7.1.5 The distal hereditary motor neuropathies

The distal hereditary motor neuropathies (dHMNs), also known as spinal CMT or distal spinal muscular atrophy (dSMA), are a clinically and genetically heterogeneous group of diseases characterised by distal lower motor neurone dysfunction. The dHMNs share considerable phenotypic overlap with CMT-I and CMT-II, however are set apart in that they are predominantly motor and generally lack sensory abnormalities, and are thus considered a third CMT subtype. The most common characteristic features of these disorders include progressive distal weakness and wasting in the limbs, usually presenting in the extensor muscles of the toes and feet with later progression to the upper limbs, and foot deformities such as *pes cavus* and hammer toes.

In 1993, Harding classified dHMN into seven subtypes (dHMN-I to VII) according to mode of inheritance and clinical features, including the distribution of muscle weakness, age of onset of the disease and clinical evolution(113). Since then, novel forms of dHMN have been reported and the classification of

the dHMN subtypes has evolved as the molecular and genetic basis of this group of disorders has become clearer. The presence of unusual characteristic features such as vocal cord paralysis, diaphragm paralysis, onset and predominance in the hands, and pyramidal tract signs can often be used to distinguish between subtypes (table 35, appendix). Due to difficulties in detecting sensory involvement in CMT-I and CMT–II, electromyography and nerve conduction tests are used to distinguish between CMT and dHMN. dHMN patients are generally considered to have normal or slightly reduced motor NCVs and normal sensory NCVs, where CMT-I and CMT–II patients show both motor and sensory involvement. However, the presence of or absence of sensory symptoms is no longer a distinctive feature of dHMN as a number of dHMN subtypes display minor sensory abnormalities. Mutations of the same gene (*HSPB1, HSPB8, GARS, TRPV4, DYNC1H1*) may be associated with either CMT-II or dHMN, and even the same mutation may cause both phenotypes(114). The dHMNs also have clinical and genetic overlap with other motor neurone diseases with proximal neuromuscular involvement amyotrophic lateral sclerosis (ALS), Kennedy's disease, and spinal muscular atrophy (SMA), and these disorders are often considered to be encompassed by the term distal hereditary motor neuropathy.

Despite successful identification of dHMN causing mutations in over 20 genes, it has been estimated that 80% of dHMN patients have mutations residing in as-yet undiscovered genes(114, 115). The genes that have been implicated in dHMN encode a functionally diverse array of proteins, including 4 heat-shock proteins (HSPB8, HSPB1, HSPB3, DNAJB2) which are produced in response to cellular stress, proteins involved in RNA metabolism (IGHMBP2, SETX), 2 tRNA synthetase proteins (HARS, GARS), microtubules motor proteins or motor complex subunits (dynactin, cytoplasmic dynein heavy chain 1), cation channels and transporters (TRPV4, ATP7A), a lipid transporter (SIGMAR1), a ubiquitination enzyme (UBE1), and a mitochondrial protein (REEP1).

This thesis describes two distinct groups of neurological conditions arising due to different mutations in the primary cholinergic transporter (CHT). Our data show that these conditions include autosomal dominantly inherited dHMNs, and autosomal recessively inherited infantile hypotonia, arise due to distinct disease mechanisms. A review of this this latter condition is provided in section 4.2.

2

CHAPTER TWO

MATERIALS AND METHODS

2 MATERIALS AND METHODS

2.1 Buffers, reagents and stock materials

Table 3. B**uffers, reagents and stock solutions and their constituents**

Agarose loading buffer	40% ficoll, 0.2% xylene cyanol, 0.1% bromophenol blue
ExoSAP	For 1 millilitre: 50 U/ml Exonuclease I 50U/ml shrimp alkaline phosphatase (both bought from New England BioLabs), ddH_2O to final volume
Denaturing loading buffer (for PAGE)	0.3% bromophenol blue, 0.3% xylene cyanol, 10mM EDTA
Amipicillin	5mg/ml Amp in ddH_2O sterilized using a 0.22µM filter unit
Kanamycin	50mg/ml Kan in ddH_2O sterilized using a 0.22µM filter unit
Carbenicillin	50mg/ml Carb in ddH_2O sterilized using a 0.22µM filter unit
SOC medium	For 1 litre: 2% (w/v) Bacto tryptone, 0.5% (w/v) Bacto yeast extract, 10mM NaCl, 2.5mM KCl, 10mM $MgCl_2$, 20mM Glucose, ddH_2O to final volume, then autoclaved
Luia Bertani (LB) broth (Sigma-Aldrich)	For 1 litre: 25g LB broth base (components: 10g/L tryptone, 5g/L yeast extract, 5g/L NaCl), ddH_2O to final volume, then autoclaved
LB Agar	For 1 Litre: 25g LB broth base, 15g Agar, ddH_2O to final volume, then autoclaved
Phosphate buffered saline (PBS) (Life technologies)	GIBCO® Dulbecco's PBS without calcium and magnesium
1X PBS/$Ca^{2+}Mg^{2+}$	1mM $MgCl_2$, 0.1mM $CaCl_2$ in PBS
1X PBS/Ca2+Mg2+/glycine	1mM $MgCl_2$, 0.1mM $CaCl_2$, 100mM glycine in PBS
Transfer buffer	25mM Tris-base, 192 mM glycin, 20% methanol, pH8.3
TBS	150mM NaCl, 10mM Tris (pH8.0) in ddH_2O, adjusted to pH8.0 with HCl
TBST	0.1% Tween-20 in TBS
Protease inhibitor (Qiagen)	Protease inhibitor solution
RIPA buffer	10mM Tris (pH7.4), 150mM NaCl, 1mM EDTA, 1% Triton X-100, 0.5% Na deoxycholate, 0.1% sodium dodecyl sulphate (SDS) in ddH_2O

Sodium chloride-Tris-EDTA (STE) buffer	100mM NaCl, 10mM Tris (pH8), 1mM EDTA (pH8) in ddH_2O
Tris/CHAPS buffer	30mM Tris HCl, 150mM, NaCl, 1% CHAPS in ddH_2O
Low concentration Triton X-100 lysis (LCTL) buffer	5mM Tris (pH7.4), 100mM NaCl, 0.5% Triton X-100 in ddH_2O
Hypertonic swell (SWELL) buffer	10mM Tris (pH8), 1mM EDTA (pH8) in ddH_2O
Salt solution	1.5M NaCl, 10mM $MgCl_2$ in ddH_2O
2X Laemmli buffer (Sigma)	277.8mM Tris-HCl (pH6.8), 4.4% LDS, 44.4% (w/v) glycerol, 0.02% bromophenol blue
4X Laemmli buffer (BIO RAD)	277.8 mM Tris-HCl, pH 6.8, 4.4% LDS, 44.4% (w/v) glycerol, 0.02% bromophenol blue
Krebs-Ringer bicarbonate buffer (KRHB)	130mM NaCl, 1.3mM KCl, 1.2mM MgSO4, 2.2mM $CaCl_2$, 1.2mM KH_2PO_4, 10mM glucose, 10mM HEPES (pH7.4)
Stripping buffer	200mM glycine, 3.5mM SDS, 1% Tween-20 in ddH_2O, adjusted to pH2.2 with HCl

2.2 Family recruitment and sample acquisition

2.2.1 Ethical Approval

Ethical approval for the research carried out at St. George's Hospital laboratories was granted by the Wandsworth Research Ethics Committee (reference 04/Q0803/78, 05/Q0803/161). Research was carried out in compliance with the Code of Practice for Human Tissue and Research provided by the Human Tissue Authority (HTA), which defines human tissue as relevant material which consists of, or contains cells (HTA CoP 9). As this project involves the use and storage of blood samples, as well as subsequent DNA extraction, the blood must be stored on HTA-licensed premises and research must be carried out in accordance with the Human Tissue act 2004.

The HT Act and the HTA's code of practice states that informed consent must be obtained in order to:

i. Store and use dead bodies
ii. Remove, store and use relevant material from a dead body
iii. Store and use relevant material from the living

(HTA CoP 1)

In accordance with the HTA's code of practice, all subjects from which blood samples were taken for analysis were adequately informed about the purpose

of the research and how their blood samples would be stored and used. Only once a subject felt sufficiently informed and satisfied with the purpose of the research, were they asked to give signed consent.

2.2.2 Data management

On receipt of blood or DNA samples from their respective collection locations, each sample was assigned a sample ID, and this as well as clinical and molecular information was recorded in a password protected database. The vessels containing the samples were anonymised and labelled with the relevant sample ID.

2.3 Molecular methods

2.3.1 DNA extraction

DNA was extracted and purified from whole blood lymphocytes using the Promega ReliaPrep^{TM} Blood gDNA Miniprep system according to the manufacturer's instructions (summarised below), or provided by St. George's Hospital molecular diagnostic laboratory.

On arrival blood samples were stored at -20°C. Prior to extraction, blood samples were thawed completely and mixed thoroughly for 10 minutes at room temperature on a rotisserie shaker. Filter pipettes and sterile microcentrifuge and collection tubes were used throughout the procedure in order to prevent contamination. For each sample, 20µl of Proteinase K was dispensed into a 1.5ml microcentrifuge tube. 200µl of blood was added to the Proteinase K and triturated to mix. 200µl cell lysis buffer was subsequently added to the tube and the contents mixed by vortexing for 10 seconds and incubated at 56°C for 10 minutes. Following incubation, 250µl of binding buffer was added to the tube and the contents mixed by vortexing for 10 seconds. At this point it was ensured that the lysate was dark green in colour. The contents of the tube were added to a ReliaPrep^{TM} binding column placed in a collection tube and centrifuged at 13,000rpm (max speed of microcentrifuge) for 1 minute. If the lysate was still visible at the top of the membrane following centrifugation, the column was spun for a further 1 minute. The column was moved to a fresh collection tube, and the

flowthrough from the old one was discarded as hazardous waste in a sharps bin. The column was then washed by adding 500µl of column wash solution to the column and centrifuging it at 13,000rpm for 3 minutes. If any of the solution remained visible on the membrane, the column was spun for a further minute. The flowthrough was discarded as hazardous waste. This wash step was repeated two more times to make a total of three washes. The column was then transferred to a clean 1.5 microcentrifuge tube and 50µl of 70°C nuclease free water added to the column which was centrifuged at 13,000rpm for 1 minute to elute the DNA. The binding column was discarded. The DNA concentration and purity of the elute was measured using the nanoDrop, and an aliquot of working stock of 10-30ng/µl was prepared by diluting the DNA with molecular grade water.

2.3.2 RNA extraction

Monocyte mRNA was extracted from whole blood collected in PAXgene Blood RNA Tubes (BRT) and purified for sequencing using the Qiagen PAXgene blood RNA kit according to the manufacturer's instructions, described below.

PAXgene BRTs were equilibrated to room temperature after storage at -20˚C and then stored at room temperature prior to commencement of the procedure. In order to avoid RNase contamination the lab work space, pipettes, tubes racks and gloves were cleaned with RNaseZAP® prior to starting the extraction, and filter tips were used throughout.

Blood samples were centrifuged at 3000xg for 10 minutes in the PAXgene BRTs in a swing-out centrifuge. The supernatant was removed by pipetting, taking care not to disturb the pellet, and 4ml RNase free H_2O was added before closing the tubes with BD Hemogard closures. The pellet was resuspended by vortexing the tubes, which were then centrifuged a 3000xg for a further 10 minutes. The supernatant was completely removed and discarded. The pellets were dissolved in 350µl resuspension buffer and vortexed to ensure completed dissolution. The samples were then transferred to 1.5ml microcentrifuge tubes and mixed with 300µl binding buffer and 40µl proteinase K by vortexing for 5 seconds. The samples were incubated at 55˚C for 10 minutes in the shaking incubator at 800rpm. The lysate was transferred into a PAXgene Shredder spin

column placed in a 2ml processing tube by pipetting and centrifuged for three minutes at maximum speed (13,000rpm) in a bench-top micro-centrifuge. The entire supernatant of the flow-through fraction was transferred to a fresh microcentrifuge tube, taking great care not to disturb the pellet in the processing tube. 350µl 100% ethanol was added to the sample and mixed by vortexing before briefly centrifuging in order to remove any drops from the inside of the lid.

A 700µl volume of sample was pipetted into a PAXgene RNA spin column placed in a 2ml processing tube and centrifuged at 10,000xg for 1 minute. The PAXgene RNA spin column was placed in a fresh 2ml processing tube, and the flow-through in the old processing tube was discarded. 350µl wash buffer 1 was pipetted into the PAXgene RNA spin column and centrifuged at 10,000xg for 1 minute. Again the spin column was placed in a fresh 2ml processing tube, and the flow-through discarded.

In a 1.5ml microcentrifuge tube, 10µl DNase I stock solution was mixed with 70µl DNA digestion buffer and mixed gently by flicking the tube before briefly centrifuging to collect the fluid at the bottom. The full volume (80µl) of this mix was then pipetted directly onto the PAXgene spin column membrane and incubated at room temperature for 15 minutes. 350µl wash buffer 1 was subsequently pipetted into the spin column and the column was centrifuged at 10,000xg for 1 minute. The spin column was transferred to a new 2ml processing tube, and the flow-through discarded. 500µl wash buffer 2 was pipetted into the spin column and the column was centrifuged at 10,000xg for 1 minute. The spin column was transferred to a fresh 2ml processing tube, and the flow-through in the old processing tube was discarded. Another 500µl wash buffer 2 was added to the spin column and the column was centrifuged at 10,000xg for 3 minutes. The spin column was transferred to a fresh 2ml processing tube, the flow-through discarded, and the spin column was centrifuged for 1 more minute at 10,000xg. The processing tube containing the flow-through was discarded and the spin column was placed in a 1.5ml microcentrifuge tube. 40µl elution buffer was pipetted directly onto the PAXgene spin column membrane and the spin column was centrifuged at 10,000xg for 1 minute in order to elute the RNA. Another 40µl elution buffer was pipetted directly onto the spin column membrane and the spin column was centrifuged at

10,000xg for 1 minute, keeping the spin column placed in the same microcentrifuge tube. The elute was incubated at 65˚C for 5 minutes in the shaking incubator to denature the RNA, and then chilled immediately on ice. RNA was stored at -80˚C and used in reverse transcription PCR (RT-PCR) followed by sequencing as described in sections 2.3.8 to 2.3.13.

2.3.3 Reverse transcription PCR (RT-PCR)

R-PCR is a technique used for the indirect amplification of RNA by first making a complimentary DNA copy for amplification and sequencing, from which the RNA sequence can be deduced.

Prior to commencement of the procedure the workspace, including the bench top, pipettes, pipette racks, and filter-tip boxes, was cleaned first with 70% ethanol and then with RNaseZap (Ambion) to eliminate any traces of RNase. Filter tips were used throughout the procedure. RNA extracted from whole blood monocytes (see 2.3.2) and stored on ice was subjected to the Titanium one-step RT-PCR kit (Clontech), according to the manufacturer's protocol.

Primers for RT-PCR were designed to anneal to exonic sequences separated by at least one intron using Primer3 software (version 0.4.0, available at (http://bioinfo.ut.ee/primer3-0.4.0/) and ordered from Sigma-Aldrich. The programme settings were altered so that primers were designed according to the following criteria:

- Primers should be at least 22 bases in length (ideally 25-30)
- Primer melting temperature should be ~70°C
- Primer should have a GC content of 45-60%

Primers were diluted to 45µM for use. A master mix was made for each control and experimental reaction comprising the constituents in table 4, and RNase free water was added to bring the total volume to 50µl. A negative control reaction containing RNase free water in place of RNA was included to control for contamination. When carrying out RT-PCR it is important to be confident that it is in fact RNA that is being amplified, and not genomic DNA. To control for this, an additional control reaction was prepared in which standard taq, used in PCR, was used in place of the Titanium taq and the RNA replaced with ddH_2O.

A positive control reaction was also run containing mouse liver total RNA and primers specific to mouse β-actin (provided with kit). The reaction mixes were placed in a Eppendorf 96-well Mastercycler, thermal cycler machine and run through the heat cycling parameters detailed in table 5.

Table 4. RT-PCR constituents and their volumes

Component	Volume (µl)	
	Positive control	Experimental reactions
10X One-Step Buffer	5	5
50X dNTP Mix	1	1
Recombinant RNase Inhibitor (40u/µl)	0.5	0.5
Thermostabilising Reagent	25	25
GC-Melt	10	10
Oligo(dT) primer	1	1
50X Titanium *Taq* RT Enzyme Mix	1	1
Control mouse liver total RNA	1	-
Control mouse β-actin primer mix	1	-
Experimental RNA sample (1ng-1µg)	-	1-5.5
Experimental PCR primer mix (45µM)	-	1
RNase free H_2O	4.5	To 50
Total Volume	**50µl**	**50µl**

Table 5. RT-PCR thermal cycling program

Number of cycles	Temperature (°C)	Time
1	50	1 hr
1	94	5 min
40	94	30 sec
	65	30 sec
	68	1 min
1	68	2 min

The size of the products were analysed by agarose gel electrophoresis (see 2.3.11), on a 2.5% gel for 90 minutes.

2.3.4 Whole-exome sequencing in dHMN-VII family

Whole-exome sequencing was performed by Dr Saeed Al-Turki and Dr Matthew Hurles at the Wellcome Trust Sanger Institute (WTSI), and also provided guidance and support with the analysis of the data. Whole-exome sequencing was carried out on a single affected member of the dHMN-VII family. Gene coding regions were captured using SureSelect All Exons Target Enrichment System (50Mb): an automatable and scalable platform, and target enrichment solutions which enrich the genomic region of interest, and sequenced on the Illumina HiSeq with 76pb paired ends. In order to call single nucleotide variants (SNVs), reads were mapped to the reference genome sequence (GRCh37), duplicate fragments were marked using Picard, and GATK (v1.0.130910) was used to recalibrate base qualities. GATK was then used to call indels using IndelGenotyper. Variants were called using GATK UnifiedGenotyper and poor quality sites were filtered out near indels using the following hard filters: QUAL < 30.0 || AB > 0.75 && DP > 15 || HRun > 5 || SB > -0.10 || DP < 4 || DP > 2000". Samtools (v0.1.7) was used to call variants only from reads mapped in good pairs (correct insert size range) within the union of the bait and design target regions. Variants were filtered out if the read depth <4x or >1200x, if the consensus quality <20, or if the SNP quality <25. Dindel was run on a list of candidates in the union of the bait and design target regions +/-25bp. All variants were annotated using dbSNP (132), and the 1000 genomes pilot study. The effect variants on protein structure was predicted by SNP Effect Predictor (VEP v2.1) based on the Ensembl database (version 61). Both the SNVs and indels called by the mentioned programs were then merged in a single file for downstream analysis.

The VCF file obtained from whole-exome sequencing underwent further custom filtering using the exome variant analysis suite (EVA) – now the family based exome variant analysis suite FEVA – a software tool developed at the Wellcome Trust Sanger Institute which applies custom filters to VCF files in order to select a subset variants of interest. *In silico* predictive analysis of the structural and functional outcomes of any candidate variants identified by whole exome sequencing was performed using PolyPhen (http://genetics.bwh.harvard.edu/pph2/), PROVEAN &SIFT (http://provean.jcvi.org/genome_submit_2.php), Mutation Taster

(http://www.mutationtaster.org/), VEP (http://www.ensembl.org/Homo_sapiens/Tools/VEP), and TMHMM (Tied mixture hidden Markov model) (http://www.cbs.dtu.dk/services/TMHMM/) online software.

2.3.5 Targeted next-generation sequencing in dHMN-V family

Sequencing libraries were prepared using the Illumina TruSight One™ sequence capture and were sequenced on an Illumina HiSeq 2500. With the use of a custom built cloud-based GATK genotyping bioinformatics pipeline offering targeted test panels from a 4800 gene menu, the following known motor neuropathy genes were analysed: *ALS2, ANG, BSCL2, C9orf72, DCTN1, FIG4, FUS, GARS, HSPB1, HSPB3, HSPB8, IGHMPB2, DYNC1H1, SLC5A7, OPTN, REEP1, SETX, SOD1, SPAST, SPG20, TARDBP, TRPV4, UBQLN2, VAPB, CMTX*. Next generation sequencing data was visualised using the Integrative Genome Viewer (IGV) software. Putative pathogenic mutations were confirmed with bi-directional Sanger sequencing.

2.3.6 Whole-exome sequencing in Turkish hypotonia family

Exome sequencing of this family was carried out in collaboration with Dr Sebahattin Cirak at Uniklinik Köln University Hospital, Germany. The exome was captured with SeqCap EZ Human Exome Library v2.0 kit (Roche NimbleGen). The finished libraries were sequenced on an Illumina HiSeq 2000 with a paired-end 2x100 bp protocol as per the manufacturer's guidelines. The Cologne Center for Genomics VARBANK pipeline v.2.12 (https://varbank.ccg.uni-koeln.de/) was used for data analysis and filtering with Burrows-Wheeler Aligner-ALN plus hg19 for mapping of reads in combination with the GATK toolkit for base quality score recalibration (BQSR), local realignment, and variant quality score recalibration (VQSR). Variant prioritization and data filtering were conducted using the VARBANK database and analysis tools.

2.3.7 Whole-exome sequencing in Hispanic hypotonia family

Exome sequencing of this family was carried out in collaboration with Dr. Omar Abdulrahman and Holly Zimmerman, based at the University of Mississippi Medical Center, USA. Coding regions were captured using the SureSelectXT Target Enrichment System for Illumina Paired-End Multiplexed Sequencing, additional probes for 1800 clinically relevant disease genes were included to improve the exome coverage. Finished libraries were sequenced on the Illumina HiSeq platform with a 100bp paired-end protocol, according to the manufacturers guidelines. Exome data was analysed using the Mercury 1.0 next generation sequence analysis pipeline. Sequencing data were converted to bcl file by Illumina CASAVA 1.8 software, and mapped with the Burrows-Wheeler Aligner (BWA) software (SourceForge). Variant calls were performed using the Baylor College of Medicine Human Genome Sequence Center (BCM-HGSC) Atlas-SNP and Atlas-indel tools and variants were annotated using BCM-HGSC-SNP-anno and BCM-HGSC-indel-anno software.

2.3.8 Primer design

Genomic DNA sequences were obtained from the Ensembl Genome Browser (February 2009 and December 2013 assemblies) database. Primers were designed for a small section of DNA sequence (200-500bp) using online Primer3 software (version 0.4.0, available at (http://bioinfo.ut.ee/primer3-0.4.0/) and ordered from Sigma-Aldrich. The guidelines for primer design are as follows:

- Primer length should be between 18-22 nucleotides.
- Difference in melting temperature between the forward and the reverse primers should be no more than 1˚C, preferably between 55-65˚C.
- Guanine-cytosine (GC) content should be between 40-60%.
- Use of self-complimentary primers with inter or intra-primer efficiency extending more than 3 bases was avoided in order to prevent the formation of primer dimers and secondary structures, which would affect the PCR.
- Primers must be 100% complimentary and unique to the region of interest to ensure only that region is amplified.

In silico PCR and BLAST analysis was carried out via the UCSC Genome Bioinformatics website to ensure primers were specific to the region of interest. To ensure that a primer is 100% complimentary to the area of interest, the corresponding sequence of DNA must not contain any single nucleotide polymorphisms (SNPs).

2.3.9 Polymerase chain reaction (PCR)

The PCR is a laboratory technique used to selectively and exponentially amplify specific DNA sequences *in vitro*, by up to 10^9 times. The reaction requires repeated temperature cycles, a buffering solution, forward and reverse primers, deoxynucleotides (dNTPs: dGTP, dCTP, dATP, dTTP), magnesium chloride ($MgCl_2$), DNA, and Taq polymerase (Thermo Scientific).

Primers, designed as described in 2.3.8, arrive as a solid dried pellet which is diluted to a 100ρM/µl stock solution and stored at -20˚C. The stock dilution is further diluted to a 5ρM/µl working solution for use in PCR. For each set of primer pairs, a master reaction mix is made up with all of the reaction components except for the DNA. The master mix volume is dependent on the number of reactions required. If using patient DNA, this is dictated by the number of samples (patients) plus positive and negative controls (See table 6 for the constituents and their volumes required for each PCR mix).

Table 6. PCR constituents and their volumes

Component	Volume (µl)	Volume (µl)
10x Dream Taq Buffer (15mM $MgCl_2$, Thermo Scientific)	1	2.5
dNTPs (10mM, Invitrogen)	0.4	1
ddH_2O	6.9	17.25
Forward Primer (5ρM/µl, Sigma-Aldrich)	0.4	1
Reverse Primer (5ρM/µl, Sigma-Alsdrich)	0.4	1
Dream Taq polymerase (5U/µl, Thermo Scientific)	0.1	0.25
DNA	0.8	2
Total Volume	**10µl**	**25µl**

The PCR mix was then run through a number of repeated heating and cooling cycles in order to melt the DNA (denaturation), bind the primer pairs to their complimentary sequence (annealing), and allow enzymatic replication of the region of interest (elongation). This was carried out in an Eppendorf 96-well Mastercycler, thermal cycler machine.

A 'touchdown' PCR protocol was used, which is a method that helps to avoid amplification of regions other than that of interest by improving the specificity of the primer binding. This is achieved by incrementally lowering the annealing temperature by 2°C every two cycles from an initial temperature that is 4°C greater than that of the annealing temperature (Tm) until the desired Tm is reached (table 7).

Table 7. Touchdown PCR thermal cycling program

Number of cycles	Temperature (°C)	Time (Sec)
1	95 (denaturation)	120
2	95 (denaturation)	30
	Tm plus 4	45
	72 (elongation)	45
2	95 (denaturation)	30
	Tm plus 2	45
	72 (elongation)	45
35	95 (denaturation)	30
	Tm (annealing)	45
	72 (elongation)	45
1	72 (elongation)	300

Before use with subject DNA samples, PCR conditions were optimised for each primer pair using control DNA samples known to amplify well from their use in previous reactions. This allowed for determination of the optimum annealing temperature of the primer pair, as well as modification of the PCR reaction mixture if necessary (see section 2.3.10- optimisation of PCR primer conditions below). When carrying out PCR both with control and subject DNA, a negative (water) control was also run to ensure that the desired DNA template was being amplified, and not DNA from a contaminant in one of the reaction constituents.

2.3.10 Optimisation of PCR primer conditions

To determine the optimal annealing temperature for primer pairs, they were trialled using a 55-67°C temperature gradient. This was carried out by running

12 reactions for each primer pair through a touchdown PCR thermal cycle, each with a different annealing temperature which increased incrementally across the PCR block from 55°C to 67°C by approximately 1°C. If the temperature gradient produced weak or no products across the range of temperatures, often due to the GC content of one or both of the primers being above 60%, a second gradient was carried out with a 10% concentration of dimethyl sulfoxide (DMSO, Fisher Scientific) in each reaction. DMSO is an organic sulphur compound which binds to cytosine residues on DNA, changing its conformity and making it more liable to heat denaturation. Should amplification still be inadequate for intended use, further temperature gradients were carried out which PCR mixtures containing varying concentrations of magnesium (1mM-3mM), in the form of magnesium chloride ($MgCl_2$). Magnesium concentration was controlled by altering the amount of 10x Dream Taq Buffer and adding an appropriate volume of ddH_2O to make up the total volume of the reacting mixture.

2.3.11 Agarose gel electrophoresis

Agarose gel electrophoresis is a technique that uses an electric current to separate molecules according to their size. The gel forms a matrix through which smaller DNA molecules migrate faster and therefore further through the gel than larger molecules. This technique was used to visualize PCR products in order to assess the success of the PCR and whether amplification of the DNA is adequate for sequencing.

A 1.5% Agarose gel was made by mixing 1.5g agarose powder (Sigma-Aldrich) with 100ml 1X tri-acetate EDTA (TAE) buffer and heating the mixture in a microwave for 3-4 minutes or until the powder had completely dissolved. 1µl of ethidium bromide (Sigma-Aldrich) was then added and the mixture left to cool for 15-20 minutes. Ethidium bromide is a DNA intercalating agent which fluoresces brightly when exposed to ultraviolet (UV) light. Rubber seals were used to close up the two open ends of the gel plate creating a sealed mould into which the gel could set. 28-toothed combs were placed at equal distances along the length of the gel plate to create loading wells in the gel. The molten gel was poured in to the gel plate and a cellophane cover was placed over it as it set to avoid light exposure as the ethidium bromide is UV sensitive.

Once the Agarose gel was set, the rubber seals were removed and the gel plate, containing the gel, was placed in an electrophoresis tank and submerged in 1X TAE buffer. 1µl DNA ladder (1Kb Plus, Invitrogen) was loaded into the first well of each row to allow assessment of the PCR product size. 5µl of each PCR product was mixed with 2µl agarose loading buffer, and loaded into one of the wells. A power pack was used to apply a 100V current across the gel for 20-30 minutes. The gel was subsequently removed from the tank and the gel plate and placed on the illuminator (UV light box with a camera), where the ethidium bromide in the gel caused the PCR products to fluoresce under UV light. The column in which the negative control was loaded should not fluoresce, if products were seen in the negative control, all the PCR products were assumed to be contaminated and the reaction was repeated.

For larger DNA fragments (>500bp), PCR products were run through a lower concentration agarose gel (0.8%-1.0%) prepared as above with a lesser amount (0.8g-1.0g) of agarose powder.

2.3.12 PCR product purification

Before sequencing of a PCR product can be carried out, any unincorporated dNTPs and primers that remain in the reaction mixture must be removed. For this 'clean-up' reaction, 2µl ExoSAP (Exonuclease-1 and shrimp alkaline phosphatase) was used to purify 5µl of each of the PCR products. The exonuclease 1 removes remaining primers and the shrimp alkaline phosphatase removes the dNTPs whilst allowing the PCR products to be salvaged. The mixture was incubated at 37˚C for 30 minutes during which the two enzymes mentioned above were active, then at 95˚C for 5 minutes in order to deactivate the enzymes.

2.3.13 Sequencing reaction

Purified PCR products underwent a sequencing reaction in order to attach to them a fluorescent dye which is read by the sequencer machine. This was carried out using the BigDye® Terminator Cycle Sequencing Kit v3.1 (ABI PRISM®, Applied Biosystems).

A master reaction mix was made for each region of interest (each of the primer sets used in the PCR) and 7µl was aliquoted into appropriately labelled 0.2ml thermo-tubes. 3µl of the appropriate PCR product was then added to each thermo-tube. For each PCR sample, two sequencing reactions were performed with the forward and the reverse primers in separate reactions. (See table 8 for the constituents and their volumes required for each sequencing reaction mix). Each of the 10µl reaction mixtures was placed into an Eppendorf 96-well mastercycler, thermal cycler machine and run through thermal cycle detailed in table 9 for a total of 25 cycles.

Table 8. Sequencing reaction constituents and their volumes

Component	Supplier	Volume (µl)
BigDye Terminator	Applied Biosystems	0.5
BigDye Terminator Buffer	Applied Biosystems	1.7
Primer (forward or reverse)	Sigma_Aldrich	0.5
ddH_2O		4.3
Cleaned PCR product		3.0
Total volume		**10**

Table 9. Sequencing reaction thermal cycler program

Number of cycles	Temperature (°C)	Time (Sec)
25	96	30
	50	15
	60	240

2.3.14 Sequencing reaction product purification

In order to prepare the samples for automated DNA sequencing, they must first be purified. Purification of the sequencing reaction products was carried out using the BigDye® XTerminator™ Purification Kit (Applied Biosystems) according to the manufacturer's instructions, described below.

The BigDye® XTerminator™ Purification Kit removes unincorporated BigDye terminators, salts and other charged molecules from sequencing reactions that may interfere with base calling and electrokinetic sample injection (Applied

Biosystems). This clean-up reaction requires two reagents: XTerminator™ Solution scavenges unincorporated dye terminators and other charged molecules; SAM™ Solution enhances the performance of the XTerminator™ Solution and stabilises the post-purification reactions (Applied Biosystems).

The sequencing reaction products were loaded into a 96-well plate. The XTerminator™ Solution was vortexed briefly and 5µl was aliquoted into each well containing the sequencing reaction products. 30µl of SAM™ Solution was also added to each well. The plate was sealed using clear adhesive film (Thermo Scientific) and vortexed for 30 minutes then briefly centrifuged. The plate was then placed into a 16-capillary 3130xl Applied Biosystems® Automated DNA Sequencer for sequencing on a 36cm array POP7 polymer programme setting.

2.3.15 Restriction digest

A restriction digest is a method used to cleave DNA fragments by digestion of a given DNA molecule, at specific sites (restriction sites) recognised by a particular restriction enzyme. Polymorphisms which create or eliminate a restriction site are called restriction fragments length polymorphisms (RFLP). Restriction digest is a technique by which an RFLP can be detected by using a restriction enzyme specific to that variation to fragment a length of DNA. Resulting DNA fragments are then sized by agarose gel electrophoresis or PAGE as in 2.3.11 and 2.3.16, respectively. This was carried out to confirm the presence of the putative disease causing variants in affected subjects, and its absence their unaffected family members, as well as control populations.

A restriction digest reaction mixture is constituted of PCR product (amplified DNA) of the area of interest, 10X buffer, the appropriate restriction endonuclease and ddH_2O. The sequence containing the variant and the wild type sequence was entered into NEBcutter V2.0 online (http://tools.neb.com/NEBcutter2/) software to identify restriction enzymes that cut the two sequences differently, and these were selected for use.

A restriction digest master mix was made with all the constituents, except for the PCR product, and 12.5µl was aliquoted into appropriately labelled 0.2ml

thermo-tubes. 2.5µl PCR product was then added to each tube, and the tubes were incubated at 37˚C overnight (8+ hours). Two methods were used to visualise the restriction digest products, agarose gel electrophoresis or PAGE. For agarose gel electrophoresis, a 3% Agarose gel was made (3g Agarose powder, 100ml 1X TAE buffer) as described in 2.3.11 and the restriction digest products loaded and run through it for 1 hour prior to being visualised in the illuminator. For PAGE see 2.3.16.

2.3.16 Denaturing polyacrylamide gel electrophoresis (PAGE)

PAGE was used in order to visualise the products from restriction digest reactions. Prior to running the restriction digest products on the PAGE gel, they were visualised by agarose gel electrophersis to determine the relative volumes of product and loading buffer required for page, according to the strength of the PCR/restriction digest product.

An 8% denaturing acrylamide gel was made from the following components: 25ml Gene Page 8% (Amresco), 40µl TEMED (N'N'N'N'-tetramethylethylenediamine, Sigma-Aldrich) and 40µl 25% APS (ammonium persulphate, Sigma-Aldrich). The components were mixed for 30 seconds with a magnetic stirrer, then poured into a gel casting apparatus and left to set for 1 hour. Once set, the gels were placed into an electrophoresis tank and the tank was filled with 1L 65°C 1X TBE. The restriction digest products were mixed with denaturing loading buffer (formamide, bromophenol blue, and xylene cyanol) and subsequently 1µl of the mixture was loaded into each well. These were electrophoresed at 100mA for an appropriate length of time to ensure sufficient separation of the different sized products.

The gel was fixed with an aqueous fixing solution (10% ethanol (BDH), 0.5% glacial acetic acid (BDH)) for 15 minutes. It was then silver stained by submersion in an aqueous solution of 0.1% silver nitrate (Sigma-Aldrich) for 10 minutes followed by submersion in an aqueous solution of 1.5% sodium hydroxide (BDH) and 0.15% formaldehyde (BDH) until visualisation of the bands had occurred (~10-15 minutes). The gel was finally fixed with an aqueous solution of 0.75% sodium carbonate (BDH) for 5 minutes. Between each of these steps the gels were rinsed thoroughly with distilled water. Following the

final wash with water the gel was wrapped in Saran wrap, appropriately labelled, and the bands analysed over a white light box.

2.3.17 Bacterial culture: growth and maintenance

Transformed DH5α competent Escherichia coli (*E. Coli*) cells were propagated both in Luria Bertani (LB) broth, and on agar plates, supplemented with antibiotic at 37°C overnight. Cells grown in liquid LB broth were used immediately for plasmid extraction once fully confluent. Cells grown on agar plates were stored at 4°C in sealed bags for later selection of colonies for further propagation. Frozen cell stocks were made by mixing 0.5ml of fully confluent liquid culture with 0.5ml 100% sterilised glycerol by vortexing, followed by storage at -80°C.

2.3.18 Heat shock transformation of chemically competent bacteria

Heat shock transformation is a process in which the membrane of chemically competent cells is made permeable by heating to allow ingestion of foreign DNA for propagation. This technique was used for propagation of pRK5α vectors containing gene constructs of interest for later use in function investigation in transiently transfected cell lines, and in sub-cloning (see 2.3.19) of wild type and mutant alleles for sequencing of separate strands from individuals with heterozygous frameshift variants. In both cases, plasmids were transformed into competent *E. coli*.

Transformation with pRK5 vector: Preparation of this reaction took place in a fume cupboard. Chemically competent Subcloning Efficiency™ DH5α™ cells (Invitrogen) were thawed on ice. 0.5µg DNA (from site directed mutagenesis reaction, 2.3.20) was added to 80µl chemically competent cells, mixed gently, and incubated on ice for 30 minutes. The cells were heat shocked at 42°C in a water bath for 45 seconds and returned immediately to ice for 2 minutes for recovery. 100µl SOC was added to the cells and they were incubated at 37°C for 1 hour in the shaking incubator. Cells were then spread on an agar plate supplemented with 100µg/ml Ampicillin and incubated overnight at 37°C.

Transformation with pCR®2.1 vector (ligation mix): Preparation of this reaction took place in a fume cupboard. BL21(DE3) Singles™ Competent *E. coli* (Novagen) were thawed on ice. Once thawed, 2µl ligation reaction product was pipetted directly into 50µl cells and mixed gently before incubating on ice for 5 minutes. The cells were subsequently heat shocked at 42˚C in a water bath for 30 seconds. The cell were then immediately transferred to ice for 2 minutes to recover. 250µl of room temperature LB broth was added to each vial and the vials were shaken horizontally at 225rpm at 37˚C for 1 hour in a shaking incubator. 100µl cells was then evenly spread across pre-prepared agar plates supplemented with 50µg/ml Kanamycin, which were then incubated overnight at 37˚C.

The plasmid vectors used in the above transformation reactions contain antibiotic resistance genes to the respective antibiotics mentioned. Any cells that did not internalise a plasmid during the heat-shock would not contain the antibiotic resistant gene and therefore should not grow on the agar supplemented with antibiotic. The introduction of antibiotic resistance into the cells was necessary to ensure that all the colonies that grew on the agar plates contained the DNAs of interest.

2.3.19 Sub-cloning of PCR products

Sequencing data containing a frame-shift or compound heterozygous mutation appears as a double trace before or after the point of change depending on whether the forward or reverse primer was used during the sequencing reaction. Should a double trace be found in a sequencing file, the two individual strands (wild type and mutant) were separated for DNA sequencing by sub-cloning. This involves incorporating a small (200 bases) length of single stranded DNA into the plasmid of chemically competent cells (transformation). Any cell that internalises a plasmid will take in only one copy of the region of interest, either the wild type or the mutant, because plasmids are single strands of DNA. This allows for clean, clear sequencing of the region of interest. Sub-cloning requires two steps: an initial ligation reaction, described below, followed by a transformation reaction as described in 2.3.17.

A ligation reaction is a type of DNA amplification, similar to PCR that uses DNA ligase to link chains and amplify the template containing the sequence in question. DNA ligases are enzymes that catalyse the joining of two DNA molecules to form a double helix. This part of the sub-cloning incorporates the length of DNA of interest into a plasmid vector (See table 10 for the constituents and their volumes required for a ligation reaction). Sub-cloning was carried out using the pCR®2.1-TOPO® Vector (Invitrogen), and the TOPO® TA Cloning® Kit (Invitrogen). PCR of the sample to be sub-cloned was undertaken, as described in 2.3.8, to produce fresh (less than 1 day old) PCR products. A master reaction mixture containing all the reagents except for the PCR product was made and 8.5µl was aliquoted into appropriately labelled thermo-tubes (positive and control). 1.5µl of fresh PCR product and 1.5µl of water was then added to the positive tube and the control tube respectively. The reaction mixture was incubated at 14°C overnight, and then at 65°C for 10 minutes to heat inactivate the T4 DNA ligase before use of the products in the transformation reaction, as described in 2.3.18.

Table 10. Ligation reaction constituents and their volumes

Component	Volume (µl)
10x Ligation Buffer	1.0
pCR®2.1 vector (25ng/µl)	2.0
T4 DNA Ligase (4.0 Weiss units/µl)	1.0
ddH_2O	4.5
Fresh PCR product	1.5
Total volume	**10**

In order to sequence the colonies of transformed cells from the agar plate, individual colonies were gently transferred to 0.2ml thermos-tubes containing 50µl molecular grade water with the use of a sterile 10µl pipette tip. 12 standard PCR reactions were made up with the same primers that were used for the PCR reaction undertaken prior to the ligation reaction. 1µl was taken from each of the 0.2ml thermos-tubes containing sole colonies and added to 1 of the 12 PCR mixes. PCR was carried out and its success analysed by agarose gel

electrophoresis, as described previously. All successful reaction products were sequenced by dideoxy Sanger sequencing (see 2.3.13)

2.3.20 Site-directed mutagenesis (SDM)

Site directed mutagenesis (SDM) is a molecular technique used to introduce specific and intentional sequence variations to a gene construct in a plasmid vector. SDM was carried out with the use of the QuickChange Lightning Site-Directed Mutagenesis kit (Agilent) according to the manufacturer's instructions (for SDM primer sequences see appendix 7.3.7), detailed below, in order to generate mutant gene constructs.

Prior to carrying out SDM, mutagenic primer pairs were individually designed according to the desired mutation. Wild type gene cDNA sequences were obtained from the Ensembl Genome Browser (February 2009 GRCh37/hg19 or December 2013 GRCh38/hg38 assembly) database, and primers were designed by eye according to the following criteria:

- Both the forward and reverse mutagenic primers must contain the desired mutation
- Both mutagenic primers must anneal to the same sequence on opposite strands of the plasmid
- Primers should be between 25 and 45 bases in length, and have a melting temperature of 78°C or greater
- The desired mutation should be positioned in the middle of the primer with between 12 and 20 bases of correct sequence flanking each side
- Primers should have a GC content ≥40%
- Primers should terminate in one or more G or C bases

A 50µl reaction mix was prepared for each pair of mutagenic primers comprising the constituents in table 11, and a 50µl control reaction mix was prepared with the constituents listed in table 12 on ice. 1 µl QuickChange Lightning Enzyme (derivative of PfuUltra™ High Fidelity DNA polymerase) was added to each reaction mix immediately prior to their being loaded in the thermal cycler and run through the heat cycling parameters detailed in table 13.

Table 11. SDM sample reaction constituents and their volumes

Component	Volume (µl)
10x QuickChange Lightning Buffer	5
pRK5 vector containing wild type gene cDNA (50ng/µl)	2
Forward mutagenic primer (65ng/µl)	2
Reverse mutagenic primer (65ng/µl)	2
dNTP mix	1
QuickSolution reagent	1.5
ddH_2O	37.5

Table 12. SDM control reaction constituents and their volumes

Component	Volume (µl)
10x QuickChange Lightning Buffer	5
pWhitescript 4.5-kb control plasmid (5ng/µl)	5
Oligonucleotide control Primer #1 (100ng/µl) **5' CCATGATTACGCCAAGCGCGCAATTAACCCTCAC 3'**	1.25
Oligonucleotide control Primer #2 (100ng/µl) **5' GTGAGGGTTAATTGCGCGCTTGGCGTAATCATGG 3'**	1.25
dNTP mix	1
QuickSolution reagent	1.5
ddH_2O	34

Table 13. SDM reaction thermal cycling program

Number of cycles	Temperature (°C)	Time (Sec)
1	95	120
18	95	20
	60	10
	68	30/kb plasmid
1	68	300

Following amplification, 2µl *DpnI* restriction enzyme was added to each sample reaction and the control reaction. The tube contents were gently mixed briefly centrifuged prior to incubation at 37°C for 5 minutes. *DpnI* digests the parental supercoil dsDNA. The resultant plasmids were transformed into Chemically Competent Subcloning Efficiency™ DH5α™ cells (see 2.3.18).

The control reaction was used to test the efficiency of mutant plasmid generation. The pWhitescript 4.5-kb control plasmid contains a stop codon in place of a glutamine codon in the β-galactose gene, and the oligonucleotide control primers #1 and #2 create a point mutation which reverts stop codon back to the wild type sequence, reintroducing the glutamine residue to the β-galactose gene product. Following transformation and propagation of transformed cells on agar plates, the presence of >100 colonies, of which >85% are blue as opposed to white, on the plate spread with the control reaction indicates successful mutagenesis.

2.3.21 Plasmid preparation and sequence verification

Following SDM and transformation, single, stand-alone colonies were picked from the agar plate using a sterile inoculating loop and transferred to 10ml LB broth supplemented with 100µg/ml Ampicillin and incubated at 37°C overnight in the shaking incubator. Once confluent, a frozen stock of each of the grown colonies was made, and the remaining cells were spun at 6000 xg for 15 minutes at 4°C, and the supernatant removed. Plasmids were extracted with the Qiagen® Plasmid Mini kit according to the manufacturer's instructions involving an alkaline lysis step and subsequent binding of plasmid DNA to an anion exchange resin under low salt and pH conditions. Medium salt washes are applied to remove impurities, followed by a higher salt solution wash to elute the plasmid DNA. Plasmid DNA was precipitated from the high salt buffer with isopropanol, desalted with 70% ethanol, and resuspended in 1x TE buffer.

The plasmids were then sequence verified by dideoxy sequencing to ensure the desired mutations had been introduced, and that no additional variations were present. For plasmids found to be sequence verified, larger scale preparations were made by transferring a scrape of cells from the frozen stocks into 200ml LB broth supplemented with 100µg/ml Ampicillin and incubating at 37°C overnight in the shaking incubator. The plasmids were then extracted using the Qiagen® Plasmid Midi kit according to the manufacturer's instructions.

2.4 *In silico* methods

2.4.1 *In silico* sequencing data analysis

The success of the sequencing was checked visually as a chromatogram using Finch TV 1.4.0 (created by Geospiza Inc. Avaialble at www.geospiza.com). Successful sequences were than compared to the wild type DNA sequence (available from the online Ensembl database) using alignment trees created in CLC Free Workbench sequence viewer 6.3 (created by CLC Bio A/S).

2.4.2 Mutation Analysis

The amino acid sequence was obtained for both the wild type and the mutant forms of the putative disease causing gene by entering the exonic DNA sequence into ExPASy software (https://www.expasy.org/). The amino acid sequences then were entered into Tied Mixture Hidden Markov Model (TMHMM) software (http://www.cbs.dtu.dk/services/TMHMM/) to produce graphs which predict probability of amino acid sequences forming transmembrane helices based on the hidden Markov model (HMM).

2.4.3 Conservation Analysis

The wild type and mutant amino acid sequences for the human disease gene of interest, and the wild type amino acid seuqences of the orthologues from 7 other species (Pan troglodytes, *Canis lupus familiaris, Bos taurus, Mus musculus, Rattus norvegicus, Gallus gallus*, and *Caernorhabditis*) were entered into CLUSTAL W2 (http://www.ebi.ac.uk/Tools/msa/clustalw2/), or CLUSTAL Omega (http://www.ebi.ac.uk/Tools/msa/clustalo/) software in FASTA format to create a multiple alignment.

2.5 Cell culture techniques

2.5.1 Cell culture

HEK-293 cells previously found to be negative for mycoplasma infection were maintained in 5% CO_2, at 37°C in growth medium: DMEM (with 4.5g/L glucose,

with L-glutamine without sodium pyruvate) (GIBCO®) supplemented with 1% penicillin-streptomycin, 1% L-glutamine, and 10% foetal bovine serum (GIBCO®).

2.5.2 Freezing cell line stocks

When fully confluent, HEK-293 cells cultured as described above were harvested and resuspended in freezing medium (growth medium with 15% DMSO) and transferred to CryoTubes. These were immediately placed into a Mr. Frosty™ Freezing Container in which they were stored overnight prior to long term storage in liquid nitrogen.

2.5.3 Cell plating

HEK-293 cells were plated in either 24-well plates with 100,000 cells/well in 1ml growth media, or in 6-well plates with 500,000 cells/well in 2ml growth media.

The procedure was carried out under a sterilised cell culture hood, and all equipment was sprayed with 70% ethanol prior to being placed in the hood to avoid infection of the culture. 1X poly-D-lysine (PDL) was dispensed into each well in order to promote adhesion of the cells to the bottom of the wells. The cells were washed by rinsing 1X phosphate buffered saline (PBS) over the inside of the cell culture flask. The PBS was removed from the cell culture flask and the cells were trypsinised in 1X trypsin to detach the cells from the flask and to break up clumps of cells. The cells were then suspended in 10ml growth media (GIBCO®) and counted using a haemocytometer. The cells were then appropriately diluted in media in order to plate the appropriate number of cells in each well. Once plated, the cells were returned to incubation at 37°C, in 5% CO_2 for 24 hours before transfection.

2.5.4 Transient transfection of cultured cells

The cells were transfected using TranIT®-LT1 transfection reagent (Mirus) in Opti-MEM® Reduced Serum Media (modification of Eagle's Minimum Essential Media, buffered with HEPES and sodium bicarbonate, and supplemented with

hypoxanthine, thymidine, sodium pyruvate, L-glutamine, trace elements, and growth factors, Invitrogen). For a 6-well plate plated with 500,000 cells/well, 1µg plasmid DNA was transfected in 3µl TranIT®-LT1 and 100µl Opti-MEM®. For 24-well plates with 100,000 cells/well, 200ng plasmid DNA was transfected in 1.5µl TranIT®-LT1 and 45µl Opti-MEM®.

Appropriate volumes of TranIT ®-LT1 and Opti-MEM® for the number of well to be transfected were mixed in a 15ml BD Falcon tube and incubated at room temperature. Appropriate volumes of the DNAs (see tables 36 and 37 in the appendix) to be transfected were each transferred to separate BD Falcon tubes and the appropriate amount of TranIT®-LT1/Opti-MEM® mix was added to each before a 20 minute room temperature incubation. The transfection mix and DNAs were then pipetted directly onto the cell containing media in the wells and the plates were swirled to ensure mixing. The plates were returned to incubation at 37°C, in 5% CO_2 for 24 hours before use in assays or for protein extraction.

2.6 Protein methods

2.6.1 Cell extract preparations

In order to detect and analyse the protein products of mutant gene constructs transiently transfected into HEK-293 cells, the proteins were first extracted.

The procedure was carried out on ice. Cells plated and transfected in 6-well plates as described were washed 2 times with warm (37°C) 1X PBS then solubilised in 400µl RIPA containing protease inhibitor on the shaker at 4°C for 1 hour. Cell lysates were scraped from the wells and transferred to 1.5 microcentrifuge tubes and spun at full speed (13,000rpm) for 20 minutes at 4°C. The supernatant was transferred to clean microcentrifuge tubes on ice, leaving the globby pellet of tissue debris behind. The protein content of the cell lysates was then quantified by a BCA protein assay.

2.6.2 Bicinchoninic acid (BCA) protein assay

A protein assay was carried out in order to quantify the amount of protein present in cell lysates of transiently transfected HEK-293 cells. 5ml BCA protein assay agent (Thermo Scientific) was prepared (BCA protein assay reagent

A:BCA protein assay reagent B , 50:1). In a 96-well plate, 10µl BCA standards (blank, 0.025mg/ml, 0.125mg/ml 0.25mg/ml 0.5mg/ml, 0.75mg/ml, 1mg/ml, 1.5mg/ml, 2mg/ml) were loaded into wells with 200µl BCA protein assay agent. 10µl of each of the protein samples obtained from the biotinylation was also loaded into wells with 200µl BCA protein assay agent. Following 20 minutes incubation at 37°C, the plate was loaded into a PHERAstar FS microplate reader (BMG Labtech) and the concentrations of each sample were calculated. Each sample was then diluted in RIPA buffer to meet the concentration of that of the lowest concentrated protein prior to their purification.

2.6.3 SDS-PAGE

A 10% SDS-PAGE running gel solution (see table 14 for SDS-PAGE running gel constituents and their volumes) was prepared and poured into a gel mould. Once set, a 10% SDS-PAGE stacking gel solution (table 15) was made and poured into the mould on top of the running gel. A 15 toothed comb was placed in the top of the mould to form the wells. Once the stacking gel had set, gel was placed in an electrophoresis tank containing 1X SDS-PAGE running buffer (24.8mM tris base, 192mM glycine, 0.1% SDS in ddH_2O). Proteins extracted from cells and normalised for concentration as described, were mixed with 20µl 2X Laemmli buffer and spun at maximum speed for 5 minutes. 10µl Spectra Multicolor Broad Range Ladder (Thermo Scientific) was loaded into one of the wells, and 20µl each protein sample was loaded into subsequent wells. The electrophoresis tank was connected to a power pack and a current of 125V was run across the gel for 1.5 hours.

Table 14. 10% SDS-PAGE running gel constituents and their volumes

Component	Supplier	Volume (ml)
ddH_2O		4
Acrylamide (30% at 29:1)	Invitrogen	3.3
1.5 Tris pH8.8		2.5
10% SDS	Invitrogen	100µl
10% APS	Invitrogen	50µl
TEMED	Invitrogen	5µl

Table 15. 10% SDS-PAGE stacking gel constituents and their volumes

Component	Supplier	Volume (ml)
ddH_2O		3.05
Acrylamide (30% at 29:1)	Invitrogen	650
0.5 Tris pH6.8		1.25
10% SDS	Invitrogen	150µl
10% APS	Invitrogen	25µl
TEMED	Invitrogen	5µl

2.6.4 Membrane transfer

The proteins separated by SDS-PAGE were transferred onto Immobilin-P blot membrane (EMD Millipore). The membrane, cut according to the size of the SDS-PAGE gel was activated with 100% methanol, and two similarly sized sheets of blotting paper were soaked in transfer buffer. The gel was removed from the electrophoresis tank, placed in contact with the Immobilin-P blot membrane, and sandwiched between the two pieces of blotting paper. A test tube was gently rolled over the ‘sandwich’ to remove air bubbles. The sandwich was then placed in a transfer tank filled with transfer buffer and connected to a power pack, and current of 20V was run through the gel for 18 hours in the cold

room. During this time, the ladder and the proteins transfer from the gel to the Immobilin-P blot membrane.

2.6.5 Western blotting

Following transfer of the proteins onto the Immobilin-P blot membrane, the blot membrane was removed from the transfer tank and blocked with 3% bovine serum albumin (BSA) in 1X TBS with1% Triton (TBST) for 30 minutes at room temperature, with gentle agitation on the Belly Dancer® (Sigma-Aldrich). The now empty gel was discarded. The 3% BSA-PBST was poured of the membrane and the membrane was probed with mouse monoclonal anti-HA antibody (m.m. anti-HA) (Abcam, ab18181) in 3% BSA-PBST (1:500) for 2 hours at room temperature on the belly dancer. The m.m. anti-HA was poured off and the membrane was washed three times in 1X TBST for 10 minutes at room temperature on the Belly Dancer. The membrane was probed with a secondary antibody, goat-anti-mouse-IgG-HRP (Abcam, ab6789) in 3% BSA-TBST (1:10,000) for 1 hour at room temperature on the Belly Dancer®. The membrane was then washed 3 times in 1X TBST for 10 minutes at room temperature on the Belly Dancer® and then submerged in 1X TBS until visualisation.

Transferred proteins probed with goat-anti-mouse-IgG-HRP secondary antibodies were detected with the use of the Western Lightning® Plus-ECL, Enhanced ChemiluminescenceSubstrate Kit (Perkin Elmer) and developed on Amersham HyperFilm™ ECL (GE Healthcare Life Sciences) in a Konica Minolta SRX-101 A-Xray film developer. In the dark room, with the lights on, 2.5ml Western Lightning –ECL Enhance Luminol Reagent (Perkin Elmer) was mixed with 2.5ml Western Lightning –ECL Oxidising Reagent (Perkin Elmer). The 1X PBS was poured off the blot membrane and the Western Lightning mix was poured on for 1 minute. The lights were then turned off. The membrane was removed from the Western Lightning mix and the excess fluid wiped off with a Kim-wipe. The membrane was placed in an exposure cassette with an Amersham Hyper-Film for varying exposure times (1minute, 30 seconds, 10 seconds and 2 seconds) and the film was immediately placed into the Konica SRX-101A-Xray Film Developer. The membrane was wrapped in Saran wrap and placed in a C-DiGit® Blot Scanner (LI-COR®) for imaging.

2.7 Functional studies

2.7.1 Cell surface biotinylation experiments in transiently transfected HEK-293 cells

This work was carried out in collaboration with Dr. Randy Blakely and Jane Wright of Vanderbilt University School of Medicine.

Biotinylation is a technique often used to detect and/or purify proteins by the process of attaching biotin to the proteins. The functional impact of the putative disease causing variants was investigated by heterologous expression of the mutant and wild type cDNAs in transiently transfected HEK-293 cells followed by biotin labelling of the wild type and mutant proteins produced. The proteins were visualised by western blotting.

HEK-293 cells were plated in 6 well plates and incubated for 24 hours to allow the cells to adhere to the bottom of the wells. The cells were then transfected with the appropriate cDNAs and incubated for a further 48 hours at 5% CO_2 at 37°C. The cells were washed twice with cold 1X PBS/$Ca^{2+}Mg^{2+}$ (1mM $MgCl_2$, 0.1mM $CaCl_2$ in 1X PBS) and incubated in 2ml/well NHS-SS-Biotin (12mg/ml Sulfo-NHS-SS-Biotin [EZ-Link^{TM}] in 1X PBS/$Ca^{2+}Mg^{2+}$) with gentle shaking at 4°C for 30 minutes. The cells were then washed twice with 2ml/well PBS/$Ca^{2+}Mg^{2+}$/glycine (1mM MgCl2, 0.1mM CaCl2, 100mM glycine in 1X PBS) and quenched in 1ml PBS/$Ca^{2+}Mg^{2+}$/glycine at 4°C with gentle shaking for a 15 minutes. The cells were washed again in 2ml/well 1X PBS/$Ca^{2+}Mg^{2+}$ and solubilised in 400µl RIPA buffer with protease inhibitor (Qiagen) on the shaker at 4°C for 1 hour. The contents of each well were transferred to 1.5 microcentrifuge tubes and spun at 13,000rpm for 3 minutes. The supernatant was transferred to clean microcentrifuge tubes and the pellets discarded. A BCA protein assay was then carried out as described previously in order to determine the protein concentrations for normalisation.

Streptavidin beads were used to purify the biotinylated proteins. Streptavidin beads were washed 4 times with RIPA buffer containing protease inhibitor. 50µl of the streptavidin beads was added to each of the lysates and the mixture was incubated at room temperature on a tilt plate for 1 hour. The samples were washed 4 times with 200µl RIPA buffer with protease inhibitor before 30µl 4X Laemmli buffer (277.8 mM Tris-HCl, pH 6.8, 4.4% LDS, 44.4% (w/v) glycerol,

0.02% bromophenol blue) was added to each and they were incubated again at 4°C on the shaker for 30 minutes. The samples were then analysed by Western blot.

2.7.2 Saturation analysis of choline uptake in HA-SLC5A7^{WT} and HA-SLC5A7^{K499N} transfected HEK-293 cells

This work was carried out in collaboration with Dr. Randy Blakely and Jane Wright of Vanderbilt University School of Medicine.

Saturation analysis was carried out in order to determine the choline concentration at which the CHT WT and CHT p.K499Nfs*13 transporters uptake activity becomes saturated. This allows confidence that any differences in transport activity observed between the two isoforms arise due to differences in rate of transport of the molecules and not due to differences in choline concentration.

Choline uptake assays were carried out as described in section 2.7.3 in HEK-293 cells transiently transfected with HA-*SLC5A7*^{WT} and HA-*SLC5A7*^{K499Nfs*13}. In each assay cells were incubated in varying concentrations of a mix of [^{3}H]-choline chloride and cold choline chloride (100nM, 300nM, 1µM, 3µM, 7µM, 10µM, 20µM, 30µM) at 37°C for 15 minutes prior to washing and scintillation counting.

2.7.3 [^{3}H]-choline uptake assay in transiently transfected HEK-293 cells

[^{3}H]-choline uptake was measured in transiently transfected HEK-293 cells in order to determine whether there was reduced CHT activity in these cells and, if so, whether that reduction was due to a reduction in choline transport V_{MAX} as opposed to a change in choline K_M.

HEK-293 cells were plated and transfected as described above in 24-well plates as previously described. Parallel experiments were carried out in multiples of 6. Transport assays were performed 24 hours later. Cells were washed 2 times KRHB with (130mM NaCl, 1.3mM KCl, 1.2mM MgSO4, 2.2mM CaCl2, 1.2mM KH2PO4, 10mM glucose, 10mM HEPES: pH7.4) prior to a 15 minute incubation

at 37°C in 200µl KRHB. The KRHB was removed and replaced with 50µl 50nM [^{3}H]-choline chloride (78.3 Ci/mmol) in KRHB and the cells were incubated at 37°C for a further 15 minutes. The fluid was removed from the cells and disposed of as radioactive waste. The cells were washed 4 times with ice cold KRHB before being lysed in 400µl scintillation fluid on the Belly Dancer® at room temperature, for 1 hour. Contents of the wells were transferred to scintillation vials and accumulated radioactivity was quantified by scintillation spectrometry (HIDEX 300SL, LabLogic). Parallel assays were conducted with cells transfected with empty pRK5 vector in order to account for the cells own choline uptake activity. Parallel plating and transfection of cells with various constructs was also carried out. These cells were lysed and the average protein concentration/well was calculated in order to calculate the choline uptake per minute per microgram of protein produced.

2.7.4 [^{3}H]-Choline uptake assay in whole blood monocytes

This work was carried out with the assistance of Dr. Ajith Sreekantan-Nair at St. George's University of London. Choline transport was measured in whole blood monocytes collected in BD Vacutainer® CPT glass cell preparation tubes from affected individuals from the dHMN-VII_family (family 1) and from healthy control individuals.

Cell preparation tubes containing blood samples were spun at 2,200rpm at 4°C for 20 minutes. Serum and buffy-coat were transferred to a fresh tube and made up to a 15ml volume with KRHB. The cells were then spun at 300xg for 10 minutes and the pellet resuspended in KRHB before protein content was determined by BCA assay as described in chapter (2.6.2). [^{3}H]-choline uptake assays were performed by incubating the cells at 37°C for 1 hour in 60nM [^{3}H]-choline chloride (85.5 Ci/mmol; Perkin Elmer) in KRHB as the substrate. 500µl ice cold KRHB was added to each sample and the cells were then pelleted and washed 3 times with KRHB. Accumulated radioactivity was quantified by liquid scintillation counting as described in Chapter 2.7.3 and counts per minute (CPM) were counted on a Beckman Coulter LS 6500 scintillation counter. Nonspecific [^{3}H]-choline uptake was quantified is assays performed in parallel with 1µM hemicholinium-3 (HC-3), which was then subtracted from the total

accumulation to yield the specific uptake. All data were normalised to protein content.

2.7.5 Co-immunoprecipitation of tagged *SLC5A7* wild type protein products and *SLC5A7* (NM_021815.2: c.1497delG; NP_068587.1: p.K499Nfs*13) mutant protein from transiently transfected HEK-293T cells

Unfortunately, due to the time constraints of my visit to Vanderbilt University, and because during the undertaking of these experiments Okuda and team(116) publish evidence that CHT forms a homo-oligomer on the cell surface, these experiments were not successfully completed. Methodology and results for these studies is included in the appendix.

2.7.6 Pulse chase analysis of CHT-WT and CHT-K499Nfs*13 in transiently transfected HEK-293 cells

Initial pulse chase analysis attempts in HEK-293T cells were unsuccessful, and due to the time constraints of my visit to Vanderbilt University further attempts were not able to be made. Methodology and results for these studies is included in the appendix.

3

CHAPTER THREE

READING FRAME ALTERATION OF THE *SLC5A7*/CHT C-TERMINUS IS ASSOCIATED WITH dHMN PHENOTYPES VIA A DOMINANT-NEGATIVE DISEASE MECHANISM

3 READING FRAME ALTERATION OF THE SLC5A7/CHT C-TERMINUS IS ASSOCIATED WITH dHMN PHENOTYPES VIA A DOMINANT-NEGATIVE DISEASE MECHANISM

3.1 Introduction

The dHMNs are a heterogeneous group of peripheral motor neurone disorders (see section 1.7.1.5 and table 35, appendix) that share a common feature of length-dependent neuropathy which results in progressive weakness and wasting of the distal limb muscles, which typically presents in the extensor muscles of the toes and feet, and later on progresses to the upper limbs(80). Unlike CMT-I and II, in dHMN there is no overt sensory involvement and motor nerve conduction velocities (mNCVs) are normal or slightly reduced. It has been hypothesised that the dysfunctional mechanisms underlying this group of diseases relate to the cell body of the neurone and not the axon(117). In addition to the progressive muscle weakness and atrophy of the distal limbs, foot deformities such as *pes cavus* and hammer toes, and diminished or no reflexes are the most commonly observed features of dHMN(117).

Distal hereditary motor neuropathy type VII (dHMN-VII or dHMN-VIIA) was first described by Young and Harper in 1980, in a large Welsh kindred, in which they observed that the disease was of autosomal dominant inheritance and displayed a large age range of onset (11-31 years), although in most affected individuals onset was in the second decade(118). *Pes cavus* was also reported. Muscle weakness and wasting distribution was unusual and presented initially in the small muscles of the hands, occurring later in the lower limbs. The main characteristic noted in this family however, was the presence of unilateral or bilateral vocal cord paresis presenting as a husky voice and difficulty in raising the voice, and which was visible on laryngoscopy. Three other dominantly inherited neuropathies in which vocal cord paresis is characteristic have been described: CMT-IIC, scapuloperoneal spinal muscular atrophy (SP-SMA), and vocal cord and pharyngeal weakness with distal myopathy (VCPDM)(119).

In a later study by Pridmore *et al.* (1992) a smaller dHMN-VII family, thought to be unrelated to that described by Young and Harper, was reported with hoarseness, slowly progressive wasting and weakness of the hands and distal forearms and later, weakness of the feet. Again, age of onset varied between

family members (4-21 years), as did the severity of the disease(120). This could be due to variable expressivity and lack of penetrance of the mutant gene(118).

McEntagart *et al.* (2002) undertook linkage analysis on the two previously described dHMN-VII families and not only found them to be distantly related, but also mapped the dHMN-VII disease locus to chromosome 2q14(119). The authors noted that dHMN-VII shows considerable phenotypic overlap with CMT-IIC (table 32, appendix), but can be distinguished by the lack of sensory involvement in dHMN-VII. The locus was further refined in 2008 by Dick *et al.* to two distinct regions of chromosome 2q14.2, one comprising of 9.2Mb defined by markers D2S3038-D2S160, and the second comprising of 4.3Mb defined by markers D2S2970-D2S2969 (figure 13)(121).

In 2003, Puls *et al.* reported a family with a second form of dHMN-VII, dHMN-VIIB(60). Similarly to the family described by Young and Harper, Pridmore *et al,*, and McEntagart *et al.*, disease transmission followed and autosomal dominant mode of inheritance with onset in early adulthood, limb muscle weakness and atrophy presented and predominated in the small muscles of the hands, and vocal cord paralysis was present. Unlike in Young and Harding's original dHMN-VII family, in addition to weakness and atrophy of the hand muscles, the neuropathy in these subjects presented as breathing difficulty due to the vocal cord paresis, and progressive facial weakness. Using genome-wide linkage analysis, Puls *et al.* (2003) mapped the disease locus to a 4Mb region on chromosome 2p13 and, after sequencing of candidate genes within the critical region, identified a mutation in *DCTN1* as underlying the disorder in this family. *DCTN1* encodes the $p150^{Glued}$ subunit of dynactin, a large complex that interacts directly with dynein via the $p150^{Glued}$ subunit where it acts as an activator and binds cargos(122). Together, and with a number of other activators, the complexes form a microtubule-based motor protein required for cytoplasmic retrograde transport of vesicles and organelles along microtubules(122). Puls and colleagues found that the disease causing variant identified in this family significantly reduced (50%) microtubule binding preventing distal enrichment of dynactin thereby inhibiting the initiation of retrograde transport. The authors suggested that motor neurones may be particularly vulnerable to the resultant defects in axonal transport due to their

unusual size and metabolic activity, and their dependence on trophic factors delivered from the periphery.

First described by Meadows and Marsden in 1969 and later classified as a subtype of the dHMNs, dHMN-V shares considerable phenotypic overlap with dHMN-VII with the exception of vocal cord paralysis(123). Similarly to dHMN-VII, dHMN-V follows an autosomal dominant mode of inheritance; is variable in both age of onset which ranges from early childhood to the fourth decade, and disease severity; is usually slow to progress; weakness and atrophy presents and predominates in the small muscles of the hands, with lower limb involvement occurring later and at a lower degree in the disease course(123-127). Several cases have been observed in which hand muscle weakness and wasting is confined exclusively to the thenar and/or interosseous dorsalis I eminences(124-126, 128). Foot deformities including *pes cavus, pes planus* and/or hammer-toes are often present, and less frequently, atrophy of the ankle extensors(129). dHMN-V canbe divided into two further subtypes, -VA and -VB, based on genetic features.

dHMN-VA is allelic with two phenotypically similar disorders, CMT-IID and Silver syndrome(85, 114, 128, 130, 131). CMT-IID (table 32, Appendix), an autosomal dominant form of axonal CMT which also presents and predominates in the hands with the addition of sensory involvement, shares with dHMN-VA, mutant *GARS* as it disease causing gene. *GARS* encodes Glycyl-tRNA synthetase, a class II aminoacyl synthetase enzyme that catalyses the synthesis of glycyl-tRNA, required for the insertion of glycine during protein synthesis(132). Its secondary function is the synthesis of dinucleoside polyphosphates, which have been suggested to play a role in the regulation of cell functions(132). Silver syndrome, a rare complex form of spastic paraplegia characterised by unilateral or bilateral upper and lower limb muscle weakness and atrophy- often involving the thenar or hypothenar muscles, *pes cavus*, pyramidal tract signs, and lower limb hyperreflexia and hypertonia, is caused by autosomal dominant mutations in *BSCL2*(133). *BSCL2* encodes the protein seipin, which plays an important role in adipocyte differentiation, its exact molecular function remains unknown, as well as lipid homeostasis by promoting adipose tissue fat storage, via the regulation of intracellular calcium homeostasis(134). Autosomal recessively-

acting *BSCL2* mutations are also known to cause Bernardinelli-Seip congenital lipodystrophy type 2, one of the most severe lipodystrophy diseases(134).

dHMN-VB is distinguishable from type-VA by genetic evidence only, and is caused by mutations in *REEP1*. *REEP1* encodes receptor expression enhancing protein 1 (REEP1), which plays an important role in the formation, shaping and remodelling of the endoplasmic reticulum by linking endoplasmic reticulum tubules to the cytoskeleton(127, 135). It has also been suggested that REEP1 may enhance cell surface expression of odorant, or olfactory receptors(136), and play a role in long-term axonal maintenance via the endoplasmic reticulum-regulation of lipid droplets(137). Loss-of-function REEP1 mutations have previously been identified in a dominant form of hereditary spastic paraplegia, SPG31, a disease associated with upper-motor neurone pathology(127).

Here, genetic and molecular studies implicate an autosomal dominantly-transmitted truncating mutation in *SLC5A7*, encoding the high-affinity choline transporter, as the cause of dHMN-VII in two families via a dominant-negative mode of action on transporter function. Interestingly we also identified a third family with a truncating dominant-negative mutation without vocal cord paralysis (VCP), in which the phenotype is more in-keeping with that of dHMN-V.

3.2 Results

PART A

3.2.1 Identification of the disease causing mutation in *SLC5A7* in a dHMN-VII family by whole-exome sequence analysis

The data regarding the discovery and analysis of the causative gene mutation was published in The American Journal of Human Genetics (Barwick KES, Wright J, Saeed Al-Turki, McEntagart MM, Nair A, Chioza B, Al-Memar A, Modarres H, Reilly MM, Dick KJ, Ruggiero AM, Blakely RD, Hurles ME, and Crosby AH (2012): 91(6): 1103-1107): *Defective presynaptic choline transport underlies hereditary motor neuropathy*.

3.2.1.1 History of clinical and pathological features of dHMN-VII family (family 1) members and previous genetic analysis

Subject family 1_V:9 (figure 10) from Young and Harper (1980) (corresponding pedigree number: III 24 of the YH1 branch of the family) was born in 1929 and initially presented at the age of 14 with bilateral wasting of the palm muscles which caused stiffness and curling of his fingers(118). By 20 years of age his voice had become husky and he was neither able to sing nor shout, and at this point he reported that the muscle weakness and wasting he had experienced in his hands has progressed to the distal lower limb muscles. Another 10 years on and muscle weakness and wasting had progressed to a point at which it severely limited his activity as walking became painful and difficult. From the age of 40 he noticed increasing dyspnoea (laboured breathing), which in addition to his muscles weakness and atrophy, contributed to impaired exercise tolerance. At 50 years he was only able to walk for short distances, had difficulty driving, and could barely hold a pen, so was no longer capable of earning his living. On examination he showed marked distal wasting and atrophy of the lower limbs with the typical “inverted champagne bottle” appearance of the legs (figure 11) and bilateral *pes cavus*. He also had severe wasting of the small muscles of the hand, in particular those of the palm, and despite exhibiting full passive movements in both hands he was unable to extend the medial three digits in either. He lacked deep tendon reflexes in both his wrists and ankles

and showed a pronounced tremor in the hands when outstretched. No sensory deficits were observed.

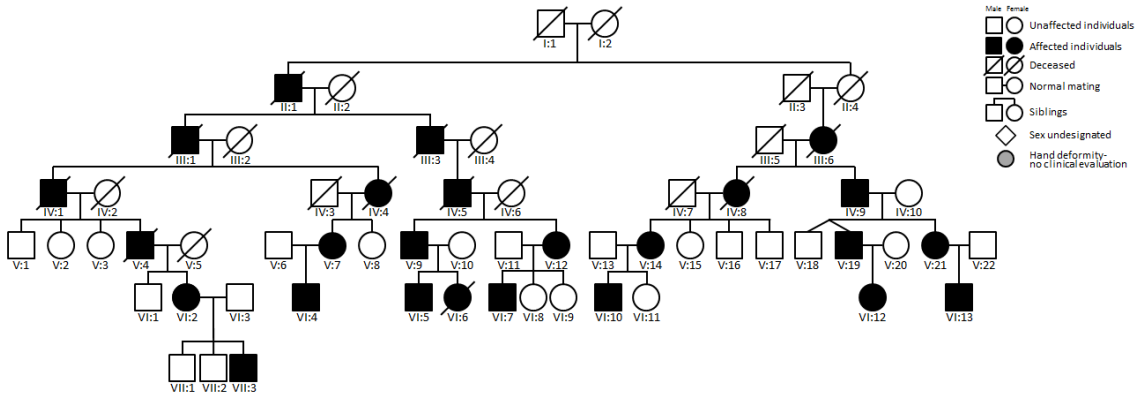

Figure 10. dHMN-VII family (family 1) pedigree

In a later study by Pridmore *et al.* (1992) a smaller Welsh dHMN-VII family - thought to be unrelated to that described by Young and Harper - was reported with hoarseness, slowly progressing weakness and wasting of the hands and distal forearms, and later weakness of the feet(120). Similarly to Young and Harper's family, age of onset of the disease varied between family members (4-21 years), as did the severity of the disease. Also as in Young and Harpers family, the disease was dominantly inherited and affected family member across at least three generations. With a diagnosis of peroneal muscular atrophy in the family history, the proband (family 1_VI:12, figure 10) was taken to hospital at the age of 6 by her parents who were concerned about her impaired hand function. The parents reported that onset of hand weakness was at age 5 when her ability to manipulate a pencil or a spoon became difficult, and she had had a slightly hoarse voice from the age of 4. On examination at age 6 family 1_VI:12 was found to have a hoarse voice in absence of facial weakness, palatal palsy, tongue atrophy, or fasciculation. This was confirmed by laryngoscopy which revealed left vocal cord paralysis. Weak grip was reported with normal muscle tone and preserved reflexes, although these were depressed in the upper limbs. Nerve conduction velocities (NCVs) and electromyography (EMG) studies were normal (table 16). She had a normal gait but poor heel walking. On later examination (age 9 years) she showed mild weakness in her grip, finger extension, and wrist flexion, but still showed no muscle wasting. The family reported that her voice had become progressively more hoarse and her writing progressively more difficult. She had bilateral *pes cavus* and the poor heel

walking persisted, as did the normal tone and preserved reflexes with depression in the upper limbs. Sensation and NCVs were normal however EMG indicated early neurogenic change (table 16).

Previous genetic studies by McEntagart *et al.* (2001) and Dick *et al*(2008) indicated that the gene responsible for dHMN-VII resides in either of two closely located genomic regions of 9.2Mb, flanked by microsatellite markers AC084377 – AC115115 proximally, or 4.4Mb, D2 S437 – D2 S5347 distally(figure 13), resulting from an unusual series of recombination events in the P2 branch of the family (figure 12). 15 candidate genes within the locus were also excluded as being disease causing by dideoxy sequence analysis(121). Pedigree identification numbers for a number of individuals in this study have varied between studies over the years since their first description with the addition of new family members; for past subject ids see appendix.

A summary of the clinical and electrophysiological findings of members from both branches of the family can be found in tables 16 and 17.

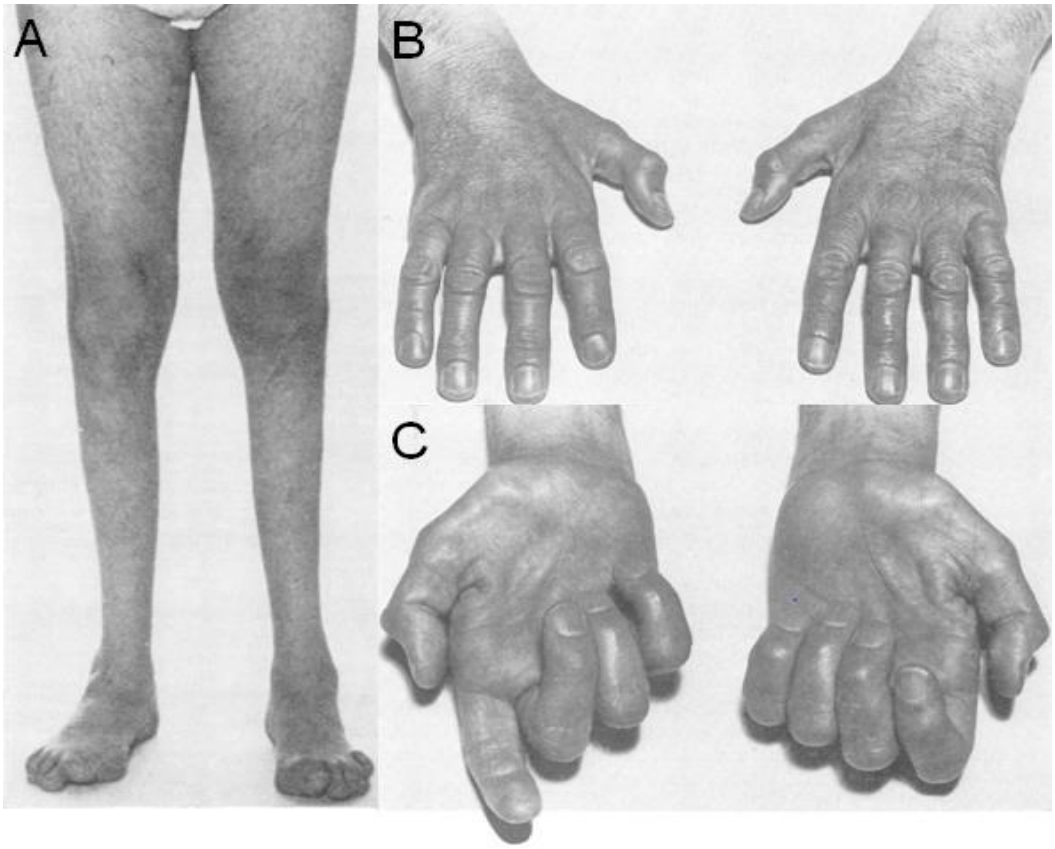

Figure 11. Distal muscle wasting of family 1_V:9 in (A) the lower limbs giving an "inverted champagne bottle" appearance, and (B & C) small hand musculature giving a claw-like positioning of the hands. Modified (Young & Harper, 1980 (118))

Table 16: Electrophysiological findings from both branches of dHMN-VII family 1

	Normal range	family 1_V:9	family 1_VI:6	family 1_V:4	family 1_VI:2	family 1_V:7	family 1_VI:4	family 1_V:12	family 1_VI:12	family 1_VI:13	family 1_V:19
Age at testing		45y	20y	46y	14y	45y	21y/24y	42y	6y/9y	11m	12
Sensory studies											
Sural nerve (post tibial)											
Velocity (m/s)							28		48/51	53	
Action potential (μV)							7		18/16	20	
Median nerve		Rt	Rt		Rt			Lft			
Amplitude (μV)		9	30		Norm			**			
Latency (ms)		3.8	2.6								
Ulnar nerve		Rt	Rt			Rt	Rt	Rt			
Amplitude (μV)		12	21	Norm		Norm	Norm	Norm			
Latency (ms)		2.5	2.1								
Motor studies											
Medial popliteal nerve			Rt Lft								
Velocity (m/s)			55 50							53	
Distal latency (ms)			4.0 3.7						3.5	5	
Distal CMAP (mV)									11	6	
F wave latency (ms)	25-32								27.5	35.5	
Median nerve (apb)					Rt			Lft			
Velocity (m/s)		NR			56			43	51		
Distal latency (ms)		NR			5.8				3.5		
Distal CMAP (mV)									3.6		
F wave latency (ms)									24		
Ulnar nerve		Rt	Rt		Rt	Rt	Rt	Rt			
Velocity (m/s)		55	57	41	56	44	31	52			
Distal latency (ms)		3.6	2.5								
Lateral popliteal nerve (edb)					Rt	Rt	Rt				
Velocity (m/s)				28	38	44	26				45
Distal latency (ms)											5.5
Distal CMAP (mV)											2.8
F wave latency (ms)											52
Common peroneal nerve			Rt								
Velocity (m/s)			40								
Distal latency (ms)			3.8								
Electromyography											
Abductor digiti minimi								***			
Extensor digitorum communis									Early NC	Normal	
First dorsal interosseous										Normal	
Tibialis anterior							*				

Abbreviations and symbols: **apb**= abductor pollicis brevis; **edb**= extensor digitorum brevis; **NR**=No response; **Rt**=Measurement taken on right side; **Lft**= Measurement taken on left side; *****Spontaneous fibrillation with reduced volitional activity; **Small, dispersed, delayed sensory action potentials; ***Spontaneous fibrillation and reduced interference pattern

Table 17: Clinical findings from both branches of dHMN-VII family 1

Subject	Sex	Age on examination (y)	Age at onset (y)	Vocal cord changes	Upper limb involvement	Lower limb involvement
family 1_V:9	M	50	14	Left cord fixed	+ + +	+ + +
family 1_VI:6	F	23	16	Hoarse voice	+ +	+
family 1_V:4	M	57	14	Right cord fixed	+ + +	+ +
family 1_VI:2	F	25	12	Left cord fixed	+ +	+
family 1_V:7	F	57	11	Bilateral palsy	+ +	+ + +
family 1_VI:4	M	33	13	Bilateral palsy	+ +	+ +
family 1_V:12	F	42	31	Hoarse voice	+ + +	+
family 1_VI:12	F	6	4	Left cord palsy	+ +	+
family 1_V:19	M	32	12	Bilateral palsy	+ + +	+
family 1_V:21	F	?	21	Hoarse voice		-
family 1_IV:9	M	63	Teens	Hoarse voice		+ +
family 1_IV:8	F	62	?	Hoarse voice		-

Abbreviations: **F**=Female; **M**=Male; **+ + +**=Severe; **+ +**=Moderate; **+**=Mild; **-**=Absent

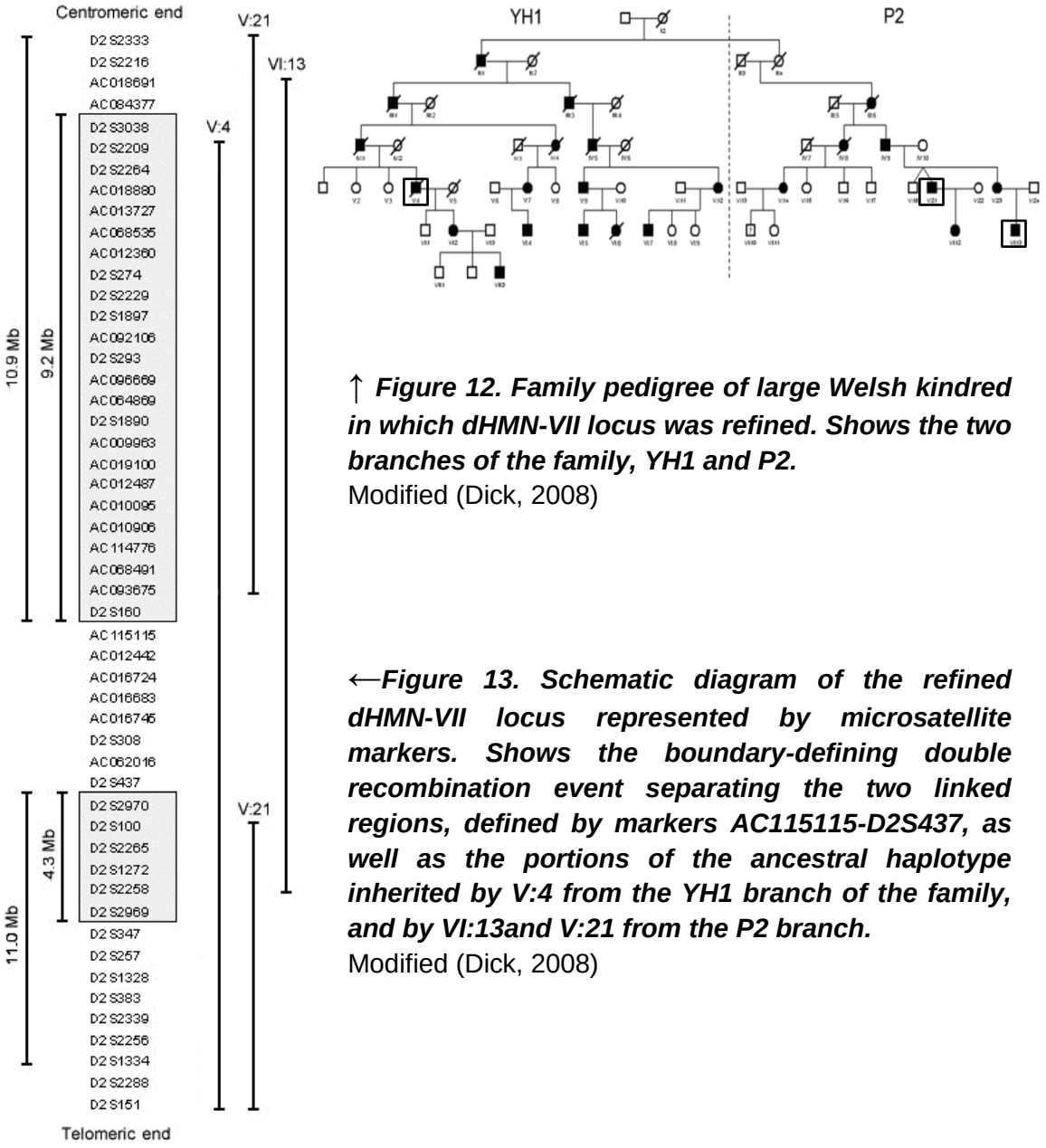

↑ ***Figure 12. Family pedigree of large Welsh kindred in which dHMN-VII locus was refined. Shows the two branches of the family, YH1 and P2.***
Modified (Dick, 2008)

←***Figure 13. Schematic diagram of the refined dHMN-VII locus represented by microsatellite markers. Shows the boundary-defining double recombination event separating the two linked regions, defined by markers AC115115-D2S437, as well as the portions of the ancestral haplotype inherited by V:4 from the YH1 branch of the family, and by VI:13and V:21 from the P2 branch.***
Modified (Dick, 2008)

3.2.1.2 Exome sequencing identifies a mutation in *SLC5A7* as the likely cause of dHMN-VII

In order to identify the gene responsible for this condition, DNA from a single affected individual (family 1_VI:5) was subjected to whole-exome sequence analysis to generate a novel variant profile in collaboration with Dr Matt Hurles at the Wellcome Trust Sanger Institute. Coding regions were captured using SureSelect All Exons (50Mb) and sequenced by Illumina HiSeq. The VCF file obtained from whole-exome sequencing yielded 9.8Gb data (~130 million reads) corresponding to 91% coverage with a mean depth of 107x and identifying 52,806 variants. See table 18 for sequencing statistics. Exome sequence analysis identified four novel potentially pathogenic variants within the chromosome 2q14 locus (table 19).

Table 18. Sequencing statistics

Bases	9,877,091,850 (9.8 Gb)
% Q20 bases	96.87%
% Q30 bases	91.57%
Reads used	131,694,558
% Duplication	7.69%
Reads mapped	120,632,748 (91.6%)
Reads mapped (high mapping quality ≥ Q30)	103,839,839 (78.8%)
Mean depth on target regions	107.5
Array	SureSelect All Exon 50Mb (solution)
Mapped to	GRCh37_53 (Human)

Table 19. dHMN-VII family 1 loci variants

Variant position	Variation	Affected gene	Predicted outcome	Cosegregates?
Chr2:108627070	Single base deletion (G)	*SLC5A7*	Non-synonymous coding p.Lys499Asnfs*13	Yes
Chr2:120404629	Single base deletion (T)	+3 in intron splice of *PCDP1*	Unlikely to affect splice site	No
Chr2:101924635	Single base substitution (T-C)	*RNF149*	Non-synonymous coding p.Asn199Asp	No
Chr2:121107178	Single base substitution (A-G)	*INHBB*	Non-synonymous coding p.Asn318Asp	No

Legend: *Novel likely deleterious varients within the dHMN-VII loci identified by whole-exome sequencing, the genes in which they appear, their predicted outcome, and results of cosegregation analysis.*

In order to determine which of these variants may represent the causative mutation, cosegregation analysis was performed on all four variants in the 24 member family (for primer sequences see table 39 appendix). Only one likely deleterious variant was found to cosegregate with the disease phenotype (table 19), a single base deletion located within the reading frame of the solute carrier family 5 (choline transporter), member 7 (*SLC5A7*) gene (c.1497delG: NM_021815.2), encoding the Na^+/Cl^- dependent, high affinity choline transporter (CHT). All *SLC5A7* exons were well covered during the exome sequencing (data not shown) including the 9th exon that harbours the c.1497delG variant under study. There are fewer reads covering the first exon due to high GC content.

The variant was found to be absent in all unaffected members of the family and present in all affected members of the family by both dideoxy sequence analysis (figure 14A), and by an *Ssp1* restriction digest (recognition sequence AATATT) visualised by PAGE (figure 14B). The variant was shown to be absent in 151 UK controls by *Ssp1* restriction digest visualised by agarose gel electrophoresis (figure 45, appendix), and was absent from online genomic databases: National Center for Biotechnology Information's (NCBI) dbSNP (http://www.ncbi.nlm.nih.gov/SNP/), 1000 Genomes Project (http://browser.1000genomes.org/), National Heart, Lung and Blood Institue's (NHLBI) Exome sequencing project (ESP6500) via the Exome Variant Server (EVS) (http://evs.gs.washington.edu/EVS/), and Exome Aggregation Consortium (ExAC) (http://exac.broadinstitute.org/).

The variant was also found to be present in monocyte mRNA of affected cases by dideoxy sequencing (PCR primers used for amplification of mRNA were 5'-TGGTCTTGGTGCAGTTTCTGCTGCT-3' and 5'-GGTGAAAGTTGAGCTGAGGGTCATGC-3') (figure 15).

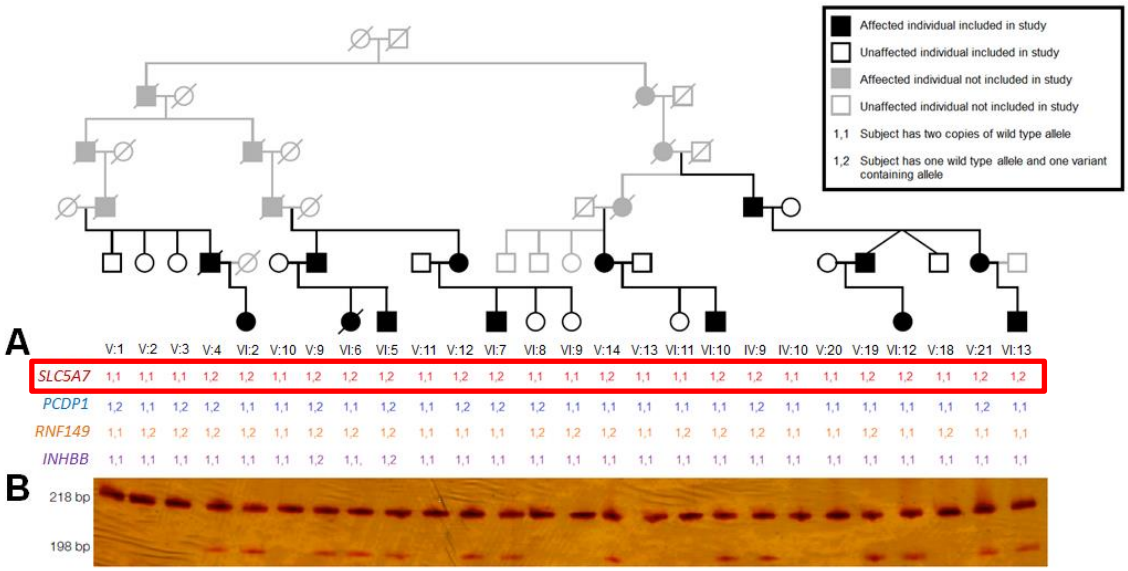

Figure 14. dHMN-VII family 1 pedigree showing A) cosegregation analysis results for each of the variants in the dHMN-VII loci identified by whole exome sequencing. Only one variant cosegregates with the disease phenotype (red box). B) Confirmation of cosegregation of c.149delG in SLC5A7. The variant results in the creation of a novel Ssp1 restriction site allowing cosegregation analysis by restriction digest of exon 9 PCR products (PCR primers used for amplification of exon 9 genomic DNA were 5'-CCCTGGCTATTACCCTGATG-3' and 5'-CACAAGTGCAAGTTCATCTAATTT-3'). Digest products were resolved by polyacrylamide gel electrophoresis (PAGE). The c.1497delG variant results in the digestion of the 218bp wild type product into two fragments of 198bp and 20bp (not shown). All unaffected subjects have only the undigested 218bp product. All affected subjects are heterozygous for the c.1497delG variant and thus have both the undigested 218bp products as well as the digested 198bp fragment.

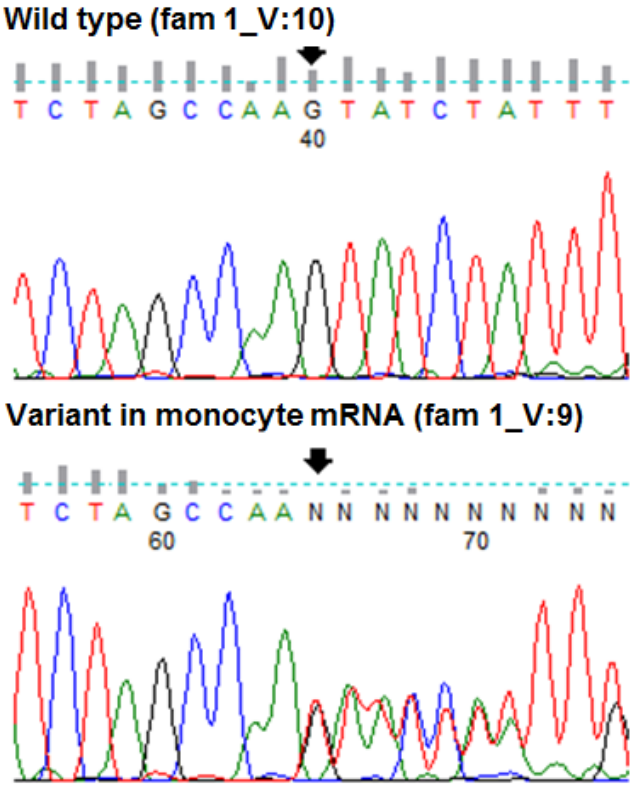

Figure 15. Chromatogram showing DNA sequence around the c.1497delG variant showing wild type sequence (upper trace) and mutant (c.1497delG) strand from monocyte mRNA (middle trace) from an affected individual (family 1_V:9).

3.2.1.3 *In silico* analysis of *SLC5A7* c.1497delG

The amino acid sequence was obtained for both the wild type and mutant molecules by entering the coding (exonic) DNA sequence into the online ExPASy translate tool (http://web.expasy.org/translate/). The wild type protein (CHT: NP_068587.1) consists of 580 amino acids predicted to comprise 13 transmembrane domains, with an extra cellular NH_2-terminus and an intracellular COOH-terminus(138, 139) (figure 16A). The *SLC5A7* c.1497delG variant at the nucleotide level is predicted to result in premature truncation of the protein by 82 amino acids, causing near complete deletion of the proteins cytoplasmic C-terminus, and the inclusion of 12 aberrant amino acids (p.K499Nfs*13) (figures 17 and 16B).

Conservation analysis indicates that the C-terminal corresponds to a region of the molecule that is highly conserved across many species (figure 46, appendix) and TMHMM analysis predicts that the c.1497delG variant will profoundly affect transmembrane morphology of the 3' terminus of the protein

(figure 47, appendix). Although it disputes the precise transmembrane topology of the *SLC5A7* gene product, from the (TMHMM) analysis (online predictive software which uses the Tied Mixture Hidden Markov Model to predict the location and orientation of alpha helices in membrane spanning proteins) it is apparent that the mutation is likely to interfere with the number or orientation of transmembrane domains(139, 140).

In silico mutation analysis programs, PROVEAN and Mutation Taster were used to create predictions of the impact of the *SLC5A7* c.1497delG mutation on the structure and function of the protein product. PROVEAN predicted c.1497delG to have a deleterious effect on the function of the protein product with a score of -55.034. Mutation taster predicted the variant to be disease causing with a score of 1.

SLC5A7 sequence analysis (for primer sequences see appendix) was also undertaken in two other unrelated families (figure 18) with dHMN-VII-like features. Both families displayed distal muscle weakness and wasting, as well as some degree of vocal cord paralysis. In the proband from dHMN-VII-like family 2 (family 2_II:2, figure 16A), onset of the disease occurred at 30 years of age with muscle weakness and wasting in the small muscles of the hands and the forearm muscles, with milder lower leg involvement and a hoarse voice. The second dHMN-VII-like family (family 3, figure 16B) display typically signs of dHMN-VII with the addition of myokymia (quivering muscles). Previous *TRPV4* screening had failed to detect mutations. No novel *SLC5A7* sequence variants were identified in these subjects (data not shown) This indicates that another as yet undiscovered gene(s) is/are also responsible for this condition.

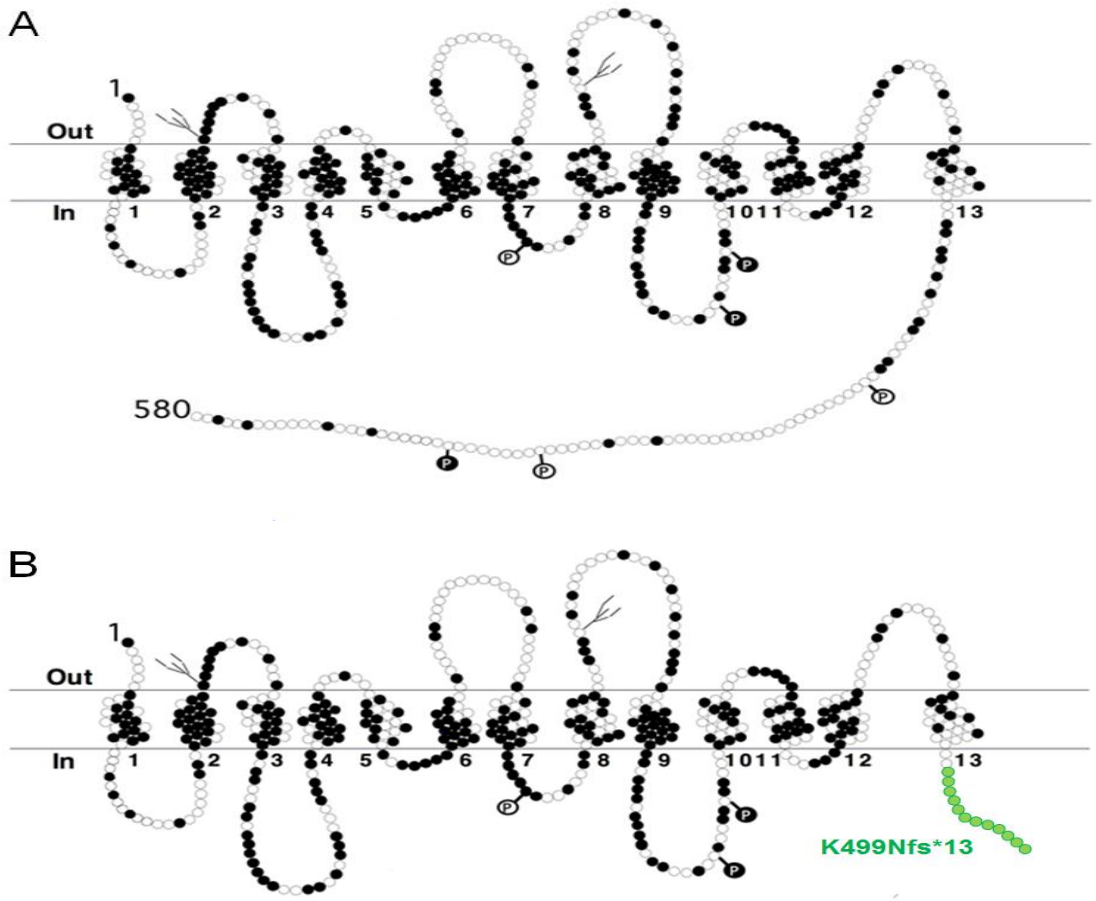

Figure 16. A) Diagram of the predicted secondary structure of the SLC5A7 gene protein product (CHT) showing 13 transmembrane domains with an extracellular N-terminus, and an intracellular C-terminus. Dark circles represent amino acids which are conserved across human CHT, mouse Cht1, and the C. elegans CHT ortholog, CHO-1. Dark circles containing the letter 'P' indicate potential protein kinase C phosphorylation sites, and light circles containing the letter 'P' represent potential protein kinase A phosphorylation sites. The fork-like structures represent potential N-glycosylation sites. B) Green circles represent the 12 ectopic amino acids encoded as a result of the c.1497delG variant, and the position of the first of these is the point from which the C-terminus is lost. Modified (Apparsundaram, 2000; Apparsundaram, 2001 (140, 141))

Figure 17. Alignment of wild type and CHT K499Nfs*13 amino acid sequences showing premature truncation of the protein product, and the inclusion of 12 ectopic amino acid residues (ClustalOmega – http://www.ebi.ac.uk/Tools/msa/clustalo/).

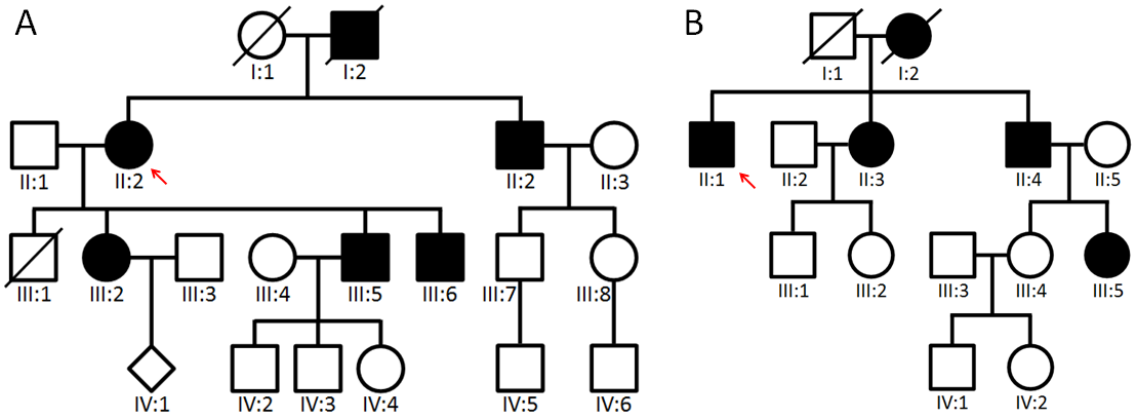

Figure 18. dHMN-VII-like family pedigrees A) family 2 B) family 3. Red arrows indcate affected individuals subjected to SLC5A7 sequencing.

3.2.1.4 Functional investigation of CHT p.K499Nfs*13

Experiments undertaken in collaboration with Prof Randy Blakely and Jane Wright in the United States.

Investigation of the functional impact of the *SLC5A7* c.1497delG (p.K499Nfs*13) variant on CHT was performed via heterologous expression of mutant (CHT p.K499N*fs13) and wild type (CHT WT) proteins in HEK-293 cells transiently transfected with the respective cDNA constructs (*SLC5A7*^{K499Nfs*13} and *SLC5A7*^{WT}) in a pRK5 vector (for cDNA transfection amounts see tables 36 and 37 appendix). As existing CHT antibodies target the C-terminus of the molecule, a hemagglutinin (HA; amino acid sequence 5'-YPYDVPDYA-3') tag was added to the N termini of both the mutant and wild type transporters by site directed mutagenesis using the Quick-Change kit, Stratagene. Cell surface biotinylation experiments and western blotting were carried out to investigate the expression and surface delivery of the two transporters, and [^{3}H]-choline transport assays were performed in order to compare the choline transport ability of the wild type and mutant molecules when expressed both individually and in combination. Choline transport activity was also measured in whole blood monocytes natively expressing CHT WT and CHT p.K499Nfs*13 collected from dHMN-VII affected individuals and healthy control individuals.

3.2.1.4.1 *SLC5A7*^{K499Nfs*13} alters CHT expression levels and surface delivery

Lysation of HA-*SLC5A7*^{WT} and HA-*SLC5A7*^{K499Nfs*13} transfected HEK-293 cells, followed by SDS-PAGE and immunoblotting with anti-HA antibody, shows that

the wild type protein migrates through the cells as two broad bands; a 48kDa band which represents an immature, core glycosylated species, and a 56kDa band which represents the mature, more highly N-glycosylated species (figure 19). CHT p.K499Nfs*13 is also shown to migrate as two species, however each as is of a smaller size than the wild type equivalent, confirming truncation of the mutant molecule (figure 19). For equivalent amounts of wild type and mutant cDNAs transfected, reduced levels of both the mature and immature protein products were observed in the HA-SLC5A7^{K499Nfs*13} transfected cells. Where double the amounts of transporter cDNAs were transfected, there is a comparable increase in CHT WT and CHT p.K499Nfs*13 protein, maintaining their relative differences in protein level.

Cell surface biotinylation experiments analysed by Western blot show the mature more substantially glycosylated form to be enriched in cell surface extracts (figure 20). When expressed individually, the surface levels of CHT WT and CHT p.K499Nfs*13 are comparable, despite differences in total expression levels. However, when the wild type and mutant cDNAs were co-expressed, the levels of total and surface protein for each transporter were significantly reduced in comparison to when these cDNAs were transfected individually. The reduction in expression is ~30% of that calculated from a simple addition of levels from individual transfections (students unpaired t-test, p=0.001, n=5). A transfection titration was carried out prior to these experiments to account for saturation of the cell's expression.

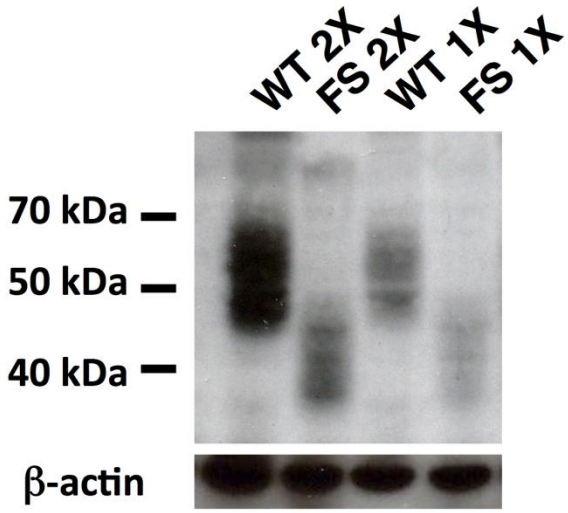

Figure 19. Total protein levels of HA-tagged CHT WT and CHT p.K499Nfs*13 in transiently transfected HEK-293 cells. Immunoblotting with anti-HA antibody of cell products run on SDS-PAGE confirms CHT p.K499Nfs*13 truncation and reveals reduced total protein expression of CHT p.K499Nfs*13 in cells transfected with both 2X (lanes 1 and 2) and 1X (lanes 3 and 4) cDNA (for amounts of DNA transfected see appendix). Stripping and blotting for β-actin reveals equal protein loaded across lanes. All experiments were conducted with the same total amount of transfected plasmid, balancing with pRK5 vector.

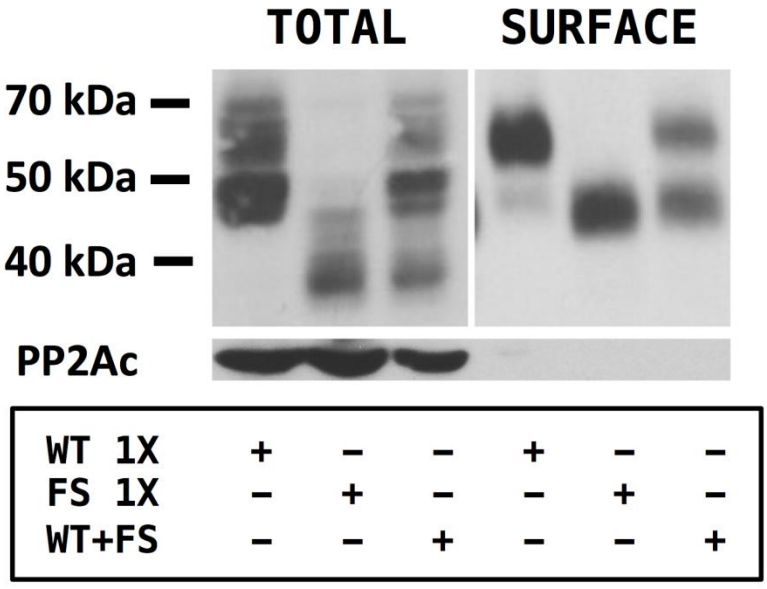

Figure 20. Total and surface levels of CHT WT and CHT p.K499Nfs*13 protein are reduced in cells co-transfected with both cDNAs at 1X levels compared to cells transfected individually at 1X levels. Stripping and blotting for PP2Ac reveals equal protein loaded across all lanes. All transfection were performed with identical amounts of total plasmid, balanced by pRK5 vector.

3.2.1.4.2 The p.K499Nfs*13 mutation significantly reduces choline transport activity in both transfected and patient cells

Saturation analysis of [^{3}H]-choline transport in HA-SLC5A7^{K499Nfs*13} transfected HEK-293 cells compared with HA-SLC5A7^{WT} transfected cells shows a 33.4% reduction in the choline transport activity of CHT p.K499Nfs*13. This reduction was accounted for by decrease in choline transport V_{MAX} (rate of transport) as opposed to a change in K_M ([^{3}H]-choline concentration) (figure 21).

Choline uptake assays showed that CHT specific uptake in cells with dual HA-SLC5A7^{WT} and HA-SLC5A7^{K499Nfs*13} cDNA transfections was significantly reduced compared to what would be expected from the summation of transport activity from cells individually expressing either CHT WT or CHT p.K499Nfs*13 (figure 22). Indeed, a far more severe impact of the c.1497delG variation arises when cells produce CHT proteins with mismatched C-termini, as is shown by the even further reduced CHT activity seen in cells co-expressing CHT WT and CHT p.K499Nfs*13 than that observed in cells transfected with CHT p.K499Nfs*13 alone. This suggests a dominant negative impact of the c.1497delG variant on CHT function.

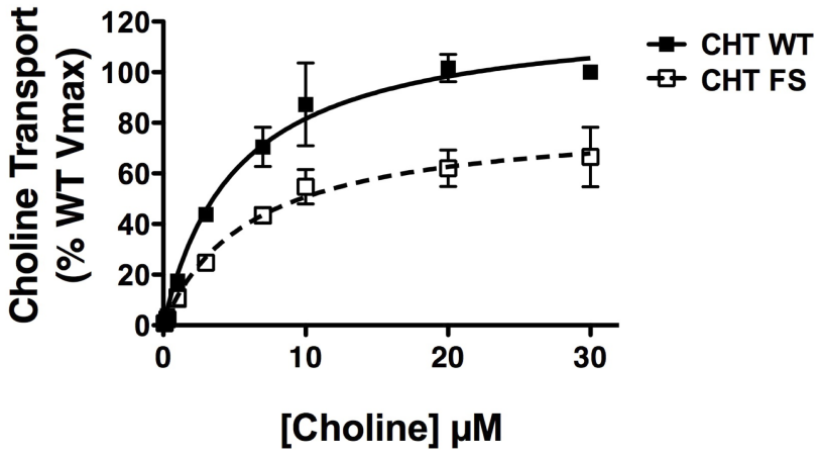

Figure 21. Saturation analysis of [3H]-choline transport activity in transfected HEK-293 cells demonstrates a significant reduction in transport activity for CHT p.K499Nfs*13 (CHT FS) compared to CHT WT. The reduced transport in CHT p.K499Nfs*13 transfected cells are accounted for by a reduction in choline transport V_{MAX} (33.4% reduction, p=0.024, student's unpaired t-test), and not a change in choline k_M (WT=5.15+/-1.12µM, FS=6.12+/-1.72µM, p=0.66, student's unpaired t-test). Specific choline uptake was determined by subtracting the uptake obtained in cells transfected with a mock vector (pRK5), from the uptake obtained from cells transfected with HA-SLC5A7^{WT} and HA-SLC5A7^{K499Nfs*13} cDNAs. Assays were conducted in parallel.

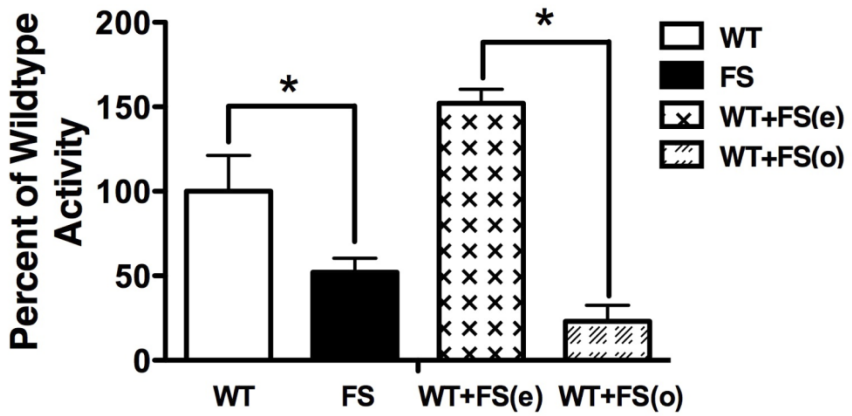

Figure 22. [3H]-choline transport activity is reduced in CHT p.K499Nfs*13 (FS) expressing HEK-293 cells compared to CHT WT (WT) expressing cells (*p=0.035, n=5, student's unpaired t-test). The transport activity observed in cells co-expressing CHT WT and CHT p.K499Nfs*13 (WT+$FS_{(O)}$) falls significantly below that expected (WT+$FS_{(e)}$) from a sum of the independent expression of these isoforms (*p=0.005, n=5, student's unpaired t-test).

Choline transport was measured in whole blood monocytes obtained from both affected subjects (n=4) and control individuals (n=11) in order to investigate whether a similar reduction in CHT activity exists in cells natively expressing CHT with the c.1497delG variant compared with cells natively expressing CHT WT (experiments carried out under assistance of Dr. Ajith Sreekantan-Nair, SGUL). Hemicholinium-3 (HC-3) sensitive choline transport was readily detected in CHT WT expressing cells from the control individuals (figure 23). In contrast, CHT activity was barely detectible in cells from affected individuals expressing CHT p.K499Nfs*13, a reduction even greater than that observed in the transfected cells. This is consistent with the severely reduced transport observed in cells co-transfected with cDNAs encoding both CHT WT and CHT p.K499Nfs*13, and supports the theory that the c.1497delG has a dominant negative impact on choline uptake activity.

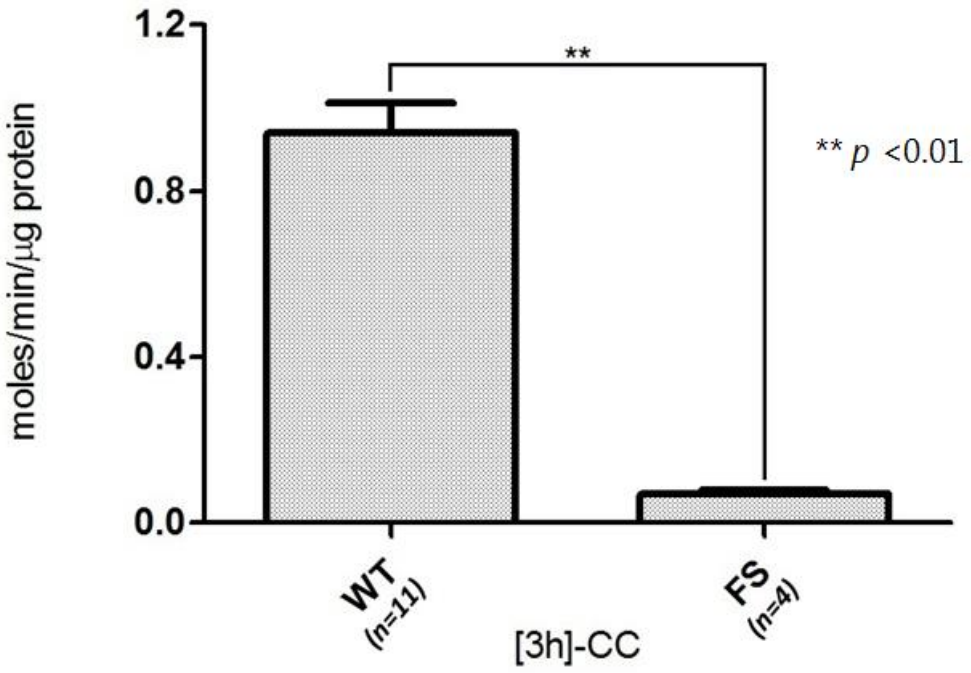

Figure 23. HC-3 sensitive choline transport activity in whole blood monocytes natively expressing CHT WT (n=11) compared with that in whole blood monocytes natively expressing both CHT WT and CHT p.K499Nfs*13 (n=4) reveals a dramatic loss (to 7.6% of controls) in dHMN-VII subjects (*p=0.72x10^{-6}, student's one-tailed t-test)

3.2.1.5 Electrophysiology recording in dHMN-VII subjects

The congenital myasthenic syndromes (CMSs) are a well recognised group of genetically heterogeneous neuromuscular disorders known to result from mutations in genes encoding presynaptic, postsynaptic, and synaptic NMJ proteins. One key characteristic of CMS is fatiguing muscle weakness with a pathological decrement on repetitive muscle stimulation or abnormal jitter and blocking on single-fiber EMG. Despite there being considerable difference in phenotype between CMS and dHMN-VII, the involvement of the NMJ in the pathogenicity of dHMN-VII prompted us to undertake specialist neuromuscular junction electrophysiology evaluation in two affected family members (table 20). This work was carried out by Dr. Meriel McEntagart, SGUL. Repetitive stimulation showed no significant decrement. EMG quantitative jitter studies showed an excess of jitter and blocking. This suggests disturbance of the NMJ but it is not clear if this is all secondary to reinnervation or if there is an element of primary disturbance of NMJ as well. The changes were less marked in the younger patient with less progressed disease.

Table 20. Fatigability and decrement EMG response

Subject	Age/Sex	Repetitive stimuation	Single fibre EMG
family 1_V:19	56y/M	Recording of right adm at rest and up to 1 min post activation showed no significant decrement.	Right edc: no spontaneous activity, an excess of complex polyphasic units on volition, quantitative jitter studies showed an excess of units with jitter and blocking.
family 1_VI:13	28y/M	Recording of right adm at rest and up to 1 min post activation showed no significant decrement.	Right edc: no spontaneous activity, an excess of stable polyphasic units noted on volition, quantitative jitter studies showed an excess of complex units with increased jitter and occasional blocking.

Abbreviations: **adm=**adductor digiti minimi; **edc=**extensor digitorum communis; **M**=male.

3.2.1.6 Identification of a second family (family 4), also from Wales, in which the same *SLC5A7* c.1497delG truncating mutation underlies dHMN-VII

Published in Practical Neurology: (Ingram G, Barwick KES, Hartley L, McEntagart MM, Crosby AH, Llewelyn G, Morris HR (2012): 0: 1-5): *Distal hereditary motor neuropathy with vocal cord paresis: from difficulty in choral singing to a molecular genetic diagnosis.*

A 52-year-old woman, proband (family 4_II:2, figure 24) and her 20-year-old daughter (family 4_III:2), both keen singers, reported a change in their voices when singing between the ages of 12 and 13 years, as if their voices were '*breaking like a boys at puberty'*. At age 15, the proband was diagnosed with a vocal cord nodule by an ear, nose and throat consultant and was referred for speech therapy. 2 years later her music college referred her for further ear, nose and throat review on the basis of hoarseness of voice and underwent partial thymectomy for a benign thymic tumour. However, her disorder continued to progress, and on more recent ear, nose and throat investigation family 4_II:2 was found to have a persistent glottic chink with poor opposition of the vocal cords due to bilateral vocal cord paralysis. Onset of motor problems did not occur until the proband was 27 years of age, following her first pregnancy when she experienced difficulty with tasks requiring manual dexterity such as changing her babies clothes and making him bottles of milk. Deterioration in hand function progressed gradually and later, she developed foot pain and calf cramps after walking as well as poor balance. Examination at

50 years after onset revealed hoarse voice but otherwise normal cranial nerves. She was also found to have bilateral weakness and atrophy of the small muscles of the hands with prominence at the thenar eminence (Figure 25), with no change in proximal strength, sensation or reflexes. High foot arches and clawing of the toes was present, but not true *pes cavus*. She displayed distal weakness of the lower limbs, especially on dorsiflexion, inversion and eversion.

Motor symptoms occurred earlier for family 4_III:2 than her mother when she also experienced difficulty with manual dexterity and suffered with hands cramps at age 14. Similarly to her mother, she experienced gradual deterioration in hand function with later progression to the lower limbs, presenting as walking induced foot pain, calf cramps and loss of balance. Both the proband and her daughter have retained independent mobility. Nerve conduction studies showed small motor action potentials and electromyography showed changes of distal chronic denervation consistent with motor neuropathy. Sensory action potentials and sensory and motor NCVs were within normal range. The clinical phenotype in this family is consistent with that of dHMN-VII.

Clinical review of the proband's mother (family 4_I:2) revealed mild weakness of the right first dorsal interosseous muscle of the hand, but no overall hand wasting or weakness. She also had high foot arches and clawing of the toes, but was considered to be clinically distinct from the proband and her daughter. The maternal aunt (family 4_I:1) had relatively high arches with toe clawing but did not display any weakness or atrophy. The proband's father (family 4_I:3) had right hand thenar wasting attributed to war injury problems in the left hand, feet or voice. He passed away in 1993 due to liver problems.

3.2.1.7 Genetic studies

Due to the diagnosis of dHMN-VII, the proband was screened and found to be a heterozygous carrier of the *SLC5A7* c.1497delG mutation. Genetic testing was not performed on any further family members.

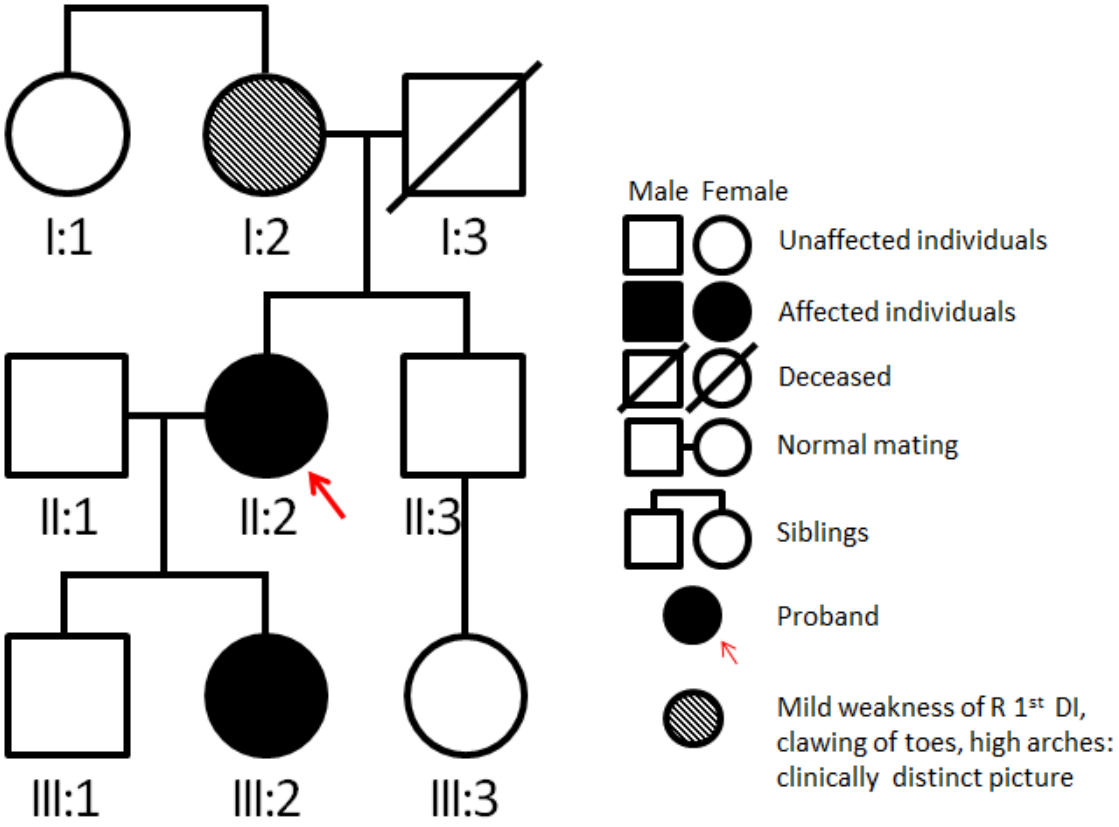

Figure 24. dHMN-VII family (family 4) pedigree

Figure 25. (A & B) Distal muscle wasting of family 4_II:2 in the small hand musculature giving a claw-like positioning of the hands. C) High arched foot and clawing of the toes in family 4_II:2. Modified (Ingram, 2016 (142))

PART B

3.2.2 Identification of a likely pathogenic, distinct *SLC5A7* truncating mutation in a family with dHMN-V (family 5) by targeted next generation sequencing

In preparation for publication: (Barwick KES, Wright J, Bower M, Russell MA, Blakely RD, McEntagart MM, Baple EL, Walk D, Crosby AH (2016)): *Dominantly-acting truncating mutations in SLC5A7 underlie adult onset dHMN*

Following our publication of *SLC5A7* mutation in dHMN-VII, we were contacted by Dr David Walk (University of Minnesota Medical Center, USA) to help with the interpretation and investigation of a putative *SLC5A7* sequence variant identified by clinical exome sequencing in a family under his care with individuals with a phenotype consistent with dHMN-V.

3.2.2.1 History and clinical findings in dHMN-V family 5 members

Clinical investigation of the dHMN-V family was carried out in collaboration with Dr David Walk, University of Minnesota Medical Center. At 27 years of age, family 5_IV:1 (figure 26) was referred with possible ALS following a 1-2 year history of progressive weakness in the hands. Sensory symptoms were absent and she claimed no prior history of weakness, developmental delay, or peripheral neuropathy. Neither was she aware of any family history of neurologic disease. Neurologic examination demonstrated normal mental state and cranial nerve examinations including voice were also normal. On motor examination family 5_IV:1 was found to have bilateral marked atrophy of the intrinsic hand muscles with normal tone and no fasciculations. On manual muscles testing (MMT), full strength was observed in all muscles required for shoulder abduction, elbow flexion, elbow extension, wrist extension, hip flexion, knee extension, knee flexion and ankle plantar flexion, and weakness was present in distal muscles as follows on the Medical Research Council (MRC) scale (table 21): bilateral mild loss of movement against resistance of the first dorsal interosseous (fdi) muscle involved in abduction of the index, middle and ring fingers from the midline of the hand; loss of rage of movement against resistance of the right abductor pollicis brevis (apb) muscle which functions as

an abductor of the thumb, and loss of range of movement both against gravity and resistance of the left; and a moderate loss of range of movement against resistance of the muscles responsible for ankle dorsiflexion. For manual muscle testing results please see table 22. She demonstrated normal perception to touch, vibration, and pinprick on sensory examination. Increased (brisk) reflexes were observed throughout, with vertical spread in the upper limbs. However, no clonus or Babinsky signs were present. Nerve conduction studies revealed markedly attenuated median and peroneal compound muscle action potentials (CMAPs) with normal conduction velocities and no focal motor conduction block, normal ulnar and tibial motor conduction studies, and normal sensory nerve action potential (*SNAP*) amplitudes. Needle electromyography demonstrated fibrillation potentials, reduced interference patterns, and high-amplitude long-duration motor unit potentials in distal muscles. Together these provide evidence of a pure motor neurogenic process without conduction block, and did not demonstrate uniform involvement of all motor nerves (tables 23-26). Immune-mediated neuropathies such as multifocal motor neuropathy were excluded from diagnosis with the use of an anti GM-1 ganglioside antibody test. IV:1 also received one dose of intravenous immunoglobulin, 1 gm/kg with no immediate improvement and chose not to continue this intervention; supporting the evidence that the disorder is not immune-mediated. Hexosaminidase A deficiency, *PMP22 and SOD1* mutations, and a number of other pathologies with similar presentations were omitted as possible causes by a range of tests including a urinary hexosaminidase-A assay, *SOD1* sequencing, cervical magnetic resonance imaging (MRI), cerebrospinal fluid (CSF) protein level measurements. The subject demonstrated no further progression of weakness over the following 6 years of follow up.

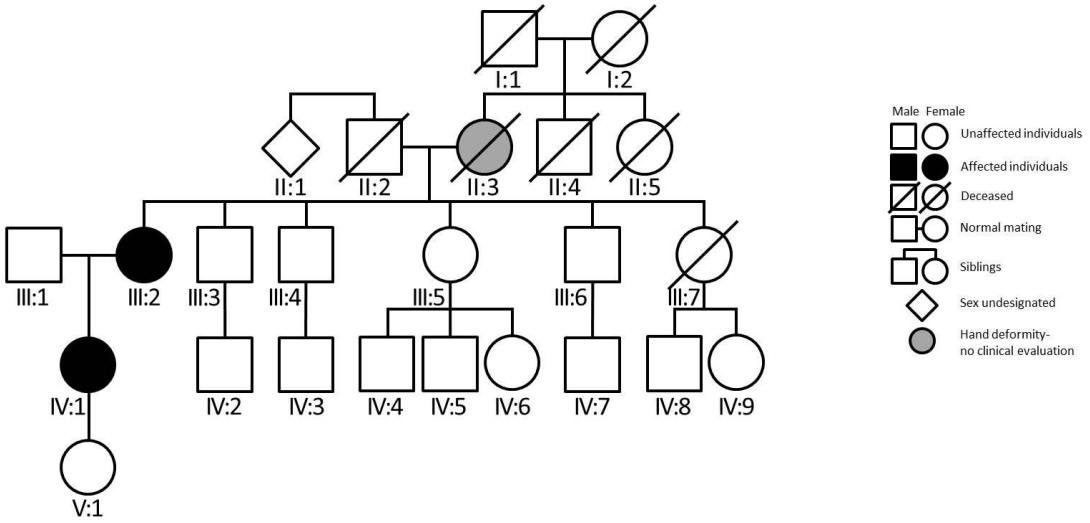

Figure 26. dHMN-V family (family 5) pedigree

More than a decade later, the subjects mother (family 5_III:2, figure 26) (60 years), presented with a 2-3 year history of gradually progressive bilateral weakness of plantarflexion of the ankle. Sensory symptoms, weakness of the proximal lower limbs, weakness of the upper limbs, and bulbar symptoms, were absent. Neurologic examination demonstrated normal mental state and cranial nerve examinations including voice were normal. On motor examination she was found to have slight atrophy of the intrinsic hand and feet muscles, with normal tone and no fasciculations. Similarly to family 5_IV:1, MMT revealed full muscle strength with the exception of the following: slight loss of range of movement against resistance of the left fdi, the left apb, and the left extensor digitorum communis (edc); moderate loss of range of movement in the right fdi and bilaterally in the muscles involved in ankle dorsiflexion; complete loss of range of movement against resistance but full range of movement against gravity of the left apb (table 22). Sensory examination of family 5_III:2 showed normal perception to touch and vibration, and demonstrated an ambiguous reduction in pinprick perception in her toes. Vertical reflex spread was observed in the upper limbs with no clonus, Babinski signs, or spasticity. Nerve conduction studies revealed weakened median, peroneal, and tibial CMAPs with normal conduction velocities and no focal motor conduction block, normal ulnar motor conduction studies, and normal SNAP amplitudes. Fibrillation potentials, reduced interference patterns, and high-amplitude long-duration motor unit potentials in distal muscles were demonstrated by needle electromyography. GM1 antibody, serum Lyme titer, vitamin B12 and copper

levels, cervical MRI, and CSF analysis were normal or negative. CSF analysis demonstrated a protein level of 42 mg/dl, glucose of 52 mg/dl, 2 white blood cells, 0 red blood cells, and negative oligoclonal bands. No paresis was observed and vocal cord function appeared normal on laryngoscopy.

The proband and her mother have been followed for 14 years and 2 years, respectively. With the exception of the development of median entrapment at the wrist, confirmed by electrodiagnostic study in family 5_IV:1, there were no clinically significant changes on examination in that time.

The patients reported that their mother/maternal grandmother (family 5_II:3) had a hand deformity late in life. However, they describe the appearance of the deformity as being different from their own, and suspect it was due to arthritis rather than atrophy. Family 5_III:2 has three living brothers and one sister, three of whom (family 5_III:3-5) have undergone neuromuscular examination and genetic testing according to a protocol approved by the University of Minnesota Institutional Review Board. None were found to have neuromuscular symptoms or findings of dHMN on examination. One demonstrated clinical and electrodiagnostic evidence of a sensory-predominant polyneuropathy, with normal needle electromyography in both distal and proximal muscles.

Table 21: Medical Research Councils manual muscle testing scale

Grade	Description
5	Muscle contracts normally against full resistance
4	Muscle strength is reduced but muscle contraction can still move joint against resistance
3	Muscle strength is further reduced such that the joint can be moved only against gravity with the examiner's resistance completely removed. As an example
2	Muscle can move only of the resistance of gravity is removed
1	Only a trace of flicker of movement is seen or felt in the muscle or fasciculations are observed in the muscle
0	No movement is observed

Table 22: Manual muscle testing

Muscle ↓	**Side**	**Grade (0 to 5)**	
Subject →		**family 5_IV:1**	**family 5_III:2**
fdi	Rt	4	4
	Lft	4	4.5
apb	Rt	2	3
	Lft	3	4.5
Ankle dorsiflexion	Rt	4	4
	Lft	4.5	4
EDC	Rt		5
	Lft		4.5

Abbreviations and symbols: **fdi=** first dorsal interosseous; **apb**= abductor pollicis brevis; **edc=** extensor digitorum communis; **Rt=** measurement taken on right side; **Lft=** measurement taken on left side

N.B. All recordings in below tables taken from the right side

Table 23: Motor nerve conduction in family 5_IV:1

	Latency (ms)	Velocity (m/s)	Amplitude (mV)	Distance (cm)	Temp (°C)
Median nerve					32
Wrist - apb	3.6		0.54	8.0	
Elbow – wrist	7.7	47.6	0.52	19.5	
(normal range)		(49-64)			
Right common peroneal					30
Ankle - edb	8.8		0.33	8.0	
fh – ankle	15.5	33.0	0.29	25.4	
pf – fh	19.1	34.6	0.32	9.0	
(normal range)		(44+)			
Tibial nerve					30
Ankle - ah	3.6		5.09	8.0	
pf – ankle	11.2	48.2	3.4	36.6	
(normal range)		(41+)			
Ulnar nerve					33
Wrist – adm	3.2		8.55		
Be elb - wrist	5.9	57.4	7.03	15.5	
Ab elb – Be elb	7.5	64.4	7.10	10.3	
Axilla – Ab elb	9.5	60.0	6.59	12.0	
Erb – Axilla	13.2	73.0	6.66	27.0	
(normal range)		(49+)			

Abbreviations and symbols: **apb**= abductor pollicis brevis; **edb**= extensor digitorum brevis; **fh**= fibular head; **pf**= popliteal fossa; **ah**= abductor hallucis; **adm**= abductor digiti minimi; **Ab elb**= above elbow; **Be Elb**= below elbow; **Erb=** Erb's point

Table 24: F-wave analysis in family 5_IV:1

Nerve	F-Latency		
	Min F	**Max F**	**Mean F**
Tibial nerve			
Ankle – ah	50.2	57.2	51.6
Ulnar nerve			
Wrist - adm	25.5	33.8	29.5

Abbreviations and symbols: **Min F=** minimum F-latency; **Max F=** maximum F-latency; **Mean F=** mean F-Latency; **ah=** abductor halluces; **adm=** adductor digiti minimi;

Table 25: Sensory nerve conduction in family 5_IV:1

	Latency (ms)	Velocity (m/s)	Amplitude (mV)	Distance (cm)	Temp (°C)
Median nerve					33
Dig. II – wrist	2.4	58.3	39.36	14.0	
(normal range)		(45-70)			
Ulnar nerve					33
Dig. V – wrist	1.9	64.4	17.35	12.5	
(normal range)		(48-74)			
Sural nerve					30
Ankle –	2.5	55.0	41.26	14.0	
(normal range)		(46-64)			

Abbreviations and symbols: **Dig**= digit;

Table 26: Electromyography findings in family 5_IV:1

Muscle (Innervation)	Ins. act.	Spontaneous action		Amp.	Dur.	Poly.	Recruit.	Firing
		Fib/PSW	Fasc.					
Rt Triceps (Radialis, c6 C7 c8)	Incr.	1+	2+	++	++	0	Red.	Norm.
Rt Trapezius	Incr.	0	1+	++	++	2+	Mild red.	Norm.
Rt Biceps (Musculotaneous, C5 c6	Incr.	1+	1+	++	++	1+	Red.	Norm.
Rt Paravert T4	Incr.	1+	1+	++	++	1+	Norm.	Norm.
Rt Paravert T8	Incr.	0	1+	+	+	1+	Norm.	Norm.
Rt Paravert T12	Incr.	0	1+	+	+	1+	Norm.	Norm.
Rt Gastroc. caput med. (Tibialis, S1 s2)	Incr.	1+	2+	++	+	1+	Norm.	Norm.
Rt Tibialis anterior (Peroneus profundus, l4 L5)	Incr.	2+	1+	++	++	1+	Red.	Norm.
Rt Vastus lateralis (Femoralis, l2 l3 L4)	Incr.	0	1+	+	++	1+	Norm.	Norm.

Abbreviations and symbols: **Rt**= right; **Gastroc. Caput med**= Gastocnemius caput mediale; **Ins. Act.**= insertional action; **Fib**= fibrillation; **PSW**= positive sharp waves; **Fasc.**= fasciculation; **Amp.**= amplitude; **Dur.**= duration; **Poly.**= poly phasic potential; **Recruit.**= recruitment pattern; **Incr.**= increased; **+**= mild abnormality ; **++**= moderate abnormality ; **+++**= severe abnormality; **Norm**= normal; **Red.**= reduced

3.2.2.2 Targeted next-generation sequence analysis identifies a novel likely pathogenic variant in *SLC5A7*

In order to identify the gene mutation causative of this condition, family 5_III:2 was subjected to next generation sequence analysis, the data from which was run through a custom built pipeline allowing the production and use of targeted test panels. Specific analysis was undertaken of the following genes: *BSCL2, DCTN1, DNAJB2, GARS, HSPB1, HSPB3, HSPB8, IGHMBP2, PLEKHG5, REEP1, SLC5A7*, and *TRPV4*. Target regions were captured using the Illumina TruSight One^{TM} sequence capture and sequenced by Illumina HiSeq 2500. Of the 25 known motor neuropathy genes targeted for analysis, next generation sequencing identified only one potentially disease causing variant, a heterozygous 2 base deletion (c.1563_1564delCA: NM_021815.2) in *SLC5A7* (figure 27). Coverage across the exon harbouring the variant (exon 9) was >300x and about half of the reads contain the c.1563_1564delCA variant. Heterozygous presence of the mutation was confirmed in both family 5_III:2 and family 5_IV:1 by bi-directional di-deoxy sequencing (figure 28).

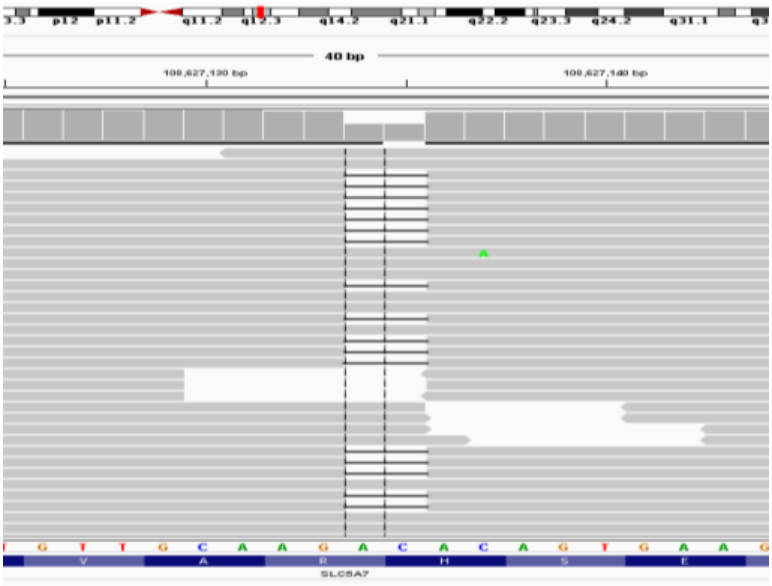

Figure 27. Next generation sequencing data for individual family 5_III-2 visualised in the integrative genome viewer (IGV). Coverage across the area of interest is >300x and half the reads contain a 2 base pair AC deletion.

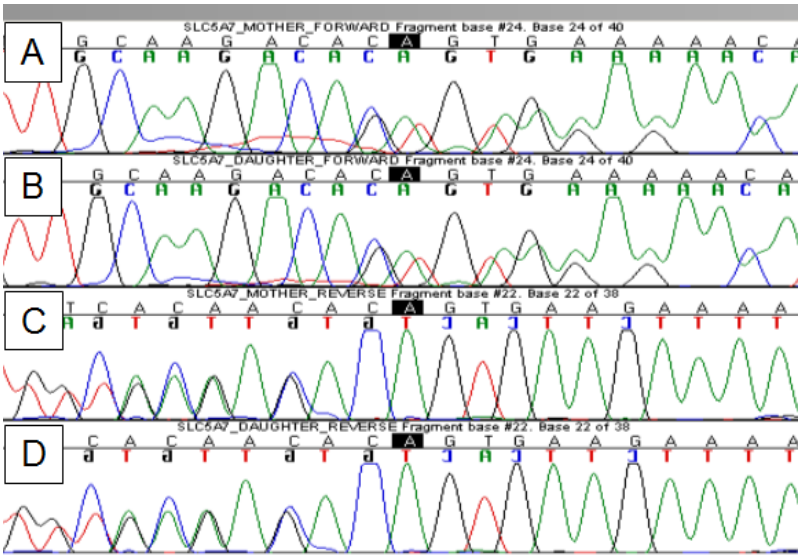

Figure 28. Chromatogram showing DNA sequence around the c.1563_1564delCA variant in (A) individual family 5_III:2 (forward strand); (B) individual family 5_IV:1 (forward strand); (C) individual family 5_III:2 (reverse strand); (D) individual family 5_IV:1 (reverse strand). The overlapping traces indicate the position of the frameshift variant.

3.2.2.3 *In silico* analysis of *SLC5A7* c.1563_1564delCA

As for c.1497delG, the amino acid sequence of *SLC5A7* c.1563_1564delCA was obtained by entering the coding (exonic) DNA sequence into the online ExPASy translate tool. The *SLC5A7* c.1563_1564delCA variant is also predicted to result in premature truncation of the protein at the C-terminus by 60 amino acids with the inclusion of 1 aberrant histidine residue (p.H521Qfs*2) (figure 29 and 30B). Conservation analysis indicated that the portion of the C-terminal that is lost contains residues that are highly conserved across many species (figure 49, appendix), and TMHMM analysis predicts a similarly profound effect on transmembrane morphology of the 3' terminus of the protein as c.1897delG in that it too is likely to interfere with the number or orientation of transmembrane domains (figure 50, appendix). *In silico* mutation analysis programs, PROVEAN and Mutation Taster predicted the variant to have deleterious effects on the protein function with scores of -14.155 and 0.999999999999999, respectively. *SLC5A7* c.1563_1564delCA was absent from dbSNP, 1000 Genomes Project, EVS and ExAC.

Figure 29. Alignment of wild type and CHT H521Qfs*2 amino acid sequences showing premature truncation of the protein product, and the inclusion of 1 (highlighted) ectopic amino acid residues (ClustalOmega - http://www.ebi.ac.uk/Tools/msa/clustalo/).

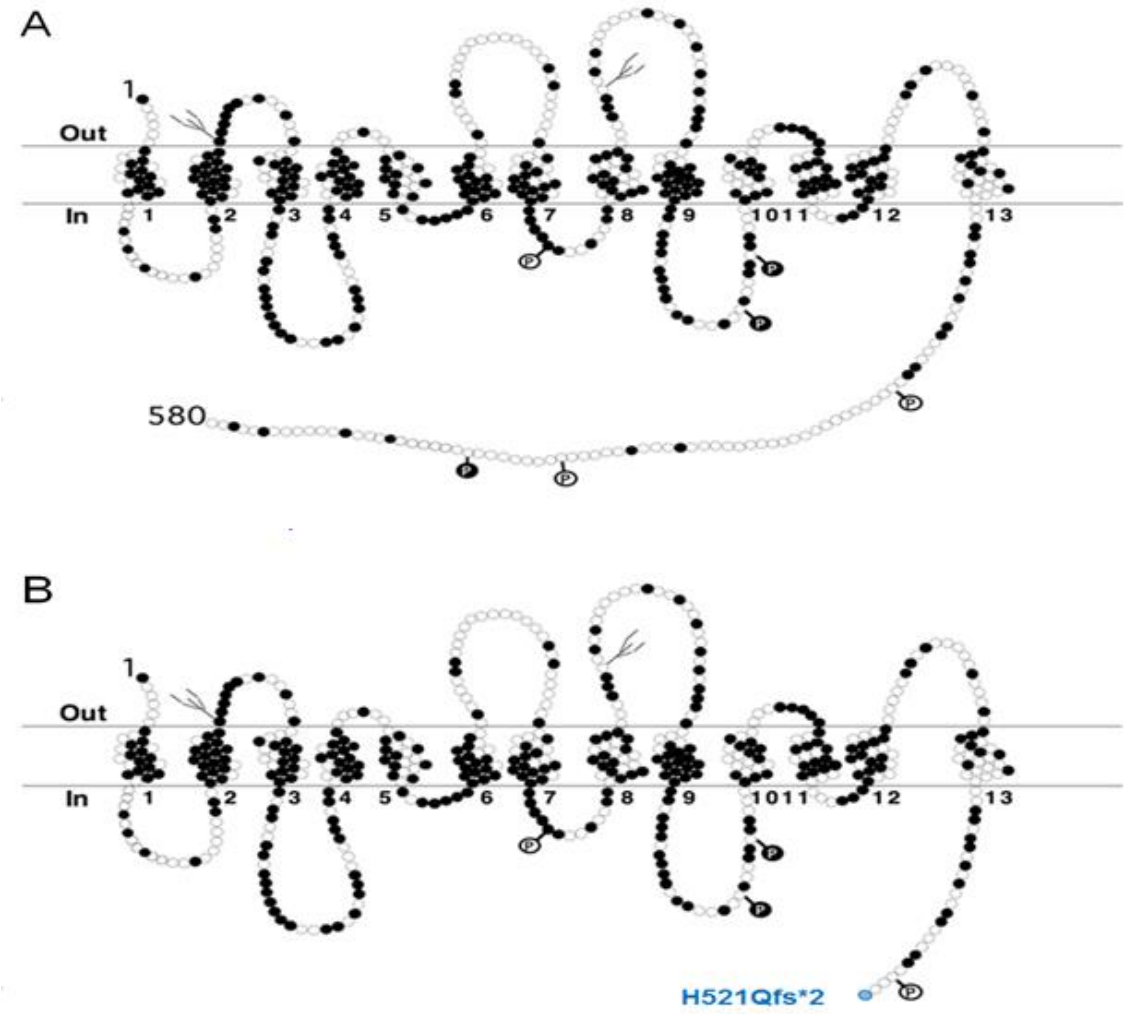

Figure 30. A) Diagram of the predicted secondary structure of the SLC5A7 gene polypeptide product (CHT) showing 13 transmembrane domains with an extracellular N-terminus, and an intracellular C-terminus. Dark circles represent amino acids which are conserved across human CHT, mouse Cht1, and the C. elegans CHT ortholog, CHO-1. Dark circles containing the letter 'P' indicate potential protein kinase C phosphorylation sites, and light circles containing the letter 'P' represent potential protein kinase A phosphorylation sites. The fork-like structures represent potential N-glycosylation sites. B) The blue circle represents the one aberrant amino acid encoded as a result of the c.1563_1564delCA variant followed by premature truncation of the cytoplasmic C-tail. Modified (Apparsundaram, 2000; Apparsundaram, 2001 (140, 141))

3.2.2.4 *SLC5A7*^{H521Qfs*2} truncates CHT, alters expression levels and reduces choline transport

In order to maintain experimental continuity, investigation of the impact of *SLC5A7* c.1563_1564delCA (p.H521Qfs*2) variant on CHT function was performed via heterologous expression of mutant (CHT p.H521Qfs*2) and wild type (CHT WT) proteins in HEK-293 cells transiently transfected with the respective cDNA constructs (*SLC5A7*^{H521Qfs*2} and *SLC5A7*^{WT}) in a pRK5 vector (for cDNA transfection amounts see tables 36 and 37 in appendix) in Prof Blakely's laboratory. Mutant cDNA constructs were produced using the QuickChange Lightning Site-Directed Mutagenesis kit (for SDM primer sequences see appendix). These experiments were undertaken in parallel with those involving the *SLC5A7* c.1497delG (p.K499Nfs*13) variant. Again, a HA-tag was added to the N-termini of both the mutant and wild type transporters by site directed mutagenesis.

Preliminary western blot analysis of cell lysates of HEK-293T and HEK-293 cells transiently transfected with HA-*SLC5A7*^{WT}, HA-*SLC5A7*^{K499Nfs*13}, and HA-*SLC5A7*^{H521Qfs*2} cDNAs, confirms truncation of the CHT p.H521Qfs*2 mutant indicates equal levels of products were produced for equivalent amounts of cDNA transfected (figure 31) (for amounts of DNA transfected into HEK-293 cells see appendix). Two additional bands are present at a much higher molecular weight (between 120 and 140kDa for wild type) for both wild type and truncated proteins, especially visible in lysates from HEK-293T cells. These may represent CHT homodimers indicating that the ability of CHT to form homodimers is not affected by these mutations.

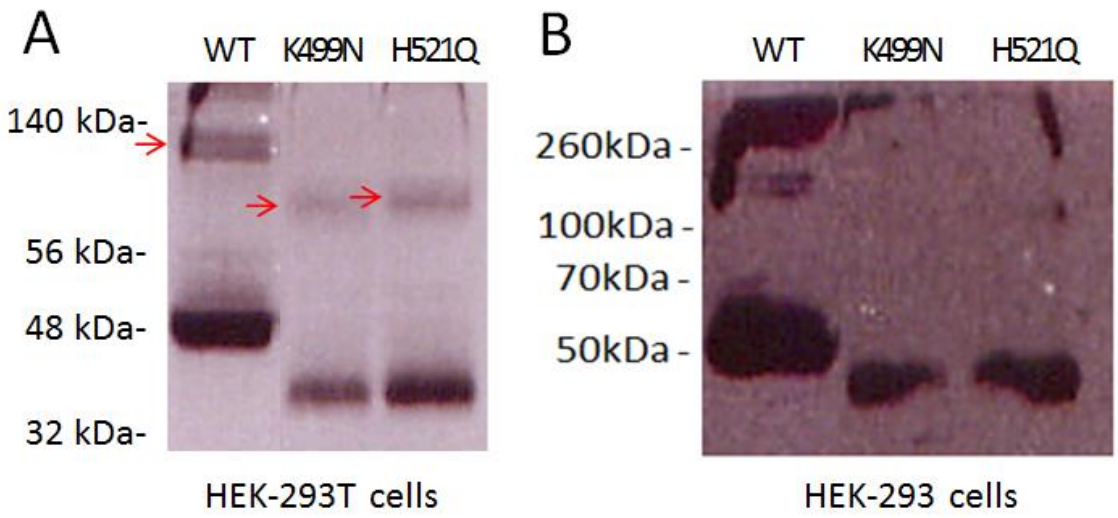

Figure 31. Preliminary western blot analysis of total protein levels of HA-CHT WT, HA-CHT p.K499Nfs*13 and HA-CHT p.H521Qfs*2 after SDS-PAGE and immunoblotting with anti-HA antibody of lysates from transiently transfected (A) HEK-293T and (B) HEK-293 cells. Truncation of HA-CHT p.H521Qfs*2 is confirmed. In A, two faint bands are visible for all proteins, between 120 and 140kDa in the wild type and between 80 and 100kDa in the lanes loaded with truncated proteins (indicated by arrows) which may represent CHT homodimers.

Preliminary choline uptake assays showed that CHT specific uptake in cell transfected with HA-*SLC5A7*^{H521Qfs*2} cDNA is ~50% of that in cells transfected with *SLC5A7*^{WT} (figure 32), similar to the reduced uptake activity observed in cells expressing HA-CHT p.K499Nfs*13.

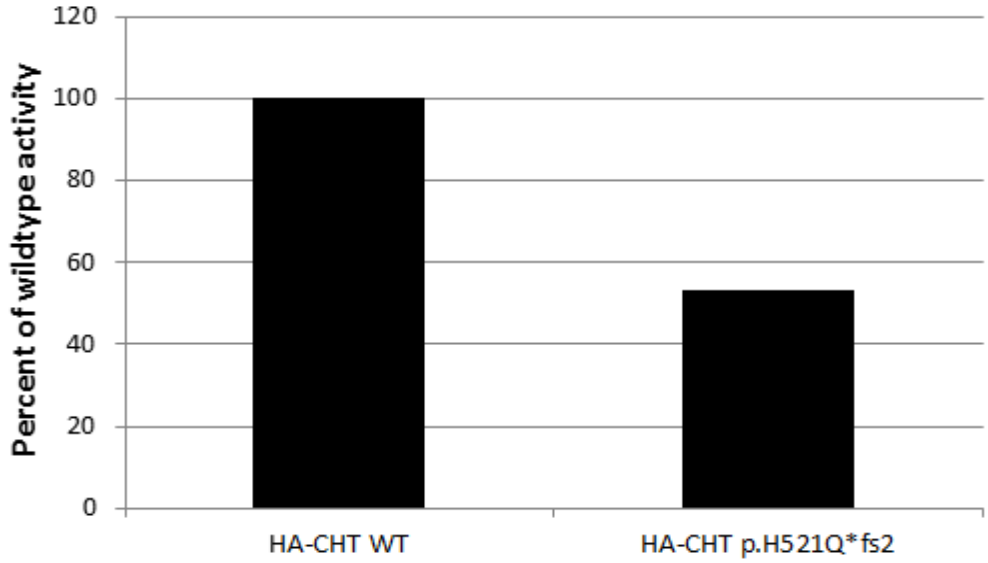

Figure 32. Preliminary choline uptake assay in HEK-293 cells transiently transfected with wild type and CHT p.H521Qfs*2 cDNAs. [3H]-choline transport activity is reduced in CHT p.H521Qfs*2 expressing HEK-293 cells compared to CHT WT expressing cells by ~50% (p=0.199, n=3, students unpaired t-test). This data is preliminary. Experiments are still underway.

3.3 Discussion

Whole-exome sequencing of one affected member of dHMN-VII family 1 with individuals with dHMN-VII identified novel variants within four genes (*SLC5A7* [MIM 608761], *PCDP1* [MIM N/A], *RNF149* [MIM N/A], *INHBB* [MIM 147390]) located within the critical region. Following cosegregation studies, four of the sequence variants identified could be excluded as each had not been inherited by at least one affected family member, indicating that each was present on the alternate (non-disease) allele in the individual investigated. Only one of the four variants was found to cosegregate with the disease phenotype and considered likely to be the pathogenic mutation, a single base deletion, c.1497delG, in *SLC5A7* encoding the Na+/Cl- dependent, high-affinity choline transporter (CHT). As well as other possible mutations located within the chromosome 2 locus that may have been missed by whole exome sequencing, an unlikely possibility also exists that there is a second region located elsewhere on the genome that also cosegregates with the disease phenotype and contains a pathogenic mutation. To exclude this possibility, whole-exome sequence analysis of a second affected subject was undertaken by Prof M Reilly and Prof H Houlden at the MRC Centre for Neuromuscular Diseases, Department of Molecular Neurosciences, UCL Institute of Neurology and National Hospital for Neurology and choline transport was measured in whole blood monocytes obtained from both affected subjects (n=4) and Neurosurgery (data not shown). This confirmed the c.1497delG variant as the only variant identified by both analyses, and strongly indicates that it is causative. Identification of a second Welsh dHMN-VII family (family 4) as carrying the c.1497delG mutation provides further evidence of this genetic variation as being causative of the disorder and indicates that both families are likely to be distantly related. These findings provide an important additional genetic test for patients with upper limb dominant distal hereditary neuropathy with vocal cord involvement, in addition to screening for *BSCL2* and *TRPV4* mutations.

SLC5A7 screening of families displaying dHMN-VII-like features (family 2 and family 3, figure 16) already found to be negative for *TRPV4* and *BSCL2* mutations, failed to detect novel sequence variants, indicating the existence of as yet undiscovered gene(s) that is(are) also responsible for this condition. Whole exome sequencing is now being undertaken in these families.

Targeted next generation sequence analysis run through a custom built test panel was carried out on one affected member of a third family (family 5) in the laboratory of Dr David Walk. Affected family members displayed a phenotype related to dHMN-VII present in the Welsh families (family 1 and family 4)), presenting with a dHMN-V which does not display vocal cord paralysis. This identified a second *SLC5A7* frameshift mutation (c.1563_1564delCA) which cosegregates with the disease phenotype and results in partial loss of the C-terminus of CHT.

CHT is a protein which consists of 580 amino acids predicted to comprise 13 transmembrane domains with an extracellular –NH2 terminus and an intracellular –COOH terminus(138, 143). CHT is enriched in motor neurones and nerve terminals(144) and is localised at the cell membrane(138). This Na+/Cl- dependent, high-affinity choline transporter is sensitive to hemicholinium-3(139) and is responsible for the choline uptake at NMJs, the rate limiting step in acetylcholine (ACh) synthesis(138, 139).

The *SLC5A7* c.1497delG variant is predicted to result in a translational frame-shift substituting lysine at amino acid position 499 for asparagine and going on to encode an additional 11 aberrant amino acids prior to a premature stop codon (p.K499Nfs*13). This alteration results in premature truncation of the protein, eliminating the transporter's ultimate 82 amino acids which is a near complete deletion of the protein's cytoplasmic C-terminus. The *SLC5A7* c.1563_1564delCA variant is also predicted to cause in a DNA reading frameshift resulting in the substitution of histidine at position 521 to glutamine followed immediately by a premature stop codon. This represents the loss of the ultimate 59 amino acids, partially eliminating the proteins C-terminus. The C-terminus amino acid sequence is highly conserved across species and encodes residues known to regulate surface trafficking(145): both evidence that loss of this domain is likely to have profound consequences on the transporter's function.

Online TMHMM software is a programme which uses the Hidden Markov model to predict the location and orientation of alpha helices in membrane spanning proteins. *In silico* TMHMM analysis of CHT WT compared with CHT p.K499Nfs*13 and CHT p.H521fs*2 suggests that both variants are likely to

alter the number of transmembrane domains of the protein, which, if the protein acts as a monomer, may change the orientation of the 3‘-terminus of the protein. Further evidence that these frameshift mutations are likely to have profound functional consequences.

Both frameshift mutations located in the last exon of the gene and therefore the transcript may not be subjected to nonsense-mediated mRNA decay (NMD). The NMD pathway mediates rapid down regulation of aberrant mRNAs that terminate translation upstream of the last splice junction(146). Following splicing, a multi-protein exon-junction complex (EJC) is deposited 20-24 nucleotides upstream of each exon-exon junction, which are then removed by the first translation event(146).If translation terminates >50-55 nucleotides upstream of the last exon-exon junction, one or more of the EJC‘s will remain associated downstream of the termination complex triggering rapid decay of the mRNA(146). If, as is likely the case in the c.1497delG and c.1563_1564delCA variants, translation is terminated <50-55 nucleotides upstream of the last exon-exon junction, no EJC‘s will remain associated and therefore NMD may be averted, potentially allowing the synthesis of the mutant molecule. While more accurate evaluation of this could be undertaken by quantitative PCR evaluations of cDNA generated from RNA extracted from patient cells, our sequencing of mRNA extracted from the blood of an affected dHMN-VII subject revealed the presence of the variant in the cDNA in approximately equimolar amounts (figure 14), providing supporting evidence that the c.1497delG variant may escape NMD and be translated to produce mutant protein.

The functional impact of the c.1497delG variant was investigated in HEK-293 cells transiently transfected with human *SLC5A7* WT and *SLC5A7* c.1497delG cDNAs. Unfortunately the only anti-CHT antibodies available target the C-terminus of the transporter, preventing their use in this investigation due to loss of the C-terminus associated with the CHT mutations. Consequently, an HA-tag was added to the N-termini of both the CHT WT and CHT p.K499Nfs*13 constructs in order to detect the proteins using western blotting. The wild type protein migrates as two species: an immature 48kDa core-glycosylated species and a mature 56kDa N-glycosylated species. The CHT p.K499Nfs*13 transporter can also be seen to migrate as two distinct species, which as expected are smaller (~38kDa and ~47kDa), confirming expression of the

truncated protein in these cells. For equivalent amounts of cDNA transfected, both at 1X and 2X, reduced levels of both the mature and immature species were observed in CHT p.K499N*13 expressing cells compared with the CHT WT expressing cells, indicative of reduced translation or stability of the CHT p.K499Nfs*13 transporter. The [3H]-choline uptake assays revealed a significant reduction in choline transport activity in heterologous CHT p.K499Nfs*13 expressing HEK-293 cells compared with the wild type expressing cells. This was accounted for by a reduction in choline transport V_{MAX} (CHT activity) and not choline K_M (a variation in choline concentration), confirming that the c.1497delG variant has a negative impact on CHT p.K499Nfs*13 transporter function. Interestingly, CHT activity observed in the uptake assays undertaken on HEK-293 cells co-expressing the two isoforms was found to be reduced significantly below that expected from the summation of transport activities from cells independently expressing CHT WT and CHT p.K499Nfs*13. This suggests that the CHT p.K499Nfs*13 exerts a dominant-negative impact on total and surface protein for both CHT isoforms. Activity seen with dual transfection was reduced even when compared to activity in cells transfected with *SLC5A7* c.1497delG alone, showing that the severity of the functional effect of the c.1497delG variant increases when the cells produce CHT proteins with mismatched C-termini. When the mutant and wild type cDNAs were co-transfected in equal amounts (1X), the combined surface levels of the two transporters were reduced greatly compared to that expected from the summation of the levels observed when the same amount of the two cDNAs were transfected individually, providing further evidence for a dominant-negative impact of the c.1497delG variant on CHT function.

When measuring choline transport in whole blood monocytes natively expressing the *SLC5A7* c.1497delG variant, obtained from affected subjects, choline transport was impacted even more significantly and barely detectable compared with that in whole blood monocytes of unaffected control individuals. This is consistent with the greatly reduced transport observed in HEK-293 cells co-transfected with both *SLC5A7* WT and *SLC5A7* c.1497delG. This, coupled with our studies in transiently transfected HEK-293 cells, provides robust evidence that the c.del1497 variation is the disease causing gene mutation in dHMN-VII, and that there is a dominant-negative impact of the mutation on

transporter function as opposed to the effects expected due to haploinsufficiency alone.

Preliminary choline uptake assays in HEK-293 cells individually transfected with wild type CHT cDNA, and CHT cDNA encoding the p.H521Qfs*2 mutant identified in dHMN-V family (family 5) revealed a reduction in choline uptake activity of CHT p.H521Qfs*13 to ~53% of that of the wild type, similar to that seen in cells individually transfected with CHT p.K499nfs*13 cDNA. Choline uptake assays in cells dually transfected with wild type and p.H521Qfs*2 cDNAs are currently ongoing. However, due to the phenotypic similarity between the dHMN-VII and dHMN-V families, the similarity in the predicted outcome of the two truncating mutations, and the similarity in functional effect observed in these preliminary studies, it is likely that there will be a similar outcome in cells dually transfected with wild type and p.H521Qfs*2 cDNAs as that seen in cells transfected with CHT wild type and CHT p.K499Nfs*13 cDNAs. Consequently the p.H521Qfs*2 mutant molecule may also be likely to exert a dominant-negative mode of action leading to a greater reduction in choline uptake activity compared to single transfections. In light of the slightly milder phenotype observed in the dHMN-V family (family 5) compared to the dHMN-VII families (families 1 and 4), and our knowledge that CHT p.H521Qfs*2 mutation spares residues of the proteins C-terminus that CHT p.K499Nfs*13 does not, perhaps the H521Qfs*2 mutation permits for slightly greater transporter activity, resulting in the milder phenotype lacking VCP. Unfortunately we are unable to test this in whole blood monocytes as patient material is not available.

In 2012, Okuda and colleagues found that co-expression of wild type CHT with partially inactive mutants N301Q and I89A revealed inhibition of wild type uptake activity in a dominant-negative manner. Although these residues do not reside in the C-terminal tail like the CHT p.K499Nfs*13 and p.H521Qfs*2 mutations, this supports our findings that mutant CHT molecules can interfere with the wild type molecule when expressed heterozygously, which may be explained by evidence that CHT functions as a homo-dimer(116). Deletion of CHT amino acid residues 499, 502, and 503 at the N-terminus of the C-tail leads to a decrease in CHT activity (30, 35, and 75% of wild type, respectively)(147). All of these are lost as a result of the *SLC5A7* c.1497delG/p.K499Nfs*13 mutation which eliminates the transporters

cytoplasmic C-terminus reducing CHT activity by ~50% of the wildtype in transfected cells, and resulting in the dHMN-VII phenotype with VCP in human carriers. On the other hand, deletion of residue 510 and 550 both result in an increase in uptake activity (120%)(147). These residues are lost as a result of both dHMN causing *SLC5A7* mutations. The authors have not commented on the effects of the above variants when expressed with the wild type. However, the increase in uptake activity associated with their deletion seems at odds with the loss of uptake activity resulting from partial or complete loss of the C-terminus, although it is not possible to draw strict correlations due to the different nature of each mutation. These findings indicate the necessity of 10 or less amino acids located at the stem of the cytoplasmic C-terminus for choline uptake activity(147). Evidence also suggests a negative effect on uptake of residues located closer to the C-terminus. CHT harbours a motif on the its C-terminus (I530,L531) similar to an acidic residue-flanked dileucine motif on the cytoplasmic C-terminus of VAChT, on which VAChT internalisation and sorting to the synaptic-like microvesicles (SLMVs) in PC12 cells is dependent(32). As it is also present on the membrane of a subpopulation of VAChT-positive synaptic vesicles, it is likely that CHT and VAChT share this common structural motif, and possibly more, for endocytic targeting to synaptic vesicles. This motif is eliminated from both the truncated proteins underlying dHMN and it is thus possible that disrupted endocytosis and vesicular sorting contribute to the dHMN phenotype.

Ruggiero *et al.* (2012) identified two sequences in the hCHT C-terminus that drive constitutive endocytosis(3). A primary endocytic motif (SEENMDKTILV-1° Motif) between CHT amino acids S522 to V532 contains a dileucine-type motif and is essential for CHT dynamin-dependent endocytosis(3). A secondary motif (DELAL-2° Motif) between D540 and L544 supports enhanced surface expression of CHT but doesn't exhibit a dominant capacity for surface trafficking(3). Both the CHT truncating mutations we have identified in dHMN result in the complete elimination of both SEENMDKTILV-1° and DELAL-2° motifs suggesting that these mutations may lead to impaired choline uptake due to the loss of dynamin-dependent endocytosis. It has also been suggested that residues 560-577 within the C-tail, also lost in dHMN subjects, may be involved in internalisation of CHT from the cell surface and in recycling of internalised

CHT back to the surface(147); possibly these residues represent a motif required for protein kinase C (PKC)-dependent CHT internalisation and thus another possible contributing factor to the reduction of CHT activity in dHMN subjects.

NMJ dysfunction has not previously been implicated in the distal hereditary motor neuropathies. However, it is a well-recognised cause of a genetically heterogeneous group of neuromuscular disorders known as the congenital myasthenic syndromes (CMS). CMS is known to result in mutation in genes that encode pre-, post and synaptic proteins at the NMJ such as choline acetyltransferase (CHAT), ACh receptors (AChRs), receptor associated protein of the synapse (RAPSN), and downstream of kinase 7 (DOK7)(148-152). CMS does not share any apparent phenotype with dHMN-VII or dHMN-V. Features of CMS include opthalmoparesis, ptosis and bulbar weakness and as suggested in the name, onset of CMS is usually at or before birth. The lack of phenotypic overlap between CMT and dHMN subjects is unexpected and prompted us to carry out electrophysiology (table 20) studies in two affected dHMN-VII family members (family 1_V:19 male 56y; family 1_VI:13 male 28y, figure 10). Repetitive stimulation did not show a significant decrement and single fibre EMG showed an excess of jitter and blocking which is suggestive of disturbance of NMJ function (data not shown) but such changes could also be secondary to reinnervation. The changes were less marked in the younger of the two subjects who has less progressed disease. Vocal cord paresis, presenting as congenital stridor (a harsh grating or vibrating sound when breathing) is a feature of CMS that is associated with mutations in *DOK7*, and less often with *CHAT*(153, 154). This suggests that it is possible that the differences between dHMN-VII and CMS may involve differences in the contribution made to NMJ signalling between CHT and the CMS related NMJ proteins.

Two forms of NMJ exist (see chapter 1.4.2.2), of which the *en plaque* twitch fibres have a role for CHT in sustained, high frequency ACh signalling. It is possible that the synapses affected in dHMN-VII and dHMN-V are more dependent on CHT due to a requirement for sustained, high frequency ACh release. Model system studies with HC-3 demonstrate a suppression of ACh release and cholinergic signalling only with sustained or higher frequency stimulation(32).

In summary, convincing genetic and functional evidence has been provided that a dominantly-acting *SLC5A7* mutation that results in near complete loss of the CHT transporter C-terminus underlies dHMN-VII in the families investigated. Moreover, we have identified a second dominant *SLC5A7* mutation, which also affects the C-terminus, resulting in partial loss of the ultimate 59 amino acids, as underlying dHMN-V. This gives rise to a possible novel disease mechanism in which CHT has role in idiopathic motor neuropathies. Knowledge of these mutations underlying dHMN-VII and -V provides a genetic test for disease risk in affected families, and may permit the development of targeted pharmacotherapies (see chapter 5).

4

CHAPTER FOUR

N-TERMINAL AUTOSOMAL RECESSIVELY-ACTING *SLC5A7*/CHT MISSENSE MUTATIONS ASSOCIATED WITH SEVERE CONGENITAL HYPOTONIA

4 N- TERMINAL AUTOSOMAL RECESSIVELY-ACTING SLC5A7/CHT MISSENSE MUTATIONS ASSOCIATED WITH SEVERE CONGENITAL HYPOTONIA

4.1 Introduction

Hypotonia is a term used to denote diminished tone of skeletal muscle in the limbs, trunk, or craniofacial muscles, associated with reduced resistance of muscles to passive stretching(155). Hypotonia is not however, a specific diagnosis, but part of a great number of distinct disorders, and its severity is extremely variable depending on the underlying aetiology. In clinical practice, the differential diagnosis of neonatal and infantile hypotonia is extremely broad and presents a diagnostic challenge, yet is crucial for prognosis, management and treatment(156). Infantile hypotonia can present due to abnormalities at all levels of both central and peripheral nervous systems including anterior horn cell disorders, congenital motor or sensory neuropathies and NMJ disorders; muscle abnormalities such as congenital myopathies and muscular dystrophies; and metabolic disorders affecting multiple systems (figure 33). As hypotonia is often the presenting sign for many benign and serious multisystem and nervous system diseases, a detailed history combined with full systemic, neurological and often genetic examination are critical in obtaining an accurate diagnosis. Despite extensive clinical and genetic examination, a lack of information regarding the genes and their respective pathways involved in neuromuscular function means a significant proportion of patients remain undiagnosed.

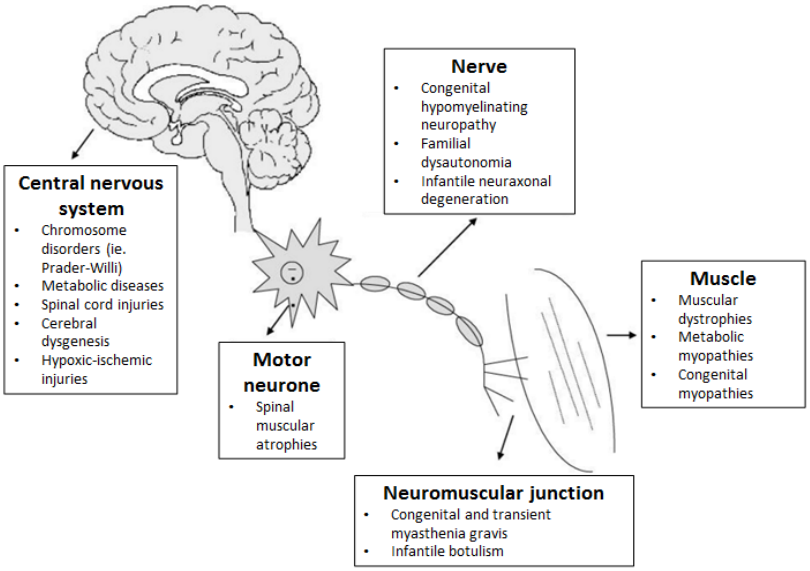

Figure 33. Schematic diagram of the anatomical-clinical correlation of infantile hypotonia, illustrating differential diagnosis. Modified (Leyenaar, 2005 (156))

When investigating the underlying cause of hypotonia in an infant, it is important to first distinguish whether the diminished muscle tone results from an abnormality in the CNS, the PNS, or an abnormality involving both systems(155). Clinical findings, in additional to hypotonia, suggestive of a CNS abnormality may include hyperreflexia, cognitive developmental delay, normal strength and seizures, where as those suggestive of PNS involvement or neuromuscular origin may include muscle weakness, muscle atrophy, lack of antigravity movements, fasciculations and diminished reflexes, usually with normal cognitive function(155). Genetic disorders associated with either congenital central, peripheral or combined hypotonia, their salient distinguishing features, and their genetic aetiology are detailed in the appendix. Loss of function mutations in *PRPS1,* causative of peripheral neuropathy CMT-5X (Rosenberg-Chutorian syndrome), have also been reported to cause Arts syndrome, a characteristic of which is congenital or early onset central hypotonia(157).

This chapter describes two consanguineous families affected by a severe congenital neuromuscular disorder presenting as combined (predominantly) central and peripheral hypotonia that have not previously been described in the literature, and provide genetic and molecular evidence implicating two autosomal recessive missense mutations in *SLC5A7* that result in complete elimination of CHT choline transport as being causative.

4.2 Results

4.2.1 Identification of a autosomal recessive mutations in *SLC5A7* in two consanguineous families with severe congenital hypotonia

In preparation for publication: (Wang H, Barwick KES, Wright J, Zimmerman HH, Karakaya M, Stüve B, Weis J, Russell MA, Wirth B, Abdul-Rahman OA, Blakely RD, Baple EL, Cirak S, Crosby AH (2016)): *Recessively-acting choline transporter mutations associated with severe neurodevelopmental delay and congenital hypotonia.*

4.2.1.1 History and clinical pathological features in Turkish hypotonia family (family 6)

A 2.5 year old female presented with severe developmental delay (family 6_IV:1, figure 34). Born at 32 weeks from gestation because of pathologic cardiotocography- a similar technology to echocardiography in that Doppler ultrasound is used to provide information on foetal heart rate- after an uneventful pregnancy. Birth weight was 1676g (50^{th} centile), and head circumference was 30cm (60^{th} centile). During postnatal period, respiratory insufficiency and lack of spontaneous movements, especially in the distal extremities were noted. In addition to diffuse hypomotoric activity, lack of eye movements and difficulties in swallowing suggested in involvement of the cranial nerves. On examination, severe generalised central hypotonia and muscle atrophy were present. Due to bulbar and respiratory insufficiency tracheostomy and gastrostomy were required during the first month of life. The child did not demonstrate any milestones within the speech, cognitive or motor domains. Remarkably, she had some spontaneous and nonpurposeful antigravity movements although she is unable to follow objects with her eyes, or react to stimuli. Metabolic work up including serum and urine amino acids, serum acyl-carnitine profile, serum creatine and cerebro-spinal fluid lactate levels were normal. No cardiac involvement or organomegaly (unusually large organs) were noted on echocardiography and abdominal ultrasound. The electroencephalogram showed reduced brain activity but no pathological discharges, and studies of evoked potentials were normal. Nerve conduction studies with repetitive stimulation revealed no responses from both median and

tibialis nerves. Cranial magnetic resonance imaging in the newborn period showed general atrophy of the brain (data not shown). A muscle biopsy showed myopathic changes with increased connective tissue and atrophic fibres together with core-like areas on electron microscopy (data not shown). This shows that despite the clinical presentation being dominated by central hypotonia, there is a degree of muscular weakness due to transmission defect on the presynaptic membrane of neuromuscular junction. The child is now almost 4 years of age.

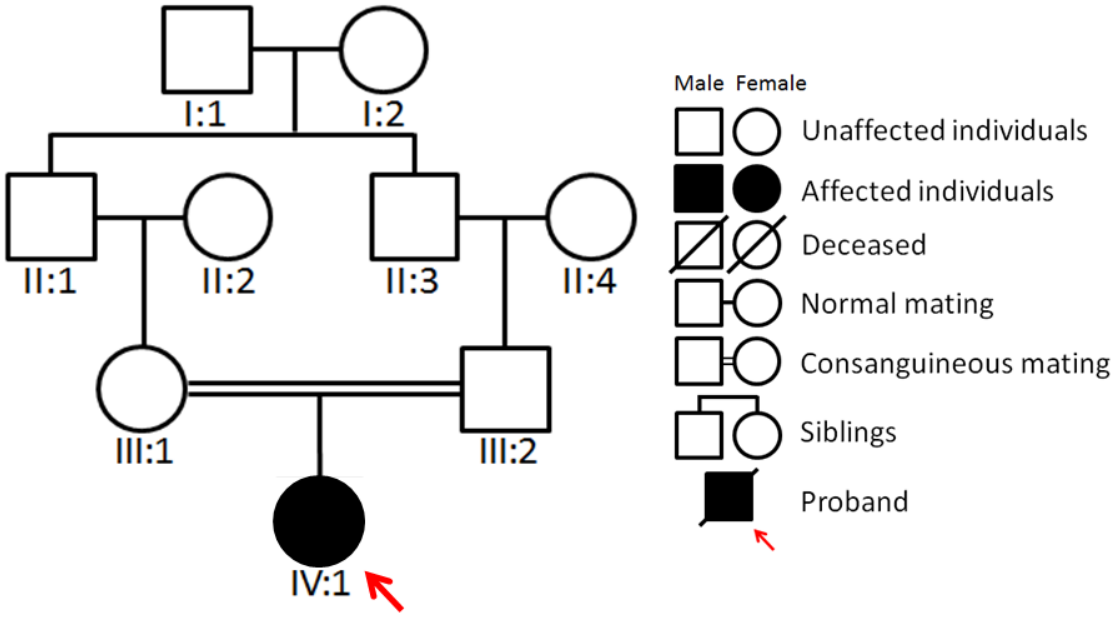

Figure 34. Turkish hypotonia family (family 6) pedigree

4.2.1.2 History and clinical pathological features in Hispanic hypotonia family (family 7)

A Hispanic male (family 7_V:3, figure 35) was born with a severe neuromuscular disorder and passed away aged 5 months. He displayed poor respiratory effort requiring a tracheotomy and ventilation. Brain magnetic resonance imaging (MRI) was normal (figure 36). Electromyography (EMG) indicated possible neuromuscular junction (NMJ) disorder with possible severe myopathy. Repeat EMG with a subdermal needle demonstrated widespread fibrillation in limb and trunk muscles with no voluntary motor unit activity. Metabolic testing, including amino acids (performed on plasma, urine and CSF), lactate and pyruvate (blood and CSF), creatinine/GAA (blood and urine),

carnitine/acylcarnitine, urine organic acids, and urine s-sulfocysteine, was normal or nondiagnostic. A neurochemistry panel was normal. Copy number of the *SMN1* gene was also normal. A SNP array of this patient revealed excessive homozygosity at 6% of the genome, consistent with the known consanguinity of the parents.

The family reported a similarly affected female sibling (family 7_V:1, figure 35) who was born a few years prior to family 7_V:3and passed away aged 10 months.

The family also reported a cousin to have a similar phenotype, however this patient is unfortunately also deceased and no clinical or genetic data available. For the clinical phenotypes of subjects family 7_V:1, family 7_V:3 and affected cousin, see table 27.

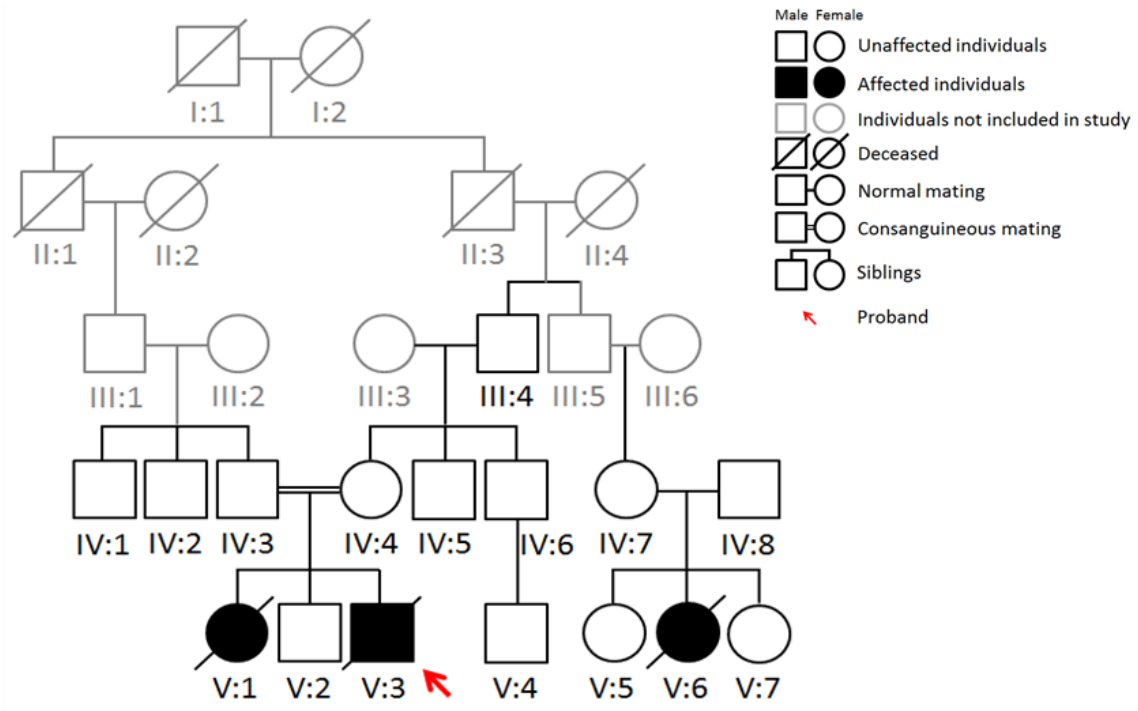

Figure 35. Hispanic hypotonia family (family 7) pedigree

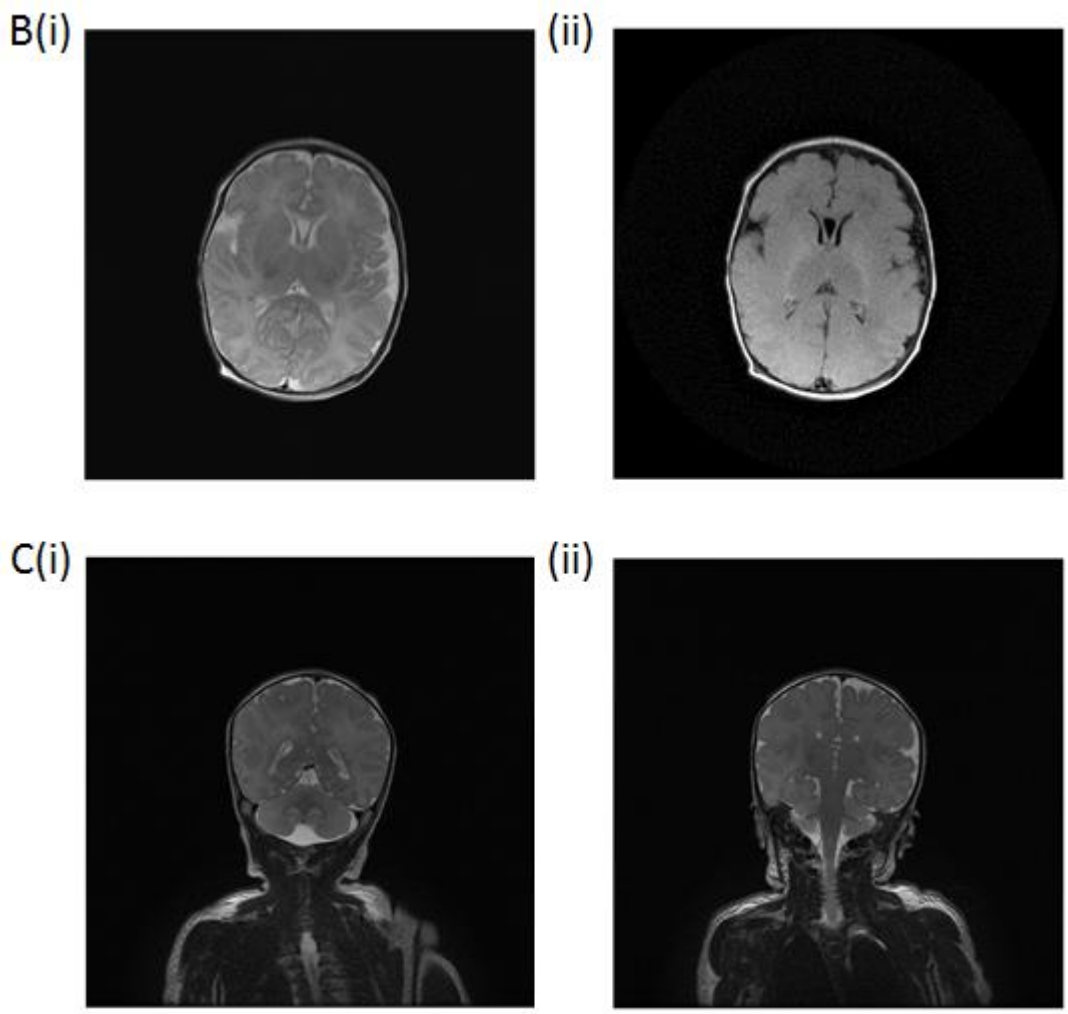

Figure 36. Brain MRI of family 7_V:3. Examination is degraded by patient motion. No significant intracranial abnormality is identified.

Table 27: Clinical phenotypes of family 7

	Proband (family 7_V:3) homozygous for *SLC5A7* c.335T>A	Full sister (family 7_V:1) homozygous for *SLC5A7* c.335T>A	Cousin (NOT TESTED)
Hypotonia	+	+	+
Stridor	+	+	
Poor respiratory effort/Respiratory support needed	+	+	+
Seizures	+	+	+
CK	198	168	20
EEG	Abnormal	Abnormal	Abnormal
EMG	Neuromuscular junction defect	Neuromuscular transmission defect	Neuromuscular transmission defect in UE and LE; diffuse myopathy
Head imaging	Normal MRI	Normal HUS	Normal HUS; initial brain MRI showed increase signal in the pituitary; f/u MRI showed cavum septum pellucidum
Muscle biopsy	Muscle atrophy	Muscle atrophy	myopathy
Death	6.5 months	11 months	11 months
Autopsy	Consistent with neuromuscular disorder	N/A	
Other details	Bowel perforation/obstruction	Bowel perforation	nystagmus
Previous Work-up (normal)	SNP array showed AOH (~6%); normal plasma amino acids, normal lactate/pyruvate, normal urine organic acids, normal urine s-sulfocysteine, normal creatine/ guinodinoacetate, normal carnitine/acylcarnitine, normal neurochemistry panel, normal SMA	Normal newborn screen, normal 60K array, normal plasma amino acids, normal urine organic acids, normal lactate/pyruvate, normal SMA	Normal echo

Abbreviations: **CK=** Creatine kinase; **EEG=** Electroencephalogram; **EMG=** Electromyography; **+ =** present; **MRI=** Magnetic resonance imaging; **HUS=** Head ultrasound scan; **AOH=** Absence of heterozygosity; **SMA=** spinal muscular atrophy.

4.2.2 Exome sequencing and mutation identification

In order to define the disease causing mutation in each family, a single affected individual (family 6_IV:1, figure 34) from the Turkish hypotonia family, family 6, and three individuals (family 7_V:3, family 7_IV:3 and family 7_IV:4) from the Hispanic hypotonia family, family 7, were subjected to whole-exome sequencing analysis to generate novel variant profiles. Exome sequencing of these families was carried out in collaboration with Dr Sebahattin Cirak at Uniklinik Köln University Hospital, Germany and Dr. Omar Abdulrahman and Holly Zimmerman, based at the University of Mississippi Medical Center, USA, for the Turkish and Hispanic families, respectively.

The exome from family 6_IV:1 was captured with SeqCap EZ Human Exome Library v2.0 kit (Roche NimbleGen) and sequenced on an Illumina HiSeq 2000 with a paired-end 2x100 bp protocol. On average, this resulted in >68 million of mapped unique sequences with a mean coverage of 92 i.e., 20x coverage for 92.9% of target sequences. Following filtering for homozygous variants and exclusion of all those with allele frequencies >0.1% in the population that do not occur within one of the homozygous intervals identified, one candidate variant was identified in family 6_IV:1; A single base substitution at chromosome 2:108608665 (*SLC5A7* c.282T>A) (figure 37A), encoding CHT.

The exome of family 7_V:3 and his parents, family 7_IV:3 and family 7_IV:4, was captured using the SureSelectXT Target Enrichment System for Illumina Paired-End Multiplexed Sequencing with the addition of 1800 clinically relevant disease genes, and sequenced on the Illumina HiSeq platform with a 100bp paired-end protocol. The following quality control metrics of the sequence data are generally achieved using this protocol: >70% reads aligned to target, >95% target bases covered at >20X, >85% target bases covered at >40X, >100X mean coverage of target bases. Whole-exome sequencing data was compared to Illumina HumanExome 12vI array data to assess sequencing quality, achieving >99% SNP concordance to genotype array. Exome sequencing identified a single base substitution at chromosome 2:108609470 (*SLC5A7* c.335T>A) that was present homozygously in family 7_V:3, and heterozygously in family 7_IV:3 and family 7_IV:4 (figure 37B). Dideoxy sequence analysis of

the affected sister of family 7_V:3, family 7_V:1, revealed homozygosity for the *SLC5A7* c.335T>A variant.

Each substitution cosegregates in each family consistent with an autosomal recessive mode of inheritance, and, whilst regional control samples remain to be investigated, neither variant is present in genomic databases: National Center for Biotechnology Information's (NCBI) dbSNP (http://www.ncbi.nlm.nih.gov/SNP/), the National Heart, Lung and Blood Institue's (NHLBI) Exome sequencing project (ESP6500) via the Exome Variant Server (EVS) (http://evs.gs.washington.edu/EVS/ , Aggregation Consortium (ExAC) server (http://exac.broadinstitute.org/), or 1000 genomes database (http://www.1000genomes.org/).

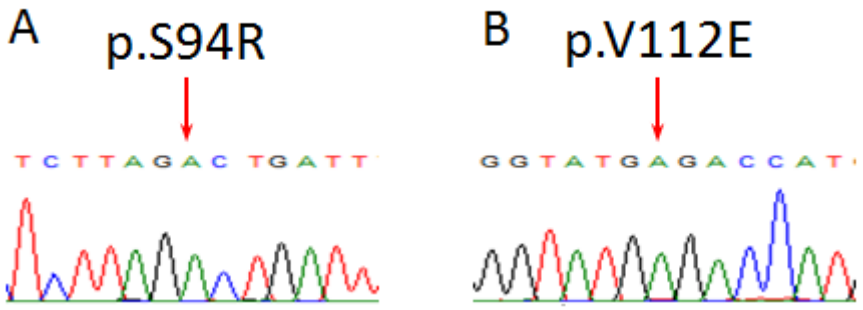

Figure 37. Chromatograms showing DNA sequence around A) the homozygous SLC5A7 c.282T>A variant in an affected individual (family 6_IV:1), and B) the homozygous SLC5A7 c.335T>A variant in affected individual (family 7_V:3), acquired by dideoxy-sequencing of genomic DNA.

4.2.3 *In silico* analysis of *SLC5A7* missense mutations

As previously, the amino acid sequence for the mutant protein was obtained using ExPASy translate software. At the nucleotide level, the *SLC5A7* c.282T>A variant is predicted to result in an amino acid substitution from serine at position 94 to arginine (p.S94R) (figure 38) affecting a residue in the third transmembrane domain of CHT (figure 39). The *SLC5A7* c.335T>A variant is predicted to result in an amino acid change from valine at position 112 to glutamic acid (p.V112E) (figure 38) affecting a residue located on the second intracellular loop between transmembrane domains 3 and 4 (figure 39).

Conservation analysis indicates that both substituted residues display high evolutionarily sequence conservation (figure 51, appendix).

In silico mutation analyses on the predicted effect of both variants on the structure and function of CHT show high damage prediction but do not predict a change in structure. PROVEAN predicted both variants c.282T>A and c.335T>A to have a deleterious effect on the function of the protein products with scores of -4.90 and -5.606, respectively. PolyPhen and Mutation Taster also predicted damaging or disease causing effects on protein function for both variants (table 28). TMHMM analysis predicted no effects of these variants on the transmembrane morphology of CHT (figure 52, appendix). An amino acid substitution at position 112 from valine to alanine (V112A) is reported in ExAC, however at an extremely low frequency ($8.25e^{-06}$) and there are no reports of homozygous cases.

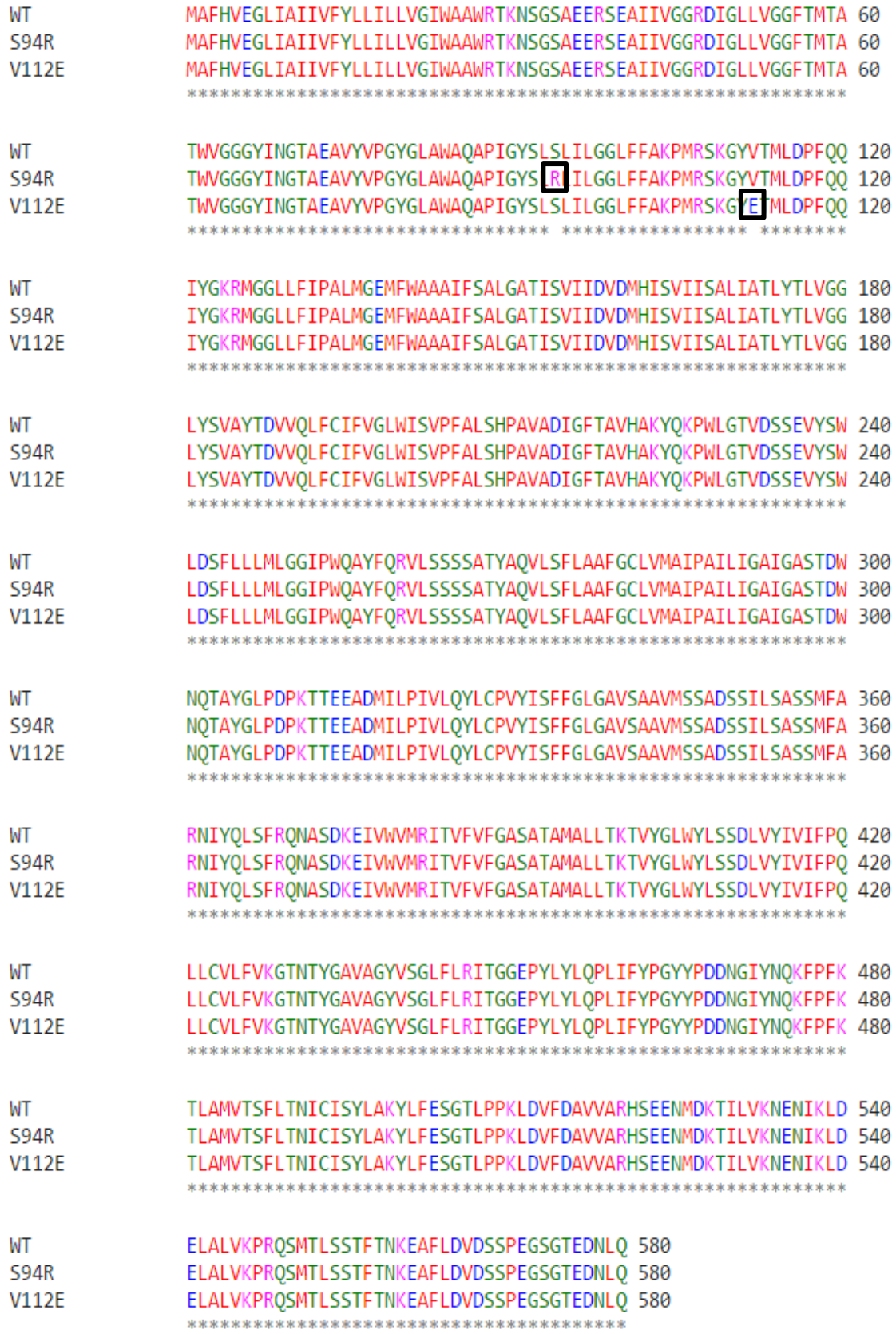

Figure 38. Alignment of wild type and CHT p.S94R and p.V112E amino acid sequences showing single residue substitutions S94R and V112E, respectively (ClustalW2).

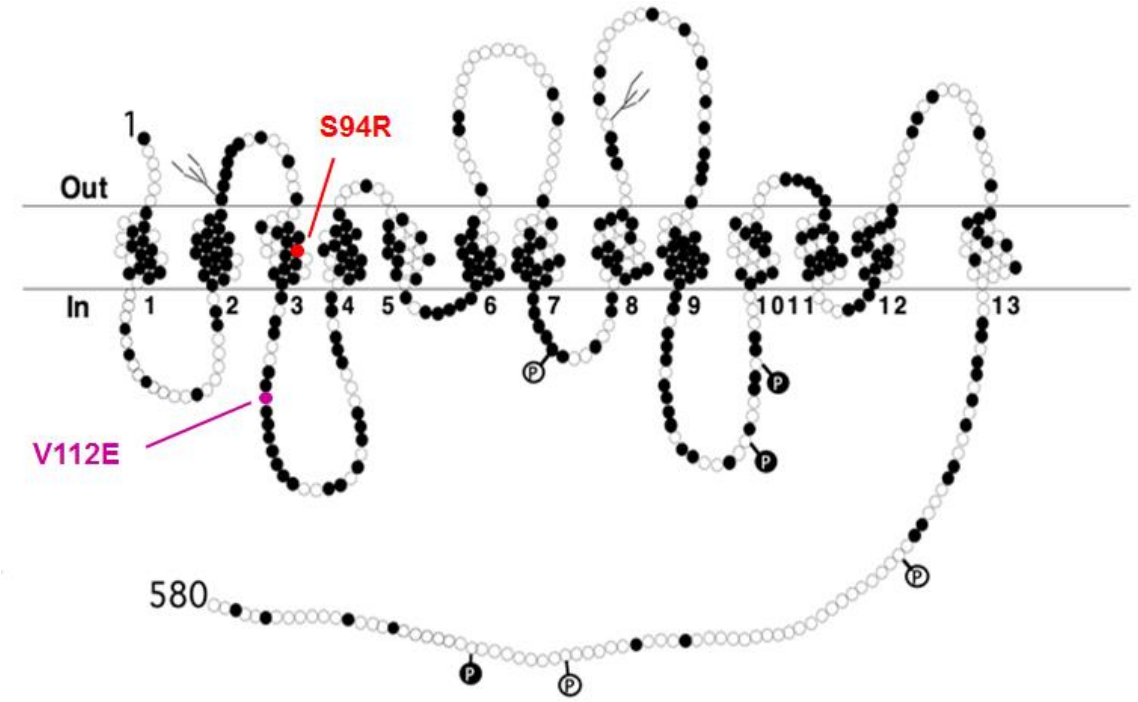

Figure 39. Diagram of the predicted secondary structure of the SLC5A7 gene protein product (CHT) showing 13 transmembrane domains with an extracellular N-terminus, and an intracellular C-terminus. As in the previous chapter, dark circles represent amino acids which are conserved across human CHT, mouse Cht1, and the C. elegans CHT ortholog, CHO-1. Dark circles containing the letter 'P' indicate potential protein kinase C phosphorylation sites, and light circles containing the letter 'P' represent potential protein kinase A phosphorylation sites. The fork-like structures represent potential N-glycosylation sites. CHT p.S94R is indicated in red, and CHT p.V112E is indicated in purple. Modified (Apparsundaram, 2000; Apparsundaram, 2001 (140, 141))

Table 28: Online *In silico* mutation analysis software results for CHT p.S94R and p.V112E

Variant	PolyPhen (HumDiv)	PolyPhen (HumVar)	Mutation Taster	PROVEAN
S94R	1.000 – probably damaging	0.996 – probably damaging	0.999999968819884 – disease causing	-4.90 – deleterious
V112E	0.996 – probably damaging	0.979 – probably damaging	0.999999999840146 – disease causing	-5.606 – deleterious

4.2.4 Functional investigation of CHT p.V112E and CHT p.S94R

To investigate the functional impact of the *SLC5A7* c. 282T>A (p.S94R) and c.335T>A (V112E) variants on CHT, similarly as with the dHMN truncating mutations, heterologous expression of mutant (CHT p.S94R and CHT p.V112E) and wild type (CHT WT) proteins in HEK-293 cells transiently transfected with the respective cDNA constructs was performed (for cDNA transfection amounts see appendix) in collaboration with Prof Randy Blakely; USA, and Dr Sebahattin Cirak, Germany. In order to maintain experimental continuity, *SLC5A7*^{S94R} and *SLC5A7*^{V112E} constructs were produced in the same plasmid vector (pRK5) and with the HA-tag included at the N-termini, as used in previous expression and uptake studies undertaken with the HA-*SLC5A7*^{K499Nfs*13} and HA-*SLC5A7*^{H521Qfs*2}. Mutant cDNA constructs were produced using the QuickChange Lightning Site-Directed Mutagenesis kit (for SDM primer sequences see appendix). Two additional sets of CHT constructs containing these variants were produced in Dr Sebahattin Cirak's laboratory. The *SLC5A7* cDNA was purchased from Origene in pCMV6-Entry vector, one with myc/DDK tag in the C-terminal and the other with C-terminal double myc- and FLAG-tags, and the missense mutations were introduced with the use of the Q5® Site-Directed Mutagenesis Kit (NEB). Cell surface biotinylation experiments and western blot analysis were performed in order to investigate the expression and surface delivery of the two transporters, as in the previous chapter. [^{3}H]-choline transport assays were also performed to compare the choline transport ability of the two mutant molecules to that of the wild type molecule when expressed individually to mimic their expression in affected homozygous mutant gene carriers. Due to the unavailability of fresh blood samples from affected individuals, it has not been possible to measure choline transport activity in whole blood monocytes natively expressing CHT p.S94R and CHTp.V112E as was done previously in dHMN-VII subjects.

4.2.4.1 *SLC5A7*^{S94R} and *SLC5A7*^{V112E} reduce surface, but not overall, CHT expression

Western blot analysis of the lysates of HEK-293 cells transfected with myc-CHT WT, myc-CHT p.S94R and myc-CHT p.V112E cDNAs shows that for equivalent

amounts of cDNA transfected, equal levels of products were produced, suggesting that these variants do not alter translation or protein stability (figure 40A). This was confirmed by assessment of protein levels by ELISA (figure 40B). Similar result were obtained on preliminary Western blot analysis of cell lysates of HEK-293T and HEK-293 cells transiently transfected with HA-*SLC5A7*^{WT}, HA-*SLC5A7*^{S94R}, and HA-*SLC5A7*^{V112E} cDNAs also shows equal levels of products were produced for equivalent amounts of cDNA transfected (figure 41). Furthermore, two additional bands are present between 120 and 140 kDa, possibly representing CHT homodimers. Myc-CHT proteins were isolated from the cell surface of HEK-293 cells transfected with myc-CHT WT, myc-CHT p.S94R and myc-CHT p.V112E cDNAs by biotinylation followed by NeutrAvidin agarose pulldown and quantified by Western blotting, and surface levels were quantified by ELISA. This showed reduced surface expression of both mutant proteins in contrast to the wild type (figure 42). Quantification of the cellular localisation of myc-CHT WT, myc-CHT p.S94R and myc-CHT p.V112E was carried out by immunofluorescent staining of the proteins in HEK-293 cells (figure 43). Compared to cells expressing wild type CHT, in cells expressing the S94R and V112E mutant proteins, a large fraction of CHT immunoreactivity showed an abnormal expression (figure 43B) pattern with large CHT aggregates in the cell body (figure 43A). These data suggest that although the CHT p.S94R and CHT p.V112E do not influence overall CHT expression, the surface localisation of the mutant proteins is reduced, and the mutants exhibit an abnormal expression pattern.

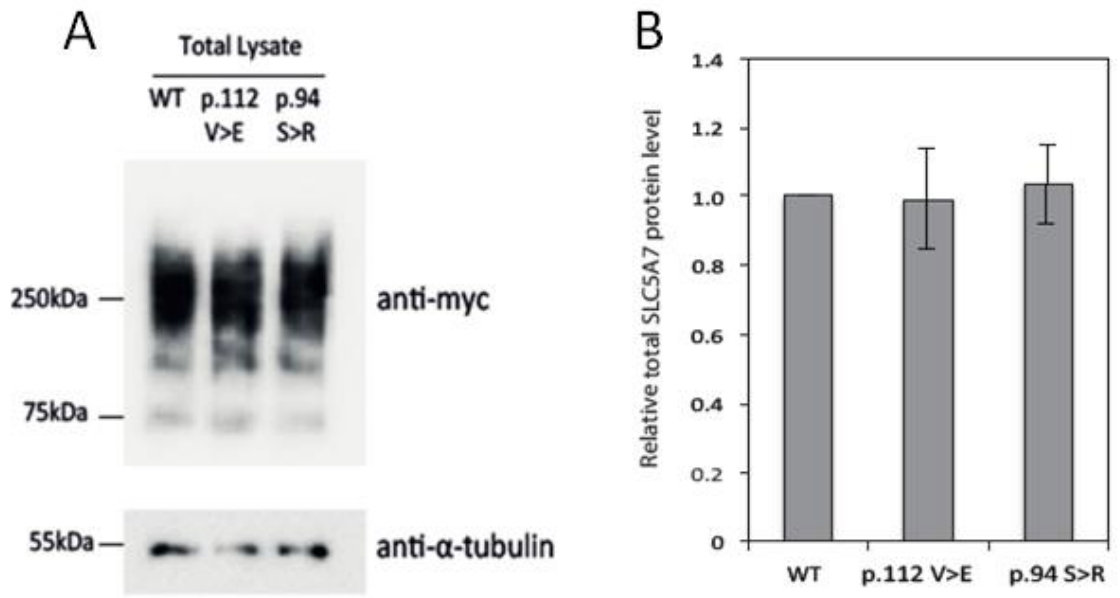

Figure 40. Western blot analysis of A) total protein levels of myc-CHT WT, myc-CHT p.S94R and myc-CHT p.V112E expressed in HEK-293 cells, after SDS-PAGE and immunoblotting with anti-myc. The α-Tubulin level was detected in stripped membrane as loading control. B) The total SLC5A7 protein level was assessed by ELISA as described in (Bogatcheva, 2007). Protein level is shown in arbitrary units (AU) as a ratio of specific horseradish peroxidase (HRP) activity of mutant to wild type SLC5A7 after anti-myc antibody binding. Results are presented as means ± SE (n = 3). (Kindly provided by Dr Cirak, Uniklinik Köln University Hospital, Germany).

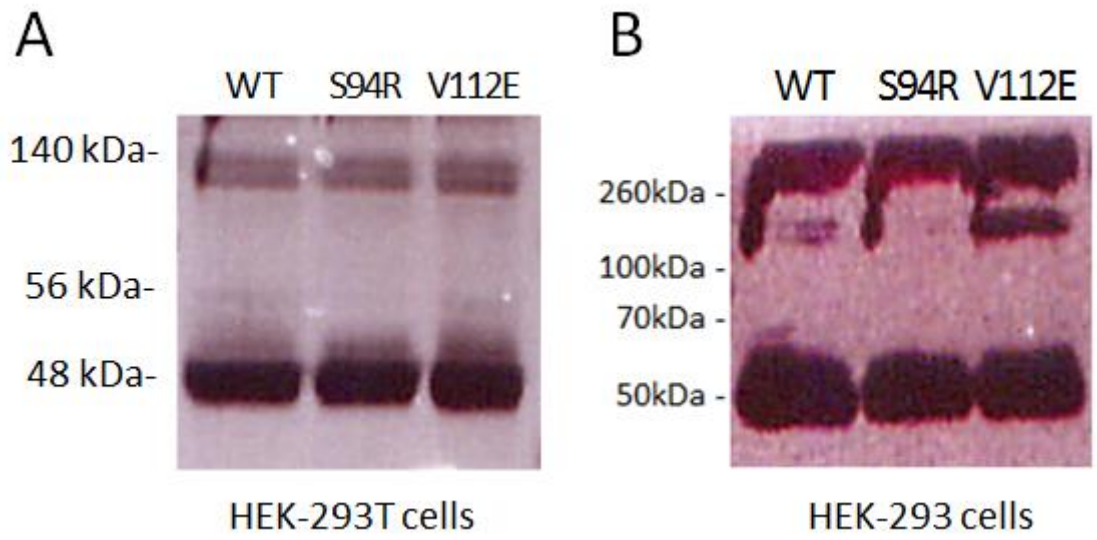

Figure 41. Preliminary western blot analysis of total protein levels of HA-CHT WT, HA-CHT p.S94R and HA-CHT p.V112E after SDS-PAGE and immunoblotting with anti-HA antibody of lysates from transiently transfected (A) HEK-293T and (B) HEK-293 cells. Both provide supporting evidence of equal expression levels of wild type and mutant proteins. The band at ~46kDa in A likely represents the immature less glycosylated species of CHT described in chapter 3. The broad band at 50kDa in B possibly represents both the immature and mature species. In both A and B two faint bands are visible for all proteins between 120 and 140kDa which may represent CHT homodimers. (Kindly provided by Prof Randy Blakely and Mrs Jane Wright).

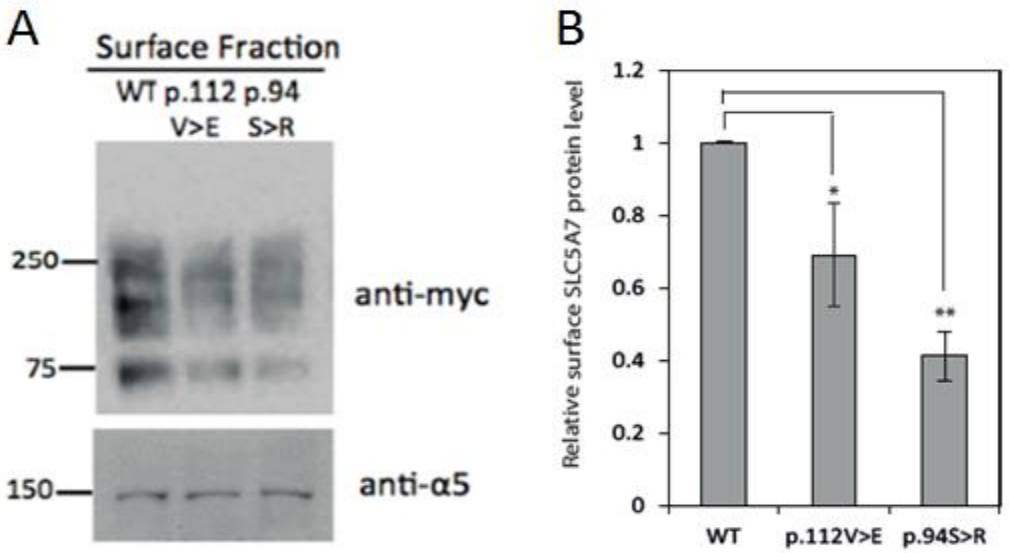

Figure 42. A) Surface protein level of SLC5A7 WT and mutants, after cell surface biotinylation, total surface protein fractions are isolated using surface isolation kit (pierce), following detection of surface SLC5A7 by SDS-PAGE and anti-myc antibody. CD49e (α5 integrin) or CD29 (β1 integrin, data not shown) level was detected in stripped membrane as loading control. B) Quantification assessed by ELISA is displayed as ration of mutant to WT of the myc antibody signal normalized to control protein signal. Means ± SE (n = 3). (Kindly provided by Dr Cirak, Uniklinik Köln University Hospital, Germany).

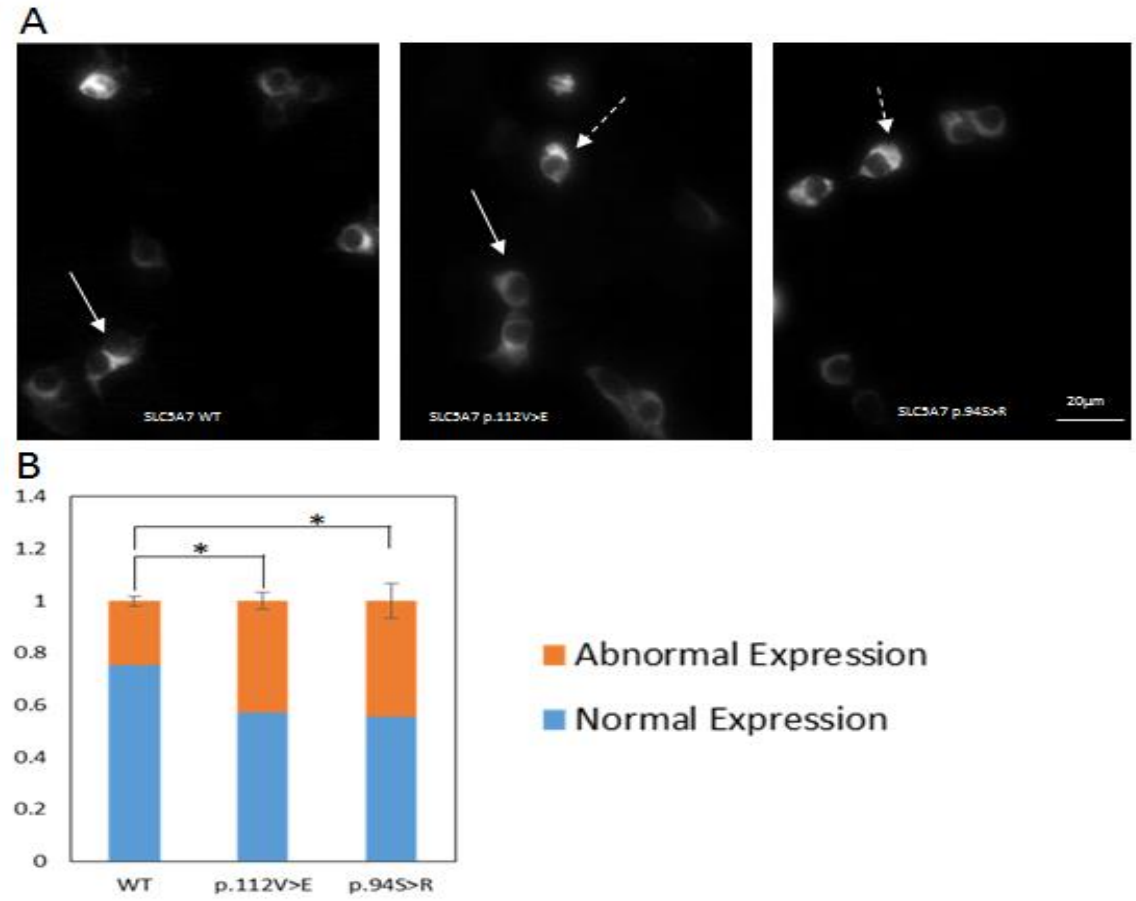

Figure 43. A) Immunostaining of transfected HEK-293T cells using anti-myc antibody shows abnormal expression of myc-CHT p.S94R and myc-CHT p.V112E compared to myc-CHT WT. Examples of cells displaying normal expression are marked with a solid white arrow, while cells displaying abnormal expression are marked with a dashed arrow. Scale bar 10µm. B) Statistical countering of cells with abnormal SLC5A7 expression (orange) and cells with normal SLC5A7 expression (blue). Means ± SE (n = 2). (Kindly provided by Dr Cirak, Uniklinik Köln University Hospital, Germany).

4.2.4.2 *SLC5A7*^{S94R} and *SLC5A7*^{V112E} abolish choline transport activity in transfected cells

To investigate the outcome of the missense sequence variants on CHT transporter activity, [3H]-choline transport assays were performed in order to compare the choline transport ability of the mutant and wild type molecules in transiently transfected HEK-293 cells. These studies are currently still underway, and the following data is preliminary. Importantly, preliminary choline uptake assays revealed complete abolishment of choline uptake activity in cells expressing mutant molecules (0%) compared to those expressing the wild type (figure 44)

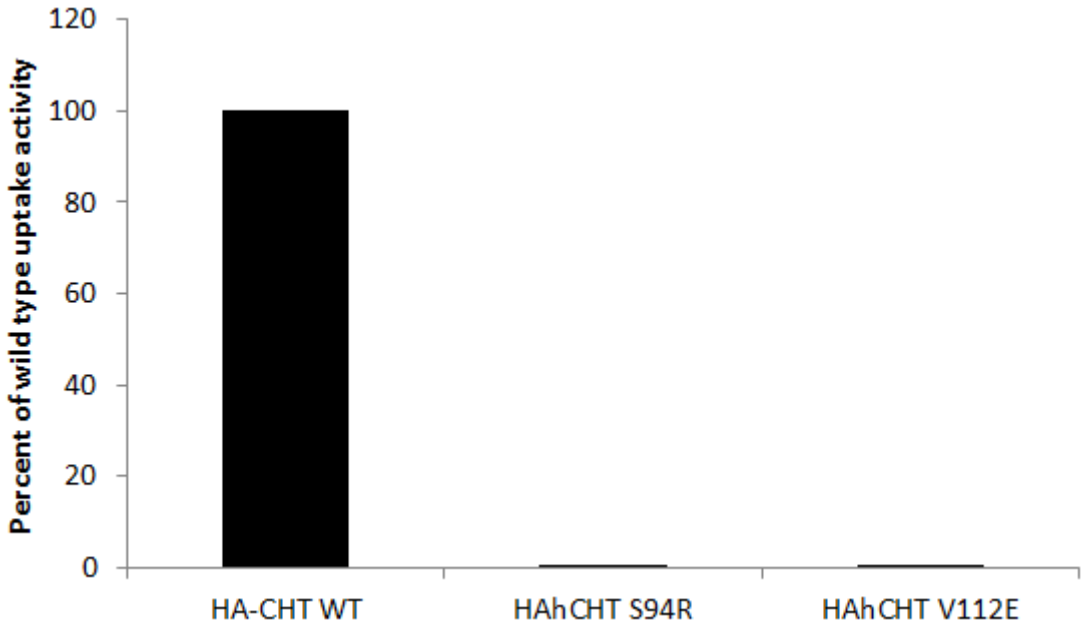

Figure 44. Preliminary choline uptake assay in HEK-293 cells transiently transfected with wild type and CHT p.S94R and p.V112E cDNAs. Choline transport activity is significantly reduced when comparing WT-CHT with CHT p.S94R (p=0.019, n=3, students unpaired t-test) and CHT p.V112E (p=0.014, n=3, students unpaired t-test). Choline uptake activity of both mutant proteins is 0% of that of the wild type, completely abolished. Specific choline uptake was determined by subtracting the uptake obtained in transfected cells with that of mock (vector) transfected cells obtained in assays conducted in parallel. This data is preliminary. Experiments are still underway.

4.3 Discussion

Investigation of the genetic cause of severe congenital, predominantly central hypotonia in two consanguineous families by whole-exome sequencing identified distinct N-terminal CHT homozygous autosomal recessively acting *SLC5A7* mutations as the likely pathogenic mutations. A single base substitution (c.282T>A) was identified in a family of Turkish origin with one affected female infant and results in a single amino acid substitution at position 94 from serine to arginine (p.S94R), affecting a residue in the third transmembrane domain of the choline transporter (CHT). In a Hispanic family with two affected infants, one male and one female who are both deceased, a single base substitution (c.335T>A) was identified resulting in an amino acid substitution from valine to glutamic acid at position 122 (p.V112E). This substitution affects a residue located in the second intracellular loop between the third and fourth transmembrane domains of CHT. Comparison of exome sequencing data and SNP array data confirmed that this variant resides within a region of homozygosity in the proband. Each variant cosegregates with the disease phenotype across each respective family, and whilst regional control samples remain to be investigated neither variant is present in genomic databases. *In silico* analysis of the variants predicted a profound impact of both on the function of CHT, but did not predict any changes in structure of the protein. Both variants affect residues in the transmembrane spanning region of CHT (figure 39). Expression studies indicated that neither variant has an effect on overall CHT expression, however abnormal cellular localisation and reduced surface expression were observed. Most importantly however, CHT transporter assays revealed complete abolition of transporter activity in transfected cells compared to wild type expressing cells.

The mechanisms underlying the genotype-phenotype relationships between the truncating and missense mutations reported in this thesis and their respective disorders, is yet to be fully elucidated. Comparison of our current knowledge of phenotypic, genetic and proteomic features of the truncating *SLC5A7* mutations described in chapter 3 and the missense mutations described here can be found in table 29. Our studies suggest the truncated p.K499Nfs*13 and p.H521Qfs*2 mutant proteins interfere with the wild type molecule exerting a dominant negative effect on transporter function due to its functioning as a

homodimer, requiring the inheritance of only one mutant allele for disease penetrance. Conversely, the lack of phenotype found in carriers of p.S94R or p.V112E missense mutations indicates that these mutations do not exeter such a dominant-negative interference effect on the wild type molecule. However due to time constraints, measurement of choline uptake activity in cells co-transfected with both wild type and p.S94R or p.V112E mutant cDNAs to investigate this further have not yet been undertaken. The severe phenotypes resulting from the missense CHT mutations in homozygous gene carriers, combined with the complete abolition of CHT transport activity and its reduced surface expression (figure 42) in *SLC5A7* p.S94R or p.V112E transfected cells, points towards roles in trafficking, internalisation, or constitutive endocytic recycling of CHT of the affected residues. As CHT choline transport is critical for ACh synthesis and signalling at all cholinergic synapses, it is interesting that while the hypotonia cases exhibit global effects of cholinergic dysfunction, neuro-dysfunction and degeneration in the dHMN cases is restricted to a specific subpopulations of neurones. This selective neuronal vulnerability may be a result of differences in the required levels of ACh synthesis to replenish stores following transmission between different subsets of cholinergic neurones, or differences in CHT expression levels.

Table 29: Comparison of *SLC5A7*/CHT mutations investigated in this study, their structural and functional effects on the choline transporter, and their associated conditions

	Truncating mutations		Missense mutations	
	p.K499Nfs*13	p.H521Qfs*2	p.S94R	p.V112E
	Phenotype			
Associated disorder	dHMN-VII	dHMN-V	Severe hypotonia	Severe hypotonia
Onset	11-31 years	25-57	Congenital	Congenital
Characteristic features	-Progressive length-dependent motor neuropathy -presents in upper limbs -VCP	-Progressive length-dependent motor neuropathy -presents in upper limbs	-Severe predominantly central hypotonia -Postnatal respiratory insufficiency -DD -Brain atrophy	-Severe predominantly central hypotonia -Postnatal respiratory insufficiency -Normal brain MRI -Infantile death
	Genetics			
MoI	AD	AD	AR	AR
Mutation type	Frameshift	Frameshift	Missense	Missense
Exon	9 (ultimate). Avoids NMD	9 (ultimate). Avoids NMD	2	3
	Protein			
Structural changes	Truncation.	Truncation.	None predicted aa substitution in membrane spanning region	None predicted aa substitution in membrane spanning region
Affected domain	C-terminus eliminated	C-terminus partially eliminated	Membrane spanning domain. (3rd transmembrane domain)	Membrane spanning domain. (2nd intracellular loop)

Effect on expression in transfected cells	Reduced overall expression compared WT in singular transfections, and reduced overall and surface expression in co-transfected cells	Reduced (less so than p.K499Nfs*13) overall expression compared WT in singularly transfected cells,	No change in overall expression. Reduced surface expression to ~70% of WT	No change in overall expression. Reduced surface expression to ~40% of WT
Functional consequence	Reduced choline transport (by ~50% in singularly transfected cells, by ~75% in co-transfected cells and by ~90% in patient cells) by a dominant negative mode of action	Reduced choline transport (by ~50% in singularly transfected cells)	Abolishes choline transport	Abolishes choline transport
Knowledge of affected amino acid residues	Loss of residues/motifs with suggested roles in: - Uptake activity regulation - Endocytic targeting to synaptic vesicles - Constitutive endocytosis	Loss of residues/motifs with suggested roles in: - Endocytic targeting to synaptic vesicles - Constitutive endocytosis	Nothing known	w/i C-terminal tyrosine-based sorting motif (YxxΦ; $Y^{111}VTM^{114}$) required for protein sorting to organelles and specific membrane regions including the somatodendritic domain of neurones

Abbreviations: **MoI=** mode of inheritance; **DD=** developmental delay; **MRI=** magnetic resonance imaging; **AD=** autosomal dominant; **AR=** autosomal recessive; **NMD=** nonsense mediated decay; **WT=** wild type; **w/i=** within

Much work has focused on the identification of CHT residues that are required for choline binding and uptake, its translocation from the cell body to the synaptic vesicles and the cell surface, its interaction with other proteins and molecules, and its internalisation from the cell surface and recycling(3, 116, 147, 158-162). V112E is located within a carboxyl-terminal tyrosine-based sorting motif (Yxxφ; $Y^{111}VTM^{114}$)(147). Tyrosine-based signals fitting the Yxxφ motif are known to mediate sorting of transmembrane proteins to endosomes, lysosomes, the basolateral plasma membrane of polarised epithelial cells, and the somatodendritic domain of neurones(163). Similarly to our CHT-V112E expressing HEK-293 cells, Y111A and M114A mutants have supposedly been found to eliminate CHT choline uptake activity [Unpublished work of Yamada H., reported by Haga (2014)](147), indicating that the residues that form this motif are necessary for choline uptake, however their specific functional role is unknown. The abnormal cellular localisation, and aggregation of CHT p.V112E in the cell body could be explained by sorting of the mutant protein due to disruption of the Yxxφ motif. The S94R amino acid substitution does not reside in any known motifs, and the residue affected has not been subject to investigation in any studies other than those pertaining to this thesis. However, both variants affect residues in the transmembrane spanning domain of CHT, which has been found to harbour residues required for choline and HC-3 binding only (E45)(147), choline uptake and binding (D48, D242, D349, D411), choline uptake but not for binding (D158, E451, R466), N-glycosylation and thus, translocation to the cell surface (N301)(116).

CHT is concentrated in cholesterol-rich lipid rafts at nerve terminals, and decreasing membrane cholesterol reduces CHT choline uptake activity and cell surface expression, diminishing cholinergic transmission by restricting the choline available for ACh synthesis(161). The association of CHT with cholesterol-rich lipid rafts is, thus, critical to CHT function. The amino acid residues required for binding to cholesterol-rich lipid rafts are not yet known. It is possible that the reduced surface levels of CHT p.S94R and CHT p.V112E compared to the wild type protein in transiently transfected HEK-293 cells, despite equal total protein expression levels, may be due to disrupted association with cholesterol-rich lipid rafts.

Choline uptake is regulated primarily by increasing the number of transporters on the presynaptic membrane, rather than altering the activity of existing transporters to support a biosynthetic response to neuronal excitation(3, 164). Data from our functional investigation of CHT p.S94R and p.V112E mutant transporters suggest that although the mutant proteins do not influence overall CHT expression, the surface localisation of the mutant proteins is reduced and the mutants exhibit an abnormal expression pattern. These mutations may therefore impact choline transport regulation and subsequent ACh synthesis. An important role of adaptor proteins (e.g. adaptor protein-3, AP-3) for CHT trafficking has been demonstrated(165), thus it is possible that these missense mutations exert their effects on surface delivery of the transporter by disrupting interactions with other molecules.

Ferguson et al. (2004) examined $CHT^{-/-}$ and $CHT^{+/-}$ mice for evidence of impaired cholinergic transmission(5). The $CHT^{-/-}$ mice were born in the Mendelian ratios that were expected but become immobile, have irregular breathing, appear cyanotic (blue colouration of skin/mucus membranes due to low oxygen), and did not live longer than an hour after birth; resembling the phenotype observed in our cases. This provides support to our conclusion that the severe phenotype in these families results from the abolition (or near abolition) of choline uptake by CHT.

It is an unlikely possibility that an alternative disease causing variant exists in each of the affected families that was missed by whole-exome sequencing, however existence of two *SLC5A7* mutations in families presenting with similar phenotypes, coupled with data indicating a profound functional impact of these mutations on CHT function, provides strong evidence that these mutations are in fact, causative of the phenotype presenting in these families. Thus, this study defines a new cause of severe congenital hypotonia.

5

CHAPTER FIVE

dHMN-VII MOUSE MODEL

5 dHMN-VII MOUSE MODEL

5.1 Introduction

5.1.1 Animal models of human disease

Animal models of neurodegenerative disease have existed for almost six decades, since resperine was used to deplete dopamine and cause a Parkinson-like phenotype in animals in 1957(166). However, until more recently human disease could only be mimicked in animals by creating lesions in specific brain regions, primarily with the use of toxins; or studies were carried out on mouse strains in which spontaneous mutations had occurred(166). In the last 2 decades, the use and importance of animal models in the elucidation of human disease mechanisms has both changed and increased drastically. The mouse has become an invaluable model system for the study of human genetics and disease, owing to its many genetic and physiological similarities, genetic malleability, and short generation time(167). Many mouse models of human genetic disorders have offered insight into anatomical, neurochemical, and behavioural effects of aberrant gene expression(168). Nevertheless, yeast, fly, worm, sheep, pig and primate neurodegenerative disease models have also been produced(166).

Animal models allow for different disease processes to be explored throughout the entire disease course, from a preclinical stage to the most advanced stages of disease. They also allow for testing of phenotype modifying agents and experimental therapies as a prelude to clinical trials with human subjects(166). We are able to alter environmental conditions to establish the intersection of genetics and environment, and study how much phenotypic variability can be accounted for by the disease causing gene mutation, and how much is due to influence from modifying genes. Animal models have even created opportunity to track specific proteins *in vivo*, and, with contribution from advancing technology, have provided researchers with the capacity to extract and analyse individual neurones, and even determine directly how different disease proteins behave in specific cell types(166). This may help us finally understand selective neuronal vulnerability.

5.1.2 The importance of animal models of motor neurone disorders

Whilst there are a number of inherited MNDs (5–10 % of all patients having a clear family history of MND), the cause of most remains unknown(169). In ‘sporadic’ cases of MND where there is no evidence of family history of the disorder, underlying factors involved may include an unknown genetic alteration, environmental factors, viral infection, or exposure to toxic substances. No consistent environmental risk factor(s) of MND have as yet been identified, suggesting the possibility that such factors may only trigger disease in genetically susceptible individuals(169). Over 100 genes have now been implicated in the causation of MND, some of which result in a very precise and consistent clinical phenotype, and others which result in more than one form of MND, even within related individuals who share the same gene mutation(169). It is therefore likely that there is significant overlap of the biological basis of many different types of MND. Despite our growing knowledge of the genetic and molecular basis of this group of disorders, at present treatment is largely palliative. Having identified the genetic basis of a form of MND in a particular group of patients, further investigation of the pathological mechanism by which the gene mutation results in the disease phenotype is often essential for the better understanding of the disease progress, and for the possibility of the development of tailored or targeted treatment strategies. As we are unable to take a biopsy of the brain or spinal cord of living MND subjects in order to better understand disease processes, the creation of mouse models allows us a way in which to do so in a biologically comparable species. There have been many successful mouse models of human disease, including neurodegenerative disorders such as PD via mutation of the mouse homologues of human disease genes, *Snca* encoding α-synuclein and *Lrrk2*(170), and HD via mutation of the huntingtin homologue *Htt*(171), the generation of which has proven invaluable for the study of these diseases. In addition to providing insight into the eitiology and progression of human genetic disease, animal models have proven a useful tool in the identification of targets of therapeutic drugs(172). It is important however, when trialling pharmacotherapies in animal models, to remember that drugs that successfully treat a disease in an animal model do not always translate to human clinical trials. Animal models may not always recreate all aspects of a human disease,

in particular mouse models for neurodegenerative diseases as these often involve cognitive deficits that mice are unable to express(172).

5.1.3 CHT-related disease treatment hypotheses

As described in chapter 3.3, CHT is a hemicholinium-3 (HC-3) sensitive, Na^+/Cl^- dependent, high affinity choline transporter responsible for the uptake of choline at the NMJ. CHT mediated choline uptake represents the rate-limiting step in ACh synthesis at the NMJ and is thus, essential for normal cholinergic transmission (figure 53, appendix). Our discovery that dominant-negatively acting *SLC5A7* frame-shift mutations underlie dHMN has enabled a better understanding of the disease mechanism whereby choline uptake activity is significantly reduced and thus, following synaptic activity there is likely insufficient ACh synthesis to support further depolarisation (figure 54, appendix). As there are currently no therapeutic agents in medical use that augment CHT-mediated choline uptake activity, we hypothesise that intervention at the post synaptic cleft with approved and available therapeutic agents might be successful in aiding cholinergic signalling at the neuromuscular junction of affected patients, thereby alleviating symptoms of dHMN-VII. On this basis, we identified two possible treatment options to trial in a dHMN-VII mouse model as a prelude to patient clinical trials:

(i) Treatment with a nicotinic acetylcholine receptor (nAChR) agonist may raise the resting potential of the postsynaptic muscle cells membrane potential, allowing the reduced amount of nAChR binding by ACh released from the presynaptic nerve terminal to increase the membrane potential to the action potential threshold (see 5.1.3.1).

(ii) Treatment with an acetylcholine esterase inhibitor (AChE) inhibitor (e.g. edrophonium, neostigmine or pyridostigmine) may prolong the presence of ACh in the synaptic cleft by inhibiting breakdown by AChE and therefore promote binding to nAChRs to allow the postsynaptic membrane action potential threshold to be accomplished (see 51.3.2).

In addition to the above treatments, the possibility of treatment with choline was also discussed in order to address the issue of reduced intracellular choline in

the presynaptic nerve cell. However, because increasing the intracellular choline concentration has been found to have an inhibitory effect on CHT-dependent ion flux(3) and increasing extracellular choline rapidly decreases cell-surface CHT expression(173), it is possible that administration of choline may further exacerbate clinical symptoms. Should targeted inhibition of clathrin-mediated and dynamin-dependent CHT endocytosis be achievable in the future, treatment with such an agent of dHMN subjects in which CHT is still partially active, might retain the higher level of CHT at the presynaptic plasma membrane following an increase in extracellular choline concentration. Thus, choline uptake activity might be sustained sufficiently to replenish ACh stores. Extensive studies have been carried out on endocytosis, including the investigation of key molecules and mechanisms that modulate dynamin dependent GTPase activity and clathrin- and dynamin-dependent vesicle formation(174, 175). A number of chemical, pharmacological and genetic inhibitors of endocytosis have been identified which target both clathrin (hypertonic sucrose, phenothiazines, pitstop, clathrin Hub mutant) and dynamin (dynasore, dynamin K44A mutant)(176). Unfortunately, most have also been reported to exert effects elsewhere in the cell including interference of macropintocytosis, phagocytosis, actin cytoskeleton and clathrin- and dynamin-independent endocytic pathways, as well as cell toxicity and changes in gene expression(176).

5.1.3.1 Treatment with a nAChR agonist

In 2013, Rilstone *et al.* reported an autosomal recessive disease presenting as infantile-onset movement disorder (parkinsonism and non-ambulation), sleep and mood disturbance, autonomic instability, and developmental delay as being caused by a *SLC18A2* c. 1160C→T mutation resulting in a proline to leucine amino acid substitution at position 387 of the vesicular monoamine transporter 2 (VMAT2)(177). VMAT2 is similar to CHT in that it is a membrane spanning transporter present on neurotransmitter containing synaptic vesicles. It translocates biogenic amines (dopamine, serotonin, adrenaline and noradrenaline) into synaptic vesicles and is essential for motor control, stable mood, and autonomic function(177). Similarly to the CHT p.K499Nfs*13 and p.H521Qfs*2 mutations responsible for dHMN, the authors reported the VMAT2

p.P387L mutation results in dramatically decreased, but not totally abolished, transport activity compared to the wild type molecule in transiently transfected COS-7 cells(177). The authors thus concluded that defective monoamine loading into synaptic vesicles, and therefore defective neurotransmission underlie the phenotype described. Affected family members had previously been treated with levodopa–carbidopa, which has dopamine receptor antagonistic properties, on the basis of Parkinsonism and diminished urinary dopamine. However this resulted in major deterioration and was discontinued. The authors gave one affected family member pramipexole, a direct dopamine receptor agonist, which resulted in in dramatic and sustained disappearance of Parkinsonism and dystonic attacks, and improvement in other symptoms(177). Other affected family members were also treated and showed continuing improvement with more substantial recovery observed in younger subjects, and minimal side effects(177). The similarity in pathogenic mechanism between dHMN-VII and the disorder investigated by Rilstone and colleagues, prompted us to hypothesis that treatment with a nAChR agonist may elicit a similar improvement in disease state of dHMN-VII animal models and human subjects (figure 55, appendix).

Two types of Ach receptor exist within the mammalian nervous system: i) muscarinic ACh receptors (mAChRs), G-protein coupled receptor complexes which display higher sensitivity to the agonistic molecule muscarine than to nicotine and exhibit a slow and prolonged response to stimulation. These occur primarily in the CNS but are also present peripherally on postganglionic membranes of the sympathetic and parasympathetic nervous systems, and ii) nAChRs which are ligand-gated ion channels that mediate fast signal transmission at synapses. These are composed of multiple subunits that combine to form many different receptor subtypes that can be of either neuronal, or muscle type. Different nAChR subtypes are involved in a wide range of physiological processes including cognitive function, learning and memory, arousal, reward, motor control, and analgesia. Muscle type nAChRs are localised to the postsynaptic muscle cell membrane at the NMJ and are composed of $\alpha 1 - \varepsilon - \alpha 1 - \beta 1 - \delta$ subunits. Ideally, for nAChR agonist treatment of dHMN-VII, an agonist that is specific to adult muscle nAChRs would be administered in order to reduced action at other cholinergic sites causing

adverse side-effects. Unfortunately however, there are currently no NMJ specific nAChR agonistic therapeutic agents available. For this reason we propose currently available, more globally acting yet safety approved pharmacological agents for which a therapeutic and safety window has already been established, such as the smoking cessation drug Varenicline (Champix®) or nicotine products used for smoking cessation.

5.1.3.2 Treatment with an AChE inhibitor

AChE inhibitors are drugs that inhibit the hydrolysis of ACh by AchE, whose action can be reversible, irreversible, or partially irreversible. Medicinally AChE inhibitors are used to treat myasthenia gravis and myasthenic syndromes(178), cognitive impairments associated with schizophrenia(179), ADi(180), PD(181), and dementia with Lewy bodies(182), as well as glaucoma(183), and to enhance rapid eye movement (REM) sleep in autistic children(184). We propose that treatment of dHMN-VII animal models and human subjects with reversible AChE inhibitors whose main site of action is the NMJ (edrophonium, neostigmine or pyridostigmine)(185) might maintain ACh levels in the post synaptic cleft following depolarisation and ACh release such that sufficient amounts remain to elicit a response despite depleted ACh pools on subsequent depolarisations (figure 56, appendix). The mentioned anticholinesterase drugs exhibit short to medium durations of action (10 minutes, 1-2 hours, and 2-3 hours respectively) and thus, all should be trialled in order to distinguish which is more effective in treating dHMN(185).

5.2 Generation of dHMN-VII mouse line, and results of preliminary phenotyping

Mouse studies were designed by Dr Darren Logan and Dr Sebastian Gerety based at the Wellcome Trust Sanger Institute in house after discussion of the human phenotype with both myself and Professor Crosby. The analysis was performed by Ms Eve Coomber, while I observed much of this work.

A patient-specific *knock-in* mouse model carrying the *SLC5A7* c.1497delG mutation identified in dHMN-VII family 1 (chapter 3) was generated using

CRISPR/Cas9-mediated gene editing. For methodology for the generation of the dHMN-VII mouse line, see appendix 7.5.2. Confirmation of expression of the patient-specific *Slc5a7*^{indelAC} allele was obtained by sequencing of mRNA extracted from spinal cord biopsy of animals found to carry the genetic alteration heterozygously that were sacrificed under the schedule 1 procedure of the Home Office Animals (Scientific Procedures) Act 1986. For methodology and results for the assay for the *knock-in* allele expression, see appendix 7.5.3.

5.2.1 Open field and grip strength testing

Animals aged 18-22 weeks were subjected to 20 minutes open field testing to assess differences in distance covered (figure 58, appendix), average velocity, or time spent moving between either *Slc5a7*$^{indelAC/+}$ or *Slc5a7*$^{+/TM1A}$ and their littermates. There were no measurable differences observed for any of the open field measurements. For methodology and results data for open field testing, see appendix 7.5.4. Grip strength measurements were taken from wild type control and mutant mice at 18-22, 23-26 and 27-31 weeks of age in order to assess difference in muscle strength between *Slc5a7*$^{indelAC/+}$ or *Slc5a7*$^{+/TM1A}$ and their respective wild type littermates. For data from grip strength testing methodology, see appendix 7.5.5.

5.2.2 Grip strength results for *Slc5a7*$^{indelAC/+}$ mice

In general, a trend can be observed whereby animals heterozygous for the patient-specific mutation (*Slc5a7*$^{indelAC/+}$) have reduced mean forepaw and all-paw grip strength compared to wild type littermates (*Slc5a7*$^{+/+}$) at almost all time points in both sexes (figure 59, appendix 7.5.5.1). This reduction is only statistically significant however in two specific comparisons: female *Slc5a7*$^{indelAC/+}$ mice had significantly less all-paw grip strength than S*lc5a7*$^{+/+}$ mice (Mean difference=44.75; p=0.0334) at time point 1 (18-22 weeks), and male *Slc5a7*$^{indelAC/+}$ mice had significantly less all-paw grip strength than *slc5a7*$^{+/+}$ matched controls (Mean difference=41.12; p=0.0411) at time point 2 (23-26 weeks). At other times points, the differences in grip strength visible on the graphs when comparing *Slc5a7*$^{indelAC/+}$ and *Slc5a7*$^{+/+}$mice are not

statistically significant (tables 42 and 43, appendix 7.5.5.1). Female *Slc5a7*$^{indelAC/+}$ mice demonstrated a statistically significant increase in all-paw grip strength between time points 1 and 3 (mean difference=35.97; *p*=0.0418; figure 59A and table 42, appendix 7.5.5.1). This may explain why the difference seen between *Slc5a7*$^{indelAC/+}$ and *slc5a7*$^{+/+}$ females at time point 1 is not seen at time point 3.

Mean forepaw grip strength decreases significantly between time points 1 and 3 across both sexes and both phenotypes (female *Slc5a7*$^{indelAC/+}$ mean difference=22.45; *p*=0.0459, female *Slc5a7*$^{+/+}$ mean difference=20.63; *p*=0.0495, male *Slc5a7*$^{indelAC/+}$ mean difference=32.05; *p*<0.0001, male *slc5a7*$^{+/+}$ mean difference=20.03; *p*=0.0261; tables 42 and 43, appendix 7.5.5.1), suggesting that although there is no clear difference between *Slc5a7*$^{indelAC/+}$ and *slc5a7*$^{+/+}$ mice in forepaw grip strength, all animals between 18 and 31 weeks appear to lose forepaw strength.

5.2.3 Grip strength results for *Slc5a7*$^{+/TM1A}$ mice

No difference can be observed between *Slc5a7*$^{+/TM1A}$ and *Slc5a7*$^{+/+}$ mice of either gender at any time point. No significant difference was observed between heterozygous null (*Slc5a7*) mice and their wild type littermates (*Slc5a7*$^{+/+}$) in forepaw or all-paw grip strength at any time point in either of the sexes. As in the *Slc5a7*$^{indelAC/+}$ animals, A significant decrease in forepaw grip strength in male *Slc5a7*$^{+/TM1A}$ mice can be seen between time points 1 and 3 (mean difference=33.48; *p*=0.0008, figure 60A and table 45, appendix 7.5.5.2). In addition to this, there is a significant decrease in male *Slc5a7*$^{+/TM1A}$ forepaw grip strength between time points 2 and 3 (mean diff=31.38; *p*=0.0019, figure 60A and table 45, appendix 7.5.5.2). This was not seen in *slc5a7*$^{+/+}$ male or either genotype of female mice. The only significant difference observed in the female animals was an increased in all-paw grip strength of *Slc5a7*$^{+/+}$ females between time points 1 and 3 (mean difference=54.86; *p*=0.0012, figure 60D and table 44, appendix 7.5.5.2) but this was not seen in the *slc5a7*$^{+/TM1A}$ littermates. There is no difference at any time point between *Slc5a7*$^{+/TM1A}$ and *Slc5a7*$^{+/+}$ mice of either gender.

5.3 Discussion

While in-depth neurological phenotyping remains to be undertaken, preliminary phenotyping data indicates that *Slc5a7*$^{indelAC/+}$ display only a very mild motor phenotype involving reduced mean forepaw and all-paw grip strength at all time points. Due to the lack of detailed phenotypical data, it is not possible to draw direct comparisons between *Slc5a7*$^{indelAC/+}$ mice and human subjects with dHMN-VII. The apparently milder phenotype presenting in mice compared to human dHMN-VII subjects expressing the same mutated protein may be due to a number of reasons, elucidation of which requires far more rigorous neurophenotyping as well as molecular investigation in biopsied tissues.

Different neuronal cells within the same organism display variable vulnerability to factors contributing to neurodegeneration. It is thus possible that human neuronal cells affected by defective CHT also differ in their vulnerability when compared to those neuronal cells in *Slc5a7*$^{indelAC/+}$ mice, that would be considered to be representative with respect to their anatomical location and the tissues which they innervate. Another possibility is that the CHT choline transport activity of *Slc5a7*$^{indelAC/+}$ mice is not reduced comparably to that of our dHMN subjects such that cholinergic signalling is better supported. Anatomical distribution of cholinergic neurones and thus, CHT, has been found to be consistent between humans and mice(141). It is therefore unlikely that the difference in severity of phenotype is due to differences in CHT distribution. It has been reported that >20% of human essential genes have nonessential mouse orthologues(186). Although CHT has been shown to be essential for mouse survival(187) it is likely that mice express different proteins involved in the trafficking and regulation of CHT to humans, and that deletion of the transporters C-terminus is not as detrimental to these essential interactions. It has been reported that the phenotype of a given single gene mutation in mouse models is often modulated by the genetic background of the strain to which the mutation is introduced(188). This phenotypic variability has been attributed to the presence of different "*modifier-genes"* in the genomes of different inbred laboratory mouse strains, which act in combination with modified gene(188). If such differences arise between different strains of the same species, it is not surprising that a number of influencing factors and thus the phenotype may differ between human and mice harbouring orthologous mutations. It is also

possible that cholinergic signalling at the mouse NMJ does not require the same rate of choline reuptake activity to replenish ACh stores following transmission. Although wild type and *Slc5a7*^{indelAC} mRNA were found to be expressed at equivalent levels in *Slc5a7*$^{indelAC/+}$ animals, without specific measurement of the CHT protein levels in neuronal tissue from these animals the possibility that the milder phenotypic presentation in mice may also be due to reduced expression of the mutant protein during translation also exists.

The weaker grip strength observed in *Slc5a7*$^{indelAC/+}$ mice than in *Slc5a7*$^{+/+}$ mice at time point 1 indicate that 18 weeks is likely too late for commencement of phenotyping. The onset of loss of grip strength in *Slc5a7*$^{indelAC/+}$ mice may occur earlier than 18 weeks of age, while age related loss of all-paw grip strength in *Slc5a7*$^{+/+}$ mice reaches a similar level to that of the *Slc5a7*$^{indelAC/+}$ animals at around time point 2. Despite this, considering the progressive nature of dHMN-VII, one may have expected significant findings at all tested time points with a progressively worse presentation of *Slc5a7*$^{indelAC/+}$ mice compared to age and sex matched wild type littermates. However, the presence of neurological outcome clearly indicates that mild neurological features are present in this model that should be explored in more detailed phenotypical assays.
Overall, the motor-phenotyping results demonstrate that mice of all genotypes (*Slc5a7*$^{indelAC/+}$, *Slc5a7*$^{+/TM1A}$, and *Slc5a7*$^{+/+}$) within our cohort display a degree of loss of forepaw grip strength between the ages of 18 and 31 weeks. As mentioned above, it is possible that a greater difference exists between younger animals than those tested, which might better represent the teenage onset of dHMN-VII in human patients. Repetition of the tests carried out in this study on the same models post-exercise may also reveal a phenotypic difference between genotypes, however licencing restrictions do not permit for these further tests to be undertaken.

5.3.1 Future work- creation of a hypomorphoc compound heterozygous *Slc5a7*$^{indelAC/TM1A}$

Discussions are currently ongoing with partners at the University of Exeter Medical School animal unit and Prof Blakely's group at Vanderbilt University to undertake more detailed phenotypical assessments of *Slc5a7*$^{indelAC/+}$ mice. An

additional avenue of animal model development to recapitulate the patient dHMN(-VII) phenotype, is to create animals with hypomorphic choline transport by a combination of existing mutant alleles. Given the putative disease mechanism, this may provide an additional suitable substrate for testing the pharmacotherapies described in section 5.1.3. This work has commenced, however is still in early stages. Intercrossing of *Slc5a7*$^{indelAC/+}$ and *Slc5a7*$^{+/TM1A}$ mice resulted in the birth of compound heterozygous animals (*Slc5a7*$^{indelAC/TM1A}$) at expected ratios, confirmed by genotyping in 3-week old pups. From the initial litter 4 *Slc5a7*$^{+/TM1A}$ pups were born, which displayed a strong phenotype ~10 weeks of age. This included a reduction in body weight of 30% compared to their wild type littermates (table 30), as well as reduced activity in their home cage, ataxia, abnormal gait, tremors, reduced rearing, poor posture, and rapid, heavy breathing. These animals were culled prior to any motor-phenotyping for humane reasons. Additional *Slc5a7*$^{indelAC/TM1A}$ animals are currently under observation as they approach 10 weeks. These preliminary results are an encouraging indication that the *Slc5a7*$^{indelAC/TM1A}$ mice might indeed be showing phenotypes representative of that seen in dHMN-VII patients. Follow-up studies are required in order to confirm these findings.

Table 30. Genotyping and initial phenotyping of litter born from intercrossing Slc5a7indelAC/+ and Slc5a7+/TM1A mice

MOUSE ID	SEX	GENOTYPE	WEIGHT	PHENOTYPE
SGAQ17.1a	male	*slc5a7*$^{indelAC/TM1A}$	19.3g	YES
SGAQ17.1b	male	*slc5a7*$^{indelAC/+}$	28.7g	NO
SGAQ17.1c	male	*slc5a7*$^{indelAC/TM1A}$	19.6g	YES
SGAQ17.1d	male	*slc5a7*$^{+/+}$	27.9g	NO
SGAQ 17.1e	female	*slc5a7*$^{indelAC/TM1A}$	16.2g	YES
SGAQ 17.1f	female	*slc5a7* $^{+/TM1A}$	22.6g	NO
SGAQ 17.1g	female	*slc5a7* $^{+/TM1A}$	23.6g	NO

Should open field and grip strength phenotyping of *Slc5a7*$^{indelAC/TM1A}$ support a disease state comparable to dHMN, we plan to carry out further phenotyping, molecular investigation of the disease mechanism, and exploration of phenotype improvement with potential treatments. Further phenotyping analyses are likely to include treadmill testing to assess stamina and the maximum velocity at which mutant mice are able to move, rotarod testing to assess balance, motor coordination and endurance, and *in vivo* compound action potential recordings to assess nerve function. Careful observation for

signs of onset of the disease in *Slc5a7*$^{indelAC/TM1A}$ pups will be made from birth, important information when considering at what point in the animals life to administer trial treatments. Biochemical analyses will provide additional important insight into disease pathogenesis and will include western blotting for CHT in protein extracts of mouse neuronal tissue to analyse expression levels, measurement of ACh and CHT levels, assessment of CHT trafficking in nerve terminal preparations, and measurement of CHT activity. As discussed in section 5.1.3, we hypothesise that treatment with either a nAChR agonist or and AChE inhibitor might prevent and or alleviate symptoms caused by cholinergic dysfunction in this animal model of dHMN. We plan to trial these treatments in *Slc5a7*$^{indelAC/TM1A}$ animal in order to establish which, if either, is the more successful in treating symptoms with minimal side effects. This will also establish the most beneficial time to commence treatment (prenatally, from birth, shortly before disease onset, or at onset), and whether administration at a progressed disease stage alleviates symptoms or if the benefits are limited to early administration. Should trials be successful in animals, this will provide the scientific basis and impetus to potentially carry out a clinical trial for the appropriate treatment with our dHMN subjects.

6

CHAPTER SIX

FINAL DISCUSSION AND FUTURE WORK

6 FINAL DISCUSSION AND FUTURE WORK

The work in this thesis describes two distinct classes of novel *SLC5A7* mutations resulting in divergent clinical outcomes; an autosomal dominant adult-onset form of distal hereditary motor neuropathy, as well as autosomal recessive severe congenital predominantly central hypotonia with respiratory insufficiency, seizures and usually, infantile death. Genetic mapping, traditional and next generation sequencing techniques were applied in order to identify the location of the disease causing gene, and the respective mutations for these disorders. Following genetic verification, the causative mutations were subjected to *in silico* and molecular functional analyses to elucidate the structural and biomolecular effects of each mutation on the protein product. These findings were of significant enough scientific and medical impact to warrant the generation of a range of mouse models by our colleagues at WTSI, with a view to confirm pathogenicity of the truncated CHT protein, and trial putative treatment options as a prelude to clinical trials with human subjects. This section provides an overview of the findings of this thesis and relates these to the current literature, highlighting areas of future research.

The identification of the biomolecular basis of neurological disease provides information crucial for the specification of putative treatment options to alter the disease course. Approximately 5% of the world's population are estimated to be living with a 'rare' disease, with over 7000 having been reported, of which over 1150 are neurological(189). Thus, these disorders collectively pose a substantial clinical and financial burden. Importantly, due to the overlap of many of the biological pathogenic pathways implicated in many neurological diseases, discoveries of the biological basis of a particular (rare) disease will likely provide far more wide-ranging benefits for other conditions with a similar biological cause. Thus, treatment benefits of knowledge of one of these disorders is likely to extend far more widely, and provide a platform from which broader research might be directed.

The findings presented in this thesis has provided important new insights into NMJ dysfunction, and defined two novel human disorders that arise due to varying degrees of defective choline transport. ACh has well-defined

widespread actions as a neurotransmitter within the mammalian central, peripheral, and autonomic nervous systems. It is responsible for the normal functioning of a wide range of physiological and behavioural functions, including movement, cardiovascular activity, gut motility, arousal, attention, and memory. Within the CNS, ACh functions as a modulator of cognitive and appetitive processes including arousal, attention, memory and reward(32, 144). Cholinergic neurones of the CNS include motor neurones of the spinal cord, neurones within the basal forebrain, and interneurones in the caudate nucleus(147). Within the autonomic nervous system (ANS), ACh controls the output of many organs, including the heart, lungs, exocrine and endocrine glands, gut, and bladder, by mediating chemical signalling by both sympathetic and parasympathetic preganglionic neurones, and acting as a neurotransmitter at parasympathetic postganglionic synapses(32). ACh is also the principal neurotransmitter at the mammalian neuromuscular junction (NMJ) where it is critical for the control of muscular contraction. Our findings indicate that severe deductions (approaching 90%) of CHT activity may be tolerated and result in no (or only very late onset) neurological disease, which seems at odds with the key biological role of this molecule. Indeed our findings in dHMN, in which clinical signs appear to be restricted to motor neurones (specifically those innervating the distal limb muscles), indicate that it is the NMJ role of ACh that is impacted initially as CHT transporter activity is reduced. It is only with yet more severe reductions in CHT activity that the core CNS functions of ACh appear to be affected, resulting in a more severe central hypotonia phenotype. In addition, it will be interesting to investigate further whether the specific truncating mutation (p.H521Qfs*2) associated with dHMN-V lacking vocal cord involvement (family 5) permits slightly more CHT activity than the truncating mutation (p.K499Nfs*13) resulting in dHMN-VII associated with VCP. A slightly less severe impact on transporter function of p.H521Qfs*2 may account associated with the dHMN-V phenotype, and provide further insight into the pattern of selective neuronal loss and clinical outcome in these conditions.

As cholinergic neurotransmission supports a wide range of physiological and behavioural functions, it is not surprising that genetic variation and/or deficits in components of cholinergic signalling have been associated with a range of disorders, including myasthenias, cardiovascular disease, attention-deficit

hyperactivity disorder (ADHD), ADi, schizophrenia, addiction, and depression(1-3). It has been well established that basal forebrain cholinergic neurones are involved in learning and memory processes, and that impairment of cholinergic transmission contributes to the cognitive deficit in ADi(32, 190). Thus, enhancement of cholinergic transmission with the use of acetylcholinesterase AChE inhibitors is used, although with limited success, as a therapy for managing Alzheimer's related cognitive decline(1, 3). Although useful in some instances, medications used in the treatment of these disorders are often insufficiently specific resulting in global side-effects, they may also exhibit dose-limiting side effects, and usually act independently of neuronal activity(3). AChE inhibitors have not previously been trialled for the treatment of motor neurone degenerative disease, however they have been considered, and rejected, as a tool for the diagnosis of progressive muscular atrophy and amyotrophic lateral sclerosis(191). Our findings may provide an explanation for this and indicate that these treatments may only be of relevance in forms of MND in which ACh / CHT malfunction is the biological basis of the disease.

The elimination of CHT in transgenic mice produces time-dependent eradication of cholinergic signalling presenting as immobility, failure to feed and cyanosis that is incompatible with life(187, 192). Consistent with this, our data indicates that elimination of CHT activity in human subjects results in a similar outcome. However, as we have not yet been unable to explore choline uptake activity in cells natively expressing CHT mutants, we are unable to conclude whether the longer lifespan of the Turkish hypotonic children (family 6) may result from a slightly increased CHT transport activity of p.S94R mutant protein compared with p.V112E. Furthermore, although $CHT^{+/-}$ mutant animals exhibit features consistent with reduced CNS and autonomic levels of ACh(193), the deficits of both the dHMN-VII and dHMN-V subjects investigated in this project are more severe than in hemizygous *Slc5a7* mice. This is supportive of our finding of a dominant negative mode of action of truncated CHT on the wild type molecule, and this aspect may be further illuminated by assessment of NMJ morphology in the affected endplates of individuals with dHMN-VII and dHMN-V and studies in *Slc5a7*$^{indelAC/+}$ and *Slc5a7*$^{indelAC/TM1A}$ transgenic mouse models.

In addition to CHT, two additional families of choline transporter exist: the intermediate-affinity choline transporter-like (CTL) family, and the organic action

transporters (OCTs). The three families of choline transporters, although similar in that they comprise a single homogeneous glycoprotein with multiple transmembrane domains, differ in their specific structure, affinity for choline, and the fate of the choline translocated(147). Where CHT is dedicated to providing choline for ACh synthesis in cholinergic nerve terminals, more widely expressed choline transporters support other aspects of choline metabolism. The ubiquitously expressed intermediate-affinity choline transporter-like (CTL1) transports choline for the production of membrane lipid phosphatidylcholine, the body's most abundant choline metabolite, constituting ~50% of the total cell membrane lipid content(190). This is thus unlikely to act as a compensator for defective CHT choline transport. OCTs 1-3 operate as polyspecific uniporters which mediate facilitated diffusion of organic cations, weak bases and some neutral compounds in both directions across the plasma membrane, including choline(194). OCT2, although predominantly expressed in basolateral membrane of the proximal tubules of the kidney, has also been reported to be localised on the synaptic vesicles of presynaptic cholinergic neurone terminals surrounding motor neurones at the spinal cord and NMJ. This suggests a possible role for this transporter in cholinergic neurones as well as a possible collaboration between OCT2 and CHT(195). There is no evidence however, suggesting a compensatory role of OCT2 in the absence or reduction of CHT activity.

Although efficacious treatments exist for acquired neuropathies such as chronic inflammatory demyelinating polyneuropathy (steroids, IVIg, or plasmapheresis) and multifocal motor neuropathy (IVIg)(196), to date no cure has been developed for hereditary motor neuropathies. Intervention for these hereditary disorders including CMT and HNPP is restricted to the management of symptoms, such as physical and occupational therapy, and orthotic devices(196). Having gained mechanistic insight into the course of dHMN, we have been able to hypothesise putative treatment interventions (chapter 5.1.3) which may augment cholinergic signalling in affected subjects and we plan to trial these putative treatments in transgenic mice as a prelude to clinical trials. If successful, this will be the first MND for which knowledge of the genetic and molecular basis of the disease has led to the identification of pharmacological intervention. Further, a number of molecules and molecular complexes are

involved in the ACh cycle at cholinergic terminals with roles ranging from the regulation of ACh vesicle formation and membrane fusion, to ACh synthesis and hydrolysis, and the transport and maintenance of its various components. In this regard, genetic variation and/or deficits in components of cholinergic signalling have been associated with a range of disorders including myasthenias, cardiovascular disease, attention-deficit hyperactivity disorder (ADHD), ADi, schizophrenia, addiction, and depression(1-3). Myasthenia Gravis and the congenital myasthenic syndromes can arise from mutations in one of multiple genes encoding proteins expressed at the NMJ. These include AChR subunits (*CHRNE, CHRNA1, CHRNB1, CHRND*), AChE subunits (*COLQ*), ion channels subunits (*SCN4A*), as well as genes encoding proteins with roles in ACh synthesis (*CHAT*), AChR clustering (*MUSK*) and stabilisation (*RAPSN*), and NMJ development (*AGRN*)(148, 149, 197). Interestingly, *CHAT* mutations have been associated with hypotonia and respiratory failure at birth, similar to the cases seen in families 6 and 7. Myasthenias are most commonly treated with AChE inhibitors (pyrosigmine) which are largely beneficial(198, 199). There are however certain subtypes such as the *DOK7*-related myasthenias that show no improvement or even deteriorate with AChE inhibitors(198). CHT polymorphisms have been associated with ADHD(2) and it has been well established that basal forebrain cholinergic neurones are involved in learning and memory processes, and that impairment of cholinergic transmission contributes to the cognitive deficit in ADi(32, 190). Although useful in some instances, medications used in the treatment of these disorders are often insufficiently specific resulting in global side-effects, and they may also exhibit dose-limiting side effects and usually act independently of neuronal activity(3). Thus should intervention of the ACh cycle at cholinergic terminals prove to be successful in the treatment of dHMN subjects, this will likely provide a platform from which investigation may be taken into developing treatment interventions targeted to different aspects of cholinergic signalling which form the basis of these other ACh-associated disorders.

7

CHAPTER SEVEN

APPENDIX

7 APPENDIX

7.1 APPENDIX CHAPTER 1

7.1.1 Table 31. Demyelinating CMT subtypes, their distinguishing features, and their associated genes and their functions

Demyelinating CMT subtype	Mode of inheritance & Distinguishing characteristics	Average mNCVs (m/s)	Gene name (symbol) chromosomal location	Protein function
CMT-IA	AD.70-80% of CMT-I cases. Less severe than CMT-IB. Onset in 1st-2nddecade. Accounts for ~50% all CMT patients.	15-20	Peripheral myelin protein-22 (*PMP22*) 17p12	Comprises 2-5% of peripheral myelin. Expressed predominantly in Schwann cells and plays a role in Schwann cell development.
CMT-IB	AD. More severe than CMT-IA. Onset from birth to second decade.	<20	Myelin protein zero (*MPZ* or P_0) 1q23	Comprises 50% of peripheral myelin. Expressed in Schwann cells and is the major myelin structural protein.
CMT-IC	AD. Distinguishable from other types of CMT-I by genetic evidence only.	16-25	Lippolysaccharide-induced tumour necrosis factor alpha factor (*LITAF*) 16p13.13	Associated with p53, known to regulate apoptosis pathways. Expressed in Schwann cells and 3 other cell types. May play a role in protein degradation pathway.
CMT-ID	AD. Distinguishable from other types of CMT-I by genetic evidence only.	26-42	Early growth response 2 (*EGR2*) 10q21.3	Induces essential myelin genes in Schwann cells.
CMT-IE	AD. CMT associated with deafness	29-43	Peripheral myelin protein-22 (*PMP22*) 17p12	See CMT-IA above
CMT-IF	AD. Increased severity compared with other CMT-I subtypes. Onset from 1-13 years.	9-20	Neurofilament protein, light polypeptide (*NEFL*) 8p21.2	Interacts with MTMR2 which is expressed in both myelin-forming and non-myelin forming Schwann cells, and both sensory and motor neurones.
HNPP	AD. Onset usually in second or third decade. Tomacular (sausage shaped) swellings cause repeated focal pressure neuropathies, eg. Peroneal palsy with foot drop.		Peripheral myelin protein-22 (*PMP22*) 17p12	Comprided 2-5% of peripheral myelin. Expressed predominantly in Schwann cells and plays a role in Schwann cell development.
CMT-IX	X-linked dominant. Affects heterozygous females more mildly than homozygous males. Stroke like presentation has been reported.	Males: 30-50 Females: 31-52	Gap junction protein, beta 1 (*GJB1*) Xq13.1	Also known as connexin-32 (*CX32*). Transmembrane channels that cluster in gap junction to allow diffusion of low molecular weight materials between cells.
CMT as yet unclassified	X-linked. Onset ~50 years. Absent sural and superficial peroneal sensory response. Normal reflexes accept	36-48	Dystrophin-related protein 2 (*DRP2*) Xq22.1	Interacts with periaxin (see CMT-4F) and dystroglycan and plays a role in the maintenance of Cajal bands of

	absent ankle jerks. Relatively rapid progression.			myelinating Schwann cells
CMT-4A	AR. Severe neuropathy with onset before 2 years. Rapidly progressive weakness and wasting. Basal laminal onion bulbs.	30	Ganglioside-induced differentiation-associated protein 1 (*GDAP1*) 8q21.11	Regulator of mitochondrial dynamics that are vital for the function of myelinated peripheral nerves by promoting mitochondrial fission. Expressed in both Schwann cells and neurones. May be involved in neuronal development. Regulates glutathione metabolism, sensitivity to apoptosis, and reactive oxygen species levels.
CMT-4B1	AR. Focally folded myelin sheaths.	0-17	Myotubularin-related protein 2 (*MTMR2*) 11q21	Phosphate that acts on lipids and phosphoinositol headgroup.
CMT-4B2	AR. Onset 5-8 years. Focally folded myelin sheaths. Juvenile-onset or congenital open-angle glaucoma may be present	<20	Myotubularin-related protein 13 or SET binding factor (*SBF2*) 11p15.4	Guanine nucleotide exchange factor (GEF) which may activate RAB28.
CMT-4B3	AR. Onset 5-11 years. Focally folded myelin sheaths, few onion bulbs and occasional regenerating clusters of axons.	<38	Myotubularin-related protein 5 or SET binding factor (*SBF1*) 22q13.33	Possible pseudophosphatase. May function as a guanine nucleotide exchange factor activating RAB28.
CMT-4C	AR. Classic CMT often with early onset severe scoliosis, often requiring surgery. Onset from infancy to 37 years. Highly variable phenotype.	19-30	SH3 domain and tetratricopeptide repeat-containing proteins 2 (*SH3TC2*) 5q32	Involved in Rab11 regulation of recycling of internalised membrane and receptors. Contains a SOX10-CREB binding element that functions as an enhancer.
CMT-4D	AR. Classic CMT with onset in 1st decade and deafness developing by the 3rd decade. Kyphoscoliosis may be present	Progressively reduced till unattainable after 15 years	NMYC downstream-regulated gene 1 (*NDRG1*) 8q24.22	May play a role in growth arrest and cell differentiation, and Schwann cell signalling. Upregulated in hypoxic cells. Expression is particularly high in Schwann cells.
CMT-4E	AR. Onse from birth to 7 years. Congenital cases show respiratory distress. Scoliosis, chest deformities, and *pes equinovarus* may be present.	0-3	Early growth response 2 (*EGR2*) 10q21.3	See CMT-ID
			Myelin protein zero (*MPZ* or P_0) 1q23	See CMT-IB
CMT-4F	AR. Variable age of onset from infancy to adulthood. When onset is in infancy, characterised as Dejerine-Sottas syndrome. Slowly progressive,	3-15	Periaxin (*PRX*) 19q13.2	Required for myelin sheath maintenance. May specifically affect the internodal length, but not other parameters.

	onion bulb formation, focal myelin swelling			
CMT-4G	AR. aka Russe-type HMSN. Severe CMT with onset by or in teenage years. Prominent sensory loss. Foot and hand deformities. Occasionally scoliosis is present.	25-37	Hexokinase-1 (*HK1*) 10q22.1	Allosteric enzyme involved in hexose metabolism.
CMT-4H	AR. Early onset with variable severity. Slow rate of progression. Hypoplasia or hypotrophy of hypothenar muscles. Distal sensory loss. Myelin out-foldings. Frequent scoliosis	8-13	FGD1-related F-actin-binding protein, FRABIN (*FGD4*) 12p11.21	GDP/GTP exchange protein for CDC42 and possesses actin filament binding activity. Role in PNS unclear. Induces CDC42-mediated cell shape changes in Schwann cells, suggesting Rho GTPase signalling is required for myelination of peripheral axons.
CMT-4J	AR.- Compound heterozygous mutation identified. Childhood onset. Progressive proximal weakness and evidence of chronic denervation in both proximal and distal muscles. Severely diminished or absent sensory NCVs.	0-16	Polyphosphoinositide phosphatase (*FIG4*) 6q21	Plays a role in the biogenesis of endosome carrier vesicles / multivesicular bodies transport intermediates from early endosomes.
CMT-4	AR. Classic CMT with intermediate NCVs	25-40	Peripheral myelin protein-22 (*PMP22*) 17p12	See CMT-IA Caused by autosomal recessive point mutations
			Myelin protein zero (*MPZ* or P_0) 1q23	See CMT-IB

Abbreviations: **AD**=Autosomal dominant; **AR**=Autosomal recessive; **aka=**also known as; **HMSN=**hereditary motor and sensory neuropathy; **PNS=**peripheral nervous system; **NCV=**nerve conduction velocity (49, 58, 73, 77, 78, 93, 97, 108, 200-237)

7.1.2 Table 32. Axonal CMT subtypes, their distinguishing features, and their associated genes and their functions

CMT-II subtype	Mode of inheritance & Distinguishing characteristics	Gene name (symbol) chromosomal location	Protein function
CMT-IIA1	AD. Distinguishable from other forms of CMT-II by genetic evidence only. Caused by mitochondrial defect. Onset in first decade.	Kinesin superfamily member 1B (*KIF1B*) 1q36.22	Motor for anterograde transport of mitochondria. Has microtubule plus end-directed motility. Plays a role in the induction of neuronal apoptosis.
CMT-IIA2	AD & AR. Distinguishable from other forms of CMT-II by genetic evidence only. Caused by mitochondrial defect. Highly variable phenotype and age of onset, and some mutation carriers may be asymptomatic.	Mitofusin (*MFN2*) 1p.36.2	Located on out mitochondrial membrane and mediates mitochondrial fusion and thus, regulates mitochondrial architecture and morphology.
CMT-IIB	AD. Frequent ulcers and infections leading to amputation of the toes. Foot pain with swelling and deformity. Scoliosis, absent ankle reflexes, decreased distal sensation and lateral-gaze nystagmus may develop.	Ras-associated protein RAB7 (*RAB7A*) 3q21.3	Key regulator of endo-lysosomal trafficking. Roles in growth factor-mediated signalling, nutrient transporter mediated nutrient uptake, neurotrophin transport, and lipid metabolism.
CMT-IIB1	AR. Onset in second decade. Proximal muscle involvement in some cases.	Lamin A/C (*LMNA*) 1q22	Encodes two structural protein components of the nuclear lamina (lamina A and C). Roles in determining nuclear assembly, chromatin organisation, and nuclear membrane and telomere dynamics.
CMT-IIB2	AR. Adult onset (28-42 years). Symmetrical weakness and wasting of the upper and lower limbs. Symmetrical ‘sock and glove’ pattern of sensory loss.	Mediator complex subunit 25 (*MED25*) 19q13.33	Component of the mediator complex, involved in the regulated transcription of nearly all RNA polymerase II-dependent genes. Significant correlation between expression of *MED25* and *PMP22.*
CMT-IIC	AD. Lateral or bilateral diaphragmatic, intercostal, and vocal cord weakness. Variable severity and age of onset.	Transient receptor potential cation channel, subfamily V, member 4 (*TRPV4*) 12q44.11	Calcium channel found on the membrane of many cells types and plays a role in a number of different functions including the sensation of pain. Also implicated in SPSMA and congenital dSMA (table 35, appendix)
CMT-IID	AD. Onset between 16 and 30 years. Presents and predominates in the hands.	Glycyl-tRNA (*GARS*) 7p14.3	Plays an important role in protein synthesis. Catalyses attachment of glycine to tRNA(Gly).
CMT-IIE	AD. Distinguishable from other forms of CMT-II by genetic evidence only. Onset between first and third decade of life.	Neurofilament protein, light polypeptide (*NEFL*) 8p21.2	Interacts with MTMR2 which is expressed in both myelinating and non-myelination Schwann cells, and both sensory and motor

			neurones.
CMT-IIF	AD. Distinguishable from other forms of CMT-II by genetic evidence only. Variable age of onset from 15 to 60 years.	Heat-shock protein 27kDa (*HSPB1*) 7q11.23	Co-expressed with *NEFL*. Expressed in response to environmental stress and involved in actin organisation.
CMT-IIG	AD. Onset between 9 and 76 years, although most present in second decade.	Unknown 12q12-q13	Unknown
CMT-IIH	AR. CMT with pyramidal syndrome. Onset between 4 and 8 years.	Unknown 8q13-q21.11	Maps to a locus containing *GDAP1*, in which mutations have been identified in other CMT cases.
CMT-IIi	AD. Onset between 47 and 70 years. Fast disease progression.	Myelin protein zero (*MPZ* or P_0) 1q23	Comprises 50% of peripheral myelin. Expressed in Schwann cells and is the major myelin structural protein.
CMT-IIJ	AD. Pupillary abnormalities and deafness/partial hearing loss. Onset between late teens and sixth decades.	Myelin protein zero (*MPZ* or P_0) 1q23	See CMT-IIi
CMT-IIK	AD & AR. Distinguishable from other forms of CMT-II by genetic evidence only. Onset in first decade for AR mutations and ranges from first to third decade for AD mutations.	Ganglioside-induced differentiation-associated protein 1 (*GDAP1*) 8q21.11	Regulator of mitochondrial dynamics that are vital for the function of myelinated peripheral nerves by promoting mitochondrial fission. Expressed in both Schwann cells and neurones. May be involved in neuronal development. Regulates glutathione metabolism, sensitivity to apoptosis, and reactive oxygen species levels.
CMT-IIL	AD. Distinguishable from other forms of CMT-II only by genetic evidence. Onset between 15 and 33 years.	Heat-shock protein 22kDa, protein 8 (HSPB8) 12q24	Inhibits protein aggregation by acting as a chaperone.
CMT-IIN	AD. Onset between 6 and 54 years. Variable severity. Occasional sensorineural deafness of varying severity.	Alanyl-tRNA synthetase (*AARS*) 16q22.1	Attaches the amino acid alanine to its appropriate tRNA. Edits incorrectly charged tRNA(Ala) via its editing domain.
CMT-IIO	AD. Childhood onset. Slowly progressive. Occasional transient paraesthesia and neuropathic lower limb pain.	Cytoplasmic dynein 1, heavy chain 1 (*DYNC1H1*)	Motor for intracellular retrograde transport of vesicles and organelles along microtubules.
CMT-IIP	AD & AR. Onset in second and fourth decades. Slowly progressive.	Leucine-rich repeat-and sterile alpha motif-containing 1 (*LRSAM1*) 9q33.3-q34.1	Involved in protein ubiquitination and plays a role in sorting endocytic and exocytic cargos.
CMT-IIQ	AD. Distinguishable from other forms of CMT-II only by genetic evidence Onset between 13 and 25 years.	Dehydrogenase E1 and transketolase domains-containing protein 1 (*DHTKD1*) 10p14	Forms part of the 2-oxoglutarate dehydrogenase complex, which catalyses the conversion of 2-oxoglutarate to succinyl-CoA and CO_2.

CMT-IIR	AR. Onset in early infancy. Tracheomalacia, respiratory insufficiency associated with vocal cord paralysis. Decreased motor and sensory amplitudes. Decreased motor and sensory nerve conduction velocities consistent with sever axonal polyneuropathy.	Tripartite motif-containing protein-2 (*TRIM2*) 4q31.3	UBE2D1-dependent E3 ubiquitin-protein ligase. Mediates ubiquitination of NEFL and phosphorylated BCL2. Plays a role in rapid ischemic tripartite-induced neuroprotection. Regulates neuronal polarisation.
CMT-IIS	AR. Onset in first decade. Presents as delayed motor development and gat difficulties, such as toe walking, foot drop, and steppage gait. Most patients require ankle foot orthoses for walking, some wheelchair bound. Hand involvement at onset or soon after.	Immunoglobulin μ-binding protein 2 (*IGHMBP2*) 11q13.3	5'-3' helicase. Binds a specific DNA sequence from the immunoglobulin mu chain switch region. Acts as a transcription regulator. Bot heterozygous and compound heterozygous mutations identified. Also mutant in dHMN-VI (table 35, appendix)
CMT-IIT	AR. Onset in third decade as unstable gait and dys/paresthesias in the distal lower limbs.	DnaJ (Hsp40) homolog, subfamily member 2 (*DNAJB2*) 2q35	Encodes heat-shock protein 40 (HSP40), a molecular co-chaperone member of the heat shock protein family.
CMT-IIU	AD. Late onset (50 to 60 years). Muscle weakness and wasting presents in both the hands and feet with equal severity and progression. Neuropathic pain in some subjects.	Methionyl-tRNA synthestase (*MARS*) 12Q13.3	Enzyme responsible for charging tRNA molecules, which is essential for protein translation in cytoplasm and mitochondria.
CMT-IIV	AD. Late onset (30 to 61 years). Presenting and dominating feature is recurrent foot pain. Some subjects develop distal upper limb parathesias. Physical and electrophysiological examination suggestive of peripheral neuropathy.	α-*N*-acetyl-glucosaminidase (*NAGLU*) 17Q21.2	Enzyme involved in the hydrolysis of terminal non-reducing N-acetyl-D-glucosamine residues in N-acetyl-α-D-glucosaminides. Involved in degradation of heparin sulphate. Patient leukocytes show average of 45% decrease in enzymatic activity.
CMT-IIW	AD. Variable age of onset (childhood to 62 years). Presents in lower limbs as gait difficulties, steppage gait, or foot deformities. Pain and hand weakness in few subjects, but upper limb involvement is rare.	Histidyl-tRNA synthetase (*HARS*) 5q31.3	Enzyme responsible for charging tRNA molecules, which is essential for protein translation in cytoplasm and mitochondria.
AR-CMT-II with neuromyotonia	AR. Onset in first decade. 'Motor greater than sensory neuropathy'- pure motor in some patients and mixed motor and sensory in others. Neuromyotonia.	Histidine triad nucleotide binding (*HINT1*) 5q23.3	Ubiquitously expressed. Binds and hydrolyses adenosine 5′-monophosphoramidate substrates. Haploinsufficient tumour suppressor genes that promotes apoptosis, inhibits the transcriptional activity of beta-catenin/TCF4, USF2 and NFkappaB, and inhibits the expression of endogenous cyclin D1 and

			TGFbeta2.
HMSNP	AD. Onset between third and fourth decade. Painful muscle cramps and fasciculations.	TRK-fused gene (*TFG*) 3q12.2	Plays a role in normal dynamic function of the endoplasmic reticulum and its associated microtubules.
CMT-II as yet unclassified	AD. Onset between early childhood and fifth decade. Variable rate of progressing and severity.	Valosin-containing protein Valosin-containing protein (*VCP*) 9p13.3	Required for export of endoplasmic reticulum into the cytosol. Associated with several essential cell protein pathways including cell cycle, homotypic membrane fusion, nuclear envelope reconstruction, DNA damage response, apoptosis suppression, and ubiquitin-dependent protein degradation.
CMT-II presenting as dHMN	Mitochondrial. Onset from 3 years to second adolescence. Variable expression and variable, and sometimes incomplete penetrance. Often presents as a purely motor neuropathy with sensory symptoms developing subsequently.	Mitochondrially encoded STP synthase 6 (*MT-ATP6*) base pairs 8,527 – 9,207	Subunit of Complex V (ATP synthase), which produces ATP from ADP in the presence of a proton gradient across the mitochondrial membrane.
HMSN-II with neurofilament accumulation	AD. Classic CMT-II with axonal swelling (giant axons). Variable severity. More severe cases also have cardiomyopathy.	DDB1- and CUL4-associated factor 8 (*DCAF8*) 1q23.2	Contains 7 WD repeats that form a β-propeller and interacts with DDB1 protein in the CUL4-DDB1 E3 ubiquitin ligase macromolecular complex, which regulates cell proliferation, DNA repair, and chromatin integrity through targeted ubiquitination of specific substrates.
Giant axonal neuropathy	AR. Onset by 3 years. Severe progressive peripheral motor and sensory neuropathy. Frizzly hair in ~60%, CNS involvement in ~90%, sensory involvement in ~50%. Giant axons caused by neurofilament accumulation.	Gigaxonin (*GAN*) 16q23.2	Ubiquitously expressed. Plays an important role in the cytoskeleton by stabilisation of the microtubule network.

Abbreviations: **AD**=Autosomal dominant; **AR**=Autosomal recessive; **tRNA**= transfer RNA (40, 52, 53, 69, 72, 74, 76, 79, 83-85, 87, 89, 115, 128, 130, 238-282)

7.1.3 Table 33. Intermediate CMT subtypes, their distinguishing features, and their associated genes and their functions

Intermediate CMT subtype	Mode of inheritance & Distinguishing characteristics	Average mNCVs (m/s)	Gene name (symbol) chromosomal location	Protein function
DI-CMTA	AD. Onset ~6 years. Slow but steady disease progression till 30 years. Rapid disease progression from 40 – 50 years until later stabilisation.	25-45	Unknown. 10q24.1-q25.1	Unknown
DI-CMTB	AD. Onset from 2 – 50 years. Shares clinical features with CMT-I and CMT-II. Cataracts and neutropenia	24-54	Dynamin-2 (*DNM2*) 19q13.2	GTPase involved in intracellular vesicle trafficking and cytoskeleton remodelling with ubiquitous tissue expression.
DI-CMTC	AD. Onset from 5-59 years. Motor symptoms predominate over sensory. Slow progression and moderate severity.	30-40	Tyrosyl-tRNA synthetase (*YARS*) 1p35.1	Essential enzyme for protein biosynthesis. Expressed ubiquitously. catalyses the aminoacylation of tRNATyr with tyrosine.
DI-CMTD	AD. Onset between 14 and 17 years. Calf hypertrophy. Aidie's pupil.	35-43	Myelin protein zero (*MPZ* or P_0) 1q23	Approximately 30% of MPZ mutations are associated with intermediate DI-CMTD. Comprises 50% of peripheral myelin. Expressed in Schwann cells and is the major myelin structural protein.
DI-CMTE	AD. Onset from 5 - 28 years. CMT associated with focal segmental glomerulosclerosis. Proteinuria. Sensory loss in 50%. Sensorineural hearing loss in 30%. Muscle cramps.	23-45	Inverted formin-2 (*INF2*) 14q32.33	Member of the diaphanousrelated formin family, which is involved in remodelling the microtubule cytoskeleton and actin. Interacts with Rho-GTPase CDC42, lymphocyte protein, and myelin-important commencement and maintenance of myelination.
DI-CMTF	AD. Onset from 10 – 45 years. Clinical severity from asymptomatic t wheelchair bound.	16-46	Guanine-nucleotide-binding protein subunit beta-4, Gβ4 (*GNB4*) 3q26.33	Forms part of a complex that form a receptor which transmits extracellular signals into cells following activation by various signalling factors. Abundant in Schwann cells and peripheral axons.
RI-CMTA	AR. Mixed features of demyelinating and axonal CMT. Severity (CMTNS>20)	25-35	Ganglioside-induced differentiation-associated protein 1 (*GDAP1*) 8q21.11	Regulator of mitochondrial dynamics that are vital for the function of myelinated peripheral nerves by promoting mitochondrial fission. Expressed in both Schwann cells and neurones. May be involved in neuronal development.

				Regulates glutathione metabolism, sensitivity to apoptosis, and reactive oxygen species levels.
RI-CMTB	AR. Dysmorphic features, developmental delay, self-abusive behaviour. and vestibular Schwannoma (benign intracranial tumour of Schwann cells)	30-40	Lysyl-tRNA synthetase (*KARS*) 16q23.1	Enzyme responsible for charging tRNA molecules, which is essential for protein translation in cytoplasm and mitochondria.
RI-CMTC	AR. Onset between first and fifth decades. Mildly increase serum creatine kinase, fatty replacement of muscle tissue.	24-39	Pleckstrin homology domain-containing family G member 5 (*PLEKHG5*) 1p36.31	Predominantly expressed in the peripheral nervous system. Dbl-homology – pleckstrin-homology motif is the minimal unit for the nucleotide exchange-promoting function of guanine nucleotide exchange factors (GEFs). Pleckstrin-homology domain plays important role in the allosteric regulation of the RhoGEF domain- initiating mechanisms that regulate neuronal shape and plasticity, dendrite growth, synapse formation, neuronal survival.

Abbreviations: **AD**=Autosomal dominant; **AR**=Autosomal recessive; **CMTNS**=Charcot-Marie-Tooth neuropathy score; **tRNA**= transfer RNA (50, 65, 75, 86, 88, 96, 283-297)

7.1.4 Table 34. X-linked CMT subtypes, their distinguishing features, and their associated genes and their functions.

CMT-X subtype	Mode of inheritance & Distinguishing characteristics	Average mNCVs (m/s)	Gene name (symbol) chromosomal location	Protein function
CMT-IX	X-linked dominant. CMT-I phenotype (table 31) Affects heterozygous females more mildly than hemizygous males. Stroke like presentation has been reported.	Males: 30-50 Females: 31-52	Gap junction protein, beta 1 (*GJB1*) Xq13.1	Also known as connexin-32 (*CX32*). Transmembrane channels that cluster in gap junction to allow diffusion of low molecular weight materials between cells.
CMT-X2	X-linked recessive. Variable age of onset. Mental retardation in some cases, normal intelligence in others.	N/A	Unknown Xp22.2	Unknown
CMT-X4 (Cowchock syndrome)	X-linked recessive. Childhood onset. Slowly progressive with deafness and cognitive impairment.	Mildly reduced or normal	Apoptosis-inducing factor (AIF) mitochondrion-associated 1 (*AIFM1*) Xq26.1	Mitochondrial flavoprotein involved in caspase-independent cell death
CMT-X5 (Rosenberg-Chutorian syndrome)	X-linked recessive. Polyneuropathy with visual impairment due to optic atrophy, and hearing loss.	43-51	Ribose-phosphate pyrophosphokinase 1 (*PRPS1*) Xq22.3	Metabolic enzyme that catalyses the synthesis of phosphoribosylpyrophosphate, essential for purine metabolism and nucleotide biosynthesis.
CMT-X6	X-linked dominant. Onset between 2 and 13 years in males, Slowly progressive but patients remain ambulant and enganged in employment or stdy. CMTNS = 11.5 ±3.3 in males; 2.0 ±2.2 in females.	38-63	Pyruvate dehydrogenase kinase, isoenzyme 3 (*PDK3*) Xp22.11	Located in mitochondrial matrix. One of 4 dehydrogenase enzymes, which negatively regulates pyruvate dehydrogenase complex activity- key enzyme linking glycolysis to Krebs cycle and lipogenic pathways.
dHMN-X (SMAX3)	X-linked recessive. Onset between 1 and 30 years. Purely motor.		Copper-transporting ATPase 1 (*ATP7A*) Xq21.1	P-type ATPase copper transporter. Also defective in Menkes disease, a sever infantile-onset neurodegenerative condition.

Abbreviations: **N/A**: information not available; **CMTNS**=Charcot-Marie-Tooth neuropathy score; **SMAX3**=Distal spinal muscular atrophy, X-linked 3 (97, 98, 100-102, 104, 105, 108, 109)

7.1.5 Table 35. Distal hereditary motor neuropathy subtypes, their distinguishing features, and their associated genes and their functions

dHMN subtype	Mode of inheritance & Distinguishing characteristics	Gene name (symbol) chromosomal location	Protein function
dHMN	AD, AR, and sporadic. Onset between 1 and 45 years. Hyporeflexia or areflexia. Normal mNCVs. Onset usually in the lower limbs.	Histidine triad nucleotide binding (*HINT1*)	Ubiquitously expressed. Binds and hydrolyses adenosine 5′-monophosphoramidate substrates. Haploinsufficient tumour suppressor genes that promotes apoptosis, inhibits the transcriptional activity of beta-catenin/TCF4, USF2 and NFkappaB, and inhibits the expression of endogenous cyclin D1 and TGFbeta2.
dHMN-I	AD. Onset by 20 years, usually first decade. Classic dHMN features	Unknown 7q34-q36	Unknown
dHMN-II	AR. Onset from early childhood to late adulthood. Variable severity. Some heterozygous gene carriers remain asymptomatic but show electrophysiological abnormalities.	Histidyl-tRNA synthetase (*HARS*) 5q31.3	Enzyme responsible for charging tRNA molecules, which is essential for protein translation in cytoplasm and mitochondria.
dHMN-IIA	AD. Onset between 15 and 20 years. Rapid disease progression with complete lower limb paralysis within 5 years of onset.	Heat shock 22-KD protein 8 (*HSPB8*) 12q24.23	Displays temperature dependent chaperone activity. Role in prevention of protein aggregation as well as roles in regulation of cell proliferation, apoptosis, and carcinogenesis.
dHMN-IIB	AD. Onset from 21 to 54 years. Slow disease progress. Presents in lower limbs and progresses to upper limbs 10 to 15 years later.	Heat shock 27-KD protein 1 (*HSPB1*) 7q11.23	Induced by environmental stress and developmental changes. Involved in stress resistance and actin organisation. Translocated from cytoplasm to nucleus in response to stress.
dHMN-IIC	AD. Onset at the start of the third decade. Slow disease progress.	Heat shock 27-KD protein 3 (*HSPB3*) 5q11.2	Muscle specific inhibitor of actin polymerisation
dHMN-IID	AD. Onset between second and fourth decades. Slowly progressive lower limb weakness and wasting. Variable severity.	F-box only protein 38 (*FBXO38*) 5q32	Contains F-box domain. May play a role in protein ubiquitination.
dHMN-VA	AD. Onset between 12 and 36. Most before 20 years. Muscle weakness and wasting presents and predominates in the upper limbs.	Glycyl-tRNA (*GARS*) 7p14.3	Plays an important role in protein synthesis. Catalyses attachment of glycine to tRNA(Gly).
		Seipin (*BSCL2*) 11q12.3	Regulator of lipid catabolism essential for adipocyte differentiation. Necessary for correct lipid storage and lipid droplets maintenance Also mutated in Silver syndrome.

dHMN-VB	AD. Onset in first or second decade. Muscle weakness and wasting presents and predominates in the upper limbs.	Receptor expression-enhancing protein 1 (*REEP1*) 2p11.2	Mitochondrial protein that serves to enhance cell surface expression of odorant receptors. Also mutant in SPG31.
dHMN-VI (dSMA6/SMARD1)	AR. Early onset- 1 or 2 months of age. Presents as respiratory distress and a weak cry due to diaphragmatic paresis.	Immunoglobulin µ-binding protein 2 (*IGHMBP2*) 11q13.3	5'-3' helicase. Binds a specific DNA sequence from the immunoglobulin mu chain switch region. Acts as a transcription regulator.
dHMN-VII	AD. Variable age of onset. Muscle weakness and wasting present in the small muscles of the hand. Vocal cord paresis presents as a husky voice due to involvement of the tenth cranial nerve.	Solute carrier family 5 [choline transporter], member 7 (*SLC5A7*) 2q12.3	Encodes the Na(+)- and Cl(-)- dependant high affinity choline transporter, CHT. Responsible for mediating choline uptake for acetylcholine synthesis at NMJ.
dHMN-VIIB	AD. Onset in early adulthood. Muscle weakness and wasting present in the small muscles of the hand. Respiratory difficulties due to vocal cord paresis.	Dynactin (*DCTN1*) 2p13.1	$p150^{Glued}$ subunit of dynactin. A complex of microtubule-based biologic motor proteins required for cytoplasmic dynein driven movement of organelles along microtubules. Interacts with dynein via $p150^{Glued}$.
dHMN-X (SMAX3)	X-linked recessive. Onset from 1 to 50 years. Very slow disease progression. Remain ambulant.	Copper-transporting ATPase 1 (*ATP7A*) Xq21.1	P-type ATPase copper transporter. Also defective in Menkes disease, a sever infantile-onset neurodegenerative condition.
dHMN Jaresh type	AR. Onset from 6 to 10 years. Weakness and atrophy progresses from lower to upper limb muscles within 2 years of onset. Mild pyramidal tract signs. Only seen in the Jaresh Jewish community.	Unknown 9p21.1-p12	Locus contains *SIGMAR1,* implicated in dSMA2
Early onset dHMN with pyramidal tract signs (ALS4)	AD. Onset between 2 and 25 years. Classic dHMN with pyramidal tract signs.	Senataxin (*SETX*) 9q34.13	DNA/RNA helicase. Has strong homology with *IGHMBP2.* Plays a role in DNA repair. May play a role in the regulation/modulation of transcription. Also mutated in AR spinocerebellar ataxia 1.
SPSMA	AD. Neurogenic amyotrophy with variable expression. Congenital absence of muscles, progressive scapuloperoneal atrophy, laryngeal palsy, progressive distal muscle weakness and wasting.	Transient receptor potential cation channel, subfamily V, member 4 (*TRPV4*) 12q44.11	Calcium channel found on the membrane of many cells types and plays a role in a number of different functions including the sensation of pain.
Congenital dSMA	AD. Onset at birth. Nonprogressive. Variable severity from weakness of the distal lower limb muscles only, to additional weakness of the pelvic girdle and truncal muscles, resulting in scoliosis.	Transient receptor potential cation channel, subfamily V, member 4 (*TRPV4*) 12q44.11	Calcium channel found on the membrane of many cells types and plays a role in a number of different functions including the sensation of pain.
dSMA2	AR. Onset between 9 and 12 years. Distal	Sigma non-opiod (*SIGMAR1*)	Involved in lipid transport from the endoplasmic

	muscle weakness and wasting presents in the lower limbs with *pes varus*, and foot drop. Hand involvement occurs later. Pyramidal tract signs and Babinski tract sign occasionally present. Progressive from onset till ~ 20 years, then stable.	9p13.3	reticulum. Involved in many cellular functions, including, BDNF signalling, EGF signalling, ion channel regulation, calcium signalling, proliferation, and cell survival and apoptosis. Also mutant in ALS16.
dSMA3	AR. Variable onset (2 months to 19 years. Variable disease progression. Those with earlier onset (1st year) loose ability to walk before 12 years and ability to write by 30 years, and have bilateral diaphragmatic paralysis. Hip subluxation and *genu recurvatum* (knee deformity) often observed. Later onset retain ability to walk but have waddling gait.	Unknown 11q13	Unknown
dSMA5	AR. Onset between 16 and 23 years. Slowly progressive weakness, hypotonia, and muscle wasting of the lower limbs, more pronounced distally. Pure motor axonal neuropathy.	DnaJ (Hsp40) homolog, subfamily member 2 (*DNAJB2*) 2q35	Encodes heat-shock protein 40 (HSP40), a molecular co-chaperone member of the heat shock protein family.
SMAX2	X-linked recessive. Infantile onset. Severe hypotonia, areflexia, and arthrogryposis (multiple congenital contractures). Infantile death.	Ubiquitin activating enzyme 1 (*UBE1*) X11.3	Catalyzes the first step in ubiquitin conjugation to mark cellular proteins for degradation through the ubiquitin-proteasome system. Essential for the formation of radiation-induced foci, timely DNA repair and for response to replication stress.
SMALED1	AD. Between birth and 7 years, most by 2 years. Non-progressive or mildly progressive. Prominent weakness and atrophy of the quadriceps muscles, moderate to severe atrophy of the hip abductors, and milder weakness in other leg muscles. Upper limbs unaffected.	Dyanin, cytoplasmic 1, heavy chain 1 (*DYNC1H1*) 14q32.31	Crucial subunit of the cytoplasmic dynein complex. Cytoplasmic dynein involved in intracellular motility, including retrograde axonal transport, protein sorting between apical and basolateral surfaces, and redistribution of organelles such as endosomes and lysosomes.
SMALED2	AD. Weakness and atrophy predominantly affecting the proximal and distal muscles of the lower limbs. Some patients show upper limb involvement, foot deformities, and mild upper motor signs.	Bicaudal D, homolog of drosophila 2 (*BICD2*) 9q22.31	Motor adaptor protein that is involved in dynein-mediated transport by linking the dynein motor complex to various cargoes. Also involved in Golgi dynamics and vesicular and mRNA transport.

SBMA (Kennedy disease)	X-linked recessive. Onset in third to fifth decades. Slowly progressive limb and bulbar muscle weakness with fasciculations, muscle atrophy, and gynecomastia.	Androgen receptor (*AR*) Xq12	Member of a group of nuclear receptors, the class I steroid receptors. Recognises canonical androgen response elements (AREs), and regulates gene expression and affects cellular proliferation and differentiation in target tissues. Also implicated in androgen insensitivity, partial androgen insensitivity with or without breast cancer, and hypospadias.

Abbreviations: **mNCV=** Motor nerve condeuctione velocities; **SPG31**= Spastic paraplegia 31; **tRNA**= transfer RNA; **dSMA**=Distal spinal muscular atrophy; **SMARD1**=Spinal muscular atrophy with respiratory distress type 1; **SPG31**=Spastic paraplegia 31; **SMAX3**=Distal spinal muscular atrophy, X-linked 3 ; **ALS4**=Amyotropic lateral sclerosis 4; **SPSMA**= Scapuloperoneal spinal muscular atrophy; **ALS16=**Amyotrophic lateral sclerosis; **BDNF**=Brain-derived neurotrophic factor; **EGF**=Epidermal growth factor; **SMALED**=Spinal muscular atrophy, lower extremity-predominant; **SBMA**=Spinobulbar muscular atrphy (43, 60, 80, 82-84, 89, 102, 115, 117, 127-129, 133, 227, 298-316)

7.2 APPENDIX CHAPTER 2

7.2.1 Table 36. Amounts of human *SLC5A7* cDNA construct transfected/500,000 cells

Label	cDNAs transfected	Amount transfected (µg)
2X PRK5	pRK5 (empty vector)	1
2X WT	HA-*SLC5A7*^{WT}	1
2X K499N	HA-*SLC5A7*^{K499Nfs*13}	1
2X H521Q	HA-*SLC5A7*^{H521Q}	1
2X V112E	HA-*SLC5A7*^{V112E}	1
2X S94R	HA-*SLC5A7*^{S94R}	1
2X pEGFP-C	pEGFP-*SLC5A7*^{WT}-C	1
2X N-GFP	*SLC5A7*-N-GFP	1
1X WT	pRK5	0.5
	HA-*SLC5A7*^{WT}	0.5
1X K499N	pRK5	0.5
	HA-*SLC5A7*^{K499Nfs*13}	0.5
1X H521Q	pRK5	0.5
	HA-*SLC5A7*^{H521Qfs*2}	0.5
1X V112E	pRK5	0.5
	HA-*SLC5A7*^{V112E}	0.5
1X S94R	pRK5	0.5
	HA-*SLC5A7*^{S94R}	0.5
1X WT /	HA-*SLC5A7*^{WT}	0.5
1X K499N	HA-*SLC5A7*^{K499Nfs*13}	0.5
1X WT /	HA-*SLC5A7*^{WT}	0.5
1X H521Q	HA-*SLC5A7*^{H521Qfs*2}	0.5
1X WT /	HA-*SLC5A7*^{WT}	0.5
1X V112E	HA-*SLC5A7*^{V112E}	0.5
1X WT /	HA-*SLC5A7*^{WT}	0.5
1X S94R	HA-*SLC5A7*^{S94R}	0.5
1X WT /	HA-*SLC5A7*^{WT}	0.5
1X pEGFP-C	pEGFP-*SLC5A7*^{WT}-C	0.5
1X WT /	HA-*SLC5A7*^{WT}	0.5
1X N-GFP		0.5

7.2.2 Table 37. Amounts of human *SLC5A7* cDNA construct transfected/100,000 cells

Label	cDNAs transfected	Amount transfected (ng)
2X PRK5	pRK5 (empty vector)	200
2X pCHT-N-GFP	pCHT-N-GFP	200
1X WT	pRK5	100
	HA-*SLC5A7*^{WT}	100
1X HA-*SLC5A7*^{K499Nfs13}	pRK5	100
	HA-*SLC5A7*^{K499Nfs*13}	100
1X HA-*SLC5A7*^{H521Qfs*2}	pRK5	100
	HA-*SLC5A7*^{H521Qfs*2}	100
1X HA-*SC5A7*^{V112E}	pRK5	100
	1X HA-*SC5A7*^{V112E}	100
1X HA-*SC5A7*^{S94R}	pRK5	100
	1X HA-*SC5A7*^{S94R}	100
1X WT *I*	HA-*SLC5A7*^{WT}	100
1X HA-*SLC5A7*^{K499Nfs*13}	HA-*SLC5A7*^{K499Nfs*13}	100
1X WT *I*	HA-*SLC5A7*^{WT}	100
1X HA-*SLC5A7*^{H521Qfs*2}	HA- *SLC5A7*^{H521Qfs*2}	100
1X WT *I*	HA-*SLC5A7*^{WT}	100
1X HA-*SC5A7*^{V112E}	1X HA-*SC5A7*^{V112E}	100
1X WT	HA-*SLC5A7*^{WT}	100
1X HA-*SC5A7*^{S94R}	1X HA-*SC5A7*^{S94R}	100

7.3 APPENDIX CHAPTER 3

7.3.1 Table 38. dHMN-VII family 1 identification numbers across studies

ID in this thesis	ID in Young and Harper 1980	ID in Pridmore *et al.* 1992	ID in McEntagart *et al.* 2001	ID in Dick *et al.* 2008	ID in Barwick *et al.* 2012
I:1				I:1	
I:2				I:2	
II:1			YH1 I:1	II:1	
II:2			YH1 I:2	II:2	
II:3				II:3	
II:4				II:4	
III:1	I 2		YH1 II:2	III:1	
III:2	I 3		YH1 II:1	III:2	
III:3	I 4		YH1 II:3	III:3	
III:4			YH1 II:4	III:4	
III:5			P2 I:1	III:5	
III:6		I.1	P2 I:2	III:6	
IV:1	II 5		YH1 III:2	IV:1	
IV:2			YH1 III:1	IV:2	
IV:3			YH1 III:4	IV:3	
IV:4	II 6		YH1 III:3	IV:4	
IV:5	II 11		YH1 III:5	IV:5	
IV:6			YH1 III:6	IV:6	
IV:7			P2 II:4	IV:7	
IV:8		II.2	P2 II:3	IV:8	
IV:9		II.1	P2 II:2	IV:9	IV:9
IV:10			P2 II:1	IV:10	IV:10
V:1	III 12		YH1 IV:1	V:1	V:1
V:2	III 13		YH1 IV:2	V:2	V:2
V:3	III 14		YH1 IV:3	V:3	V:3
V:4	III 15		YH1 IV:4	V:4	V:4
V:5			YH1 IV:5	V:5	
V:6			YH1 IV:6	V:6	
V:7	III17		YH1 IV:7	V:7	
V:8				V:8	
V:9	III 24		YH1 IV:8	V:9	V:10
V:10			YH1 IV:9	V:10	V:9
V:11			YH1 IV:10	V:11	V:11
V:12	III 25		YH1 IV:11	V:12	V:12
V:13			P2 III:4	V:13	V:17
V:14			P2 III:5	V:14	V:16
V:15			P2 III:6	V:15	
V:16		III.5	P2 III:7	V:16	
V:17			P2 III:8	V:17	
V:18		III.3	P2 III:3	V:18	V:20
V:19		III.2	P2 III:2	V:21	V:19
V:20			P2 III:1	V:22	V:18
V:21		III.4		V:23	V:21
V:22				V:24	
VI:1	IV 22			VI:1	

VI:2	IV 23		YH1 V:2	VI:2	
VI:3			YH1 V:1	VI:3	
VI:4	IV 24		YH1 V:3	VI:4	
VI:5	IV 26		YH1 V:4	VI:5	VI:5
VI:6	IV 25		YH1 V:5	VI:6	VI:4
VI:7	IV 29		YH1 V:8	VI:7	VI:6
VI:8			YH1 V:6	VI:8	VI:7
VI:9			YH1 V:7	VI:9	VI:8
VI:10				VI:10	VI:10
VI:11			P2 IV:2	VI:11	VI:9
VI:12		IV.3	P2 IV:1	VI:12	VI:11
VI:13		IV.4			VI:12
VI:14		IV.7		VI:13	
VII:1				VII:1	
VII:2				VII:2	
VII:3			VI:1	VII:3	

7.3.2 Table 39. Primer sequences for cosegregation analysis of four candidate variants within dHMN-VII locus

Variant (gene symbol)	**Forward**	**Reverse**
Chr2:108627070 G/- (*SLC5A7*)	CCCTGGCTATTACCCTGATG	CACAAGTGCAAGTTCATCTAATTT
Chr2:120404629 T/- (*PCDP1*)	ACAGCTGCGATTCCTTCAAT	GTTCCTCACAGCACCTCACA
Chr2:101924635 T/C (*RNF149*)	AGGGCCAACCCTGAAGAC	GACACGCGCTTCTTCGTG
Chr2:121107178 A/G (*INHBB*)	CCCTTTGTGGTGGTGCAG	GTGGAAGGAGGAGGCAGAG

7.3.3 Table 40. *SLC5A7* primer sequences

Primer name	Forward	Reverse
SLC5A7_1	ACGCCCTAGCACCACTCTC	GCGTCCCTCCCCTCTAAAAC
SLC5A7_2	TGAGCCAGCTGGTTTATTCC	TGTCACTCTGAAGCCACACG
SLC5A7_3	CTTCTAGTAGCCACTGGTTTGG	TCAGAGTGTTTGACTTGTTATTCCA
SLC5A7_4	TTCCTTGATAAATGGCAGCA	AAGCCAAGGCTGAGGAAAGT
SLC5A7_5	TGTTTTCATCCACTGCATTTC	CAGTCCAATGGAGAGCACAC
SLC5A7_6	TGAGCTGTGCAGTGTGTGAG	GAGCCCACAAGCACATTTT
SLC5A7_7	TGTGGCTACATGCCACATTT	GTGGAGGAAAGAGGGGAGTG
SLC5A7_8	CCAGCACATGGACTTCACAC	TCTCGTATGCTTAAAGTACAGTCAGA
SLC5A7_9a	GAGCCATTTGAACCAGGAGA	TGATGTAACCATGGCAAGTG
SLC5A7_9b	TTCTGGCCTCTTCCTGAGAA	TGCTGCATACCATCTCTCCA
SLC5A7_9c	CAGAAGGGTCTGGGACTGAA	AATTCATTGCACCATTCAAGG

7.3.4 *SLC5A7* c.1497delG screening in regional control subjects

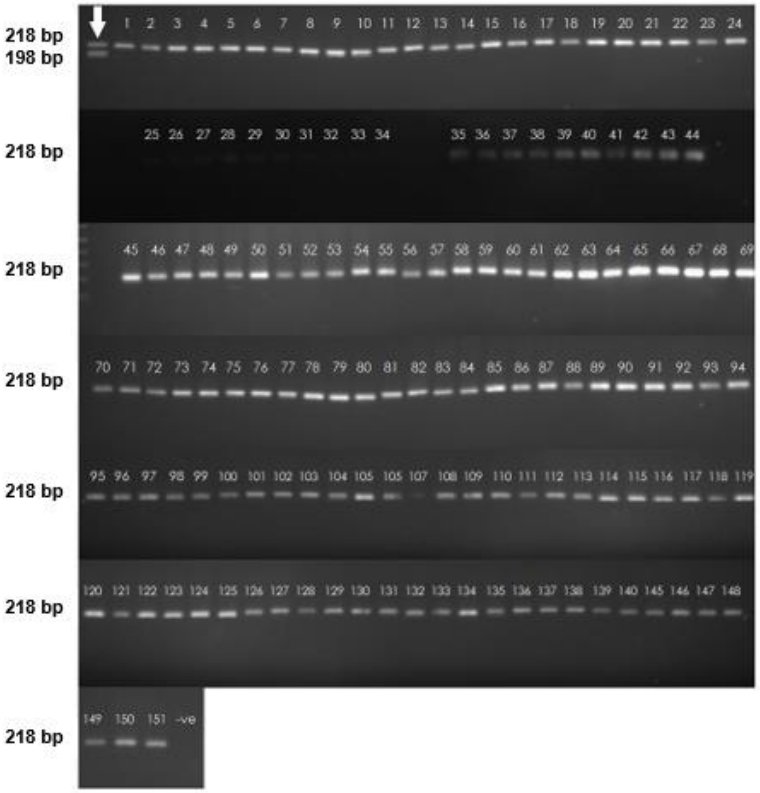

Figure 45. Restriction digest showing the presence of the c.1497delG variant in one dHMN-VII affected individual (indicated by white arrow), and its absence in 151 subjects control individuals.

7.3.5 Species conservation of CHT C-terminus compared to p.K499Nfs*13 mutant protein

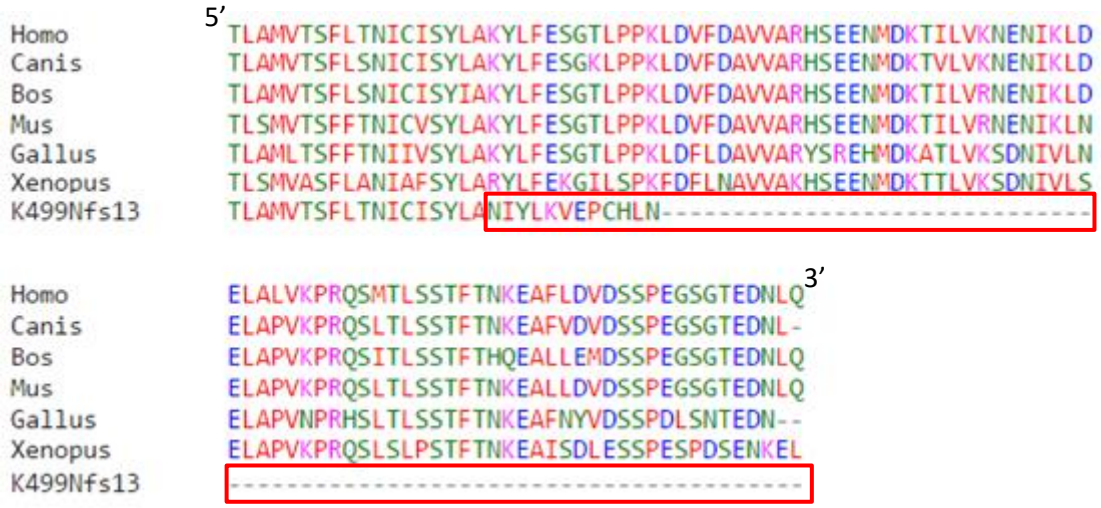

Figure 46. Protein homology of the C-terminus of the SLC5A7 genes protein product in various species compared with the c.1497delG mutant molecule. The C-terminus contains amino acid residues that are highly conserved across species (Clustal Omega)

7.3.6 TMHMM analysis of CHT p.K499Nfs*13

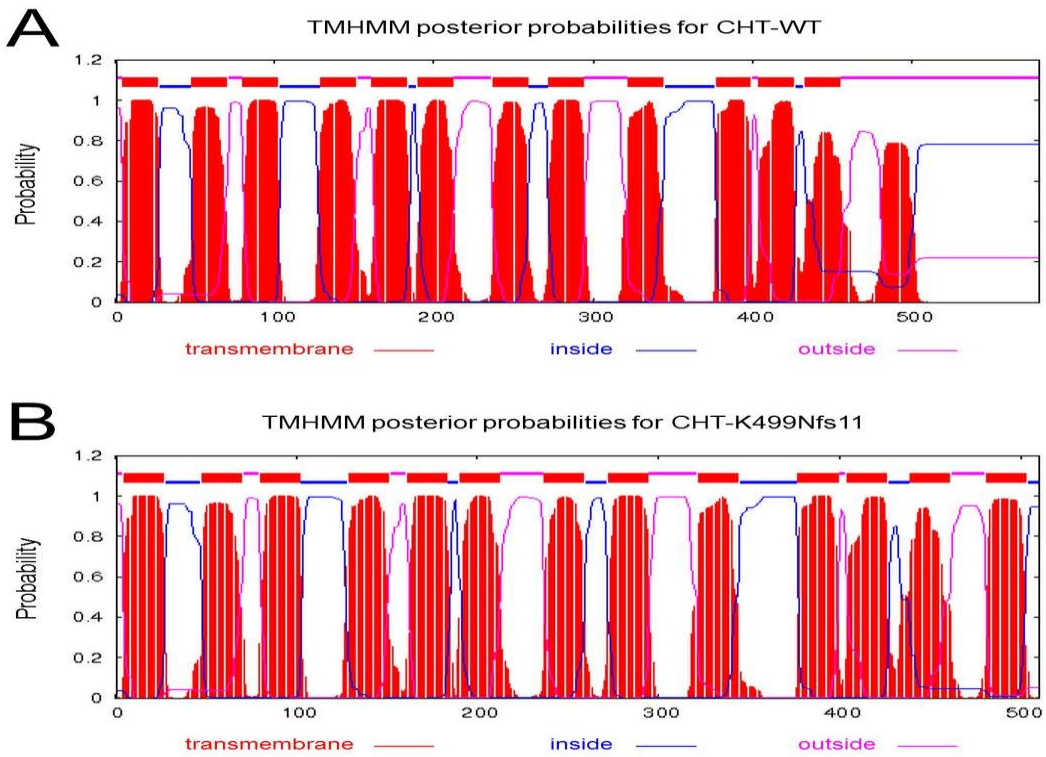

Figure 47. TMHMM transmembrane predictions of the SLC5A7 protein product of wild type and p.K499Nfs*13 mutant molecules. A) The wild type protein is predicted to have 12 transmembrane domains with the 3' terminus not reaching the threshold to be considered a transmembrane region. Both the 5' prime and the 3'terminals are predicted to be located extracellularly. B) The mutant proteins that results from the c.1497delG variant is predicted to create a more hydrophobic 3' terminus which is considered more likely a transmembrane location such that the molecule now comprises 13 transmembrane regions. The 3' terminus is now predicted to be situated intracellularly, on the cytoplasmic side of the membrane.

7.3.7 *SLC5A7* c.1563_1564delCA/p.H521Qfs*2 site-directed mutagenesis (SDM) primers

SDM oligonucleotides were designed according to the QuickChange Lightning Site-Directed Mutagenesis kit guidelines. The deleted bases are bracketed and highlighted in yellow (these were not present in the oligonucleotide), the incorporation of which results in the H521Qfs*2 amino acid change leading to protein truncation.

Primer name	Sequence
CHT_H521Qfs*2_forward	GATGCTGTTGTTGCAAGACAGTGAAGAAAACA(CA)TGGATAAGAC
CHT_H521Qfs*2_reverse	GTCTTATCCA(TG)TGTTTTCTTCACTGTCTTGCAACAACAGCATC

7.3.8 Co-immunoprecipitation of tagged *SLC5A7* wild type protein products and *SLC5A7* c.1497delG/p.K499Nfs*13 mutant protein from transiently transfected HEK-293T cells

Immunoprecipitation studies were undertaken in order to determine whether CHT functions as a multimer and how the *SLC5A7* c.1497delG/p.K499Nfs*13 variant effects multimerisation. This was carried out by co-transfecting HEK-293T cells with wild type and mutant DNA constructs with and without HA- and various other tags, followed by immunoprecipitation with anti-HA agarose beads and western blot analysis of the pulled-down proteins.

7.3.8.1 Methodology

HEK-293T cells were plated and transfected in 6-well plates as previously described. As RIPA buffer can disrupt protein interactions due to its Triton X-100 content, parallel transfections were performed using different lysis buffers in order to identify which did not interfere with the CHT proteins self-interactions should it form a multimer.

After 24 hours incubation at 37°C following transfection, cells were washed twice with warm (37°C) 1X PBS before lysis with either one of the following:

Sodium chloride-Tris-EDTA (STE) buffer, Tris/Chaps buffer, low concentration Triton X-100 lysis (LCTL) buffer, or RIPA buffer, each containing protease inhibitors. Cells lysed with STE buffer were washed twice with STE, then 2ml STE was added to prior to the cells being scraped from the bottom of the wells and transferred to 2ml microcentrifuge tubes and spun at 1,500rpm for 3 minutes at 4°C. The supernatant was removed, the pellet resuspended in STE, the spin repeated and again, the supernatant removed. 1ml SWELL buffer was added and the cells were incubated on ice for 10 minutes. The cells were then dounced 25-30 times and the salt concentration of the lysates was adjusted to 0.15M with salt solution. Cells lysed in Tris/Chaps, LCTL, and RIPA were done so in 400µl of the respective buffers on the shaker for 1 hour a 4°C. Should a white pellet of DNA be visible in the lysates, it was removed with a pipette before the lysates were transferred to microcentrifuge tubes. Samples lysed in all of the various buffers were spun at maximum speed for 30 minutes, the supernatant was transferred to fresh tubes, and the globby pellet of cell debris was discarded. A BCA protein assay was then carried out as described previously in order to determine the protein concentrations for normalisation.

Anti-HA agarose beads were prepared by washing 4 times in the various lysis buffers used earlier. The final wash was removed and 50µl of the respective lysis buffers was added. 30µl of each of the cell lysates was mixed with 30µl of beads in the appropriate buffer in microcentrifuge tubes and incubated at 4°C on the rotator overnight.

The samples were spun at full speed for 5 minutes. The supernatant was removed, and that of the samples in RIPA buffer was prepared for western blot analysis. The supernatant from the other samples was discarded. The beds were washed 4 times with the appropriate lysis buffers, and the last wash removed to leave the beads almost dry. 30µl 4X Laemmli buffer was added to each sample before heating at 50°C for 10 minutes and subsequent centrifugation at full speed for 5 minutes. The samples were analysed by Western blot as described in chapter 2.6.5. Blots were probed with mouse monoclonal (m.m.) anti-HA primary antibody and goat-anti-mouse (GAM) secondary antibody as described to ensure HA-tagged proteins had been successfully immunoprecipitated by the anti-HA agarose beads. Blots were stripped in stripping buffer for 20 minutes at 50°C and washed 4 times for 15

minutes in 1X TBST. The blot was then probed again, this time with a rabbit polyclonal (r.p.) anti-CHT primary antibody in TBST with 3% BSA (1:1000), at 4°C overnight. The blot was washed 4 times with TBST, blocked for 1 hour in 3% BSA in TBST, then probed with mouse anti rabbit (MAR) secondary antibody (1:10,000) for 1 hour at room temperature before development with the use of the Western Lightning® Plus-ECL, Enhanced ChemiluminescenceSubstrate Kit and Konica Minolta SRX-101 A-Xray film developer as described.

Tris/CHAPS buffer and LCTL buffer were found not to disrupt the protein interaction. The above procedure was repeated with these buffers with various CHT constructs incorporating various tags. However, following normalisation of the protein concentrations and prior to immunoprecipitation with anti-HA agarose beads, 20µl of each sample was removed and mixed with 10µl 4X Laemmli buffer for Western blot analysis of the total protein content. Western blot analysis of the immunoprecipitated proteins was carried out in duplicate. One of the blots was probed with m.m. anti-HA (1:1,000) primary antibody at room temperature for 2 hours and then in GAM (1:10,000) secondary antibody for 45 minutes. The other was probed with rabbit polyclonal (r.p.) anti-CHT (ab89875) (1:1000) primary antibody over night at 4°C, and mouse-anti-rabbit-IgG MAR (1:10,000) secondary antibody for 1 hour at room temperature. Both blots were developed as above, then stripped and probed with m.m. anti-CHT (1:1000) primary antibody at 4°C overnight and GAM (1:10,000) secondary antibody for 1 hour at room temperature, and redeveloped.

7.3.8.2 Results

Unfortunately, due to the time constraints of my visit to Vanderbilt University, and because during the undertaking of these experiments Okuda and team(116) publish evidence that CHT forms a homo-oligomer on the cell surface, these experiments were not successfully completed.

7.3.9 Pulse chase analysis of CHT-WT and CHT-K499Nfs*13 in transiently transfected HEK-293T cells

7.3.9.1 Methodology

Pulse chase analysis was undertaken in order to determine whether the CHT p.K499Nfs*13 molecule exhibits altered constitutive trafficking compared to the wild type molecule; whether its biosynthesis, surface delivery, and stability are perturbed; and whether it effects the rate of transport to the cell surface of both itself and the wild type molecule.

The following was carried out in a designated radioactivity laboratory, and conducted in conjunction with health and safety regulations. HEK-293T cells were plated in 6-well plates, and were transfected with 2X HA-*SLC5A7*^{K499Nfs*13}, 2X HA-*SLC5A7*^{WT}, or co-transfected with 1X of each in replicates of 5 as described previously, and incubated at 37°C for 24 hours. Cells were washed 3 times with DMEM (without glutamine, methionine and cysteine) (GIBCO®) supplemented with 1% penicillin-streptomycin, 1% L-glutamine, and 10% dialysed foetal bovine serum (cys/met free DMEM). The cells were then incubated in 500µl cys/met free DMEM containing 50µCi/ml [^{35}S]methionine and [^{35}S]cysteine at 37°C for 10 minutes. The time of commencement of incubation was noted as zero hour. The labelled medium was removed and disposed of as radioactive waste, and replaced with 2ml unlabelled complete medium, and the cells were incubated in 5% CO_2 at 37°C. One well transfected with each of the three cDNA transfections mentioned above was solubilised in RIPA buffer with protease inhibitor as previously described -with all media and washes removed from the cells being disposed of as radioactive waste- at the following time intervals from zero hour: 30 minutes, 2 hours, 4 hours, 8 hours, and 24 hours. All lysates were then processed according to the protocol below.

Following solubilisation in RIPA buffer with protease inhibitor, lysates were scraped from the bottom of the wells, transferred to 2ml microcentrifuge tubes and spun at full speed (13,000rpm) for 30 minutes at 4°C. Supernatants were transferred to fresh tubes and the pelleted cell debris was disposed of as radioactive waste. 20µl of each sample was mixed with 10µl 4X Laemmli buffer for Western blot analysis of the total protein content. Anti-HA agarose beads were prepared with RIPA containing protease inhibitors as done previously.

30µl beads were mixed with the lysates and put on the rotator overnight at 4°C. The beads were washed 4 times with RIPA buffer and all the liquid was removed. Each sample was mixed with 30µl 4X Laemmli buffer and put on the shaker for 30 minutes then stored at 4°C until all samples had been processed for SDS-PAGE. SDS-PAGE was carried out as before. The gel was fixed for 20 minutes in 50% methanol and 10% acetic acid in ddH_2O, rinsed in water, and placed in the autoradiography enhancing solution, Enlightening (New England Nuclear) for 20 minutes at room temperature before a second rinse. The gel was dried in a vacuum dryer for 2 hours at 65°C then placed in an exposure cassette with an X-ray film and exposed for 1 week at -80°C.

7.3.9.2 Results

Initial pulse chase analysis attempts in HEK-293T cells were unsuccessful (figure 48). Although CHT protein is visible for all three transfections in cells lysed at 30 minutes post incubation with cys/met free DMEM containing 50µCi/ml [^{35}S]methionine and [^{35}S]cysteine (figure 48A, white arrows), at 2 hours post incubation in radiolabelled medium HT is no longer visible. Transiently transfected cells only express the transfected gene for a finite period of time because the gene is not integrated into their genome and is thus, lost and not replicated on cell division. The loss of CHT visible from cells lysed at 2 or more hours after zero hour could be due to further division of cells and there for a fewer portion of cells expressing the transfected proteins, resulting in insufficient levels of protein in the lysates to detect. Plans to carry out further pulse chase analysis in HEK-293T cells, which are derived from HEK-293 cells but are neomycin resistant and stably express the expression enhancer-binding SVA40 large T antigen, and had been found in-house to express higher protein levels than HEK-293 cells when transfected with CHT cDNA. Unfortunately, due to the time constraints of my visit to Vanderbilt University, I was unable to progress past trouble-shooting for these experiments.

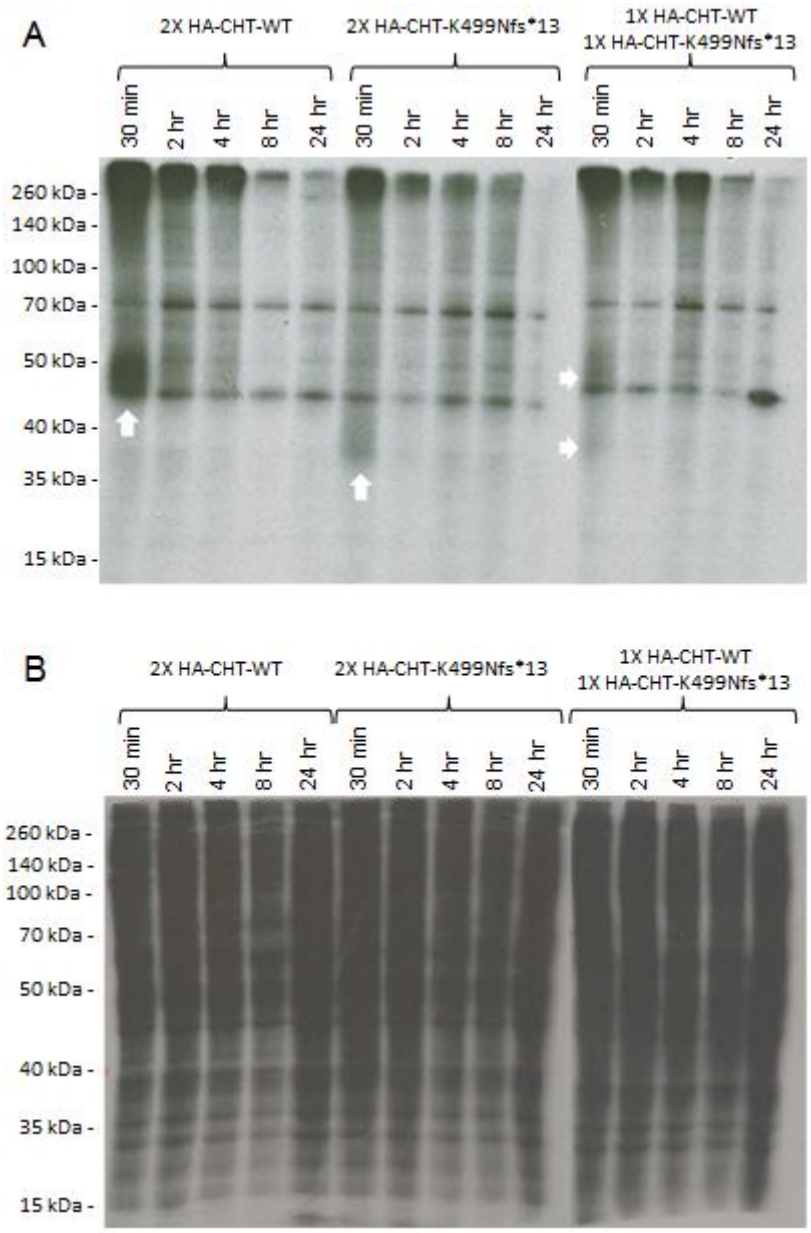

Figure 48. Preliminary pulse chase analysis HEK-293 cells transiently transfected with 2X HA-SLC5A7^{WT}, 2X HA-SLC5A7^{K499Nfs*13}, or 1X HA-SLC5A7^{WT} with 1X HA-SLC5A7^{K499Nfs*13}. A) Radiolabelled HA-tagged CHT proteins were pulled-down from total cell lysates with anti-HA agarose beads and run on SDS-PAGE. B) Total proteins from cell lysates run on SDS-PAGE.

7.3.10 Species conservation of CHT C-terminus compared to p.H521Q*fs2 mutant protein

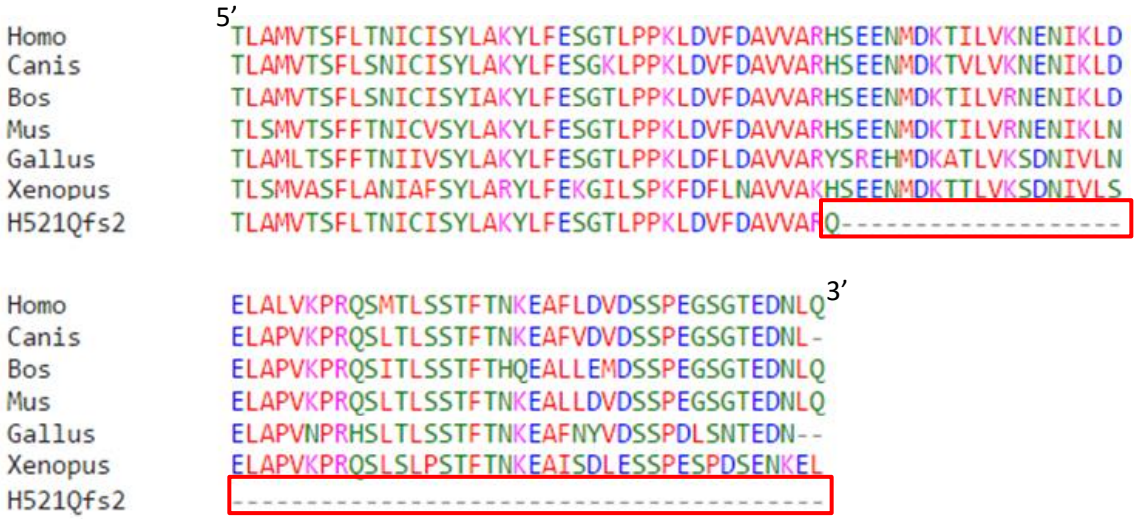

Figure 49. Protein homology of the C-terminus of the SLC5A7 genes protein product in various species compared with the c.1563_1564delCA mutant molecule. The C-terminus contains amino acid residues that are highly conserved across species (Clustal Omega)

7.3.11 TMHMM analysis of CHT p.H521Q*fs2

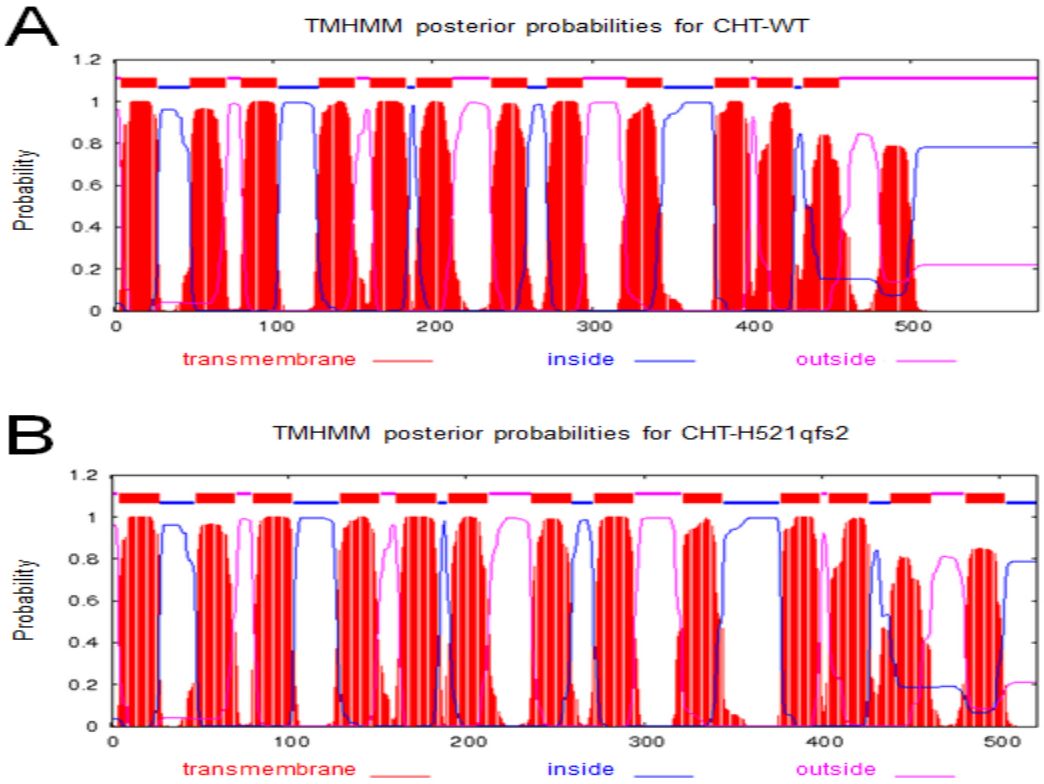

Figure 50. TMHMM transmembrane predictions of the SLC5A7 protein product of wild type and p.H521Qfs*2 mutant molecules. A) The wild type protein is predicted to have 12 transmembrane domains with the 3' terminus not reaching the threshold to be considered a transmembrane region. Both the 5' prime and the 3'terminals are predicted to be located extracellularly. B) The mutant protein that results from the c.1563_1564delCA variant is predicted to create a more hydrophobic 3' terminus which is considered more likely a transmembrane location such that the molecule now comprises 13 transmembrane regions. The 3' terminus is now predicted to be situated intracellularly, on the cytoplasmic side of the membrane.

7.4 APPENDIX CHAPTER 4

7.4.1 Table 41. Disorders featuring congenital central, peripheral, and combined hypotonia

Disorder(s)	Features	Genetics
Congenital central hypotonia		
Prader-Willi syndrome	Central hypotonia, global developmental delay, short stature, genital hypoplasia, and failure to thrive in infancy leading to hyperphasia at ~1 year.	Deletion, uniparental disomy of paternal Chr15q11-13 .
Angelman syndrome	Central hyopotonia, global developmental delay, acquired microcephaly, seizures, prognathism, and skin hypopigmentation.	Deletion, imprinting defect, uniparental disomy of maternal Chr15q11-13, or mutation of *UBE3A.*
Rett syndrome	Central hypotonia, acquired microcephaly, seizures, repetitive hand movements, and regression.	X-linked. *MECP2* and *CDKL5* mutations
Peroxisomal disorders	Spectrum of disorders of varying severity. Central hypotonia, liver abnormalities, seizures, cataracts/retinal dystrophy, hearing loss, chondrodysplasia punctata, and flattened facies with large anterior fontanelle.	AR. Mutation in 1 of 12 *PEX* genes. Most commonly *PEX1.*
Smith–Lemli–Opitz (SLO) syndrome	Central hypotonia, growth delay, global developmental delay, Y-shaped two/three-toe syndactyly, cleft palate, cataracts, heart defects, genital abnormalities, down slanting palpebral fissures with epicanthal folds, and anteverted nares.	AR. *DHCR7* mutations.
Creatine transporter deficiency	Central hypotonia, global developmental delay (most prominently with speech), mild seizures, and brain atrophy on MRI.	X-linked. *SLC6A8* mutations.
Congenital peripheral hypotonia		
Spinal muscular atrophy type 1 (SMA1)	Severe peripheral hypotonia, gross motor delay, mild contractures, particularly at the knees, and absence of tendon reflexes, poor head control, weak cry, poor feeding. Normal cognition. Fasciculations of the tongue are common.	AR. *SMN1*mutations (*SMN1* mutations account for 95% of all SMA0, 1, 2, 3 cases and 70% of SMA4 cases).
Distal SMA6 (SMARD1)	Peripheral hypotonia with distal weakness, respiratory distress due to hemidiaphragmatic palsy, and absent deep tendon reflexes. Onset rages from birth to 6 months	AR. *IGHMBP2* mutations
Congenital myotonic dystrophy	Peripheral hypotonia, facial diplegia, weak cry/poor suck, possible developmental delay/cognitive impairment, maternal family history of facial weakness and contraction myotonia, diabetes type II, and/or cataracts.	AD. Expansion of the CTG trinucleotide repeat in the 3′ untranslated region of the *DMPK.*
Congenital muscular dystrophies	Heterogeneous group of disorders with clinical features ranging from sever e often with early fatality, so mild. In addition to peripheral hypotonia may include kyphoscoliosis, torticollis, joint contractures, joint hypermobility , increased signal intensity of brain white matter on MRI, progressive spinal rigidity, and scoliosis.	AR. *LAMA2, COL6A1, 2,* and *3,* and *SEPN1* mutations.
Congenital myopathies	Group of disorders generally presenting with peripheral hypotonia, muscle weakness, delayed motor milestones, feeding difficulties, facial and oral muscle weakness. Serum creatine kinase may be normal or slightly raised.	*RYR1* mutations in central core/multi-minicore disease, *ACTA1, CFL2, NEB, TPM2* and *3, TNNT1* mutations in

	Deep tendon reflexes may be diminished or abolished. Variable severity.	Nemaline myopathy, and *MTM1* in myotubular myopathy.
Congenital myasthenic syndromes	A group of syndromes whose features include peripheral muscle weakness that worsens with physical exertion, delayed motor milestones, poor suck/weak cry, ptosis, craniofacial weakness, and possible arthrogryposis.	NMJ protein encoding *CHRNE, RAPSN, CHAT, COLQ, DOK7* mutations. *CPT2* mutations in Carnitine palmitoyltransferase deficiency type 2, *GAA* in Pompe disease, X-linked *TAZ* mutations in Barth syndrome.
CMT poly-neuropathies	Peripheral hypotonia with distal weakness, atrophy, sensory loss, and decreased deep tendon reflexes.	AR; AD. *PMP22, MPZ,* and *ERG2* mutations.
Marfan syndrome	Mild peripheral hypotonia, joint hypermobility, aortic root or dilatation, scoliosis, pectus excavatum or carinatum, arachnodactyly, and tall stature.	AD. *FBN1* mutations.
Loeys-Dietz syndrome	Mild peripheral hypotonia, hypertelorism bifid uvula or cleft palate, tortuous blood vessels on magnetic resonance angiography, and craniosynostosis.	AD. *TGFBR1,* and *1* mutations.
Congenital combined central and peripheral hypotonia		
Canavan disease	Combined hypotonia, global developmental delay, macrocephaly, optic atrophy, seizures, 'spongy' degeneration of white matter on MRI of the brain, and Ashkenazi Jewish ethnicity.	AR. 98% of Ashkenazi Jewish cases result from E285A or Y231X mutations in *ASPA* .
Marinesco–Sjogren syndrome	Central hypotonia and myopathy, global developmental delay, cerebellar atrophy, and ataxia, cataracts.	AR. *SIL1* mutations.
Mitochondrial encephalopathies	Extremely variable presentations. Features include: central hypotonia or myopathy, exercise intolerance, seizures and/or migraines, ataxia, cardiomyopathy, external ophthalmoplegia, sensorineural hearing loss, optic atrophy, hypothyroidism, diabetes mellitus, and maternal family history of any of these features.	Mitochondrial DNA or specific nuclear mitochondrial related gene mutations.

Abbreviations: **AD**=Autosomal dominant; **AR**=Autosomal recessive; **SLO=**Smith–Lemli–Opitz syndrome; **SMA**=Spinal muscular atrophy; **SMARD1**=Spinal muscular atrophy with respiratory distress type 1; **CMT=**Charcot-Marie-Tooth (155, 317)

7.4.2 Species conservation of CHT C-terminus compared to p.S94R and p.V112E mutant proteins

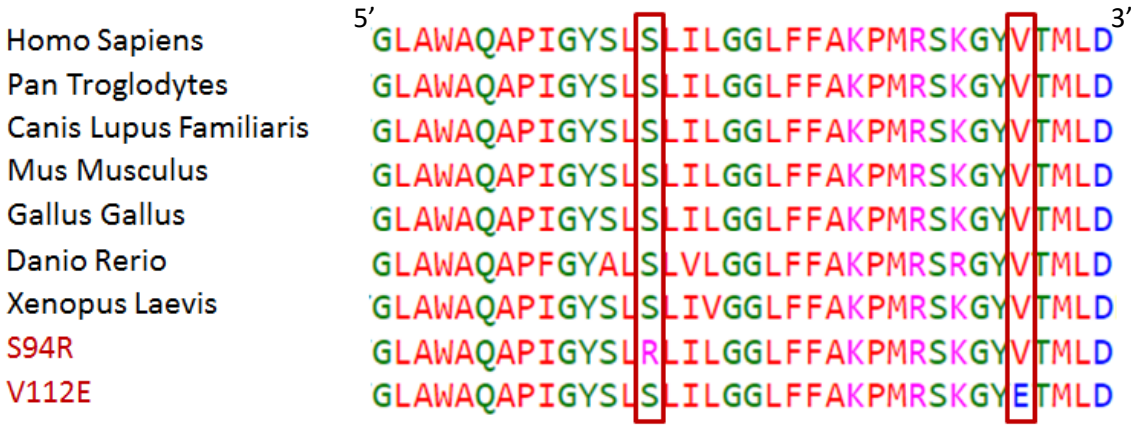

Figure 51. Protein homology of CHT at the amino acid positions of CHT p.S94R and p.V112E in various species and human wild type. The effected residues are highly conserves across species. (ClustalW2)

7.4.3 TMHMM analysis of CHT p.S94R and p.V112E

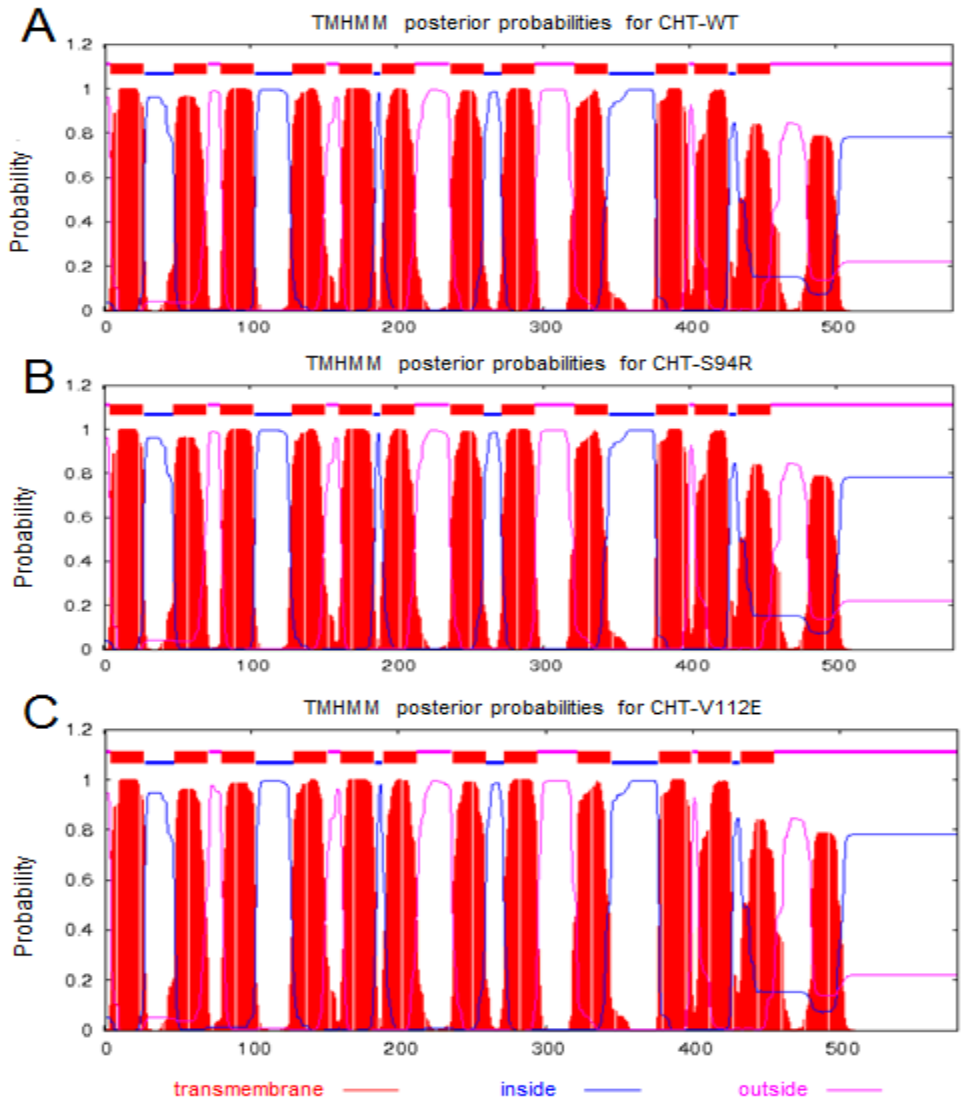

Figure 52. TMHMM transmembrane predictions of the SLC5A7 protein product of wild type and p.S94R and p.V112E mutant molecules. A) The wild type protein is predicted to have 12 transmembrane domains with the 3' terminus not reaching the threshold to be considered a transmembrane region. Both the 5' prime and the 3'terminals are predicted to be located extracellularly. B and C) No alteration in transmembrane topology is predicted as a result of the SLC5A7 c.282T>A, and c.335T>A variants.

7.4.4 *SLC5A7* c.282T>A/ p.S94R and c.335T>A/V112E site-directed mutagenesis (SDM) primers

SDM oligonucleotides were designed according to the QuickChange Lightning Site-Directed Mutagenesis kit guidelines. Mutated bases are highlighted in yellow, the incorporation of which results in the Ser94Arge and Val112Glu amino acid substitutions.

Primer name	Sequence
CHT_S94R_forward	GCACAATTGGATATTCTCTTAGACTGATTTTAGGTGGCTG
CHT_S94R_reverse	CAGCCACCTAAAATCAGTCTAAGAGAATATCCAATTGTGC
CHT_V112E_forward	CCTATGCGTTCAAAGGGGTATGAGACCATGTTAGACCCG
CHT_V112E_reverse	CGGGTCTAACATGGTCTCATACCCCTTTGAACGCATAGG

7.5 APPENDIX CHAPTER 5

7.5.1 CHT-related disease treatment hypotheses figures

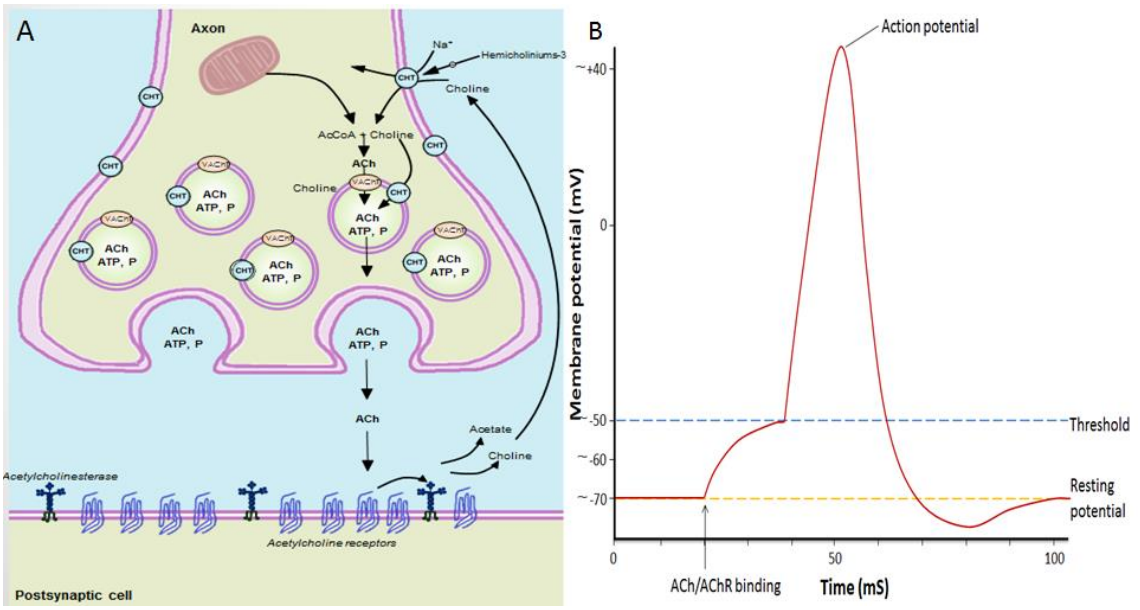

Figure 53. Normal cholinergic transmission at the NMJ.
(A) Schematic diagram of a normal cholinergic transmission at the NMJ. Choline, the precursor of ACh, is synthesised in the neuronal soma and then transported to the axon terminal via CHT, where it is acetylated with acetyl coenzyme A (AcCoA) by choline actyltransferase (ChAT) to produce ACh. ACh is stored in presynaptic vesicles (ACh transport is indicated by thin black arrows) until depolarisation of the cell stimulates its release into the synaptic cleft via an influx of Ca^{2+} at the motor terminal (not shown). ACh binds to membrane bound nicotinic ACh receptors (nAChRs) on the postsynaptic muscles cell, causing ion channels to open which allows Na^{+} to flow into the muscle cell (not shown). This stimulates a depolarisation response of the muscle cells membrane, the degree of which is dependent on the number of activated nAChRs. Following postsynaptic depolarisation, ACh is rapidly cleaved back into choline and AcCoA by actelycholinesterase (AChE), which terminates synaptic transmission and prevents prolongation of muscle contraction and multiple depolarisations. CHT is responsible for choline reuptake into the presynaptic terminal for recycling, as well as choline transport into presynaptic vesicles. Choline reuptake is the rate limiting step in ACh synthesis and is therefore crucial to cholinergic transmission at the NMJ.
(B) Simplified schematic of the postsynaptic membrane potential during normal cholinergic signalling at the NMJ. nAChR binding on the motor end plate and the subsequent inward flow of Na^{+} results in a relatively slow increase in the postsynaptic cells membrane potential from its resting potential of ~-70mV. If the membrane potential reaches -50mV, an action potential is elicited in the muscle cell via an influx of Na^{+}, during which the membrane depolarises to ~+40mV and causes the muscle to contract. The ion channels then slowly close and the membrane potential reverses dropping back to the resting potential.

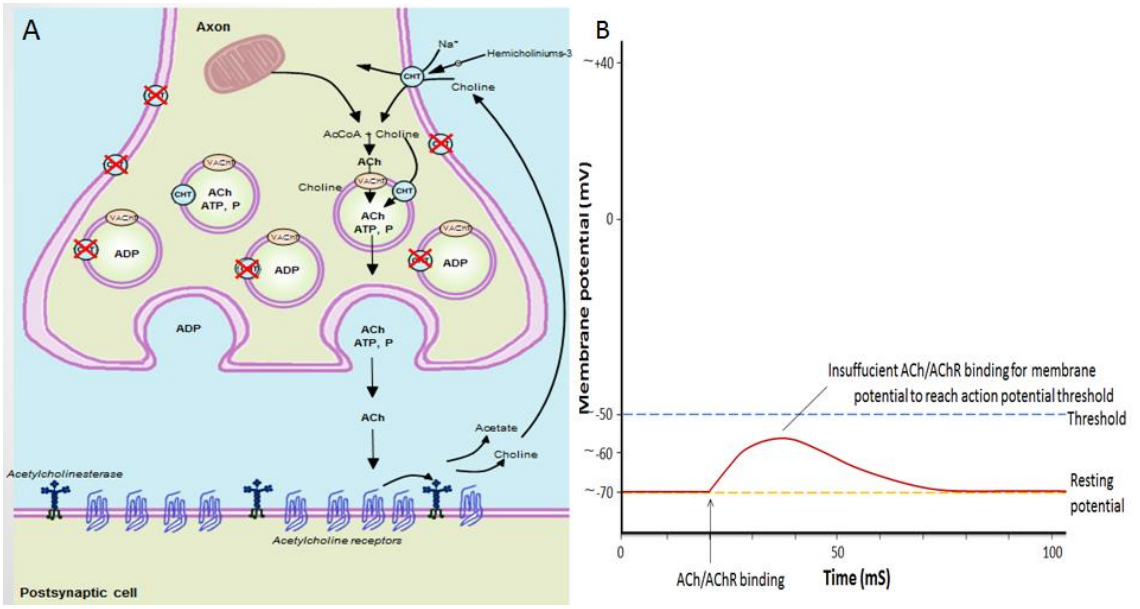

Figure 54. Defective cholinergic transmission at the NMJ due to the SLC5A7 c.1497delG.

(A) Schematic diagram of defective cholinergic signalling at the NMJ due to the SLC5A7 c.1497delG (p.K499Nfs*13) mutation. c.1497delG results in significantly reduced Choline transport by, which in turn results in a reduction in ACh synthesis and diminished vesicular ACh pools. On depolarisation of the presynaptic nerve terminal and the subsequent release of the contents of the presynaptic vesicles into the synaptic cleft, there is an insufficient amount of ACh release to saturate the postsynaptic nAChRs. This causes an insufficient increase in the postsynaptic membrane potential to elicit an action potential and subsequent muscle contraction.

(B) Simplified schematic of the postsynaptic membrane potential during defective cholinergic signalling at the NMJ due to the SLC5A7 c.1497delG mutation. Reduced release of ACh from the presynaptic nerve terminal and subsequent nAChR binding on the motor end plate causes ion channels to open and allows Na^+ to flow into the muscle cell (not shown). Due to incomplete saturation of the nAChRs by Ach, the membrane potential fails to reach the ~-50mV action potential threshold. The membrane potential returns to resting potential due to AcCoA action and muscle contraction does not occur.

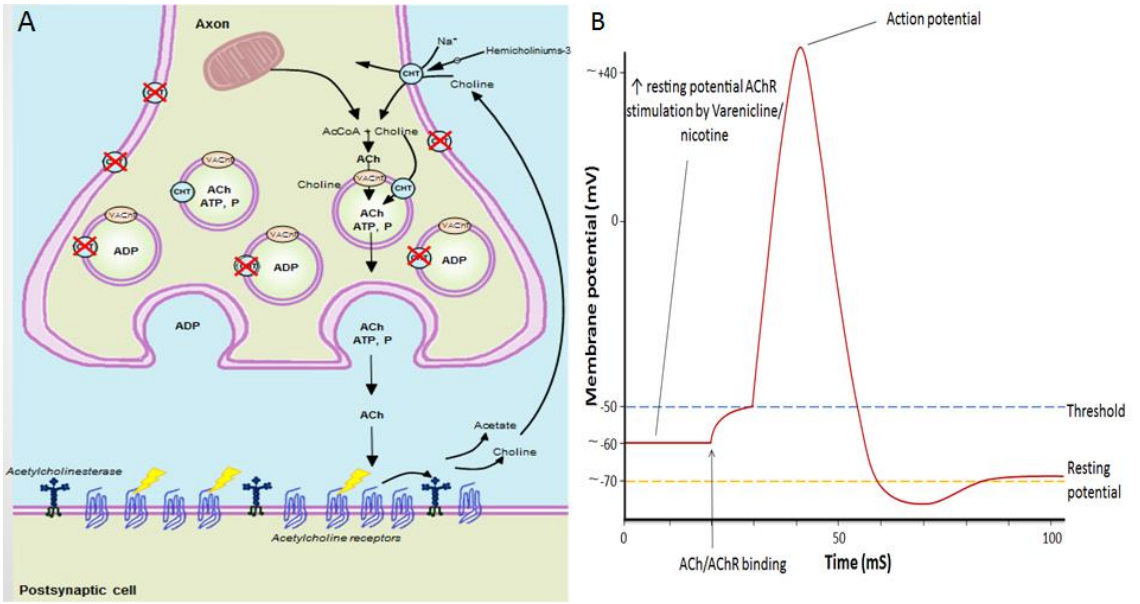

Figure 55. dHMN-VII treatment hypothesis (i) nAChR agonist.
(A) Schematic diagram of proposed mechanism of action at the NMJ of a nAChR agonist as a treatment for dHMN-VII. It is hypothesised that administration of a nAChR agonist, which binds to and stimulates postsynaptic nAChRs, will provide extra nAChR stimulation at the NMJ, raising the resting potential of the postsynaptic muscle cells membrane. This will allow saturation of the postsynaptic nAChRs by the diminished amount of ACh released from presynaptic vesicles on depolarisation of the motor neurone, causing the muscle cells membrane potential to reach the action potential threshold and broadcast the action potential to the entire muscle membrane leading to muscle contraction.
(B) Simplified schematic of the predicted postsynaptic membrane potential during cholinergic signalling at the dHMN-VII NMJ in the presence of a nAChR agonist. The presence of a nAChR agonist is hypothesised to result in an increased resting potential (>-70mV) of the postsynaptic muscle cells resting membrane potential. On nAChR binding of ACh a lesser increase in membrane potential is required in order to reach the action potential threshold and rapid depolarisation of the muscle cell.

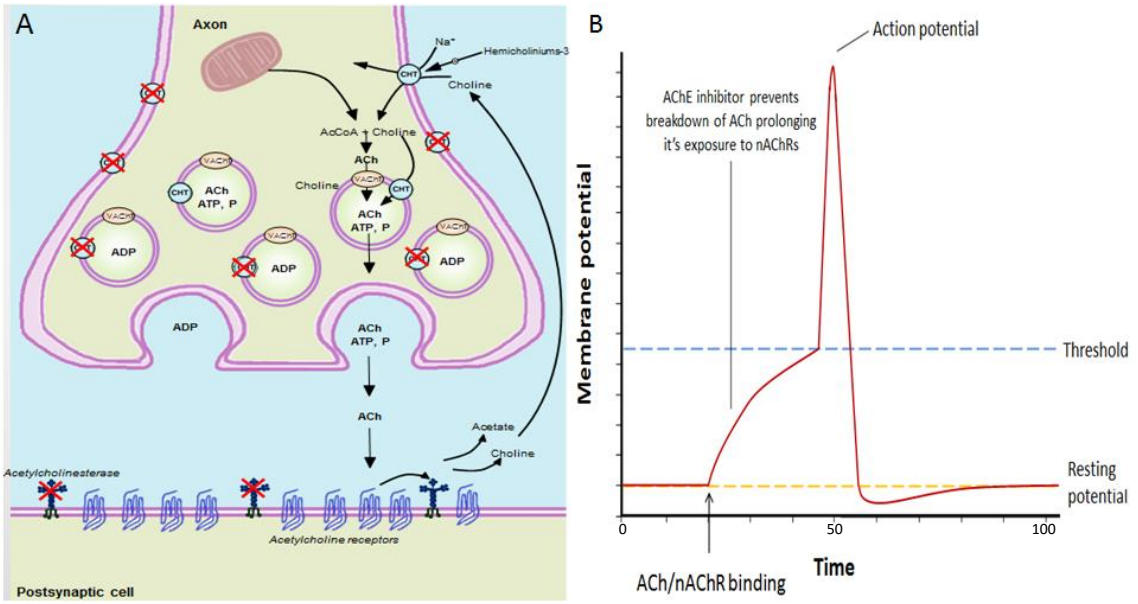

Figure 56 dHMN-VII treatment hypothesis (ii) AChE inhibitor.
(G) Schematic diagram of proposed mechanism of action at the NMJ of AChE inhibitors as a treatment for dHMN-VII. It is hypothesised that administration of AChE inhibitor, which inhibits the rapid breakdown of ACh by AChE, will prolong the time ACh remains within the synaptic cleft and therefore increase the chance of nAChR saturation, allowing postsynaptic action potential propagation.
(H) Simplified schematic of the predicted postsynaptic membrane potential during cholinergic signalling at the dHMN-VII NMJ in the presence of AChE inhibitors. The presence of an AChE inhibitor is hypothesised to result in sufficient amounts of ACh to remain in the synaptic cleft for nAChR saturation. This will allow substantial flow of Na^+ into the muscle cell for the slow increase in membrane potential to reach the action potential threshold leading to rapid depolarisation and muscle contraction.

7.5.2 Approach to mouse model generation

In order to generate a patient-specific *knock-in* mouse model carrying the *SLC5A7* c.1497delG mutation identified in dHMN-VII family 1 (chapter 3), CRISPR/Cas9-mediated gene editing(318) was employed. The homologous region of human *SLC5A7* c.1497delG in the mouse genome was targeted by a specifically designed guide RNA (protospacer adjacent motif (PAM) sequence: GCCAAGTATCTATTTGAAAG). A *S. pyogenes* SF370 plasmid containing the Cas9 open reading frame (319) was transcribed *in vitro* to produce Cas9 mRNA with the use of the Thermo Fisher Scientific mMESSAGE mMACHINE® T7 Transcription kit. An oligonucleotide was then designed in order to introduce both silent and codon altering changes to mimic the human c.1497delG mutation with 50 bases of homologous flanking sequence on either side (targeting oligonucleotide sequence: TTGTCCATGTTCTCTTCACTGTGCCTTGCGACAACAGCATCAAATACATCTA ATTTAGGTGGCAAGGTTCGACCTTCAGGTATATGTTGGCTAGATAAGAAAC ACAAATGTTGGTAAAGAATGAGGTAACCATGGAGAGAG). By microinjection, the guide RNA (50 ng/µl), Cas9 mRNA (100 ng/µl), and targeting oligonucleotide (100 ng/µl) were introduced into C57 black 6 mouse zygotes, and the zygotes were transferred into pseudo-pregnant female mice (318). Founder mosaic mice born from these zygote transfers were genotyped by ear punch biopsy followed by PCR and dideoxy Sanger sequence analysis for the presence of the exogenous oligo sequence present at the correct genomic location. Animals found to be positive for the mutation were cross-bread with wildtype C57Bl/6 mice from which germline transmission of the desired allele, termed *Slc5a7*^{indelAC} (figure 57A).

Due to the apparent dominant-negative mode of action of the c.1497delG/p.K499Nfs*13 mutant protein on wild type transporter function, it was imperative to compare any apparent phenotypes observed in *Slc5a7*$^{indelAC/+}$ mice with those of the heterozygous loss-of-function model, allowing identification of aspects of the phenotype that are due to haploinsufficiency. Thus, animals carrying an *Slc5a7* loss-of-function allele (*Slc5a7*^{TM1A}) generated by the Sanger Institute Mouse Genetics Programme(320), were examined in parallel.

Mice were maintained in a specific pathogen-free unit under a 12 hr light, 12 hr dark cycle with ad libitum access to water and food. The care and use of mice were in accordance with the UK Home Office regulations, UK Animals (Scientific Procedures) Act of 1986. Animals were monitored for signs of motor weakness, fatigue, and gait defects. Any findings were recorded and animal weights taken prior to culling.

7.5.3 Assay for *knock-in* allele expression

In order to confirm expression of the patient-specific *Slc5a7*^{indelAC} allele at the mRNA level, adult *Slc5a7*$^{indelAC/+}$ animals were sacrificed under the schedule 1 procedure of the Home Office Animals (Scientific Procedures) Act 1986. Following confirmation of death, a spinal cord tissues biopsy was taken and mRNA extracted with the use of Invitrogen TRIzol® reagent. cDNA was generated from samples taken from both wild type control and *knock-in* mutant mice, and subjected to PCR to amplify the desired region followed by dideoxy Sanger sequencing. Equivalent expression levels of both wild type and *Slc5a7*^{indelAC} mRNA in the *Slc5a7*$^{indelAC/+}$ mice was confirmed (figure 57B).

Figure 57. Confirmation of knock-in allele expression. Diedeoxy Sanger sequencing analysis of A) genomic DNA from Slc5a7$^{indelAC/+}$ pups, followed by the DNA and peptide sequences flanking the mutation in wild type and heterozygous mutant animals, as well as the mutant peptide sequence in dHMN-VII family 1 subjects; and B) spinal mRNA from from adult Slc5a7$^{indelAC/+}$ mice. The overlapping traces indicate the position of the frameshift variant and confirm the presence of both the wild type and mutant allele at both the DNA and mRNA levels. The DNA sequence of the Slc5a7$^{indelAC/+}$ animals doe not match that of dHMN-VII affected humans because silent and codon altering changes were introduced to the mouse DNA to mimic the human c.1497delG mutation with 50 bases of homologous flanking sequence on either side.

7.5.4 Open field testing - methodology and results

Following 30 minutes acclimatisation in the test room, control and mutant mice aged 18-22 weeks were placed in a clean 73 x 73cm open field arena for 20 minutes under bright light conditions. Time spent moving, time spent stationary, and average velocity and distance travelled was tracked with the use of overhead infrared video cameras, and recorded and analysed using Ethovision XT 8.5 automated video tracking software from Noldus Information Technology, Wageningen, The Netherlands. Movement was defined as a velocity of 2 cm/s over two frames and non-movement was defined when velocity was lower than 1.75 cm/s over two frames. There are no differences in distance covered (figure 58), average velocity (not shown), or time spent moving (not shown) between either *Slc5a7*$^{indelAC/+}$ or *Slc5a7*$^{+/TM1A}$ and their littermates.

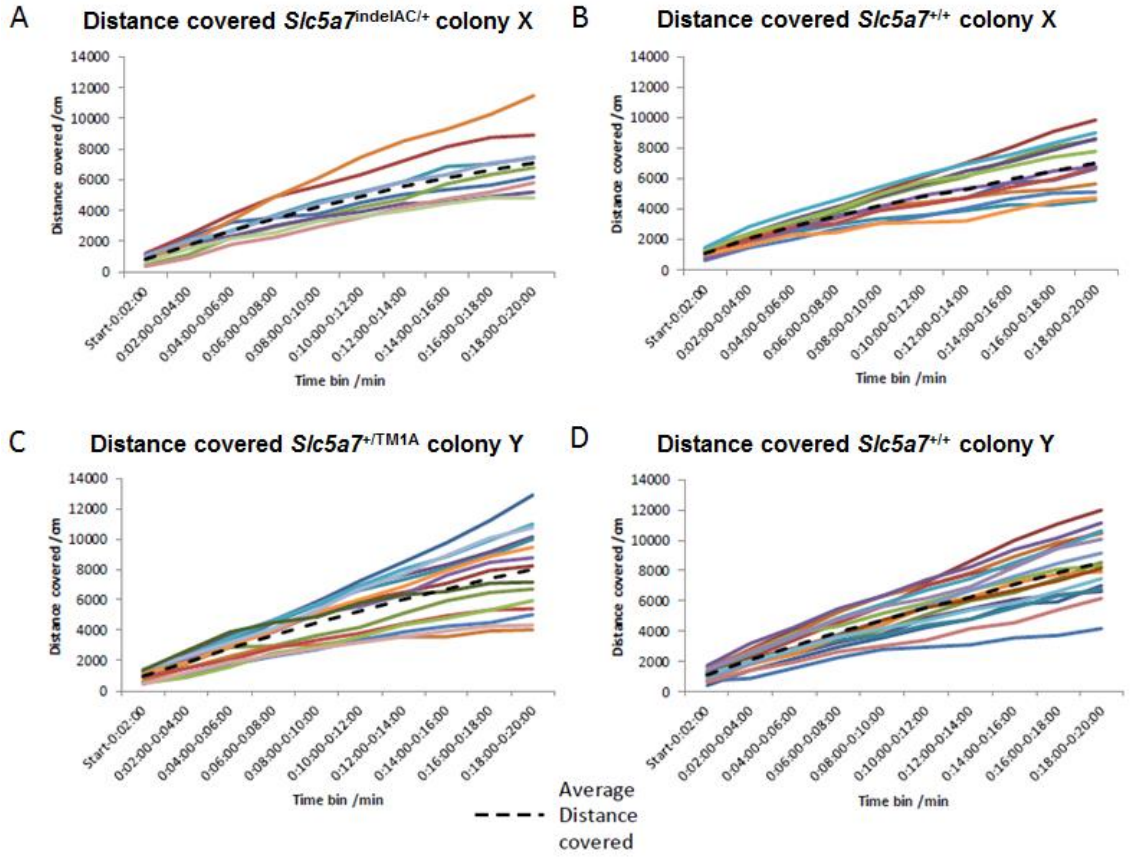

Figure 58. Distance covered in open field testing of 18-22 week old A) Slc5a7$^{indelAC/+}$ mice and B) their Slc5a7$^{+/+}$ wild type littermates, and C) Slc5a7$^{+/TM1A}$ mice and D) their wild type littermates. The 20 minute open field analysis was split into time bins of 2 minutes in order to determine whether mutant animals tire more quickly than wild type controls.

7.5.5 Grip strength testing - methodology and results raw data

Grip strength measurements were taken from wild type control and mutant mice at 18-22, 23-26 and 27-31 weeks of age. Mouse muscle strength was measured with the use of a Grip Strength Test BIO-GS3 force transducer meter from BIOSEB, and recorded in grams. Forepaw measurements were taken by holding the animal to be tested by the tail and lowering it to the metal grid attached to the force transducer meter until its front paws grasp the grid. The animals was then lowered by its tail such that its body was position almost horizontally before gently pulling the tail in the direction of the axle of the sensor until the animal released its grasp. All-paw measurements were carried out as forepaw measurements; however the animal was lowered as to allow for all four paws to grasp the grid. Forepaw and all-paw measurements were repeated 3 times for each time point and the maximum measurement of each was used in analysis. Measurements were discarded if the mouse failed to have paws gripping over the bar or if they were asymmetrically arranged on the bars.

7.5.5.1 Grip strength testing in *Slc5a7*$^{indelAC/+}$ mice

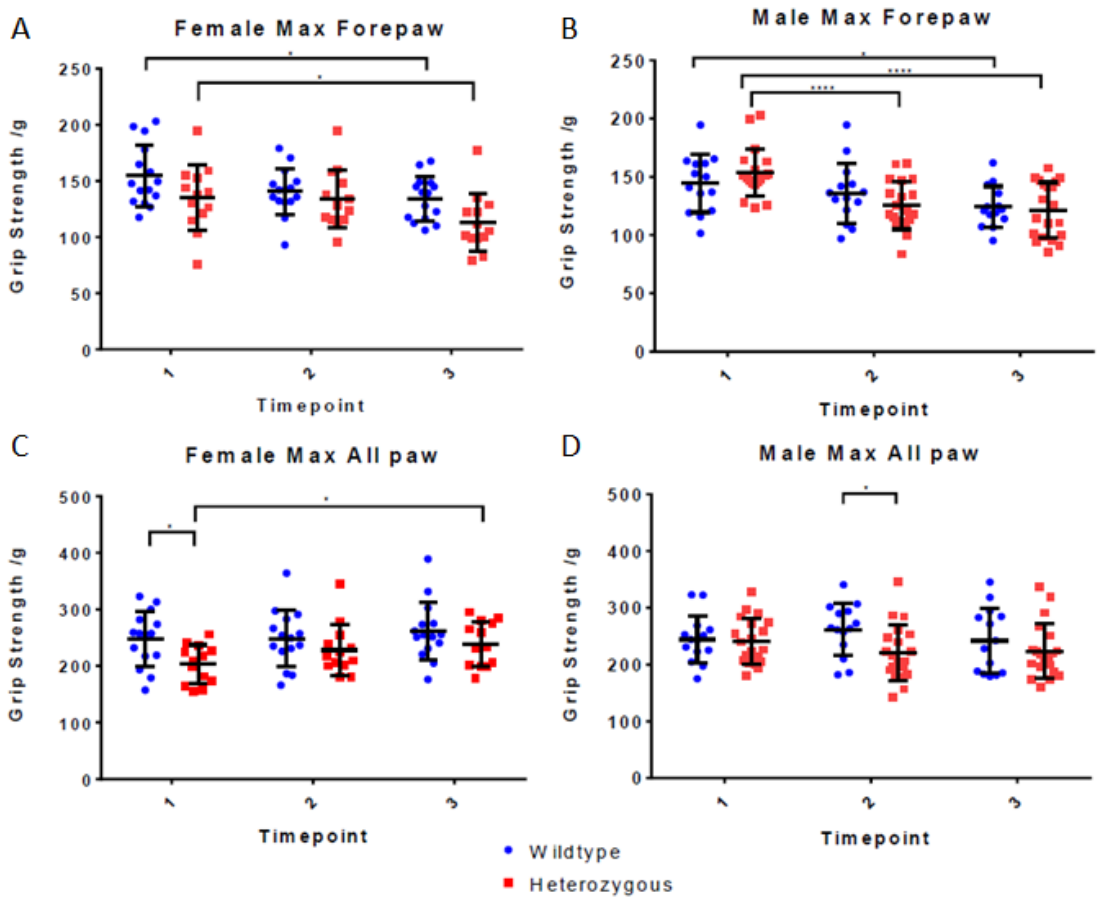

Figure 59. Grip strength test results taken at time points 1 (18-22 weeks), 2 (23-26 weeks) and 3 (27-31 weeks) from wild type (blue) vs. Slc5a7$^{indelAC/+}$ (red) A) female mice forepaws, B) male mice forepaws, C) female mice all-paws and D) male mice all-paws. Difference of statistical significance are indicated by * where p=<0.05, and * where p=<0.0001***

Table 42. Female *Slc5a7*$^{indelCA/+}$ mice grip strength summary statistics

Female max forepaw			**WT**	**HET**	
		N	15	13	
Wildtype vs. Het					
Time point	**Mean 1**	**Mean 2**	**Mean diff**	**Significance**	**Adjusted *p* value**
1	154.7	135.1	19.64	ns	0.1159
2	140.7	134.1	6.574	ns	0.865
3	134.1	112.6	21.46	ns	0.0741
Wildtype	**Mean 1**	**Mean 2**	**Mean diff**	**Significance**	**Adjusted *p* value**
1 vs. 2	154.7	140.7	14.01	ns	0.2377
1 vs. 3	154.7	134.1	20.63	*	0.0495
2 vs. 3	140.7	134.1	6.619	ns	0.7196
Heterozygous					
1 vs. 2	135.1	134.1	0.9446	ns	0.9942
1 vs. 3	135.1	112.6	22.45	*	0.0459
2 vs. 3	134.1	112.6	21.51	ns	0.0583
Female max All Paw			**WT**	**HET**	
		N	15	13	
Wildtype vs. Het					
Time point	**Mean 1**	**Mean 2**	**Mean diff**	**Significance**	**Adjusted *p* value**
1	248	203.3	44.75	*	0.0334
2	248.4	228.3	20.19	ns	0.5696
3	261.4	239.2	22.15	ns	0.4928
Wildtype	**Mean 1**	**Mean 2**	**Mean diff**	**Significance**	**Adjusted *p* value**
1 vs. 2	248	248.4	-0.4407	ns	0.9994
1 vs. 3	248	261.4	-13.37	ns	0.584
2 vs. 3	248.4	261.4	-12.93	ns	0.6045
Heterozygous					
1 vs. 2	203.3	228.3	-25	ns	0.2039
1 vs. 3	203.3	239.2	-35.97	*	0.0418
2 vs. 3	228.3	239.2	-10.97	ns	0.7295

Abbreviations: **WT=** wild type; **HET=** heterozygous SLC5A7$^{indelCA/+}$**; diff=** difference

Table 43. Male *Slc5a7*$^{indelCA/+}$ mice grip strength summary statistics

Male max Forepaw			**WT**	**HET**	
		N	14	20	
Wildtype vs. Het					
Time point	**Mean 1**	**Mean 2**	**Mean diff**	**Significance**	**Adjusted *p* value**
1	144.3	153.6	-9.353	ns	0.5416
2	135.9	125.3	10.66	ns	0.4299
3	124.3	121.6	2.674	ns	0.9803
Wildtype	**Mean 1**	**Mean 2**	**Mean diff**	**Significance**	**Adjusted *p* value**
1 vs. 2	144.3	135.9	8.333	ns	0.5124
1 vs. 3	144.3	124.3	20.03	*	0.0261
2 vs. 3	135.9	124.3	11.69	ns	0.2723
Heterozygous					
1 vs. 2	153.6	125.3	28.35	****	< 0.0001
1 vs. 3	153.6	121.6	32.05	****	< 0.0001
2 vs. 3	125.3	121.6	3.709	ns	0.8262
Male max All Paw			**WT**	**HET**	
		N	14	20	
Wildtype vs. Het					
Time point	**Mean 1**	**Mean 2**	**Mean diff**	**Significance**	**Adjusted *p* value**
1	244.5	240.9	3.643	ns	0.9946
2	261.8	220.7	41.12	*	0.0411
3	242	223.5	18.46	ns	0.6005
Wildtype	**Mean 1**	**Mean 2**	**Mean diff**	**Significance**	**Adjusted *p* value**
1 vs. 2	244.5	261.8	-17.29	ns	0.5668
1 vs. 3	244.5	242	2.549	ns	0.9876
2 vs. 3	261.8	242	19.84	ns	0.4748
Heterozygous					
1 vs. 2	240.9	220.7	20.19	ns	0.3349
1 vs. 3	240.9	223.5	17.36	ns	0.4432
2 vs. 3	220.7	223.5	-2.823	ns	0.9784

Abbreviations: **WT=** wild type; **HET=** heterozygous SLC5A7$^{indelCA/+}$**; diff=** difference

7.5.5.2 Grip strength testing in *Slc5a7*$^{+/TM1A}$ mice

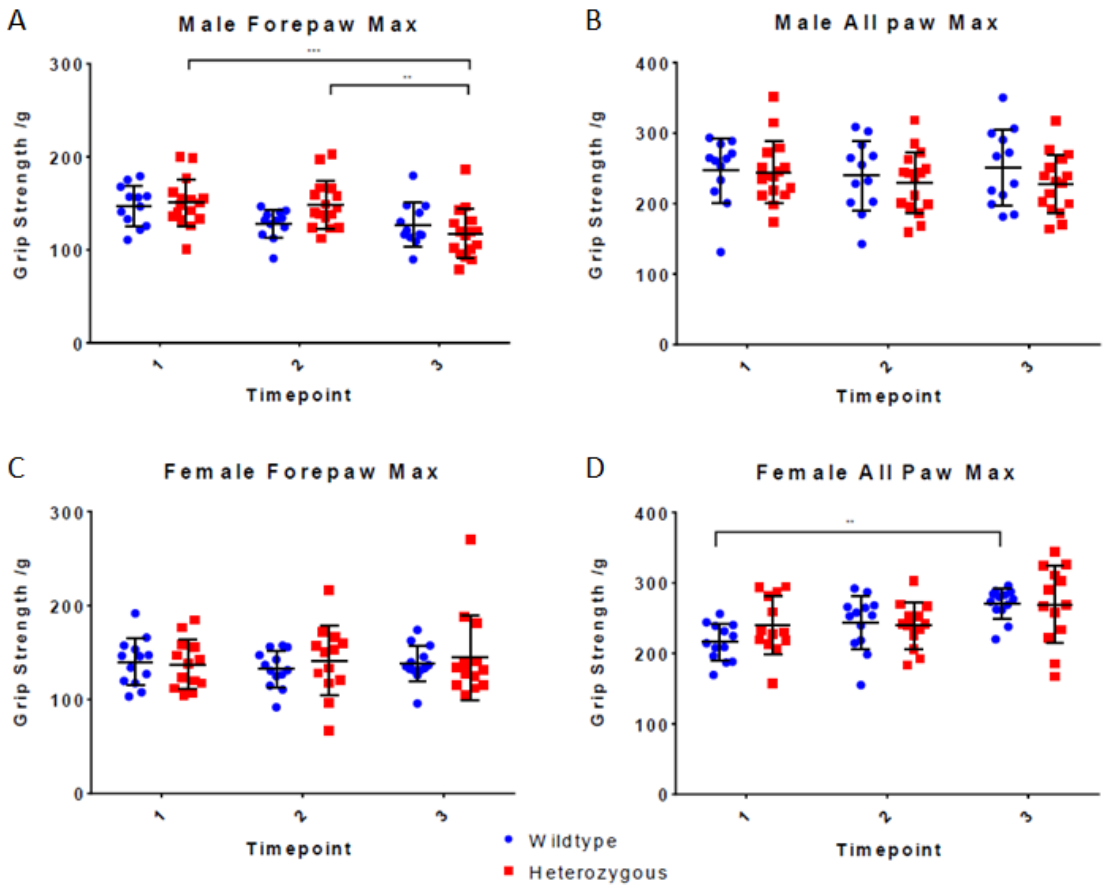

Figure 60. Grip strength test results taken at time points 1 (18-22 weeks), 2 (23-26 weeks) and 3 (27-31 weeks) from wild type (blue) vs. Slc5a7$^{+/TM1A}$ (red) A) Male mice forepaws, B) male mice all-paws, C) female mice forepaws and D) female mice all-paws. Difference of statistical significance are indicated by * where p=<0.05, and * where p=<0.0001***

Table 44. Female *Slc5a7*$^{+/TM1A}$ mice grip strength summary statistics

Female max forepaw			**WT**	**HET**	
		N	13	13	
Wildtype vs. Het					
Timepoint	**Mean 1**	**Mean 2**	**Mean diff**	**Significance**	**Adjusted *p* value**
1	139.9	137.7	2.194	ns	ns
2	132.8	141.6	-8.732	ns	ns
3	138.6	145	-6.321	ns	ns
Wildtype	**Mean 1**	**Mean 2**	**Mean diff**	**Significance**	**Adjusted *p* value**
1 vs. 2	139.9	132.8	7.02	ns	0.9909
1 vs. 3	139.9	138.6	1.229	ns	> 0.9999
2 vs. 3	132.8	138.6	-5.792	ns	0.9968
Heterozygous					
1 vs. 2	137.7	141.6	-3.906	ns	0.9997
1 vs. 3	137.7	145	-7.286	ns	0.989
2 vs. 3	141.6	145	-3.38	ns	0.9999
Female max All Paw			**WT**	**HET**	
		N	13	13	
Wildtype vs. Het					
Timepoint	**Mean 1**	**Mean 2**	**Mean diff**	**Significance**	**Adjusted *p* value**
1	216.1	240.2	-24.14	ns	0.2788
2	243.7	239.2	4.512	ns	0.9859
3	270.9	269.3	1.623	ns	0.9993
Wildtype	**Mean 1**	**Mean 2**	**Mean diff**	**Significance**	**Adjusted *p* value**
1 vs. 2	216.1	243.7	-27.69	ns	0.2534
1 vs. 3	216.1	270.9	-54.86	**	0.0012
2 vs. 3	243.7	270.9	-27.17	ns	0.2726
Heterozygous					
1 vs. 2	240.2	239.2	0.9619	ns	> 0.9999
1 vs. 3	240.2	269.3	-29.1	ns	0.206
2 vs. 3	239.2	269.3	-30.06	ns	0.1776

Abbreviations: **WT=** wild type; **HET=** heterozygous SLC5A7$^{+/TM2A}$**; diff=** difference

Table 45. Male *Slc5a7*$^{+/TM1A}$ mice grip strength summary statistics

Male max Forepaw			**WT**	**HET**	
		N	14	20	
Wildtype vs. Het					
Timepoint	**Mean 1**	**Mean 2**	**Mean diff**	**Significance**	**Adjusted *p* value**
1	147.6	150.6	-3.043	ns	0.9821
2	127.9	148.5	-20.57	ns	0.0767
3	127.2	117.1	10.04	ns	0.6144
Wildtype	**Mean 1**	**Mean 2**	**Mean diff**	**Significance**	**Adjusted *p* value**
1 vs. 2	147.6	127.9	19.64	ns	0.2236
1 vs. 3	147.6	127.2	20.4	ns	0.189
2 vs. 3	127.9	127.2	0.7605	ns	> 0.9999
Heterozygous					
1 vs. 2	150.6	148.5	2.104	ns	> 0.9999
1 vs. 3	150.6	117.1	33.48	***	0.0008
2 vs. 3	148.5	117.1	31.38	**	0.0019
Male max All Paw			**WT**	**HET**	
		N	14	20	
Wildtype vs. Het					
Timepoint	**Mean 1**	**Mean 2**	**Mean diff**	**Significance**	**Adjusted *p* value**
1	246.9	244.6	2.282	ns	0.9989
2	239.4	229.7	9.757	ns	0.9275
3	250.8	227.9	22.87	ns	0.4885
Wildtype	**Mean 1**	**Mean 2**	**Mean diff**	**Significance**	**Adjusted *p* value**
1 vs. 2	246.9	239.4	7.462	ns	0.9994
1 vs. 3	246.9	250.8	-3.899	ns	> 0.9999
2 vs. 3	239.4	250.8	-11.36	ns	0.9934
Heterozygous					
1 vs. 2	244.6	229.7	14.94	ns	0.9461
1 vs. 3	244.6	227.9	16.69	ns	0.9117
2 vs. 3	229.7	227.9	1.75	ns	> 0.9999

Abbreviations: **WT=** wild type; **HET=** heterozygous SLC5A7$^{+/TM2A}$**; diff=** difference

REFERENCES

1. Matthies DS, Fleming PA, Wilkes DM, Blakely RD. The Caenorhabditis elegans choline transporter CHO-1 sustains acetylcholine synthesis and motor function in an activity-dependent manner. J Neurosci. 2006 Jun;26(23):6200-12. PubMed PMID: 16763028. eng.

2. English BA, Hahn MK, Gizer IR, Mazei-Robison M, Steele A, Kurnik DM, et al. Choline transporter gene variation is associated with attention-deficit hyperactivity disorder. J Neurodev Disord. 2009 Dec;1(4):252-63. PubMed PMID: 21547719. Pubmed Central PMCID: PMC3164006. eng.

3. Ruggiero AM, Wright J, Ferguson SM, Lewis M, Emerson KS, Iwamoto H, et al. Nonoisotopic assay for the presynaptic choline transporter reveals capacity for allosteric modulation of choline uptake. ACS Chem Neurosci. 2012 Oct;3(10):767-81. PubMed PMID: 23077721. Pubmed Central PMCID: PMC3474274. eng.

4. Hahn MK, Blackford JU, Haman K, Mazei-Robison M, English BA, Prasad HC, et al. Multivariate permutation analysis associates multiple polymorphisms with subphenotypes of major depression. Genes Brain Behav. 2008 Jun;7(4):487-95. PubMed PMID: 18081710. Pubmed Central PMCID: PMC2670227. eng.

5. Ferguson SM, Bazalakova M, Savchenko V, Tapia JC, Wright J, Blakely RD. Lethal impairment of cholinergic neurotransmission in hemicholinium-3-sensitive choline transporter knockout mice. Proc Natl Acad Sci U S A. 2004 Jun;101(23):8762-7. PubMed PMID: 15173594. Pubmed Central PMCID: PMC423269. eng.

6. Wright C, Calhoun VD, Ehrlich S, Wang L, Turner JA, Bizzozero NI. Meta gene set enrichment analyses link miR-137-regulated pathways with schizophrenia risk. Front Genet. 2015;6:147. PubMed PMID: 25941532. Pubmed Central PMCID: PMC4403556. eng.

7. Adams HH, de Bruijn RF, Hofman A, Uitterlinden AG, van Duijn CM, Vernooij MW, et al. Genetic risk of neurodegenerative diseases is associated with mild cognitive impairment and conversion to dementia. Alzheimers Dement. 2015 Apr. PubMed PMID: 25916564. ENG.

8. Flint Beal M, Lang AE, Ludolph AC. Neurodegenerative Diseases: Neurobiology, Pathogenesis and Therapeutics: Cambridge University Press; 2005.

9. Wilkie A. Measuring up: improving the collection of neurological data and intelligence The Neurological Alliance Website: Neurological Alliance; 2014 [cited 2015 24/06/2015]. Available from: http://www.neural.org.uk/store/assets/files/380/original/Final_-_Measuring_up_30_April_2014_.pdf.

10. Hardiman O, Doherty CP. Neurodegenerative disorders : a clinical guide. London: Springer; 2011.
11. Ramanan VK, Saykin AJ. Pathways to neurodegeneration: mechanistic insights from GWAS in Alzheimer's disease, Parkinson's disease, and related disorders. Am J Neurodegener Dis. 2013;2(3):145-75. PubMed PMID: 24093081. Pubmed Central PMCID: PMC3783830. eng.
12. Saghazadeh A, Rezaei N. MicroRNA machinery in Parkinson's disease: a platform for neurodegenerative diseases. Expert Rev Neurother. 2015 Nov:1-27. PubMed PMID: 26574782. ENG.
13. Mitchell B, Sharma R. Embryology: An illustrated colour text. 2nd ed. USAUK Churchill LivingstoneElsevier 2009. 72 p.
14. Schoenwolf GC, Bleyl SB, Brauer PR, Francis-West PH. Larsen's Human Embryology. 4th ed. Philadelphia, USA: Churhill LivingstoneElsevier 2009. 643 p.
15. Sadler TW. Langman's Medical Embryology. 12th ed. USA: Lippincott Williams & Wilkins; 2012. 344 p.
16. Moore KL, Persaud T, Torchia MG. Before we are born: Essentials of embryology and birth defects. 8th ed. Philadelphia, USA: SaundersElsevier 2013. 320 p.
17. Waxman SG. Clinical neuroanatomy. 27th ed. China: McGraw Hill Education; 2013. 345 p.
18. Melton KR, Iulianella A, Trainor PA. Gene expression and regulation of hindbrain and spinal cord development. Front Biosci. 2004 Jan;9:117-38. PubMed PMID: 14766352. eng.
19. Rowitch DH, Kriegstein AR. Developmental genetics of vertebrate glial-cell specification. Nature. 2010 Nov;468(7321):214-22. PubMed PMID: 21068830. eng.
20. Stiles J, Jernigan TL. The basics of brain development. Neuropsychol Rev. 2010 Dec;20(4):327-48. PubMed PMID: 21042938. Pubmed Central PMCID: PMC2989000. eng.
21. Hawryluk GW, Ruff CA, Fehlings MG. Development and maturation of the spinal cord: implications of molecular and genetic defects. Handb Clin Neurol. 2012;109:3-30. PubMed PMID: 23098703. eng.
22. Matise MP. Molecular genetic control of cell patterning and fate determination in the developing ventral spinal cord. Wiley Interdiscip Rev Dev Biol. 2013 2013 May-Jun;2(3):419-25. PubMed PMID: 23799585. eng.
23. College TC. Anatomy and Physiology 2401 Online: SkyBlue; 2014 [cited 2015 05 July]. Online access to learning].

24. Duval N, Daubas P, Bourcier de Carbon C, St Cloment C, Tinevez JY, Lopes M, et al. Msx1 and Msx2 act as essential activators of Atoh1 expression in the murine spinal cord. Development. 2014 Apr;141(8):1726-36. PubMed PMID: 24715462. eng.

25. Lai T, Jabaudon D, Molyneaux BJ, Azim E, Arlotta P, Menezes JR, et al. SOX5 controls the sequential generation of distinct corticofugal neuron subtypes. Neuron. 2008 Jan;57(2):232-47. PubMed PMID: 18215621. eng.

26. Bodea GO, Blaess S. Establishing diversity in the dopaminergic system. FEBS Lett. 2015 Sep. PubMed PMID: 26431946. ENG.

27. Schuenke M, Schulte E, Schumacher U. Thieme Atlas of Anatomy: Head and Neuroanatomy. StuttgartNew York Thieme; 2010. 383 p.

28. Drake RL, Vogl AW, Mitchell AW. Gray's Anatomy for Students. 3rd ed. Philadelphia, USA: Churchill LivingstoneElsevier 2014. 1135 p.

29. Martini F, Timmons MJ, Tallitsch RB. Human anatomy. 7th ed. ed. Glenview, Ill. ; Harlow: Pearson Education; 2012.

30. Mancall EL, Brock DG. Clinical neuroanatomy: the anatomic basis for clinical neuroscience. Philadelphia: Elsevier Saunders; 2011.

31. Patestas MA, Gartner LP. A text book of neuroanatomy. Malden, USA: Blackwell Science Ltd.; 2006.

32. Ferguson SM, Blakely RD. The choline transporter resurfaces: new roles for synaptic vesicles? Mol Interv. 2004 Feb;4(1):22-37. PubMed PMID: 14993474. eng.

33. Rizzoli SO, Betz WJ. Synaptic vesicle pools. Nat Rev Neurosci. 2005 Jan;6(1):57-69. PubMed PMID: 15611727. eng.

34. Bertholet AM, Delerue T, Millet AM, Moulis MF, David C, Daloyau M, et al. Mitochondrial fusion/fission dynamics in neurodegeneration and neuronal plasticity. Neurobiol Dis. 2015 Oct. PubMed PMID: 26494254. ENG.

35. Komine O, Yamanaka K. Neuroinflammation in motor neuron disease. Nagoya J Med Sci. 2015 Nov;77(4):537-49. PubMed PMID: 26663933. Pubmed Central PMCID: PMC4664586. eng.

36. Krols M, van Isterdael G, Asselbergh B, Kremer A, Lippens S, Timmerman V, et al. Mitochondria-associated membranes as hubs for neurodegeneration. Acta Neuropathol. 2016 Jan. PubMed PMID: 26744348. ENG.

37. Kiriyama Y, Nochi H. The Function of Autophagy in Neurodegenerative Diseases. Int J Mol Sci. 2015;16(11):26797-812. PubMed PMID: 26569220. Pubmed Central PMCID: PMC4661849. eng.

38. Mattsson N, Schott JM, Hardy J, Turner MR, Zetterberg H. Selective vulnerability in neurodegeneration: insights from clinical variants of Alzheimer's disease. J Neurol Neurosurg Psychiatry. 2016 Jan. PubMed PMID: 26746185. ENG.

39. Wellington CL, Hayden MR. Caspases and neurodegeneration: on the cutting edge of new therapeutic approaches. Clin Genet. 2000 Jan;57(1):1-10. PubMed PMID: 10733228. eng.

40. Crimella C, Tonelli A, Airoldi G, Baschirotto C, D'Angelo MG, Bonato S, et al. The GST domain of GDAP1 is a frequent target of mutations in the dominant form of axonal Charcot Marie Tooth type 2K. J Med Genet. 2010 Oct;47(10):712-6. PubMed PMID: 20685671. eng.

41. Rinaldi C, Grunseich C, Sevrioukova IF, Schindler A, Horkayne-Szakaly I, Lamperti C, et al. Cowchock syndrome is associated with a mutation in apoptosis-inducing factor. Am J Hum Genet. 2012 Dec;91(6):1095-102. PubMed PMID: 23217327. Pubmed Central PMCID: PMC3516602. eng.

42. Mizushima N, Levine B, Cuervo AM, Klionsky DJ. Autophagy fights disease through cellular self-digestion. Nature. 2008 Feb;451(7182):1069-75. PubMed PMID: 18305538. Pubmed Central PMCID: PMC2670399. eng.

43. Harms MB, Ori-McKenney KM, Scoto M, Tuck EP, Bell S, Ma D, et al. Mutations in the tail domain of DYNC1H1 cause dominant spinal muscular atrophy. Neurology. 2012 May;78(22):1714-20. PubMed PMID: 22459677. Pubmed Central PMCID: PMC3359582. eng.

44. Anandatheerthavarada HK, Devi L. Amyloid precursor protein and mitochondrial dysfunction in Alzheimer's disease. Neuroscientist. 2007 Dec;13(6):626-38. PubMed PMID: 17911214. eng.

45. Garcia-Cazorla A, Artuch R. Neurotransmitter disorders. In: Rosenberg RN, Pascual JM, editors. Rosenberg's Molecular and Genetic Basis of Neurological and Psychiatric Disease. 5th ed. USA: Elsevier Inc; 2015. p. 703-12.

46. Bird TD, Davis MY. Genotype-Phenotype Correlations. In: Rosenberg RN, Pascual JM, editors. Rosenberg's Molecular and Genetic Basis of Neurological and Psychiatric Disease. USA: Elsevier Inc; 2015. p. 29-38.

47. Hellwig CT, Passante E, Rehm M. The molecular machinery regulating apoptosis signal transduction and its implication in human physiology and pathophysiologies. Curr Mol Med. 2011 Feb;11(1):31-47. PubMed PMID: 21189119. eng.

48. Friedlander RM. Apoptosis and caspases in neurodegenerative diseases. N Engl J Med. 2003 Apr;348(14):1365-75. PubMed PMID: 12672865. eng.

49. Baxter RV, Ben Othmane K, Rochelle JM, Stajich JE, Hulette C, Dew-Knight S, et al. Ganglioside-induced differentiation-associated protein-1 is mutant in Charcot-Marie-Tooth disease type 4A/8q21. Nat Genet. 2002 Jan;30(1):21-2. PubMed PMID: 11743579. eng.

50. Nelis E, Erdem S, Van Den Bergh PY, Belpaire-Dethiou MC, Ceuterick C, Van Gerwen V, et al. Mutations in GDAP1: autosomal recessive CMT with demyelination and axonopathy. Neurology. 2002 Dec;59(12):1865-72. PubMed PMID: 12499475. eng.

51. Ghavami S, Shojaei S, Yeganeh B, Ande SR, Jangamreddy JR, Mehrpour M, et al. Autophagy and apoptosis dysfunction in neurodegenerative disorders. Prog Neurobiol. 2014 Jan;112:24-49. PubMed PMID: 24211851. eng.

52. Nicholson GA, Magdelaine C, Zhu D, Grew S, Ryan MM, Sturtz F, et al. Severe early-onset axonal neuropathy with homozygous and compound heterozygous MFN2 mutations. Neurology. 2008 May;70(19):1678-81. PubMed PMID: 18458227. eng.

53. Weedon MN, Hastings R, Caswell R, Xie W, Paszkiewicz K, Antoniadi T, et al. Exome sequencing identifies a DYNC1H1 mutation in a large pedigree with dominant axonal Charcot-Marie-Tooth disease. Am J Hum Genet. 2011 Aug;89(2):308-12. PubMed PMID: 21820100. Pubmed Central PMCID: PMC3155164. eng.

54. Hroudová J, Singh N, Fišar Z. Mitochondrial dysfunctions in neurodegenerative diseases: relevance to Alzheimer's disease. Biomed Res Int. 2014;2014:175062. PubMed PMID: 24900954. Pubmed Central PMCID: PMC4036420. eng.

55. Dias V, Junn E, Mouradian MM. The role of oxidative stress in Parkinson's disease. J Parkinsons Dis. 2013;3(4):461-91. PubMed PMID: 24252804. Pubmed Central PMCID: PMC4135313. eng.

56. Malkus KA, Tsika E, Ischiropoulos H. Oxidative modifications, mitochondrial dysfunction, and impaired protein degradation in Parkinson's disease: how neurons are lost in the Bermuda triangle. Mol Neurodegener. 2009;4:24. PubMed PMID: 19500376. Pubmed Central PMCID: PMC2701947. eng.

57. Millecamps S, Julien JP. Axonal transport deficits and neurodegenerative diseases. Nat Rev Neurosci. 2013 Mar;14(3):161-76. PubMed PMID: 23361386. eng.

58. Jordanova A, De Jonghe P, Boerkoel CF, Takashima H, De Vriendt E, Ceuterick C, et al. Mutations in the neurofilament light chain gene (NEFL) cause early onset severe Charcot-Marie-Tooth disease. Brain. 2003 Mar;126(Pt 3):590-7. PubMed PMID: 12566280. eng.

59. Chevalier-Larsen E, Holzbaur EL. Axonal transport and neurodegenerative disease. Biochim Biophys Acta. 2006 2006 Nov-Dec;1762(11-12):1094-108. PubMed PMID: 16730956. eng.

60. Puls I, Jonnakuty C, LaMonte BH, Holzbaur EL, Tokito M, Mann E, et al. Mutant dynactin in motor neuron disease. Nat Genet. 2003 Apr;33(4):455-6. PubMed PMID: 12627231. eng.

61. Cappellano G, Carecchio M, Fleetwood T, Magistrelli L, Cantello R, Dianzani U, et al. Immunity and inflammation in neurodegenerative diseases. Am J Neurodegener

Dis. 2013;2(2):89-107. PubMed PMID: 23844334. Pubmed Central PMCID: PMC3703122. eng.

62. Association M. Different types of MND: © 2015 MND Association: Registered in England. Registered Charity no. 294354; 2015 [cited 2015 15th Septhember]. Available from: http://www.mndassociation.org/what-is-mnd/different-types-of-mnd/.

63. NINDS. Motor neurone disease factsheet Online: National Institute of Neurological Disorders and Stroke (NINDS); 2015 [cited 2015 15 September]. Available from: http://www.ninds.nih.gov/disorders/motor_neuron_diseases/detail_motor_neuron_diseases.htm.

64. Reilly MM. Classification of the hereditary motor and sensory neuropathies. Curr Opin Neurol. 2000 Oct;13(5):561-4. PubMed PMID: 11073363. eng.

65. Liu L, Zhang R. Intermediate Charcot-Marie-Tooth disease. Neurosci Bull. 2014 Dec;30(6):999-1009. PubMed PMID: 25326399. eng.

66. Timmerman V, Strickland AV, Züchner S. Genetics of Charcot-Marie-Tooth (CMT) Disease within the Frame of the Human Genome Project Success. Genes (Basel). 2014;5(1):13-32. PubMed PMID: 24705285. Pubmed Central PMCID: PMC3978509. eng.

67. Klein CJ, Duan X, Shy ME. Inherited neuropathies: clinical overview and update. Muscle Nerve. 2013 Oct;48(4):604-22. PubMed PMID: 23801417. Pubmed Central PMCID: PMC3918879. eng.

68. Scherer SS, Kleopa KA, Benson MD. Peripheral Neuropathies. In: Rosenberg RN, Pascual JM, editors. Rosenberg's Molecular and Genetic Basis of Neurological and Psychiatric Disease. 5th ed. USA: Elsevier Inc; 2015. p. 1051-74.

69. Koop O, Schirmacher A, Nelis E, Timmerman V, De Jonghe P, Ringelstein B, et al. Genotype-phenotype analysis in patients with giant axonal neuropathy (GAN). Neuromuscul Disord. 2007 Aug;17(8):624-30. PubMed PMID: 17587580. eng.

70. Wilkinson IMS, Lennox G. Essential neurology. 4th ed. ed. Oxford: Blackwell Science; 2005.

71. Shy ME, Lupski JR, Chance PF, Klein CJ, Dyck PJ. Hereditary motor and sensory neuropathies: an overview of clinical, genetic, electrophysiologic, and pathologic features. In: PJ D, PK T, editors. Peripheral neuropathy. 2. 4th ed. Philadelphia: Saunders; 2005. p. 1623-58.

72. De Sandre-Giovannoli A, Chaouch M, Kozlov S, Vallat JM, Tazir M, Kassouri N, et al. Homozygous defects in LMNA, encoding lamin A/C nuclear-envelope proteins, cause autosomal recessive axonal neuropathy in human (Charcot-Marie-Tooth disorder type 2) and mouse. Am J Hum Genet. 2002 Mar;70(3):726-36. PubMed PMID: 11799477. Pubmed Central PMCID: PMC384949. eng.

73. Hayasaka K, Himoro M, Sato W, Takada G, Uyemura K, Shimizu N, et al. Charcot-Marie-Tooth neuropathy type 1B is associated with mutations of the myelin P0 gene. Nat Genet. 1993 Sep;5(1):31-4. PubMed PMID: 7693129. eng.

74. Zhao C, Takita J, Tanaka Y, Setou M, Nakagawa T, Takeda S, et al. Charcot-Marie-Tooth disease type 2A caused by mutation in a microtubule motor KIF1Bbeta. Cell. 2001 Jun;105(5):587-97. PubMed PMID: 11389829. eng.

75. Abath O, Martins CeA, Carvalho M, Chadi G, Seitz KW, Oliveira AS, et al. DNM2 mutations in a cohort of sporadic patients with centronuclear myopathy. Genet Mol Biol. 2015 May;38(2):147-51. PubMed PMID: 26273216. Pubmed Central PMCID: PMC4530644. eng.

76. Cogli L, Piro F, Bucci C. Rab7 and the CMT2B disease. Biochem Soc Trans. 2009 Oct;37(Pt 5):1027-31. PubMed PMID: 19754445. eng.

77. Warner LE, Mancias P, Butler IJ, McDonald CM, Keppen L, Koob KG, et al. Mutations in the early growth response 2 (EGR2) gene are associated with hereditary myelinopathies. Nat Genet. 1998 Apr;18(4):382-4. PubMed PMID: 9537424. eng.

78. Street VA, Bennett CL, Goldy JD, Shirk AJ, Kleopa KA, Tempel BL, et al. Mutation of a putative protein degradation gene LITAF/SIMPLE in Charcot-Marie-Tooth disease 1C. Neurology. 2003 Jan;60(1):22-6. PubMed PMID: 12525712. eng.

79. Tang BS, Zhao GH, Luo W, Xia K, Cai F, Pan Q, et al. Small heat-shock protein 22 mutated in autosomal dominant Charcot-Marie-Tooth disease type 2L. Hum Genet. 2005 Feb;116(3):222-4. PubMed PMID: 15565283. eng.

80. Irobi J, Van Impe K, Seeman P, Jordanova A, Dierick I, Verpoorten N, et al. Hot-spot residue in small heat-shock protein 22 causes distal motor neuropathy. Nat Genet. 2004 Jun;36(6):597-601. PubMed PMID: 15122253. eng.

81. Evgrafov OV, Mersiyanova I, Irobi J, Van Den Bosch L, Dierick I, Leung CL, et al. Mutant small heat-shock protein 27 causes axonal Charcot-Marie-Tooth disease and distal hereditary motor neuropathy. Nat Genet. 2004 Jun;36(6):602-6. PubMed PMID: 15122254. eng.

82. Kolb SJ, Snyder PJ, Poi EJ, Renard EA, Bartlett A, Gu S, et al. Mutant small heat shock protein B3 causes motor neuropathy: utility of a candidate gene approach. Neurology. 2010 Feb;74(6):502-6. PubMed PMID: 20142617. eng.

83. Blumen SC, Astord S, Robin V, Vignaud L, Toumi N, Cieslik A, et al. A rare recessive distal hereditary motor neuropathy with HSJ1 chaperone mutation. Ann Neurol. 2012 Apr;71(4):509-19. PubMed PMID: 22522442. eng.

84. Gess B, Auer-Grumbach M, Schirmacher A, Strom T, Zitzelsberger M, Rudnik-Schöneborn S, et al. HSJ1-related hereditary neuropathies: novel mutations and extended clinical spectrum. Neurology. 2014 Nov;83(19):1726-32. PubMed PMID: 25274842. eng.

85. Abe A, Hayasaka K. The GARS gene is rarely mutated in Japanese patients with Charcot-Marie-Tooth neuropathy. J Hum Genet. 2009 May;54(5):310-2. PubMed PMID: 19329989. eng.

86. Jordanova A, Irobi J, Thomas FP, Van Dijck P, Meerschaert K, Dewil M, et al. Disrupted function and axonal distribution of mutant tyrosyl-tRNA synthetase in dominant intermediate Charcot-Marie-Tooth neuropathy. Nat Genet. 2006 Feb;38(2):197-202. PubMed PMID: 16429158. eng.

87. Latour P, Thauvin-Robinet C, Baudelet-Méry C, Soichot P, Cusin V, Faivre L, et al. A major determinant for binding and aminoacylation of tRNA(Ala) in cytoplasmic Alanyl-tRNA synthetase is mutated in dominant axonal Charcot-Marie-Tooth disease. Am J Hum Genet. 2010 Jan;86(1):77-82. PubMed PMID: 20045102. Pubmed Central PMCID: PMC2801750. eng.

88. McLaughlin HM, Sakaguchi R, Liu C, Igarashi T, Pehlivan D, Chu K, et al. Compound heterozygosity for loss-of-function lysyl-tRNA synthetase mutations in a patient with peripheral neuropathy. Am J Hum Genet. 2010 Oct;87(4):560-6. PubMed PMID: 20920668. Pubmed Central PMCID: PMC2948804. eng.

89. Safka Brozkova D, Deconinck T, Griffin LB, Ferbert A, Haberlova J, Mazanec R, et al. Loss of function mutations in HARS cause a spectrum of inherited peripheral neuropathies. Brain. 2015 Aug;138(Pt 8):2161-72. PubMed PMID: 26072516. eng.

90. Wallen RC, Antonellis A. To charge or not to charge: mechanistic insights into neuropathy-associated tRNA synthetase mutations. Curr Opin Genet Dev. 2013 Jun;23(3):302-9. PubMed PMID: 23465884. Pubmed Central PMCID: PMC3703498. eng.

91. Raeymaekers P, Timmerman V, Nelis E, De Jonghe P, Hoogendijk JE, Baas F, et al. Duplication in chromosome 17p11.2 in Charcot-Marie-Tooth neuropathy type 1a (CMT 1a). The HMSN Collaborative Research Group. Neuromuscul Disord. 1991;1(2):93-7. PubMed PMID: 1822787. eng.

92. Dyck PJ, Chance P, Lebo R, J.A. C. Hereditary motor and sensory neuropathies. In: Dyck PJ, Thomas PK, Griffin JW, Low PA, Podulso JF, editors. Peripheral neuropathy. 2. 3rd ed. Philadelphia: Saunders; 1993. p. 11094-1134.

93. Gagic M, Markovic MK, Kecmanovic M, Keckarevic D, Mladenovic J, Dackovic J, et al. Analysis of PMP22 duplication and deletion using a panel of six dinucleotide tandem repeats. Clin Chem Lab Med. 2015 Oct. PubMed PMID: 26479344. ENG.

94. Szigeti K, Lupski JR. Charcot-Marie-Tooth disease. Eur J Hum Genet. 2009 Jun;17(6):703-10. PubMed PMID: 19277060. Pubmed Central PMCID: PMC2947101. eng.

95. Thomas PK, King RH, Small JR, Robertson AM. The pathology of charcot-marie-tooth disease and related disorders. Neuropathol Appl Neurobiol. 1996 Aug;22(4):269-84. PubMed PMID: 8875461. eng.

96. Davis CJ, Bradley WG, Madrid R. The peroneal muscular atrophy syndrome: clinical, genetic, electrophysiological and nerve biopsy studies. I. Clinical, genetic and electrophysiological findings and classification. J Genet Hum. 1978 Dec;26(4):311-49. PubMed PMID: 752065. eng.

97. Yiu EM, Geevasinga N, Nicholson GA, Fagan ER, Ryan MM, Ouvrier RA. A retrospective review of X-linked Charcot-Marie-Tooth disease in childhood. Neurology. 2011 Feb;76(5):461-6. PubMed PMID: 21282593. eng.

98. Ionasescu VV, Trofatter J, Haines JL, Summers AM, Ionasescu R, Searby C. X-linked recessive Charcot-Marie-Tooth neuropathy: clinical and genetic study. Muscle Nerve. 1992 Mar;15(3):368-73. PubMed PMID: 1557086. eng.

99. Phillips LH, Kelly TE, Schnatterly P, Parker D. Hereditary motor-sensory neuropathy (HMSN): possible X-linked dominant inheritance. Neurology. 1985 Apr;35(4):498-502. PubMed PMID: 3856757. eng.

100. Kim HJ, Hong SH, Ki CS, Kim BJ, Shim JS, Cho SH, et al. A novel locus for X-linked recessive CMT with deafness and optic neuropathy maps to Xq21.32-q24. Neurology. 2005 Jun;64(11):1964-7. PubMed PMID: 15955956. eng.

101. Kennerson ML, Yiu EM, Chuang DT, Kidambi A, Tso SC, Ly C, et al. A new locus for X-linked dominant Charcot-Marie-Tooth disease (CMTX6) is caused by mutations in the pyruvate dehydrogenase kinase isoenzyme 3 (PDK3) gene. Hum Mol Genet. 2013 Apr;22(7):1404-16. PubMed PMID: 23297365. Pubmed Central PMCID: PMC3596851. eng.

102. Kennerson ML, Nicholson GA, Kaler SG, Kowalski B, Mercer JF, Tang J, et al. Missense mutations in the copper transporter gene ATP7A cause X-linked distal hereditary motor neuropathy. Am J Hum Genet. 2010 Mar;86(3):343-52. PubMed PMID: 20170900. Pubmed Central PMCID: PMC2833394. eng.

103. Bergoffen J, Scherer SS, Wang S, Scott MO, Bone LJ, Paul DL, et al. Connexin mutations in X-linked Charcot-Marie-Tooth disease. Science. 1993 Dec;262(5142):2039-42. PubMed PMID: 8266101. eng.

104. Kim HJ, Sohn KM, Shy ME, Krajewski KM, Hwang M, Park JH, et al. Mutations in PRPS1, which encodes the phosphoribosyl pyrophosphate synthetase enzyme critical for nucleotide biosynthesis, cause hereditary peripheral neuropathy with hearing loss and optic neuropathy (cmtx5). Am J Hum Genet. 2007 Sep;81(3):552-8. PubMed PMID: 17701900. Pubmed Central PMCID: PMC1950833. eng.

105. Ionasescu VV. Charcot-Marie-Tooth neuropathies: from clinical description to molecular genetics. Muscle Nerve. 1995 Mar;18(3):267-75. PubMed PMID: 7870103. eng.

106. Diodato D, Tasca G, Verrigni D, D'Amico A, Rizza T, Tozzi G, et al. A novel AIFM1 mutation expands the phenotype to an infantile motor neuron disease. Eur J Hum Genet. 2015 Jul. PubMed PMID: 26173962. ENG.

107. Scherer SS, Deschênes SM, Xu YT, Grinspan JB, Fischbeck KH, Paul DL. Connexin32 is a myelin-related protein in the PNS and CNS. J Neurosci. 1995 Dec;15(12):8281-94. PubMed PMID: 8613761. eng.

108. Sagnelli A, Piscosquito G, Chiapparini L, Ciano C, Salsano E, Saveri P, et al. X-linked Charcot-Marie-Tooth type 1: stroke-like presentation of a novel GJB1 mutation. J Peripher Nerv Syst. 2014 Jun;19(2):183-6. PubMed PMID: 24863494. eng.

109. Karadima G, Koutsis G, Raftopoulou M, Floroskufi P, Karletidi KM, Panas M. Four novel connexin 32 mutations in X-linked Charcot-Marie-Tooth disease. Phenotypic variability and central nervous system involvement. J Neurol Sci. 2014 Jun;341(1-2):158-61. PubMed PMID: 24768312. eng.

110. Becker MA, Smith PR, Taylor W, Mustafi R, Switzer RL. The genetic and functional basis of purine nucleotide feedback-resistant phosphoribosylpyrophosphate synthetase superactivity. J Clin Invest. 1995 Nov;96(5):2133-41. PubMed PMID: 7593598. Pubmed Central PMCID: PMC185862. eng.

111. de Brouwer AP, Williams KL, Duley JA, van Kuilenburg AB, Nabuurs SB, Egmont-Petersen M, et al. Arts syndrome is caused by loss-of-function mutations in PRPS1. Am J Hum Genet. 2007 Sep;81(3):507-18. PubMed PMID: 17701896. Pubmed Central PMCID: PMC1950830. eng.

112. Liu X, Han D, Li J, Han B, Ouyang X, Cheng J, et al. Loss-of-function mutations in the PRPS1 gene cause a type of nonsyndromic X-linked sensorineural deafness, DFN2. Am J Hum Genet. 2010 Jan;86(1):65-71. PubMed PMID: 20021999. Pubmed Central PMCID: PMC2801751. eng.

113. Harding A. Inherited neuronal atrophy and degeneration predominantly of lower motor neurons. In: Dyck P, Thomas P, editors. Peripheral Neuropathy. 2. Philadelphia: W. B. Saunders; 1993. p. 1051-64.

114. Rossor AM, Kalmar B, Greensmith L, Reilly MM. The distal hereditary motor neuropathies. J Neurol Neurosurg Psychiatry. 2012 Jan;83(1):6-14. PubMed PMID: 22028385. eng.

115. Zhao H, Race V, Matthijs G, De Jonghe P, Robberecht W, Lambrechts D, et al. Exome sequencing reveals HINT1 mutations as a cause of distal hereditary motor neuropathy. Eur J Hum Genet. 2014 Jun;22(6):847-50. PubMed PMID: 24105373. Pubmed Central PMCID: PMC4023208. eng.

116. Okuda T, Osawa C, Yamada H, Hayashi K, Nishikawa S, Ushio T, et al. Transmembrane topology and oligomeric structure of the high-affinity choline transporter. J Biol Chem. 2012 Dec;287(51):42826-34. PubMed PMID: 23132865. Pubmed Central PMCID: PMC3522279. eng.

117. Irobi J, Dierick I, Jordanova A, Claeys KG, De Jonghe P, Timmerman V. Unraveling the genetics of distal hereditary motor neuronopathies. Neuromolecular Med. 2006;8(1-2):131-46. PubMed PMID: 16775372. eng.

118. Young ID, Harper PS. Hereditary distal spinal muscular atrophy with vocal cord paralysis. J Neurol Neurosurg Psychiatry. 1980 May;43(5):413-8. PubMed PMID: 7420092. Pubmed Central PMCID: PMC490568. eng.

119. McEntagart M, Dunstan M, Bell C, Boltshauser E, Donaghy M, Harper PS, et al. Clinical and genetic heterogeneity in peroneal muscular atrophy associated with vocal cord weakness. J Neurol Neurosurg Psychiatry. 2002 Dec;73(6):762-5. PubMed PMID: 12438487. Pubmed Central PMCID: PMC1757353. eng.

120. Pridmore C, Baraitser M, Brett EM, Harding AE. Distal spinal muscular atrophy with vocal cord paralysis. J Med Genet. 1992 Mar;29(3):197-9. PubMed PMID: 1552559. Pubmed Central PMCID: PMC1015897. eng.

121. Dick KJ, McEntagart M, Alwan W, Reilly M, Crosby AH. Refinement of the locus for distal hereditary motor neuronopathy VII (dHMN-VII) and exclusion of candidate genes. Genome. 2008 Nov;51(11):959-62. PubMed PMID: 18956029. eng.

122. Fu MM, Holzbaur EL. Integrated regulation of motor-driven organelle transport by scaffolding proteins. Trends Cell Biol. 2014 Oct;24(10):564-74. PubMed PMID: 24953741. Pubmed Central PMCID: PMC4177981. eng.

123. Meadows JC, Marsden CD. A distal form of chronic spinal muscular atrophy. Neurology. 1969 Jan;19(1):53-8. PubMed PMID: 5813127. eng.

124. Christodoulou K, Kyriakides T, Hristova AH, Georgiou DM, Kalaydjieva L, Yshpekova B, et al. Mapping of a distal form of spinal muscular atrophy with upper limb predominance to chromosome 7p. Hum Mol Genet. 1995 Sep;4(9):1629-32. PubMed PMID: 8541851. eng.

125. Sambuughin N, Sivakumar K, Selenge B, Lee HS, Friedlich D, Baasanjav D, et al. Autosomal dominant distal spinal muscular atrophy type V (dSMA-V) and Charcot-Marie-Tooth disease type 2D (CMT2D) segregate within a single large kindred and map to a refined region on chromosome 7p15. J Neurol Sci. 1998 Nov;161(1):23-8. PubMed PMID: 9879677. eng.

126. Auer-Grumbach M, Löscher WN, Wagner K, Petek E, Körner E, Offenbacher H, et al. Phenotypic and genotypic heterogeneity in hereditary motor neuronopathy type V: a clinical, electrophysiological and genetic study. Brain. 2000 Aug;123 (Pt 8):1612-23. PubMed PMID: 10908191. eng.

127. Beetz C, Pieber TR, Hertel N, Schabhüttl M, Fischer C, Trajanoski S, et al. Exome sequencing identifies a REEP1 mutation involved in distal hereditary motor neuropathy type V. Am J Hum Genet. 2012 Jul;91(1):139-45. PubMed PMID: 22703882. Pubmed Central PMCID: PMC3397265. eng.

128. Antonellis A, Ellsworth RE, Sambuughin N, Puls I, Abel A, Lee-Lin SQ, et al. Glycyl tRNA synthetase mutations in Charcot-Marie-Tooth disease type 2D and distal spinal muscular atrophy type V. Am J Hum Genet. 2003 May;72(5):1293-9. PubMed PMID: 12690580. Pubmed Central PMCID: PMC1180282. eng.

129. Auer-Grumbach M, Olschewski A, Papić L, Kremer H, McEntagart ME, Uhrig S, et al. Alterations in the ankyrin domain of TRPV4 cause congenital distal SMA, scapuloperoneal SMA and HMSN2C. Nat Genet. 2010 Feb;42(2):160-4. PubMed PMID: 20037588. Pubmed Central PMCID: PMC3272392. eng.

130. Lin KP, Soong BW, Yang CC, Huang LW, Chang MH, Lee IH, et al. The mutational spectrum in a cohort of Charcot-Marie-Tooth disease type 2 among the Han Chinese in Taiwan. PLoS One. 2011;6(12):e29393. PubMed PMID: 22206013. Pubmed Central PMCID: PMC3242783. eng.

131. Rohkamm B, Reilly MM, Lochmüller H, Schlotter-Weigel B, Barisic N, Schöls L, et al. Further evidence for genetic heterogeneity of distal HMN type V, CMT2 with predominant hand involvement and Silver syndrome. J Neurol Sci. 2007 Dec;263(1-2):100-6. PubMed PMID: 17663003. Pubmed Central PMCID: PMC3272403. eng.

132. Freist W, Logan DT, Gauss DH. Glycyl-tRNA synthetase. Biol Chem Hoppe Seyler. 1996 Jun;377(6):343-56. PubMed PMID: 8839980. eng.

133. Windpassinger C, Auer-Grumbach M, Irobi J, Patel H, Petek E, Hörl G, et al. Heterozygous missense mutations in BSCL2 are associated with distal hereditary motor neuropathy and Silver syndrome. Nat Genet. 2004 Mar;36(3):271-6. PubMed PMID: 14981520. eng.

134. Bi J, Wang W, Liu Z, Huang X, Jiang Q, Liu G, et al. Seipin promotes adipose tissue fat storage through the ER Ca^{2+}-ATPase SERCA. Cell Metab. 2014 May;19(5):861-71. PubMed PMID: 24807223. eng.

135. Park SH, Zhu PP, Parker RL, Blackstone C. Hereditary spastic paraplegia proteins REEP1, spastin, and atlastin-1 coordinate microtubule interactions with the tubular ER network. J Clin Invest. 2010 Apr;120(4):1097-110. PubMed PMID: 20200447. Pubmed Central PMCID: PMC2846052. eng.

136. Saito H, Kubota M, Roberts RW, Chi Q, Matsunami H. RTP family members induce functional expression of mammalian odorant receptors. Cell. 2004 Nov;119(5):679-91. PubMed PMID: 15550249. eng.

137. Falk J, Rohde M, Bekhite MM, Neugebauer S, Hemmerich P, Kiehntopf M, et al. Functional mutation analysis provides evidence for a role of REEP1 in lipid droplet biology. Hum Mutat. 2014 Apr;35(4):497-504. PubMed PMID: 24478229. eng.

138. Apparsundaram S, Ferguson SM, George AL, Blakely RD. Molecular cloning of a human, hemicholinium-3-sensitive choline transporter. Biochem Biophys Res Commun. 2000 Oct;276(3):862-7. PubMed PMID: 11027560. eng.

139. Okuda T, Haga T. Functional characterization of the human high-affinity choline transporter. FEBS Lett. 2000 Nov;484(2):92-7. PubMed PMID: 11068039. eng.

140. Apparsundaram S, Ferguson SM, George AL, Blakely RD. Molecular cloning of a human, hemicholinium-3-sensitive choline transporter. Biochem Biophys Res Commun. 2000 Oct;276(3):862-7. PubMed PMID: 11027560. eng.

141. Apparsundaram S, Ferguson SM, Blakely RD. Molecular cloning and characterization of a murine hemicholinium-3-sensitive choline transporter. Biochem Soc Trans. 2001 Nov;29(Pt 6):711-6. PubMed PMID: 11709061. eng.

142. Ingram G, Barwick KE, Hartley L, McEntagart M, Crosby AH, Llewelyn G, et al. Distal hereditary motor neuropathy with vocal cord paresis: from difficulty in choral singing to a molecular genetic diagnosis. Pract Neurol. 2016 Jun;16(3):247-51. PubMed PMID: 26786006. eng.

143. Okuda T, Haga T, Kanai Y, Endou H, Ishihara T, Katsura I. Identification and characterization of the high-affinity choline transporter. Nat Neurosci. 2000 Feb;3(2):120-5. PubMed PMID: 10649566. eng.

144. Ferguson SM, Savchenko V, Apparsundaram S, Zwick M, Wright J, Heilman CJ, et al. Vesicular localization and activity-dependent trafficking of presynaptic choline transporters. J Neurosci. 2003 Oct;23(30):9697-709. PubMed PMID: 14585997. eng.

145. Ribeiro FM, Black SA, Cregan SP, Prado VF, Prado MA, Rylett RJ, et al. Constitutive high-affinity choline transporter endocytosis is determined by a carboxyl-terminal tail dileucine motif. J Neurochem. 2005 Jul;94(1):86-96. PubMed PMID: 15953352. eng.

146. Singh G, Lykke-Andersen J. New insights into the formation of active nonsense-mediated decay complexes. Trends Biochem Sci. 2003 Sep;28(9):464-6. PubMed PMID: 13678954. eng.

147. Haga T. Molecular properties of the high-affinity choline transporter CHT1. J Biochem. 2014 Oct;156(4):181-94. PubMed PMID: 25073461. eng.

148. Barišić N, Chaouch A, Müller JS, Lochmüller H. Genetic heterogeneity and pathophysiological mechanisms in congenital myasthenic syndromes. Eur J Paediatr Neurol. 2011 May;15(3):189-96. PubMed PMID: 21498094. eng.

149. Beeson D, Higuchi O, Palace J, Cossins J, Spearman H, Maxwell S, et al. Dok-7 mutations underlie a neuromuscular junction synaptopathy. Science. 2006 Sep;313(5795):1975-8. PubMed PMID: 16917026. eng.

150. Ohno K, Quiram PA, Milone M, Wang HL, Harper MC, Pruitt JN, et al. Congenital myasthenic syndromes due to heteroallelic nonsense/missense mutations in the acetylcholine receptor epsilon subunit gene: identification and functional characterization of six new mutations. Hum Mol Genet. 1997 May;6(5):753-66. PubMed PMID: 9158150. eng.

151. Ohno K, Engel AG, Shen XM, Selcen D, Brengman J, Harper CM, et al. Rapsyn mutations in humans cause endplate acetylcholine-receptor deficiency and myasthenic syndrome. Am J Hum Genet. 2002 Apr;70(4):875-85. PubMed PMID: 11791205. Pubmed Central PMCID: PMC379116. eng.

152. Quiram PA, Ohno K, Milone M, Patterson MC, Pruitt NJ, Brengman JM, et al. Mutation causing congenital myasthenia reveals acetylcholine receptor beta/delta subunit interaction essential for assembly. J Clin Invest. 1999 Nov;104(10):1403-10. PubMed PMID: 10562302. Pubmed Central PMCID: PMC409847. eng.

153. Kinali M, Beeson D, Pitt MC, Jungbluth H, Simonds AK, Aloysius A, et al. Congenital myasthenic syndromes in childhood: diagnostic and management challenges. J Neuroimmunol. 2008 Sep;201-202:6-12. PubMed PMID: 18707767. eng.

154. Jephson CG, Mills NA, Pitt MC, Beeson D, Aloysius A, Muntoni F, et al. Congenital stridor with feeding difficulty as a presenting symptom of Dok7 congenital myasthenic syndrome. Int J Pediatr Otorhinolaryngol. 2010 Sep;74(9):991-4. PubMed PMID: 20554332. eng.

155. Lisi EC, Cohn RD. Genetic evaluation of the pediatric patient with hypotonia: perspective from a hypotonia specialty clinic and review of the literature. Dev Med Child Neurol. 2011 Jul;53(7):586-99. PubMed PMID: 21418198. eng.

156. Leyenaar J, Camfield P, Camfield C. A schematic approach to hypotonia in infancy. Paediatr Child Health. 2005 Sep;10(7):397-400. PubMed PMID: 19668647. Pubmed Central PMCID: PMC2722561. eng.

157. Synofzik M, Müller vom Hagen J, Haack TB, Wilhelm C, Lindig T, Beck-Wödl S, et al. X-linked Charcot-Marie-Tooth disease, Arts syndrome, and prelingual non-syndromic deafness form a disease continuum: evidence from a family with a novel PRPS1 mutation. Orphanet J Rare Dis. 2014;9:24. PubMed PMID: 24528855. Pubmed Central PMCID: PMC3931488. eng.

158. Iwamoto H, Blakely RD, De Felice LJ. Na+, Cl-, and pH dependence of the human choline transporter (hCHT) in Xenopus oocytes: the proton inactivation hypothesis of hCHT in synaptic vesicles. J Neurosci. 2006 Sep;26(39):9851-9. PubMed PMID: 17005849. eng.

159. Gates J, Ferguson SM, Blakely RD, Apparsundaram S. Regulation of choline transporter surface expression and phosphorylation by protein kinase C and protein phosphatase 1/2A. J Pharmacol Exp Ther. 2004 Aug;310(2):536-45. PubMed PMID: 15064333. eng.

160. Yamada H, Imajoh-Ohmi S, Haga T. The high-affinity choline transporter CHT1 is regulated by the ubiquitin ligase Nedd4-2. Biomed Res. 2012 Feb;33(1):1-8. PubMed PMID: 22361880. eng.

161. Cuddy LK, Winick-Ng W, Rylett RJ. Regulation of the high-affinity choline transporter activity and trafficking by its association with cholesterol-rich lipid rafts. J Neurochem. 2014 Mar;128(5):725-40. PubMed PMID: 24127780. eng.

162. Hartnett S, Zhang F, Abitz A, Li Y. Ubiquitin C-terminal hydrolase L1 interacts with choline transporter in cholinergic cells. Neurosci Lett. 2014 Apr;564:115-9. PubMed PMID: 24525247. Pubmed Central PMCID: PMC4024205. eng.

163. Mardones GA, Burgos PV, Lin Y, Kloer DP, Magadán JG, Hurley JH, et al. Structural basis for the recognition of tyrosine-based sorting signals by the μ3A subunit of the AP-3 adaptor complex. J Biol Chem. 2013 Mar;288(13):9563-71. PubMed PMID: 23404500. Pubmed Central PMCID: PMC3611023. eng.

164. Blakely RD, Edwards RH. Vesicular and plasma membrane transporters for neurotransmitters. Cold Spring Harb Perspect Biol. 2012 Feb;4(2). PubMed PMID: 22199021. Pubmed Central PMCID: PMC3281572. eng.

165. Misawa H, Fujigaya H, Nishimura T, Moriwaki Y, Okuda T, Kawashima K, et al. Aberrant trafficking of the high-affinity choline transporter in AP-3-deficient mice. Eur J Neurosci. 2008 Jun;27(12):3109-17. PubMed PMID: 18554297. eng.

166. Young AB. Four decades of neurodegenerative disease research: how far we have come! J Neurosci. 2009 Oct;29(41):12722-8. PubMed PMID: 19828782. Pubmed Central PMCID: PMC2807668. eng.

167. Douglas DS, Popko B. Mouse forward genetics in the study of the peripheral nervous system and human peripheral neuropathy. Neurochem Res. 2009 Jan;34(1):124-37. PubMed PMID: 18481175. Pubmed Central PMCID: PMC2759972. eng.

168. Bailey KR, Rustay NR, Crawley JN. Behavioral phenotyping of transgenic and knockout mice: practical concerns and potential pitfalls. ILAR J. 2006;47(2):124-31. PubMed PMID: 16547369. eng.

169. Smith L, Cupid BC, Dickie BG, Al-Chalabi A, Morrison KE, Shaw CE, et al. Establishing the UK DNA Bank for motor neuron disease (MND). BMC Genet. 2015;16:84. PubMed PMID: 26170009. Pubmed Central PMCID: PMC4501191. eng.

170. Blesa J, Phani S, Jackson-Lewis V, Przedborski S. Classic and new animal models of Parkinson's disease. J Biomed Biotechnol. 2012;2012:845618. PubMed PMID: 22536024. Pubmed Central PMCID: PMC3321500. eng.

171. Ehrnhoefer DE, Butland SL, Pouladi MA, Hayden MR. Mouse models of Huntington disease: variations on a theme. Dis Model Mech. 2009 2009 Mar-Apr;2(3-4):123-9. PubMed PMID: 19259385. Pubmed Central PMCID: PMC2650190. eng.

172. Simmons D. The use of animal models in studying genetic disease: transgenesis and induced mutation. Nature Education. 2008;1(1).

173. Okuda T, Okamura M, Kaitsuka C, Haga T, Gurwitz D. Single nucleotide polymorphism of the human high affinity choline transporter alters transport rate. J Biol Chem. 2002 Nov;277(47):45315-22. PubMed PMID: 12237312. eng.

174. Takei K, Yoshida Y, Yamada H. Regulatory mechanisms of dynamin-dependent endocytosis. J Biochem. 2005 Mar;137(3):243-7. PubMed PMID: 15809324. eng.

175. Dutta D, Donaldson JG. Search for inhibitors of endocytosis: Intended specificity and unintended consequences. Cell Logist. 2012 Oct;2(4):203-8. PubMed PMID: 23538558. Pubmed Central PMCID: PMC3607622. ENG.

176. Doherty GJ, McMahon HT. Mechanisms of endocytosis. Annu Rev Biochem. 2009;78:857-902. PubMed PMID: 19317650. eng.

177. Rilstone JJ, Alkhater RA, Minassian BA. Brain dopamine-serotonin vesicular transport disease and its treatment. N Engl J Med. 2013 Feb;368(6):543-50. PubMed PMID: 23363473. eng.

178. Mehndiratta MM, Pandey S, Kuntzer T. Acetylcholinesterase inhibitor treatment for myasthenia gravis. Cochrane Database Syst Rev. 2014;10:CD006986. PubMed PMID: 25310725. eng.

179. Choi KH, Wykes T, Kurtz MM. Adjunctive pharmacotherapy for cognitive deficits in schizophrenia: meta-analytical investigation of efficacy. Br J Psychiatry. 2013 Sep;203(3):172-8. PubMed PMID: 23999481. Pubmed Central PMCID: PMC3759029. eng.

180. Waite LM. Treatment for Alzheimer's disease: has anything changed? Aust Prescr. 2015 Apr;38(2):60-3. PubMed PMID: 26648618. Pubmed Central PMCID: PMC4653985. eng.

181. Pagano G, Rengo G, Pasqualetti G, Femminella GD, Monzani F, Ferrara N, et al. Cholinesterase inhibitors for Parkinson's disease: a systematic review and meta-analysis. J Neurol Neurosurg Psychiatry. 2015 Jul;86(7):767-73. PubMed PMID: 25224676. eng.

182. Mayo MC, Bordelon Y. Dementia with Lewy bodies. Semin Neurol. 2014 Apr;34(2):182-8. PubMed PMID: 24963677. eng.

183. Hoyng PF, van Beek LM. Pharmacological therapy for glaucoma: a review. Drugs. 2000 Mar;59(3):411-34. PubMed PMID: 10776828. eng.

184. Buckley AW, Sassower K, Rodriguez AJ, Jennison K, Wingert K, Buckley J, et al. An open label trial of donepezil for enhancement of rapid eye movement sleep in young children with autism spectrum disorders. J Child Adolesc Psychopharmacol. 2011 Aug;21(4):353-7. PubMed PMID: 21851192. Pubmed Central PMCID: PMC3157749. eng.

185. Rang HP, Dale MM. Rang and Dale's pharmacology. Edinburgh ; New York: Elsevier/Churchill Livingstone,; 2012. Available from: http://www.clinicalkey.com/dura/browse/bookChapter/3-s2.0-C2009060489X.

186. Liao BY, Zhang J. Null mutations in human and mouse orthologs frequently result in different phenotypes. Proc Natl Acad Sci U S A. 2008 May;105(19):6987-92. PubMed PMID: 18458337. Pubmed Central PMCID: PMC2383943. eng.

187. Ferguson SM, Bazalakova M, Savchenko V, Tapia JC, Wright J, Blakely RD. Lethal impairment of cholinergic neurotransmission in hemicholinium-3-sensitive choline transporter knockout mice. Proc Natl Acad Sci U S A. 2004 Jun;101(23):8762-7. PubMed PMID: 15173594. Pubmed Central PMCID: PMC423269. eng.

188. Montagutelli X. Effect of the genetic background on the phenotype of mouse mutations. J Am Soc Nephrol. 2000 Nov;11 Suppl 16:S101-5. PubMed PMID: 11065339. eng.

189. Aronson JK. Rare diseases and orphan drugs. Br J Clin Pharmacol. 2006 Mar;61(3):243-5. PubMed PMID: 16487216. Pubmed Central PMCID: PMC1885017. eng.

190. Michel V, Yuan Z, Ramsubir S, Bakovic M. Choline transport for phospholipid synthesis. Exp Biol Med (Maywood). 2006 May;231(5):490-504. PubMed PMID: 16636297. eng.

191. Rasool CG, Bradley WG, Connolly B, Baruah JK. Acetylcholinesterase and ATPases in motor neuron degenerative diseases. Muscle Nerve. 1983 1983 Jul-Aug;6(6):430-5. PubMed PMID: 6137769. eng.

192. Holmstrand EC, Lund D, Cherian AK, Wright J, Martin RF, Ennis EA, et al. Transgenic overexpression of the presynaptic choline transporter elevates acetylcholine levels and augments motor endurance. Neurochem Int. 2014 Jul;73:217-28. PubMed PMID: 24274995. Pubmed Central PMCID: PMC4104494. eng.

193. Bazalakova MH, Blakely RD. The high-affinity choline transporter: a critical protein for sustaining cholinergic signaling as revealed in studies of genetically altered mice. Handb Exp Pharmacol. 2006 (175):525-44. PubMed PMID: 16722248. eng.

194. Koepsell H. The SLC22 family with transporters of organic cations, anions and zwitterions. Mol Aspects Med. 2013 2013 Apr-Jun;34(2-3):413-35. PubMed PMID: 23506881. eng.

195. Nakata T, Matsui T, Kobayashi K, Kobayashi Y, Anzai N. Organic cation transporter 2 (SLC22A2), a low-affinity and high-capacity choline transporter, is preferentially enriched on synaptic vesicles in cholinergic neurons. Neuroscience. 2013 Nov;252:212-21. PubMed PMID: 23958595. eng.

196. Trivedi JR, Phillips L, Chhabra A. Hereditary and acquired polyneuropathy conditions of the peripheral nerves: clinical considerations and MR neurography imaging. Semin Musculoskelet Radiol. 2015 Apr;19(2):130-6. PubMed PMID: 25764237. eng.

197. Müller JS, Mihaylova V, Abicht A, Lochmüller H. Congenital myasthenic syndromes: spotlight on genetic defects of neuromuscular transmission. Expert Rev Mol Med. 2007;9(22):1-20. PubMed PMID: 17686188. eng.

198. Engel AG. The therapy of congenital myasthenic syndromes. Neurotherapeutics. 2007 Apr;4(2):252-7. PubMed PMID: 17395135. Pubmed Central PMCID: PMC1978489. eng.

199. Schara U, Lochmüller H. Therapeutic strategies in congenital myasthenic syndromes. Neurotherapeutics. 2008 Oct;5(4):542-7. PubMed PMID: 19019305. Pubmed Central PMCID: PMC4514706. eng.

200. Bird TD, Ott J, Giblett ER. Evidence for linkage of Charcot-Marie-Tooth neuropathy to the Duffy locus on chromosome 1. Am J Hum Genet. 1982 May;34(3):388-94. PubMed PMID: 6952764. Pubmed Central PMCID: PMC1685353. eng.

201. Boerkoel CF, Takashima H, Bacino CA, Daentl D, Lupski JR. EGR2 mutation R359W causes a spectrum of Dejerine-Sottas neuropathy. Neurogenetics. 2001 Jul;3(3):153-7. PubMed PMID: 11523566. eng.

202. Kamholz J, Menichella D, Jani A, Garbern J, Lewis RA, Krajewski KM, et al. Charcot-Marie-Tooth disease type 1: molecular pathogenesis to gene therapy. Brain. 2000 Feb;123 (Pt 2):222-33. PubMed PMID: 10648431. eng.

203. Kovach MJ, Lin JP, Boyadjiev S, Campbell K, Mazzeo L, Herman K, et al. A unique point mutation in the PMP22 gene is associated with Charcot-Marie-Tooth disease and deafness. Am J Hum Genet. 1999 Jun;64(6):1580-93. PubMed PMID: 10330345. Pubmed Central PMCID: PMC1377901. eng.

204. Magyar JP, Martini R, Ruelicke T, Aguzzi A, Adlkofer K, Dembic Z, et al. Impaired differentiation of Schwann cells in transgenic mice with increased PMP22 gene dosage. J Neurosci. 1996 Sep;16(17):5351-60. PubMed PMID: 8757248. eng.

205. Matsunami N, Smith B, Ballard L, Lensch MW, Robertson M, Albertsen H, et al. Peripheral myelin protein-22 gene maps in the duplication in chromosome 17p11.2 associated with Charcot-Marie-Tooth 1A. Nat Genet. 1992 Jun;1(3):176-9. PubMed PMID: 1303231. eng.

206. Nagarajan R, Svaren J, Le N, Araki T, Watson M, Milbrandt J. EGR2 mutations in inherited neuropathies dominant-negatively inhibit myelin gene expression. Neuron. 2001 May;30(2):355-68. PubMed PMID: 11394999. eng.

207. Sambuughin N, de Bantel A, McWilliams S, Sivakumar K. Deafness and CMT disease associated with a novel four amino acid deletion in the PMP22 gene. Neurology. 2003 Feb;60(3):506-8. PubMed PMID: 12578939. eng.

208. Yum SW, Zhang J, Mo K, Li J, Scherer SS. A novel recessive Nefl mutation causes a severe, early-onset axonal neuropathy. Ann Neurol. 2009 Dec;66(6):759-70. PubMed PMID: 20039262. eng.

209. Othmane KB, Loeb D, Hayworth-Hodgte R, Hentati F, Rao N, Roses AD, et al. Physical and genetic mapping of the CMT4A locus and exclusion of PMP-2 as the defect in CMT4A. Genomics. 1995 Jul;28(2):286-90. PubMed PMID: 8530038. eng.

210. Quattrone A, Gambardella A, Bono F, Aguglia U, Bolino A, Bruni AC, et al. Autosomal recessive hereditary motor and sensory neuropathy with focally folded myelin sheaths: clinical, electrophysiologic, and genetic aspects of a large family. Neurology. 1996 May;46(5):1318-24. PubMed PMID: 8628474. eng.

211. Kiwaki T, Umehara F, Takashima H, Nakagawa M, Kamimura K, Kashio N, et al. Hereditary motor and sensory neuropathy with myelin folding and juvenile onset glaucoma. Neurology. 2000 Aug;55(3):392-7. PubMed PMID: 10932274. eng.

212. Azzedine H, Bolino A, Taïeb T, Birouk N, Di Duca M, Bouhouche A, et al. Mutations in MTMR13, a new pseudophosphatase homologue of MTMR2 and Sbf1, in two families with an autosomal recessive demyelinating form of Charcot-Marie-Tooth disease associated with early-onset glaucoma. Am J Hum Genet. 2003 May;72(5):1141-53. PubMed PMID: 12687498. Pubmed Central PMCID: PMC1180267. eng.

213. Conforti FL, Muglia M, Mazzei R, Patitucci A, Valentino P, Magariello A, et al. A new SBF2 mutation in a family with recessive demyelinating Charcot-Marie-Tooth (CMT4B2). Neurology. 2004 Oct;63(7):1327-8. PubMed PMID: 15477569. eng.

214. Yoshimura S, Gerondopoulos A, Linford A, Rigden DJ, Barr FA. Family-wide characterization of the DENN domain Rab GDP-GTP exchange factors. J Cell Biol. 2010 Oct;191(2):367-81. PubMed PMID: 20937701. Pubmed Central PMCID: PMC2958468. eng.

215. Nakhro K, Park JM, Hong YB, Park JH, Nam SH, Yoon BR, et al. SET binding factor 1 (SBF1) mutation causes Charcot-Marie-Tooth disease type 4B3. Neurology. 2013 Jul;81(2):165-73. PubMed PMID: 23749797. eng.

216. Kalaydjieva L, Gresham D, Gooding R, Heather L, Baas F, de Jonge R, et al. N-myc downstream-regulated gene 1 is mutated in hereditary motor and sensory neuropathy-Lom. Am J Hum Genet. 2000 Jul;67(1):47-58. PubMed PMID: 10831399. Pubmed Central PMCID: PMC1287101. eng.

217. Park H, Adams MA, Lachat P, Bosman F, Pang SC, Graham CH. Hypoxia induces the expression of a 43-kDa protein (PROXY-1) in normal and malignant cells. Biochem Biophys Res Commun. 2000 Sep;276(1):321-8. PubMed PMID: 11006124. eng.

218. Azzedine H, Ravisé N, Verny C, Gabrëels-Festen A, Lammens M, Grid D, et al. Spine deformities in Charcot-Marie-Tooth 4C caused by SH3TC2 gene mutations. Neurology. 2006 Aug;67(4):602-6. PubMed PMID: 16924012. eng.

219. Colomer J, Gooding R, Angelicheva D, King RH, Guillén-Navarro E, Parman Y, et al. Clinical spectrum of CMT4C disease in patients homozygous for the p.Arg1109X mutation in SH3TC2. Neuromuscul Disord. 2006 Jul;16(7):449-53. PubMed PMID: 16806930. eng.

220. Senderek J, Bergmann C, Weber S, Ketelsen UP, Schorle H, Rudnik-Schöneborn S, et al. Mutation of the SBF2 gene, encoding a novel member of the myotubularin family, in Charcot-Marie-Tooth neuropathy type 4B2/11p15. Hum Mol Genet. 2003 Feb;12(3):349-56. PubMed PMID: 12554688. eng.

221. Roberts RC, Peden AA, Buss F, Bright NA, Latouche M, Reilly MM, et al. Mistargeting of SH3TC2 away from the recycling endosome causes Charcot-Marie-Tooth disease type 4C. Hum Mol Genet. 2010 Mar;19(6):1009-18. PubMed PMID: 20028792. Pubmed Central PMCID: PMC2830826. eng.

222. Brewer MH, Ma KH, Beecham GW, Gopinath C, Baas F, Choi BO, et al. Haplotype-specific modulation of a SOX10/CREB response element at the Charcot-Marie-Tooth disease type 4C locus SH3TC2. Hum Mol Genet. 2014 Oct;23(19):5171-87. PubMed PMID: 24833716. Pubmed Central PMCID: PMC4168306. eng.

223. Okamoto Y, Goksungur MT, Pehlivan D, Beck CR, Gonzaga-Jauregui C, Muzny DM, et al. Exonic duplication CNV of NDRG1 associated with autosomal-recessive HMSN-Lom/CMT4D. Genet Med. 2014 May;16(5):386-94. PubMed PMID: 24136616. Pubmed Central PMCID: PMC4224029. eng.

224. Kochanski A, Drac H, Kabzińska D, Ryniewicz B, Rowińska-Marcińska K, Nowakowski A, et al. A novel MPZ gene mutation in congenital neuropathy with hypomyelination. Neurology. 2004 Jun;62(11):2122-3. PubMed PMID: 15184631. eng.

225. Tokunaga S, Hashiguchi A, Yoshimura A, Maeda K, Suzuki T, Haruki H, et al. Late-onset Charcot-Marie-Tooth disease 4F caused by periaxin gene mutation. Neurogenetics. 2012 Nov;13(4):359-65. PubMed PMID: 22847150. eng.

226. Marchesi C, Milani M, Morbin M, Cesani M, Lauria G, Scaioli V, et al. Four novel cases of periaxin-related neuropathy and review of the literature. Neurology. 2010 Nov;75(20):1830-8. PubMed PMID: 21079185. eng.

227. Li X, Hu Z, Liu L, Xie Y, Zhan Y, Zi X, et al. A SIGMAR1 splice-site mutation causes distal hereditary motor neuropathy. Neurology. 2015 Jun;84(24):2430-7. PubMed PMID: 26078401. eng.

228. Rogers T, Chandler D, Angelicheva D, Thomas PK, Youl B, Tournev I, et al. A novel locus for autosomal recessive peripheral neuropathy in the EGR2 region on 10q23. Am J Hum Genet. 2000 Sep;67(3):664-71. PubMed PMID: 10915613. Pubmed Central PMCID: PMC1287526. eng.

229. Thomas PK, Kalaydjieva L, Youl B, Rogers T, Angelicheva D, King RH, et al. Hereditary motor and sensory neuropathy-russe: new autosomal recessive neuropathy in Balkan Gypsies. Ann Neurol. 2001 Oct;50(4):452-7. PubMed PMID: 11601496. eng.

230. Sevilla T, Martínez-Rubio D, Márquez C, Paradas C, Colomer J, Jaijo T, et al. Genetics of the Charcot-Marie-Tooth disease in the Spanish Gypsy population: the hereditary motor and sensory neuropathy-Russe in depth. Clin Genet. 2013 Jun;83(6):565-70. PubMed PMID: 22978647. eng.

231. Brennan KM, Bai Y, Pisciotta C, Wang S, Feely SM, Hoegger M, et al. Absence of Dystrophin Related Protein-2 disrupts Cajal bands in a patient with Charcot-Marie-Tooth disease. Neuromuscul Disord. 2015 Oct;25(10):786-93. PubMed PMID: 26227883. eng.

232. Houlden H, Hammans S, Katifi H, Reilly MM. A novel Frabin (FGD4) nonsense mutation p.R275X associated with phenotypic variability in CMT4H. Neurology. 2009 Feb;72(7):617-20. PubMed PMID: 19221294. Pubmed Central PMCID: PMC2677538. eng.

233. Fabrizi GM, Taioli F, Cavallaro T, Ferrari S, Bertolasi L, Casarotto M, et al. Further evidence that mutations in FGD4/frabin cause Charcot-Marie-Tooth disease type 4H. Neurology. 2009 Mar;72(13):1160-4. PubMed PMID: 19332693. eng.

234. Hyun YS, Lee J, Kim HJ, Hong YB, Koo H, Smith AS, et al. Charcot-Marie-Tooth Disease Type 4H Resulting from Compound Heterozygous Mutations in FGD4 from Nonconsanguineous Korean Families. Ann Hum Genet. 2015 Nov;79(6):460-9. PubMed PMID: 26400421. eng.

235. Cottenie E, Menezes MP, Rossor AM, Morrow JM, Yousry TA, Dick DJ, et al. Rapidly progressive asymmetrical weakness in Charcot-Marie-Tooth disease type 4J

resembles chronic inflammatory demyelinating polyneuropathy. Neuromuscul Disord. 2013 May;23(5):399-403. PubMed PMID: 23489662. eng.

236. Menezes MP, Waddell L, Lenk GM, Kaur S, MacArthur DG, Meisler MH, et al. Whole exome sequencing identifies three recessive FIG4 mutations in an apparently dominant pedigree with Charcot-Marie-Tooth disease. Neuromuscul Disord. 2014 Aug;24(8):666-70. PubMed PMID: 24878229. Pubmed Central PMCID: PMC4096049. eng.

237. van Paassen BW, van der Kooi AJ, van Spaendonck-Zwarts KY, Verhamme C, Baas F, de Visser M. PMP22 related neuropathies: Charcot-Marie-Tooth disease type 1A and Hereditary Neuropathy with liability to Pressure Palsies. Orphanet J Rare Dis. 2014;9:38. PubMed PMID: 24646194. Pubmed Central PMCID: PMC3994927. eng.

238. Ben Othmane K, Middleton LT, Loprest LJ, Wilkinson KM, Lennon F, Rozear MP, et al. Localization of a gene (CMT2A) for autosomal dominant Charcot-Marie-Tooth disease type 2 to chromosome 1p and evidence of genetic heterogeneity. Genomics. 1993 Aug;17(2):370-5. PubMed PMID: 8406488. eng.

239. Bouhouche A, Benomar A, Birouk N, Mularoni A, Meggouh F, Tassin J, et al. A locus for an axonal form of autosomal recessive Charcot-Marie-Tooth disease maps to chromosome 1q21.2-q21.3. Am J Hum Genet. 1999 Sep;65(3):722-7. PubMed PMID: 10441578. Pubmed Central PMCID: PMC1377978. eng.

240. Georgiou DM, Zidar J, Korosec M, Middleton LT, Kyriakides T, Christodoulou K. A novel NF-L mutation Pro22Ser is associated with CMT2 in a large Slovenian family. Neurogenetics. 2002 Oct;4(2):93-6. PubMed PMID: 12481988. eng.

241. Houlden H, King RH, Muddle JR, Warner TT, Reilly MM, Orrell RW, et al. A novel RAB7 mutation associated with ulcero-mutilating neuropathy. Ann Neurol. 2004 Oct;56(4):586-90. PubMed PMID: 15455439. eng.

242. Leal A, Huehne K, Bauer F, Sticht H, Berger P, Suter U, et al. Identification of the variant Ala335Val of MED25 as responsible for CMT2B2: molecular data, functional studies of the SH3 recognition motif and correlation between wild-type MED25 and PMP22 RNA levels in CMT1A animal models. Neurogenetics. 2009 Sep. PubMed PMID: 19730899. Pubmed Central PMCID: PMC2847162. ENG.

243. McEntagart ME, Reid SL, Irrthum A, Irtthum A, Douglas JB, Eyre KE, et al. Confirmation of a hereditary motor and sensory neuropathy IIC locus at chromosome 12q23-q24. Ann Neurol. 2005 Feb;57(2):293-7. PubMed PMID: 15668982. eng.

244. Del Bo R, Moggio M, Rango M, Bonato S, D'Angelo MG, Ghezzi S, et al. Mutated mitofusin 2 presents with intrafamilial variability and brain mitochondrial dysfunction. Neurology. 2008 Dec;71(24):1959-66. PubMed PMID: 18946002. eng.

245. Meggouh F, Bienfait HM, Weterman MA, de Visser M, Baas F. Charcot-Marie-Tooth disease due to a de novo mutation of the RAB7 gene. Neurology. 2006 Oct;67(8):1476-8. PubMed PMID: 17060578. eng.

246. Birouk N, Azzedine H, Dubourg O, Muriel MP, Benomar A, Hamadouche T, et al. Phenotypical features of a Moroccan family with autosomal recessive Charcot-Marie-Tooth disease associated with the S194X mutation in the GDAP1 gene. Arch Neurol. 2003 Apr;60(4):598-604. PubMed PMID: 12707075. eng.

247. Chung KW, Kim SM, Sunwoo IN, Cho SY, Hwang SJ, Kim J, et al. A novel GDAP1 Q218E mutation in autosomal dominant Charcot-Marie-Tooth disease. J Hum Genet. 2008;53(4):360-4. PubMed PMID: 18231710. eng.

248. De Jonghe P, Timmerman V, Ceuterick C, Nelis E, De Vriendt E, Löfgren A, et al. The Thr124Met mutation in the peripheral myelin protein zero (MPZ) gene is associated with a clinically distinct Charcot-Marie-Tooth phenotype. Brain. 1999 Feb;122 (Pt 2):281-90. PubMed PMID: 10071056. eng.

249. Xin B, Puffenberger E, Nye L, Wiznitzer M, Wang H. A novel mutation in the GDAP1 gene is associated with autosomal recessive Charcot-Marie-Tooth disease in an Amish family. Clin Genet. 2008 Sep;74(3):274-8. PubMed PMID: 18492089. eng.

250. Le Guern E, Ravise N, Gugenheim M, Vignal A, Penet C, Bouche P, et al. Linkage analyses between dominant X-linked Charcot-Marie-Tooth disease, and 15 Xq11-Xq21 microsatellites in a new large family: three new markers are closely linked to the gene. Neuromuscul Disord. 1994 1994 Sep-Nov;4(5-6):463-9. PubMed PMID: 7881290. eng.

251. Hahn AF, Brown WF, Koopman WJ, Feasby TE. X-linked dominant hereditary motor and sensory neuropathy. Brain. 1990 Oct;113 (Pt 5):1511-25. PubMed PMID: 2245309. eng.

252. Fain PR, Barker DF, Chance PF. Refined genetic mapping of X-linked Charcot-Marie-Tooth neuropathy. Am J Hum Genet. 1994 Feb;54(2):229-35. PubMed PMID: 8304339. Pubmed Central PMCID: PMC1918155. eng.

253. Claramunt R, Pedrola L, Sevilla T, López de Munain A, Berciano J, Cuesta A, et al. Genetics of Charcot-Marie-Tooth disease type 4A: mutations, inheritance, phenotypic variability, and founder effect. J Med Genet. 2005 Apr;42(4):358-65. PubMed PMID: 15805163. Pubmed Central PMCID: PMC1736030. eng.

254. Ionasescu V, Ionasescu R, Searby C. Correlation between connexin 32 gene mutations and clinical phenotype in X-linked dominant Charcot-Marie-Tooth neuropathy. Am J Med Genet. 1996 Jun;63(3):486-91. PubMed PMID: 8737658. eng.

255. Ismailov SM, Fedotov VP, Dadali EL, Polyakov AV, Van Broeckhoven C, Ivanov VI, et al. A new locus for autosomal dominant Charcot-Marie-Tooth disease type 2

(CMT2F) maps to chromosome 7q11-q21. Eur J Hum Genet. 2001 Aug;9(8):646-50. PubMed PMID: 11528513. eng.

256. Tang BS, Luo W, Xia K, Xiao JF, Jiang H, Shen L, et al. A new locus for autosomal dominant Charcot-Marie-Tooth disease type 2 (CMT2L) maps to chromosome 12q24. Hum Genet. 2004 May;114(6):527-33. PubMed PMID: 15021985. eng.

257. Kabzińska D, Korwin-Piotrowska T, Drechsler H, Drac H, Hausmanowa-Petrusewicz I, Kochański A. Late-onset Charcot-Marie-Tooth type 2 disease with hearing impairment associated with a novel Pro105Thr mutation in the MPZ gene. Am J Med Genet A. 2007 Sep;143A(18):2196-9. PubMed PMID: 17663472. eng.

258. Miltenberger-Miltenyi G, Janecke AR, Wanschitz JV, Timmerman V, Windpassinger C, Auer-Grumbach M, et al. Clinical and electrophysiological features in Charcot-Marie-Tooth disease with mutations in the NEFL gene. Arch Neurol. 2007 Jul;64(7):966-70. PubMed PMID: 17620486. eng.

259. Nelis E, Berciano J, Verpoorten N, Coen K, Dierick I, Van Gerwen V, et al. Autosomal dominant axonal Charcot-Marie-Tooth disease type 2 (CMT2G) maps to chromosome 12q12-q13.3. J Med Genet. 2004 Mar;41(3):193-7. PubMed PMID: 14985381. Pubmed Central PMCID: PMC1735709. eng.

260. Barhoumi C, Amouri R, Ben Hamida C, Ben Hamida M, Machghoul S, Gueddiche M, et al. Linkage of a new locus for autosomal recessive axonal form of Charcot-Marie-Tooth disease to chromosome 8q21.3. Neuromuscul Disord. 2001 Jan;11(1):27-34. PubMed PMID: 11166163. eng.

261. Senderek J, Hermanns B, Lehmann U, Bergmann C, Marx G, Kabus C, et al. Charcot-Marie-Tooth neuropathy type 2 and P0 point mutations: two novel amino acid substitutions (Asp61Gly; Tyr119Cys) and a possible "hotspot" on Thr124Met. Brain Pathol. 2000 Apr;10(2):235-48. PubMed PMID: 10764043. eng.

262. Auer-Grumbach M, Strasser-Fuchs S, Robl T, Windpassinger C, Wagner K. Late onset Charcot-Marie-Tooth 2 syndrome caused by two novel mutations in the MPZ gene. Neurology. 2003 Nov;61(10):1435-7. PubMed PMID: 14638973. eng.

263. Zimoń M, Baets J, Fabrizi GM, Jaakkola E, Kabzińska D, Pilch J, et al. Dominant GDAP1 mutations cause predominantly mild CMT phenotypes. Neurology. 2011 Aug;77(6):540-8. PubMed PMID: 21753178. Pubmed Central PMCID: PMC3272385. eng.

264. Berciano J, Combarros O, Figols J, Calleja J, Cabello A, Silos I, et al. Hereditary motor and sensory neuropathy type II. Clinicopathological study of a family. Brain. 1986 Oct;109 (Pt 5):897-914. PubMed PMID: 3022865. eng.

265. McLaughlin HM, Sakaguchi R, Giblin W, Wilson TE, Biesecker L, Lupski JR, et al. A recurrent loss-of-function alanyl-tRNA synthetase (AARS) mutation in patients

with Charcot-Marie-Tooth disease type 2N (CMT2N). Hum Mutat. 2012 Jan;33(1):244-53. PubMed PMID: 22009580. Pubmed Central PMCID: PMC3240693. eng.

266. Guernsey DL, Jiang H, Bedard K, Evans SC, Ferguson M, Matsuoka M, et al. Mutation in the gene encoding ubiquitin ligase LRSAM1 in patients with Charcot-Marie-Tooth disease. PLoS Genet. 2010 Aug;6(8). PubMed PMID: 20865121. Pubmed Central PMCID: PMC2928813. eng.

267. Xu WY, Gu MM, Sun LH, Guo WT, Zhu HB, Ma JF, et al. A nonsense mutation in DHTKD1 causes Charcot-Marie-Tooth disease type 2 in a large Chinese pedigree. Am J Hum Genet. 2012 Dec;91(6):1088-94. PubMed PMID: 23141294. Pubmed Central PMCID: PMC3516600. eng.

268. Ishiura H, Sako W, Yoshida M, Kawarai T, Tanabe O, Goto J, et al. The TRK-fused gene is mutated in hereditary motor and sensory neuropathy with proximal dominant involvement. Am J Hum Genet. 2012 Aug;91(2):320-9. PubMed PMID: 22883144. Pubmed Central PMCID: PMC3415534. eng.

269. Gonzalez MA, Feely SM, Speziani F, Strickland AV, Danzi M, Bacon C, et al. A novel mutation in VCP causes Charcot-Marie-Tooth Type 2 disease. Brain. 2014 Nov;137(Pt 11):2897-902. PubMed PMID: 25125609. Pubmed Central PMCID: PMC4208462. eng.

270. Watts GD, Wymer J, Kovach MJ, Mehta SG, Mumm S, Darvish D, et al. Inclusion body myopathy associated with Paget disease of bone and frontotemporal dementia is caused by mutant valosin-containing protein. Nat Genet. 2004 Apr;36(4):377-81. PubMed PMID: 15034582. eng.

271. Khazaei MR, Bunk EC, Hillje AL, Jahn HM, Riegler EM, Knoblich JA, et al. The E3-ubiquitin ligase TRIM2 regulates neuronal polarization. J Neurochem. 2011 Apr;117(1):29-37. PubMed PMID: 20796172. eng.

272. Thompson S, Pearson AN, Ashley MD, Jessick V, Murphy BM, Gafken P, et al. Identification of a novel Bcl-2-interacting mediator of cell death (Bim) E3 ligase, tripartite motif-containing protein 2 (TRIM2), and its role in rapid ischemic tolerance-induced neuroprotection. J Biol Chem. 2011 Jun;286(22):19331-9. PubMed PMID: 21478148. Pubmed Central PMCID: PMC3103311. eng.

273. Ylikallio E, Pöyhönen R, Zimon M, De Vriendt E, Hilander T, Paetau A, et al. Deficiency of the E3 ubiquitin ligase TRIM2 in early-onset axonal neuropathy. Hum Mol Genet. 2013 Aug;22(15):2975-83. PubMed PMID: 23562820. eng.

274. Pehlivan D, Coban Akdemir Z, Karaca E, Bayram Y, Jhangiani S, Yildiz EP, et al. Exome sequencing reveals homozygous TRIM2 mutation in a patient with early onset CMT and bilateral vocal cord paralysis. Hum Genet. 2015 Jun;134(6):671-3. PubMed PMID: 25893792. Pubmed Central PMCID: PMC4426057. eng.

275. Zimoń M, Baets J, Almeida-Souza L, De Vriendt E, Nikodinovic J, Parman Y, et al. Loss-of-function mutations in HINT1 cause axonal neuropathy with neuromyotonia. Nat Genet. 2012 Oct;44(10):1080-3. PubMed PMID: 22961002. eng.

276. Klein CJ, Wu Y, Vogel P, Goebel HH, Bönnemann C, Zukosky K, et al. Ubiquitin ligase defect by DCAF8 mutation causes HMSN2 with giant axons. Neurology. 2014 Mar;82(10):873-8. PubMed PMID: 24500646. Pubmed Central PMCID: PMC3959756. eng.

277. Vogel P, Gabriel M, Goebel HH, Dyck PJ. Hereditary motor sensory neuropathy type II with neurofilament accumulation: new finding or new disorder? Ann Neurol. 1985 May;17(5):455-61. PubMed PMID: 3859241. eng.

278. Cottenie E, Kochanski A, Jordanova A, Bansagi B, Zimon M, Horga A, et al. Truncating and missense mutations in IGHMBP2 cause Charcot-Marie Tooth disease type 2. Am J Hum Genet. 2014 Nov;95(5):590-601. PubMed PMID: 25439726. Pubmed Central PMCID: PMC4225647. eng.

279. Gonzalez M, McLaughlin H, Houlden H, Guo M, Yo-Tsen L, Hadjivassilious M, et al. Exome sequencing identifies a significant variant in methionyl-tRNA synthetase (MARS) in a family with late-onset CMT2. J Neurol Neurosurg Psychiatry. 2013 Nov;84(11):1247-9. PubMed PMID: 23729695. Pubmed Central PMCID: PMC3796032. eng.

280. Hyun YS, Park HJ, Heo SH, Yoon BR, Nam SH, Kim SB, et al. Rare variants in methionyl- and tyrosyl-tRNA synthetase genes in late-onset autosomal dominant Charcot-Marie-Tooth neuropathy. Clin Genet. 2014 Dec;86(6):592-4. PubMed PMID: 24354524. eng.

281. Tétreault M, Gonzalez M, Dicaire MJ, Allard P, Gehring K, Leblanc D, et al. Adult-onset painful axonal polyneuropathy caused by a dominant NAGLU mutation. Brain. 2015 Jun;138(Pt 6):1477-83. PubMed PMID: 25818867. Pubmed Central PMCID: PMC4542621. eng.

282. Pitceathly RD, Murphy SM, Cottenie E, Chalasani A, Sweeney MG, Woodward C, et al. Genetic dysfunction of MT-ATP6 causes axonal Charcot-Marie-Tooth disease. Neurology. 2012 Sep;79(11):1145-54. PubMed PMID: 22933740. Pubmed Central PMCID: PMC3525307. eng.

283. Verhoeven K, Villanova M, Rossi A, Malandrini A, De Jonghe P, Timmerman V. Localization of the gene for the intermediate form of Charcot-Marie-Tooth to chromosome 10q24.1-q25.1. Am J Hum Genet. 2001 Oct;69(4):889-94. PubMed PMID: 11533914. Pubmed Central PMCID: PMC1226075. eng.

284. Züchner S, Noureddine M, Kennerson M, Verhoeven K, Claeys K, De Jonghe P, et al. Mutations in the pleckstrin homology domain of dynamin 2 cause dominant

intermediate Charcot-Marie-Tooth disease. Nat Genet. 2005 Mar;37(3):289-94. PubMed PMID: 15731758. eng.

285. Zhu D, Kennerson M, Merory J, Chrast R, Verheijen M, Lemke G, et al. Refined localization of dominant intermediate Charcot-Marie-Tooth neuropathy and exclusion of seven known candidate genes in the region. Neurogenetics. 2003 Aug;4(4):179-83. PubMed PMID: 12761657. eng.

286. Kennerson ML, Zhu D, Gardner RJ, Storey E, Merory J, Robertson SP, et al. Dominant intermediate Charcot-Marie-Tooth neuropathy maps to chromosome 19p12-p13.2. Am J Hum Genet. 2001 Oct;69(4):883-8. PubMed PMID: 11533912. Pubmed Central PMCID: PMC1226074. eng.

287. Jordanova A, Thomas FP, Guergueltcheva V, Tournev I, Gondim FA, Ishpekova B, et al. Dominant intermediate Charcot-Marie-Tooth type C maps to chromosome 1p34-p35. Am J Hum Genet. 2003 Dec;73(6):1423-30. PubMed PMID: 14606043. Pubmed Central PMCID: PMC1180404. eng.

288. Banchs I, Casasnovas C, Montero J, Volpini V, Martínez-Matos JA. Charcot-Marie-Tooth disease with intermediate conduction velocities caused by a novel mutation in the MPZ gene. Muscle Nerve. 2010 Aug;42(2):184-8. PubMed PMID: 20544920. eng.

289. Mastaglia FL, Nowak KJ, Stell R, Phillips BA, Edmondston JE, Dorosz SM, et al. Novel mutation in the myelin protein zero gene in a family with intermediate hereditary motor and sensory neuropathy. J Neurol Neurosurg Psychiatry. 1999 Aug;67(2):174-9. PubMed PMID: 10406984. Pubmed Central PMCID: PMC1736462. eng.

290. Mathis S, Funalot B, Boyer O, Lacroix C, Marcorelles P, Magy L, et al. Neuropathologic characterization of INF2-related Charcot-Marie-Tooth disease: evidence for a Schwann cell actinopathy. J Neuropathol Exp Neurol. 2014 Mar;73(3):223-33. PubMed PMID: 24487800. eng.

291. Park HJ, Kim HJ, Hong YB, Nam SH, Chung KW, Choi BO. A novel INF2 mutation in a Korean family with autosomal dominant intermediate Charcot-Marie-Tooth disease and focal segmental glomerulosclerosis. J Peripher Nerv Syst. 2014 Jun;19(2):175-9. PubMed PMID: 24750328. eng.

292. Boyer O, Nevo F, Plaisier E, Funalot B, Gribouval O, Benoit G, et al. INF2 mutations in Charcot-Marie-Tooth disease with glomerulopathy. N Engl J Med. 2011 Dec;365(25):2377-88. PubMed PMID: 22187985. eng.

293. Lee YC, Lee TC, Lin KP, Lin MW, Chang MH, Soong BW. Clinical characterization and genetic analysis of a possible novel type of dominant Charcot-Marie-Tooth disease. Neuromuscul Disord. 2010 Aug;20(8):534-9. PubMed PMID: 20627571. eng.

294. Soong BW, Huang YH, Tsai PC, Huang CC, Pan HC, Lu YC, et al. Exome sequencing identifies GNB4 mutations as a cause of dominant intermediate Charcot-Marie-Tooth disease. Am J Hum Genet. 2013 Mar;92(3):422-30. PubMed PMID: 23434117. Pubmed Central PMCID: PMC3591844. eng.

295. Nicholson G, Ouvrier R. GDAP1 mutations in CMT4: axonal and demyelinating phenotypes?: The exception "proves the rule". Neurology. 2002 Dec;59(12):1835-6. PubMed PMID: 12499472. eng.

296. Kim HJ, Hong YB, Park JM, Choi YR, Kim YJ, Yoon BR, et al. Mutations in the PLEKHG5 gene is relevant with autosomal recessive intermediate Charcot-Marie-Tooth disease. Orphanet J Rare Dis. 2013;8:104. PubMed PMID: 23844677. Pubmed Central PMCID: PMC3728151. eng.

297. Azzedine H, Zavadakova P, Planté-Bordeneuve V, Vaz Pato M, Pinto N, Bartesaghi L, et al. PLEKHG5 deficiency leads to an intermediate form of autosomal-recessive Charcot-Marie-Tooth disease. Hum Mol Genet. 2013 Oct;22(20):4224-32. PubMed PMID: 23777631. Pubmed Central PMCID: PMC3983407. eng.

298. Gopinath S, Blair IP, Kennerson ML, Durnall JC, Nicholson GA. A novel locus for distal motor neuron degeneration maps to chromosome 7q34-q36. Hum Genet. 2007 Jun;121(5):559-64. PubMed PMID: 17354000. eng.

299. Carra S, Sivilotti M, Chávez Zobel AT, Lambert H, Landry J. HspB8, a small heat shock protein mutated in human neuromuscular disorders, has in vivo chaperone activity in cultured cells. Hum Mol Genet. 2005 Jun;14(12):1659-69. PubMed PMID: 15879436. eng.

300. Houlden H, Laura M, Wavrant-De Vrièze F, Blake J, Wood N, Reilly MM. Mutations in the HSP27 (HSPB1) gene cause dominant, recessive, and sporadic distal HMN/CMT type 2. Neurology. 2008 Nov;71(21):1660-8. PubMed PMID: 18832141. eng.

301. Sumner CJ, d'Ydewalle C, Wooley J, Fawcett KA, Hernandez D, Gardiner AR, et al. A dominant mutation in FBXO38 causes distal spinal muscular atrophy with calf predominance. Am J Hum Genet. 2013 Nov;93(5):976-83. PubMed PMID: 24207122. Pubmed Central PMCID: PMC3824115. eng.

302. Grohmann K, Varon R, Stolz P, Schuelke M, Janetzki C, Bertini E, et al. Infantile spinal muscular atrophy with respiratory distress type 1 (SMARD1). Ann Neurol. 2003 Dec;54(6):719-24. PubMed PMID: 14681881. eng.

303. Takata RI, Speck Martins CE, Passosbueno MR, Abe KT, Nishimura AL, Da Silva MD, et al. A new locus for recessive distal spinal muscular atrophy at Xq13.1-q21. J Med Genet. 2004 Mar;41(3):224-9. PubMed PMID: 14985388. Pubmed Central PMCID: PMC1735691. eng.

304. Chen YZ, Bennett CL, Huynh HM, Blair IP, Puls I, Irobi J, et al. DNA/RNA helicase gene mutations in a form of juvenile amyotrophic lateral sclerosis (ALS4). Am J Hum Genet. 2004 Jun;74(6):1128-35. PubMed PMID: 15106121. Pubmed Central PMCID: PMC1182077. eng.

305. Deng HX, Klein CJ, Yan J, Shi Y, Wu Y, Fecto F, et al. Scapuloperoneal spinal muscular atrophy and CMT2C are allelic disorders caused by alterations in TRPV4. Nat Genet. 2010 Feb;42(2):165-9. PubMed PMID: 20037587. Pubmed Central PMCID: PMC3786192. eng.

306. DeLong R, Siddique T. A large New England kindred with autosomal dominant neurogenic scapuloperoneal amyotrophy with unique features. Arch Neurol. 1992 Sep;49(9):905-8. PubMed PMID: 1520078. eng.

307. van der Vleuten AJ, van Ravenswaaij-Arts CM, Frijns CJ, Smits AP, Hageman G, Padberg GW, et al. Localisation of the gene for a dominant congenital spinal muscular atrophy predominantly affecting the lower limbs to chromosome 12q23-q24. Eur J Hum Genet. 1998 1998 Jul-Aug;6(4):376-82. PubMed PMID: 9781046. eng.

308. Harms MB, Allred P, Gardner R, Fernandes Filho JA, Florence J, Pestronk A, et al. Dominant spinal muscular atrophy with lower extremity predominance: linkage to 14q32. Neurology. 2010 Aug;75(6):539-46. PubMed PMID: 20697106. Pubmed Central PMCID: PMC2918478. eng.

309. Oates EC, Rossor AM, Hafezparast M, Gonzalez M, Speziani F, MacArthur DG, et al. Mutations in BICD2 cause dominant congenital spinal muscular atrophy and hereditary spastic paraplegia. Am J Hum Genet. 2013 Jun;92(6):965-73. PubMed PMID: 23664120. Pubmed Central PMCID: PMC3675232. eng.

310. Teuling E, van Dis V, Wulf PS, Haasdijk ED, Akhmanova A, Hoogenraad CC, et al. A novel mouse model with impaired dynein/dynactin function develops amyotrophic lateral sclerosis (ALS)-like features in motor neurons and improves lifespan in SOD1-ALS mice. Hum Mol Genet. 2008 Sep;17(18):2849-62. PubMed PMID: 18579581. eng.

311. Neveling K, Martinez-Carrera LA, Hölker I, Heister A, Verrips A, Hosseini-Barkooie SM, et al. Mutations in BICD2, which encodes a golgin and important motor adaptor, cause congenital autosomal-dominant spinal muscular atrophy. Am J Hum Genet. 2013 Jun;92(6):946-54. PubMed PMID: 23664116. Pubmed Central PMCID: PMC3675237. eng.

312. Christodoulou K, Zamba E, Tsingis M, Mubaidin A, Horani K, Abu-Sheik S, et al. A novel form of distal hereditary motor neuronopathy maps to chromosome 9p21.1-p12. Ann Neurol. 2000 Dec;48(6):877-84. PubMed PMID: 11117544. eng.

313. Viollet L, Barois A, Rebeiz JG, Rifai Z, Burlet P, Zarhrate M, et al. Mapping of autosomal recessive chronic distal spinal muscular atrophy to chromosome 11q13. Ann Neurol. 2002 May;51(5):585-92. PubMed PMID: 12112104. eng.

314. La Spada AR, Wilson EM, Lubahn DB, Harding AE, Fischbeck KH. Androgen receptor gene mutations in X-linked spinal and bulbar muscular atrophy. Nature. 1991 Jul;352(6330):77-9. PubMed PMID: 2062380. eng.

315. Ramser J, Ahearn ME, Lenski C, Yariz KO, Hellebrand H, von Rhein M, et al. Rare missense and synonymous variants in UBE1 are associated with X-linked infantile spinal muscular atrophy. Am J Hum Genet. 2008 Jan;82(1):188-93. PubMed PMID: 18179898. Pubmed Central PMCID: PMC2253959. eng.

316. Moudry P, Lukas C, Macurek L, Hanzlikova H, Hodny Z, Lukas J, et al. Ubiquitin-activating enzyme UBA1 is required for cellular response to DNA damage. Cell Cycle. 2012 Apr;11(8):1573-82. PubMed PMID: 22456334. eng.

317. Elsheikh BH, Arnold WD, Kissel JT. Spinal Muscular Atrophy. In: Rosenberg RN, Pascual JM, editors. Rosenberg's Molecular and Genetic Basis of Neurological and Psychiatric Disease. 5th ed. USA: Elsevier Inc; 2015. p. 1075-88.

318. Wang H, Yang H, Shivalila CS, Dawlaty MM, Cheng AW, Zhang F, et al. One-step generation of mice carrying mutations in multiple genes by CRISPR/Cas-mediated genome engineering. Cell. 2013 May;153(4):910-8. PubMed PMID: 23643243. Pubmed Central PMCID: PMC3969854. eng.

319. Cong L, Ran FA, Cox D, Lin S, Barretto R, Habib N, et al. Multiplex genome engineering using CRISPR/Cas systems. Science. 2013 Feb;339(6121):819-23. PubMed PMID: 23287718. Pubmed Central PMCID: PMC3795411. eng.

320. White JK, Gerdin AK, Karp NA, Ryder E, Buljan M, Bussell JN, et al. Genome-wide generation and systematic phenotyping of knockout mice reveals new roles for many genes. Cell. 2013 Jul;154(2):452-64. PubMed PMID: 23870131. Pubmed Central PMCID: PMC3717207. eng.

PUBLICATIONS ARISING FROM THIS THEIS AND RELATED STUDIES

Defective presynaptic choline transport underlies hereditary motor neuropathy. (2012) **Barwick K.E.S.**, Wright J., Al-Turki S., McEntagart M.M., Sreekantan-Nair A., Chioza B., Al-Memar A., Modarres H., Reilly M.M., Dick K.J., Ruggiero A.M., Balekly R.D., Hurles M.E., Crosby A.H. *The American Journal of Human Genetics.* 91(6): 1103-1107

Distal spinal muscular atrophy with vocal paresis: from the Welsh choir to genes. (2013) Ingram G., **Barwick K.E.S.**, McEntagart M.M., Crosby A.H., Hartley L., Llewlyn G., Morris H. *Journal of Neurology, neurosurgery, and psychiatry*. 84(11): 0

Mutations in KPTN Cause Macrocephaly, Neurodevelopmental Delay, and Seizures. (2014) Baple E.L., Maroofian R., Chioza B.A., Izadi M., Cross H.E., Al-Turki S., **Barwick K.**, Skrzypiec A., Pawlak R., Wagner K., Coblentz R., Zainy T., Patton M.A., Mansour S., Rich P., Qualmann B., Hurles M.E., Kessels M.M., Crosby A.H. *The American Journal of Human Genetics*. 94(1): 87-94

Distal hereditary motor neuropathy with vocal cord paresis: from difficulty in choral singing to a molecular genetic diagnosis. (2016) Ingram G., **Barwick K.E.S.**, Hartley L., McEntagart M.M., Crosby A.H., Llewelyn G., Morris H.R. *Practical Neurology.,* 0: 1-5

In addition to these manuscripts, three additional publications are currently in preparation:

Dominantly-acting truncating mutations in SLC5A7 underlie adult onset dHMN. (Barwick et al. 2016)

Recessively-acting mutations in SLC5A7 link defective choline transporter activity with predominantly central hypotonia. (Barwick et al. 2016)

A novel GAN mutation presenting as Charcot-Marie-Tooth II. (Barwick et al. 2016)